Specificity of 26S Proteasome Regulation in Plants

Dissertation

der Mathematisch-Naturwissenschaftlichen Fakultät

der Eberhard Karls Universität Tübingen

zur Erlangung des Grades eines

Doktors der Naturwissenschaften

(Dr. rer. nat.)

vorgelegt von

Gautier Langin

aus Toulouse/Frankreich

Tübingen

2024

Gedruckt mit Genehmigung der Mathematisch-Naturwissenschaftlichen Fakultät der Eberhard Karls Universität Tübingen.

Tag der mündlichen Qualifikation:	29.04.2025
Dekan:	Prof. Dr. Thilo Stehle
1. Berichterstatter/-in:	Prof. Dr. Suayb Üstün
2. Berichterstatter/-in:	Prof. Dr. Marja Timmermans

The following thesis is the result of my PhD research achieved from March 2019 to December 2022 at the Eberhard Karls Universität Tübingen, in the Zentrum Für Molekularbiolgie der Pflanzen and from January 2023 to December 2023 at the Ruhr Universität Bochum, in the department Pflanzliche Zellbiologie under the supervision of Professor Suayb Uestuen.

The text will be articulated around multiple publications included in the thesis and for which my participation in the authorship will be clearly specified.

The entire document is an original work and therefore any resemblance with other uncited works is fortuitous.

Table of Contents

Abbreviations

ABA: ABscisic Acid

ATP: Adenosine triphosphate

CAMTA: Calmodulin Associated Transcriptional Activators

CDC48: Cell Division Cycle protein 48

CHLORAD: CHLOroplast-Associated Protein Degradation

DDI: DNA Damage Inducible

DNA: DesoxyriboNucleic Acids

eIF: eukaryotic Initiation Factor

EMSA: Electro Mobility Shift Assay

ER: Endoplasmic Reticulum

ERAD: ER-Associated Degradation

ERAPS: ER-Anchored Protein Sorting

HRD1: HMG-CoA Reductase Degradation protein 1

IDR: Intrinsically Disordered Region

LHC: Light Harvesting Complex

LUCA: Last Universal Common Ancestor

MLP: Major Latey Protein

mRNA: messenger RiboNucleic Acids

NAC: No apical meristem/ATAF1/Cup-shaped cotyledon 2

Nrf1: Nuclear Factor like 1

ORF: Open Reading Frame

PBB: Proteasome subunit Beta type-2

PBE: Proteasome subunit Beta type-5

PhANGs: Photosynthesis Associated Nuclear Genes

PI4Kγ: Phosphatidylinositol 4-kinase gamma

Pma: Pseudomonas syringae pv. maculicola str. ES4326

PRCE: Proteasome Regulatory Cis-Element

PROTAC: PROteolysis TArgeting Chimeras

PSA: Photosystem 1

Pst: Pseudomonas syringae pv. tomato DC3000

PTM: Post-Translational Modification

Rpn4p: Regulatory Particle Non-ATPase 4 protein

RPT: Regulatory ParTicle

SA: Salicylic Acid

SAUR: Small Auxin Upregulated RNA

SH3P2: Src homology 3 domain-containing protein 2

TF: Transcription Factor

tRNA: transfer RiboNucleic Acids

UPS: Ubiquitin Proteasome System

UTR: UnTranslated Region

WT: Wild Type

XopL: Xanthomonas Outer Protein L

Summary

The diversity and complexity of living organisms are driven by the specificity of their proteome, which is tightly regulated through controlled protein production, utilization, and degradation. To mediate this regulation, conserved and sophisticated mechanisms have evolved to form a molecular network that maintains cellular protein homeostasis, known as proteostasis. Among these mechanisms, proteolytic pathways are key determinants in proteome regulation, with proteolysis being essential for clearing unwanted proteins, especially under environmental stress. In eukaryotes, the primary proteolytic pathway is the ubiquitin-proteasome system (UPS). This system relies on the post-translational modification of target proteins with ubiquitin peptides, which marks them for recognition and specific degradation by the 26S proteasome holoenzyme. The latter identifies ubiquitinated substrates, unfolds them, and degrades them via a proteolytic core. Proteasomal degradation is responsible for the majority of protein turnover in cells and is crucial for maintaining cellular proteome balance. Under stress, however, the accumulation of proteasome substrates can exceed proteasomal capacity, resulting in proteotoxic stress. Defects in proteasomal turnover are associated with numerous medical and agricultural challenges. To counteract such stress, eukaryotes have evolved a feedback mechanism that ensures adequate proteasomal capacity. This mechanism involves a negative feedback loop in which transcriptional activators of proteasome genes are themselves substrates for proteasomal degradation, enabling constant monitoring of proteasome capacity and a rapid response under stress conditions. While this mechanism has been characterized in yeast and mammals, it remains poorly understood in plants. In this study, we investigated the role of proteolytic pathways in plant-pathogen interactions, with a focus on the importance of the ubiquitin-proteasome system in this context. We developed a pipeline to assess proteasome status under stress conditions and characterized the proteasome feedback loop in plants. We found that a sorting mechanism at the endoplasmic reticulum mediates both the degradation and nuclear translocation of the proteasome transcriptional activators NAC53 and NAC78 when proteasomal capacity is exceeded. Once in the nucleus, NAC53 and NAC78 activate proteasome gene expression and simultaneously repress photosynthesis-associated nuclear genes. This cross-talk enables an increase in proteasome capacity while reducing the accumulation of proteasome substrates. We identified this cross-talk as a core response to stress in plants. This work reveals an intricate regulatory network linking protein production, degradation, and energy metabolism, providing a conceptual framework for further exploration of proteostasis maintenance in eukaryotes.

I. Introduction - The significance of Proteostasis

a. The Proteome: working force of the cell

The uniqueness of our planet is certainly the presence of innumerable known (and yet to be discovered) living organisms crossing paths since the emergence of life. While the precise process and conditions which permitted the appearance of the last universal common ancestor (LUCA), remain elusive (Arndt and Nisbet, 2012), it eventually led to the formation of a living cell, a closed structure working as a molecular factory able to self-replicate. A living cell is characterized by the presence of nucleic acid chains, in the form of DNA (DesoxyriboNucleic Acids) and RNA (RiboNucleic Acids); encoding the genetic information allowing the formation of large molecules, the proteins. Since the time of LUCA, approximately 3.5-3.8 billion years ago (Mann, 2012), evolution has driven the diversification and complexity of life, leading to a wide array of organisms, from the deadly *Yersinia pestis,* the delicious *Boletus engelii*, to the giant *Sequoiadendron giganteum* and the swift *Acinonyx jubatus*. At first sight these organisms look nothing alike as they display drastically different developmental and behavioral phenotypes (**Figure 1A**), however they are all formed from cells directed by the same fundamental molecular principles. Therefore, what led to this diversity is not determined by the cellular mechanisms themselves, but rather by the nature of the 'workers' involved in these processes.

Any organism needs to be replicated, to produce energy and to rapidly adapt to sudden environmental changes. To do so every known living cell employs many thousands of proteins involved in various molecular pathways intertwined in a complex regulatory network. This network is specific to each individual, as every organism has a unique DNA sequence, known as the genome, composed of four nucleic acids: Adenine (A), Thymine (T), Guanine (G) and Cytosine (C). At the molecular level, the genome consists of a double stranded helix of nucleotide chains packed into single or multiple large molecular structures: the chromosomes. Each chromosome contains specific genomic regions responsible for the encoding of proteins, the genes. A gene is transcribed by the RNA polymerase complex into a single stranded nucleotide chain called the RNA molecule. These molecules are constituted from the same nucleotides as the gene itself, except for Thymines which are substituted by Uraciles (U). The RNA molecule is matured into a shorter version called the messenger RNA (mRNA) which serves as a template for protein translation. This mRNA will be recognized by the translation machinery leading to the translation of the mRNA into a protein.

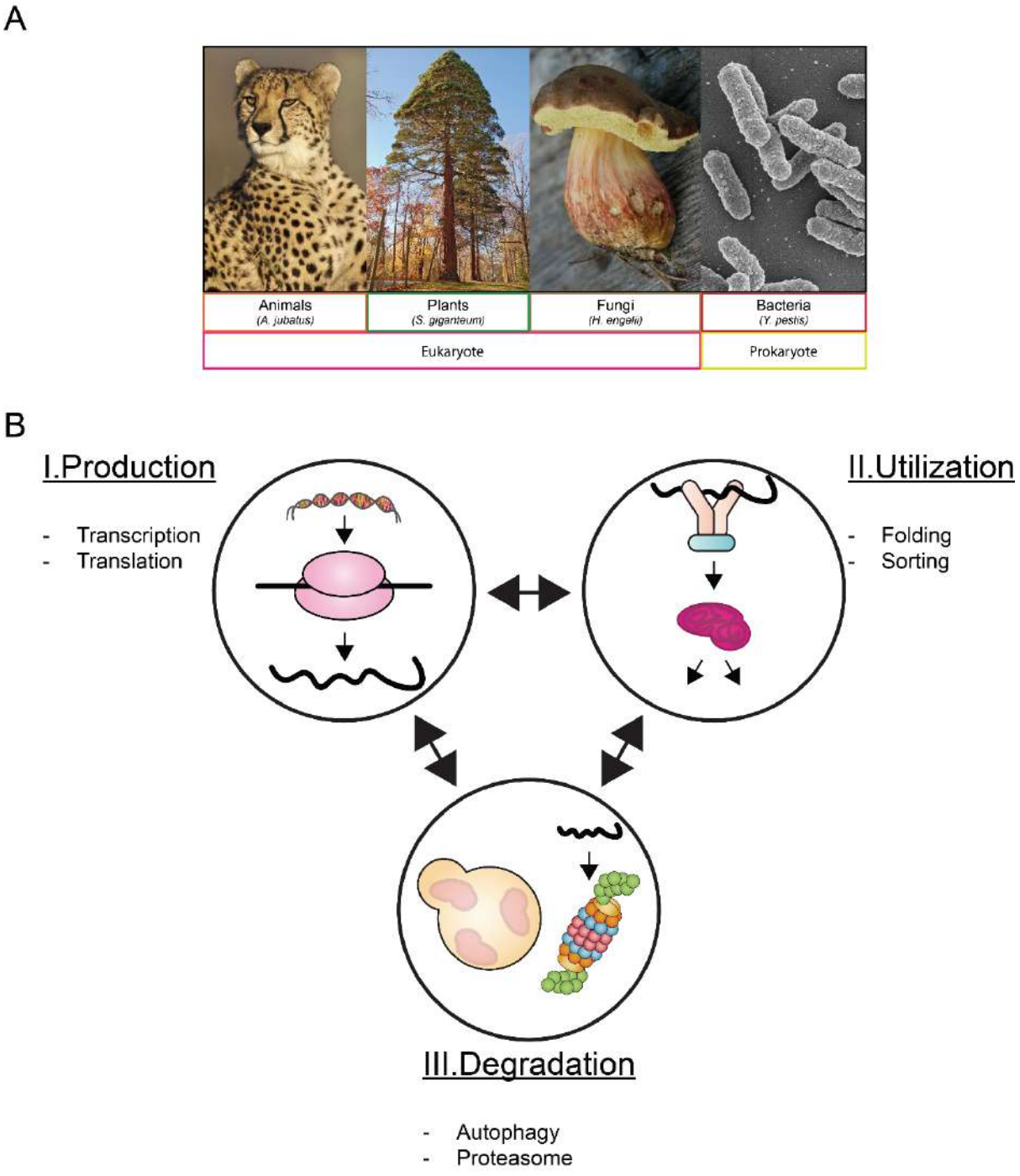

Figure 1. Regulation of the Proteome as the driver for phenotypic diversity of life

A. Representation of the phenotypic diversity observed on the planet earth. Animals, plants, fungi and bacteria are the most studied kingdoms of life. Evolution has driven an astonishing diversity of morphology from monocellular microorganisms to giant organisms. **B.** The eukaryotic triangle of proteostasis: The proteome equilibrium is controlled through protein production, utilization and degradation.

The specificity of this translation process is due to a conserved genetic code. This code relies on the correspondence between the succession of three nucleotides, a codon, to one of the 20 encoded amino acids or to a stop codon, the signal for translation termination (Koonin and Novozhilov, 2017). The sequential attachment of corresponding amino acids forms a polypeptide chain which folds into a large three-dimensional structure, creating a functional molecule known as a protein. In *homo sapiens*, protein sizes range from a few dozen to more than 35 000 amino acids (Consortium, 2022; Mayans et al., 1998). Clearly, this principle permits a nearly infinite number of possible proteins based on their size and sequence constitution. Hence, the specific suite of proteins encoded by the genome of an organism, termed as the proteome, defines the molecular working force mediating its development and adaptation to the environment.

Over billions of years life has been experienced on earth, the genome (and consequently the proteome) of each species has been precisely shaped by evolution, leading to the diversity of life we observe today. Classification of proteins, via sequence comparison, permitted to establish the evolutionary link between the proteome members of many species across the tree of life and highlighted the presence of protein families (Paysan-Lafosse et al., 2022). In addition, biochemical and molecular studies carried out since decades, identified the modes of action for many of these families, revealing the nature of the cellular “workers”. Strikingly, previous work has uncovered that a large portion of every proteome consists of very similar proteins (Koonin et al., 2004), consistent with the conservation of the fundamental molecular principles, described above, which have emerged at the early stages of life. Morevoer, it highlighted the global degree of species differentiation. Indeed, each kingdom possesses unique characteristics which are reflected in their proteome. For instance, bacterial populations can coordinate growth using quorum sensing (Miller and Bassler, 2001); plants have the ability to convert solar energy into sugar via photosynthesis (Eberhard et al., 2008) and animals can move dynamically through space using muscular organs (Fagan et al., 2013).

To accomplish their function within a cell, proteins employ several modes of action. These modes of action depend on the biophysical and biochemical properties of the protein. These properties are defined by the protein amino acid composition (Harms and Thornton, 2013). The physical properties depend on the size, shape and flexibility of the molecular structure. These aspects determine how the protein will behave in the cellular environment. It permits to associate with other proteins, to be mobile or to serve as a scaffold to maintain subcellular structures. The biochemical properties of the protein are given by the chemical nature of the exposed amino acids when the protein is properly folded. For instance, many proteins possess typical interfaces allowing the catalysis of chemical reactions within the cell. These proteins are called enzymes. Enzymes can act on small molecules to mediate their modification; this

permits the production of specific molecules used in a plethora of cellular processes (Agarwal, 2006). It includes the production of neurotransmitters for cerebral function, the synthesis of chlorophyll pigments for the absorption of sunlight during photosynthesis or the formation of defense compounds, such as antibiotics, to combat against invasive organisms (Agarwal, 2006). All these chemical reactions comprise cellular metabolism. Enzymes can also act on other proteins to modify their function. These post-translational modifications (PTM) happen via linking certain molecules to certain amino acids on the target protein, leading to specific subcellular targeting. It can result in novel functions of the modified protein or its degradation depending on the signal. Most of these modifications are reversible: For instance, the attachment of a phosphate group (phosphorylation) is mediated by kinases, while its removal is mediated by phosphatases. Additionally, enzymes can breakdown the protein structure via two means: (i) protein unfolding, and (ii) removal of bound amino acids, the latter called proteolysis (Brix, 2013).

This set of properties are the signature of what is called a protein domain (Paysan-Lafosse et al., 2022). A single protein can contain one or multiple domains. In addition, association of multiple proteins can lead to a highly elaborated molecular complex mediating precise functions such as the RNA polymerase complex for gene transcription, the ribosomal machinery for protein translation, the photosystem apparatus for photosynthetic reactions or the proteasome complex for protein degradation.

Since the correct function of a cell depends on the concerted action of many thousand proteins, a single modification in the sequence of a single protein can result in large modification of the overall molecular machinery and therefore the fate of the organism. Although the underlying principles for molecular biology and maintenance of cellular processes are sophisticated, many mechanisms are error prone. Thus, the action of a single protein and maintenance of the global proteome within each cell requires a tight regulation in time and space. Consequently, it is essential to understand how living organisms control their proteomes to comprehend the principles of molecular biology.

b. The Maintenance of Proteostasis

As mentioned above the proteome is composed of many thousand proteins with each of them working together in a complex molecular network. However, the cellular machinery does not rely on a single copy of each protein to function. Indeed, proteins are present in several forms or amounts, in specific cells from the same organism and/or at a defined developmental stage.

For the proper functions of cells proteins need to be produced in specific amounts, transported to their place of action and recycled when their function is accomplished to remove unwanted effects. This equilibrium of the “birth” of a protein to its “death” is shaping the proteome and is known as proteostasis, the dynamic regulation of a balanced, functional proteome. The regulation of proteostasis can be divided into three major regulatory modules: 1) protein production; 2) protein utilization and 3) protein degradation (**Figure 1b**).

1. Transcriptional Regulation

Gene expression is the initial step in regulating the proteome to induce the formation of mRNAs that serve as templates for protein production. To fully understand this regulation, it is important to know that all genes share a similar genomic structure. This structure consists primarily of a region called ORF (open-reading frame) carrying protein coding information. Additionally, apart from regions coding for the protein information, called exons, it can contain introns, genomic regions which are not translated into protein (**Figure 2**). The ORF can be flanked by two UTRs (UnTranslated Regions) referred to as upstream 5’UTR and downstream 3’UTR. These regions are transcribed alongside the coding region and used, with the introns, for transcriptional and/or post-transcriptional regulation. Finally, the upstream of the gene is the promoter region, a non-transcribed region, essential for the regulation of gene expression by the RNA polymerase complex (**Figure 2**).

DNA accessibility is the first regulatory aspect controlling gene expression. It comes from the physical structure of the chromosome carrying the gene of interest. Indeed, DNA molecules are packed around specific proteins, called histones, in a DNA-protein structure referred to as the chromatin. This structure is locally flexible depending on further histone interacting proteins and permits to “open” the chromatin, either to render a local region accessible, or to “close” the chromatin (Klemm et al., 2019), **Figure 2**). Once the chromatin is in an open state, the genetic region of interest is accessible for another class of proteins, the transcription factors (TFs) (**Figure 2**). TFs are essential proteins that permit the fine-tuning of gene expression. They are characterized by their ability to bind to specific DNA motifs, mainly found in the promoter region or the 5’UTR of the target gene.

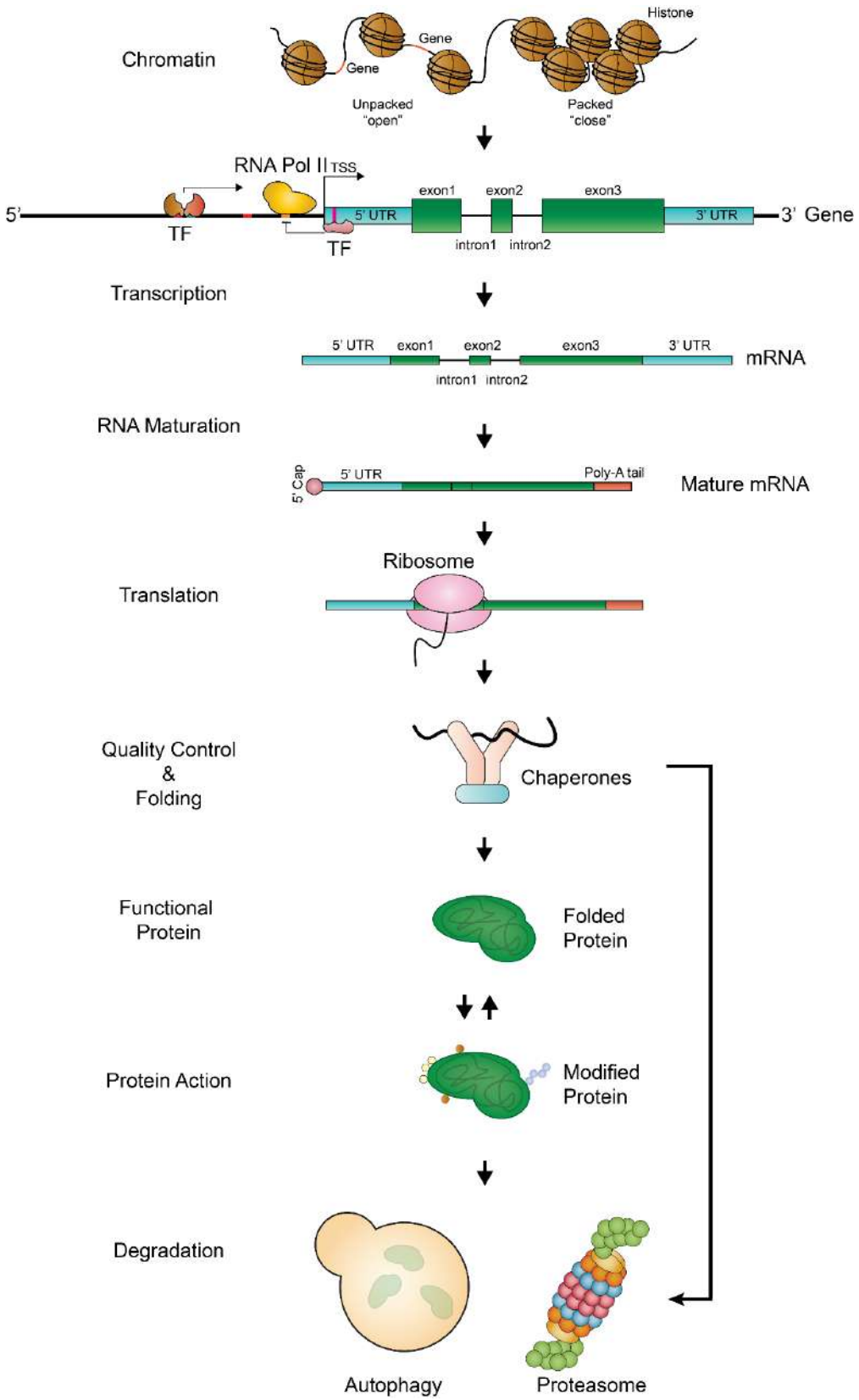

Figure 2. Regulation of protein from production to degradation.

Protein regulation from its production to its regulation is tightly regulated through multi-layered process. Production is initially regulated by chromatin accessibility regulating access of the protein genic region for the transcriptional regulators. Upon transcription the protein mRNA molecule is subjected to maturation before serving as template for the translational process. Nascent peptide from the ribosome is recognized by quality control and folding chaperones, facilitating protein folding or sending the peptide for degradation is necessary. Once folded, the functional protein can be subjected to multiple modifications to regulate its function before it is subjected to degradation once its function as been fulfilled.

Upon binding of a TF to its DNA motif it will modify the protein environment in proximity to the transcription starting site of the target gene. This modification is reflected by the recruitment of partner proteins leading to the association of the RNA polymerase complex with the DNA in case of gene expression activation; or conversely hindering the access of the RNA polymerase complex to the DNA in case of repression of gene expression. TFs can act on multiple genes simultaneously, in concert with other TFs or as a TFs cascade to finely modulate the transcriptome (Neph et al., 2012; Song et al., 2016).

There are multiple TF families, largely characterized by their protein domains allowing association with the DNA molecule. Some of these families are present in all living organisms, others are exclusive to certain species and drivers of lineage specific features (de Mendoza and Sebé-Pedrós, 2019). For instance, GATA TFs are widespread eukaryotic regulators which recognize conserved DNA motifs (Kim et al., 2021; Lentjes et al., 2016). They are involved in diverse functions in all organisms, showing the versatility of conserved transcription factors in being adapted to achieve specific functions. In contrast, the NAC TFs family is a plant specific transcription factor family that has evolved predating the emergence of land plants (Maugarny-Calès et al., 2016). In *Arabidopsis thaliana*, this family comprises 138 members which makes it one of the largest. Multiple studies have shown that NAC TFs are involved in several functions from plant developmental process to stress response (Welner et al., 2016). Contrary to GATAs, reports on diverse NAC members have shown a broad range of recognized DNA motifs (Welner et al., 2016). Furthermore, while most studies have found NAC TFs to act as transcriptional activators, a report has characterized the NAC domain as a transcriptional repressor (Hao et al., 2010). Last, TF activity can be highly influenced by other domains than the DNA recognition domain. This is the case for a sub-clade of the NAC which members possess a transmembrane domain at their C-terminal allowing membrane anchoring for specific subcellular localization (Kim et al., 2007). This type of anchoring is present in multiple TFs families and is essential for the TF activation (Seo et al., 2008). The NAC family illustrates the complexity behind TFs function where a conserved protein domain can mediate recognition of distinct DNA motifs, possess opposite transcriptional outcome and can require subcellular regulation for their activity. Two of these NAC, NAC53 and NAC78, are the main actors described and characterized in **Chapter V.**

The regulation of the transcriptome is the first step to control and adjust the cellular proteome being essential for many cellular processes such as development and response to environmental changes (Vogel and Marcotte, 2012).

2. Translational Regulation and Protein Quality Control

Protein synthesis constitutes another crucial step for the maintenance of proteostasis. As mentioned above, upon transcription, the synthesized RNA molecule possesses regulatory regions that will not serve for protein translation. However, in eukaryotic organisms, these regions are important for the translational processes since they define the mature version of the mRNA template as well as its stability and availability to the ribosomal complex (Gilbert and Nachtergaele, 2023; Lee and Rio, 2015). After transcription, the pre-mRNA molecule is modified by several proteins in a mechanism called post-transcriptional processing. This mechanism involves the splicing of existing intronic regions, defining the codon succession usage to encode the resulting protein. Splicing is an essential mechanisms as alternative splicing could result in different template sequences; leading to the production of a different protein (Lee and Rio, 2015). Another regulatory step is the capping of the RNA molecule upstream of the 5'UTR region, which consists of the attachment of a 7-methylguanosine molecule to the pre-mRNA molecule. This modification of the pre-mRNA molecule at protects it from degradation by exoribonucleases (Gilbert and Nachtergaele, 2023). Finally, the third step of post-transcriptional processing in eukaryotes is the addition of a poly-adenine chain downstream of the RNA 3'UTR. This poly-A sequence will serve as a docking site for specific proteins that protect the mRNA from degradation at this end (Gilbert and Nachtergaele, 2023). Altogether, these steps are required for the maturation of pre-mRNA into mature mRNA (**Figure 2**). They are essential for the fate of the RNA molecule, driving its final form and serving as checkpoints prior to being used for protein translation.

Once the mRNA molecule is matured it is used as a template by the ribosomal complex. The ribosomal complex is a macromolecular machine formed by two protein subcomplexes, known as the 40S ribosomes for the "small" subunits and the 60S ribosomes for the "big" subunits (Jackson et al., 2010). This complex works in concert with other proteins to mediate several steps of the translational process. In eukaryotes, the 40S ribosomal subunits associates with several members of the eukaryotic translation initiation factors (eIFs) protein family to allow the recruitment of the target mRNA to the ribosome and thus leading to the initiation of translation (Jackson et al., 2010). After recognition of the mRNA, 60S subunits associate with 40S subunits to form the complete ribosome that embraces the mRNA in the complex (**Figure 2**). Translation elongation of is performed by the utilization of transfer-RNA (tRNA) molecules by 60S subunits. As mentioned above the amino acids sequence of a protein is determined by the codon succession of the mRNA template; hence the tRNAs are RNA molecules bearing a complementary codon sequence attached to the amino acid molecule corresponding to this codon (Dever et al., 2018). With the help of the eukaryotic elongation factor, the ribosome will

associate with a tRNA, check for matching sequences between the scanned codon from the mRNA and the complementary tRNA codon, and, if matching, attach the corresponding amino acids to the nascent polypeptide chain. This process happens repeatedly until the mRNA scanning reaches the stop codon, which triggers the termination of translation resulting in the dissociation of the ribosomal complex and release of the mRNA (Dever et al., 2018).

After completion of translation, emerging nascent proteins need to be folded to form their final molecular structures. Upon translation, the polypeptide chain is in form of a linear succession of amino acids, which is termed the primary structure (Dever et al., 2018). This linear structure will rapidly form the protein secondary structure due to intramolecular hydrogen bonds forming between amino acids, resulting into sub-molecular structure known as alpha helix or beta sheets. This secondary structure will then be folded into a final tertiary structure due to hydrophilic and hydrophobic properties of the amino acids. Of note, some proteins do not form alpha helix or beta sheets and are naturally unstructured. These regions are called intrinsically disordered regions (IDRs) (van der Lee et al., 2014). The folding process is essential for the correct function of the protein. In case of misfolding, the disruption of the protein structure will lead to a disruption of the chemical properties of the protein which can significantly perturb the function of global proteome. Therefore, cells employ quality control systems to monitor misfolded proteins, relying on specific proteins termed chaperones. Chaperones are found directly in association with the ribosomes and are immediately acting downstream of them (Balchin et al., 2016). Chaperones serve as a check point to ensure proper folding of the nascent proteins. If the protein is not totally folded or partially misfolded, chaperones will facilitate the process to ensure that the protein is folded in its native active state. If the native state can be achieved, the protein will be targeted to the localization where it is required to fulfil its function within the proteome. Otherwise it will be subjected for immediate degradation (**Figure 2**) (Balchin et al., 2016).

3. Protein sorting and degradation

Production of protein from genes is a complex multi-layered process involving many regulatory steps. However, once the protein is formed it still needs to be properly transported to the correct compartment in the cell. And, conversely, it needs to be efficiently removed if it is not wanted or if it has completed its function.

Protein targeting is a particularly essential principle in eukaryotic cells which are characterized by a high level of subcellular compartmentalization compared to prokaryotes. It permits

efficient clustering of molecular mechanisms allowing better control in space and time. This eukaryotic characteristic is notably defined by the presence of, so-called, organelles separated from the cellular environment by lipidic membranes (Shibata et al., 2009). These organelles are involved in precise cellular functions. For instance, in animals and fungi, energy metabolism relies on mitochondria, while plants mainly utilize chloroplasts to maintain their energy metabolism. The secretion of proteins or metabolites in the secretory pathway is controlled by the endomembrane system consisting of the endoplasmic reticulum, golgi apparatus and plasma membrane. All three compartments are major contributors for intracellular trafficking, permitting protein exchange and transport within the cell (Yuen et al., 2023). Detoxification of deleterious compounds are stored in compartments called lysosomes or vacuoles. And gene expression is regulated in the nuclear environment. Targeting of proteins to the right compartments usually depends on specific protein sequences, known as signal peptide, which will be recognized in parallel or downstream of the folding process to correctly shuttle the protein (Grudnik et al., 2009). Additionally, organelles are inter-connected and impact each other's activity (Cohen et al., 2018). Therefore, this high degree of compartmentalization requires efficient inter-organellar communication to adjust the subcellular proteome. Indeed, apart from mitochondria and chloroplast which encode a small number of their respective intra-organellar proteome, all proteins originate from the nuclear genome (Gray, 1999). It implies that communication between organelles and the nucleus is an essential aspect of the maintenance of subcellular proteostasis.

As such, the complexity of the maintenance of the eukaryotic proteome does not allow us to rely only on the regulation of protein production from the nucleus. Adaptation of the transcriptome and regulation of translation are essential mechanisms but not sufficient to control big proteomes and to react to sudden changes in the environment. Therefore, the cell requires efficient mechanisms for protein quality control. These mechanisms rely on enzymes that degrade proteins (Brix, 2013). These enzymes, named proteases, can break down association between amino acids of a protein, leading to the cleavage of proteins into smaller peptides and ultimately releasing free amino acids that can be eventually reused in the translation process. This enzymatic action, called proteolysis, is exergonic (Brix, 2013). Thus, proteolysis should not happen spontaneously and needs to be tightly controlled to avoid stochastic degradation of functional and necessary proteins. Consequently, evolution has driven compartmentalization of protein degradation systems within the cell (Brix, 2013). Life has developed two major ways to mediate this compartmentalization. One way, is the presence of proteases in the lysosomal or vacuolar environment, separated from the rest of the cell by a lipid membrane (Knop et al., 1993). These proteases work in concert with degradation pathway relying on cellular trafficking, delivering proteins to be degraded to the

lysosome/vacuole via vesicular structures. The major process implying vesicle-mediated degradation is the autophagy pathway and is described in the context of plant-microbe interactions in **Chapter II**. The second major way is based on the formation of cylindric macromolecular structures. It consists of the association of proteases with other proteins to enclose their proteolytic active sites on the inner side of a cylinder, avoiding exposure to the cellular environment. These cylinders are usually capped by proteins that will regulate their opening state with energy, permitting a tight control of the protease's accessibility. These macromolecular structures are called proteasomes. The major type of proteasome complex in eukaryote is called the 26S Proteasome. The transcriptional regulation of this complex is the main topic of this thesis. Details about the 26S Proteasome function can be found in **Chapter II**, **III** and **IV**.

c. Coping with proteotoxicity

The previous chapter emphasized how the maintenance of proteostasis involves many mechanisms to coordinates the cellular proteome. The latter, being a complex intricated molecular network needs to be precisely sensed by the cell to adapt to its demands. Therefore, a significant challenge that any organism faces is to maintain proteostasis in response to sudden changes in the cellular environment. Indeed, external stimuli such as heat, excess of sun or drought (referred to as abiotic stress) or microbial infections by viruses or bacteria, (referred to as biotic stress) can strongly affect the proteome, notably through accumulation of aberrant proteins (Orosa et al., 2020). It can occur due to physical changes such as temperature rising or UV blast leading to genomic modification, protein misfolding or protein accumulation. In addition, pathogens willing to perturb host proteome for their own benefit will also trigger the presence of unwanted or dysfunctional proteins (see **Chapter II** and **IV**). These proteins, in excess, will strongly hinder the proteome network resulting in toxicity, an outcome known as proteotoxicity (Hightower, 1991).

Therefore, eukaryotic cells need mechanisms to efficiently sense perturbations in the proteostasis network and remodel its proteome to avoid proteotoxicity. This remodeling often implies a trade-off between developmental processes which need to be repressed and stress responsive pathways which need to be activated (He et al., 2022; Pakos-Zebrucka et al., 2016). In addition, enhanced activation of proteolytic pathways is required to remove the proteins at the origin of proteotoxicity. Being a global process, this remodeling needs to mediate a systemic coordination of the cellular proteome acting at every level during proteostasis. This aspect is particularly interesting in the scope of eukaryotic cells with a highly

compartmentalized cellular environment. Indeed, proteotoxicity can originate from a specific subcellular site and needs to be precisely sensed to activate a counter response. In turn, the perception needs to be transmitted into a signal which can permit the required adjustments on the overall proteome.

Since 26S Proteasome-dependent proteolysis is responsible for the degradation of proteins from multiple subcellular compartments, it appears to be one of the key components to cope with proteotoxicity. Additionally, the known regulatory feedback loop regulating the 26S Proteasome homeostasis, in yeast and animals, can constitute an interesting system for proteotoxic signal transduction, see **Chapter V**, (Marshall and Vierstra, 2019). In the main work of the thesis, **Chapter V**, we will address how by studying the 26S Proteasome regulation we identified a sorting mechanism that is responsible for remodeling the transcriptome in response to proteotoxicity.

In the following chapters we will, (i) describe the relevance of studying proteolytic pathways during biotic stress, (ii) review the importance of proteasomal degradation in plant-pathogen interactions, (iii) propose a pipeline to investigate the 26S proteasome regulation in such context and (iv) characterize the regulation of the 26S proteasome regulation in plant and how this regulation connects subcellular proteostasis.

II. Proteolytic Pathways are essential to cope with biotic stress

This chapter compiles three publications highlighting the importance of proteolysis in an agricultural relevant context: Plant Immunity. As described in the following publications, during infection, phytopathogenic organisms employ various mechanisms to inject protein effectors into plant cells. These effectors are utilized to manipulate several host cellular mechanisms to cause disease. The function of pathogen effector is not limited to the manipulation of a single pathway. As such, their effect has a strong impact on the overall cellular proteome. In addition, pathogen effectors have been characterized to directly hijack host proteolytic pathways, thus affecting proteostasis in the host.

In the manuscript “Microbial Effector Proteins – A Journey through the Proteolytic Landscape”, published in 2019, we described current knowledge and recent findings concerning microbial pathogen effector proteins targeting the plant autophagy and ubiquitin proteasome system (UPS). In addition, a network analysis of targeted proteins and host interaction partners allowed us to map how several plant pathways are impacted and highlighted the interconnections between mechanisms of proteostasis maintenance during microbial invasion.

In the manuscript “Selective Autophagy: Adding Precision to Plant Immunity”, published in 2022, we focused on the role of selective autophagy during plant immunity. We summarized the different types of selective autophagy and highlighted recent findings on how selective autophagy is involved during plant-pathogen infections. Given their importance during immune responses, we proposed an *in-silico* analysis, identifying putative selective autophagy receptor candidates based, (i) on their ability to recognize ubiquitinated proteins via specific protein domain, (ii) on possible recruitment to autophagosomes based on previous studies reporting predicted or putative interactions with ATG8 protein and (iii) on their transcript levels upon several immune-related context.

In the manuscript “A bacterial effector counteracts host autophagy by promoting degradation of an autophagy component”, published in 2022, we uncovered how the *Xanthomonas campestris pv. vesicatoria* bacterial effector XopL manipulates plant autophagy to promote bacterial infection. In this study we elucidated how XopL functions as an E3 ligase to promote proteasomal degradation of the plant specific autophagy component SH3P2 which results in a disruption of the host autophagy machinery.

a. Microbial Effector Proteins – A Journey through the Proteolytic Landscape

Scientific contributions: Scientific ideas 33%, Protein Network Analysis 100%.

Details about writing contributions: Writing of the section “Hijacking the UPS: Degrade, Stabilize and Suppress” under supervision of SÜ. Minor help on the sections “Proteolytic Landscape in Plants – A Battleground for Pathogens”, “Is the Targeting of Protein Degradation Pathways a Strategy to Force the Interplay between Different Cellular Pathways?” and “Concluding Remarks”.

Citation: Langin G, Gouguet P, Üstün S. Microbial Effector Proteins - A Journey through the Proteolytic Landscape. Trends Microbiol. 2020 Jul;28(7):523-535. doi: 10.1016/j.tim.2020.02.010. Epub 2020 Apr 2. PMID: 32544439.

CellPress
REVIEWS

Opinion

Microbial Effector Proteins – A Journey through the Proteolytic Landscape

Gautier Langin,[1] Paul Gouguet,[1] and Suayib Üstün [1,*]

In the evolutionary arms race between pathogens and plants, pathogens evolved effector molecules that they secrete into the host to subvert plant cellular responses in a process termed the effector-targeted pathway (ETP). During recent years the repertoire of ETPs has increased and mounting evidence indicates that the proteasome and autophagy pathways are central hubs of microbial effectors. Both degradation pathways are implicated in a broad array of cellular responses and thus constitute an attractive target for effector proteins to have a broader impact on the host. In this article we first summarize recent findings on how effectors from various pathogens modulate proteolytic pathways and then provide a network analysis of established effector targets implicated in proteolytic degradation machineries. With this network we emphasize the idea that effectors targeting proteolytic degradation pathways will affect the protein synthesis-transport and degradation triangle. We put in perspective that, in utilizing the effector diversity of microbes, we produce excellent tools to study diverse cellular pathways and their possible interplay with each other.

Highlights

Pathogens evolved effector proteins that are secreted into the host and mediate the outcome of plant–microbe interactions.

Tremendous efforts in the effector biology community have revealed how effectors target host pathways – such as RNA silencing, vesicle trafficking, transcription, cell signaling, and innate immunity – for the benefit of the pathogen.

Many effectors converge on conserved proteolytic degradation pathways such as the proteasome and autophagy.

Targeting the proteasome and the autophagy machinery opens the possibility to perturb the host cell on a global scale.

Network analysis of effector targets reveals novel possible interplays between the protein synthesis-transport-degradation triangle.

Proteolytic Landscape in Plants – A Battleground for Pathogens

The concept of the evolutionary arms race between plants and pathogens, and how it shapes the interaction between host organism and invader, has been discussed in many excellent reviews [1,2]. To adapt to new hosts and surrounding microbes, both sides undergo neofunctionalization of their gene repertoire and diversification during coevolution. This adaptation process results in a diversity of molecular players controlling colonization of plants or strengthening defense against pathogens. Despite diversification there are a common set of molecular players on the host and pathogen sides that determine the outcome of plant–microbe interactions. For instance, plants have acquired surface-localized pattern-recognition receptors (PRRs) that are able to perceive conserved pathogen-associated molecular patterns (PAMPs), to induce PAMP-triggered immunity (PTI) that confers broad resistance to various phytopathogens [3,4]. In turn, adapted plant pathogens are able to overcome PTI responses by delivering microbial effector proteins into host cells. These effectors are able to manipulate the host for the benefit of the pathogen [5]. However, this process in itself makes effectors also vulnerable because plants evolved resistance proteins to track their action and elicit the third layer of defense – termed effector-triggered immunity (ETI) [1]. Hence, effectors are the major actors in plant–microbe interaction as they largely determine the outcome of the battle between host and pathogen. Consequently, understanding the function of effectors is critical to understand how plant pathogens colonize host organisms. Identification of effector host targets revealed many 'old' and 'new' players in plant immunity, illustrating how microbial effectors can also serve as molecular probes to decipher novel key components and pathways of plant immunity.

For years, research concentrated on single effector targets such as surface-localized receptors, classical defense components, or hormone signaling, all of which are integral parts of plant immunity [5]. However, it is becoming evident that plants not only rely on classical immune system

[1]University of Tübingen, Center for Plant Molecular Biology (ZMBP), Tübingen, Germany

*Correspondence:
suayib.uestuen@zmbp.uni-tuebingen.de (S. Üstün).

components but also that microbial effectors perturb whole pathways (ETPs) rather than affecting single proteins with little impact in the host. The term ETP was first introduced by Chaparro-Garcia *et al.* in 2012 and centered around the idea that effectors target key plant processes such as RNA silencing, vesicle trafficking, transcription, cell signaling, and innate immunity for the benefit of the pathogen [6]. Since then, the repertoire of ETPs or 'hubs' has increased tremendously and now includes proteolytic degradation pathways such as those involving the proteasome and autophagy machinery [7–10]. Targeting and convergence of effectors on these essential eukaryotic pathways is not surprising as the initiation and maintenance of defense responses not only involves *de novo* synthesis of regulatory proteins and enzymes but also their regulated degradation. Thus, tailoring the proteome during plant defense response is essential to maintaining an efficient response to external change. The ubiquitin–proteasome system (UPS), and autophagy were identified as essential components of plant immunity, influencing the outcome of plant–microbe interactions [11–13]. In eukaryotes, the UPS is essential for proteostasis through the selective elimination of misfolded or otherwise defective proteins, as well as short-lived regulatory proteins [14] (Box 1). In addition to the UPS, autophagy is another major degradation pathway implicated mainly in cellular homeostasis, stress tolerance, and pathogen defense in eukaryotic organisms [15], forming double-membrane vesicles, termed autophagosomes, which deliver cargo to the vacuole for degradation [15] (Box 1). Evidence has accumulated that regulated protein turnover, via UPS and autophagy, controls multiple aspects of plant immunity, including pathogen recognition, immune receptor accumulation, and downstream defense signaling [12,13]. Therefore, many microbial effectors perturb or exploit proteolytic degradation to dampen plant immune responses resulting in a broad impact on the plant. Because microbial effectors are key determinants of disease progression, it is perhaps not surprising that they target essential plant pathways to operate in the most effective way. In this article we highlight recent advances in the understanding of microbial effector targeting (from viruses, bacteria, fungi, and oomycetes), and exploitation of degradation machineries (the UPS and autophagy). We suggest the concept that it is inevitable to look beyond the classical

Box 1. Proteasome and Autophagy – Major Degradation Pathways in Eukaryotes

Proteasome-mediated Protein Degradation

Selective protein degradation by the proteasome system proceeds from the ligation of one or more ubiquitin proteins to the ε-amino group of a lysine residue within specific target proteins catalyzed by E1, E2, and E3 enzymes. Activated ubiquitin binds to E1 and is transferred to the ubiquitin-conjugating enzyme (E2). The E2 carries the activated ubiquitin to the ubiquitin ligase (E3), which facilitates the transfer of the ubiquitin from the E2 to a lysine residue in the target protein. The ubiquitinated target protein is then recognized by the 26S proteasome for degradation. The 26S proteasome itself is a 2.5 MDa ATP-dependent protease complex composed of a 20S core protease (CP) and two 19S regulatory particles (RPs), each of which contains a lid and a base subunit. The CP is a broad-spectrum ATP- and ubiquitin-independent protease complex harboring peptidase activity. The CP peptidases cleave a broad array of polypeptides, with the β1, β2, and β5 active sites providing trypsin-like, chymotrypsin-like and caspase-like cleavage properties, respectively. The RP subcomplex is responsible for recognizing ubiquitinated target proteins and for opening the channel of the CP to insert the unfolded substrates into the CP chamber for degradation [55].

Autophagy (Greek: 'self-eating')

Autophagic mechanisms rely on a core set of conserved AuTophaGy-related (ATG) genes to form double-membrane vesicles, termed autophagosomes, that sequester and deliver cytoplasmic cargo to lytic compartments (i.e., lysosomes/vacuoles) for breakdown and recycling [15]. Autophagosome formation is initiated at the phagophore assembly site (PAS) and involves expansion and sealing of the phagophore around the cargo. ATG8 proteins are required for membrane expansion and are found on autophagosomes until their lytic destruction [15]. While autophagy has been regarded for a long time as a largely nonspecific ('bulk') catabolic and recycling process upon nutrient limitation, increasing evidence now indicates that autophagy also acts as a selective mechanism to degrade protein aggregates, organelles, and specific proteins, for example, in cellular quality control and under stress conditions [89]. ATG8 proteins play a major role during selective autophagy responses as they serve as a docking platform for selective autophagy adaptors and receptors that interact with ATG8 via an ATG8-interacting motif (AIM) or newly identified ubiquitin-interacting motif (UIM) [80].

view of one effector and one particular target protein and reintroduce the concept of ETPs. Based on this, we further emphasize the idea that the function of effectors targeting degradation machineries might have a broader impact on host cellular pathways and perturb the protein synthesis-transport-degradation triangle (Figure 1).

Hijacking the UPS: Degrade, Stabilize, and Suppress

During the past decade, an increasing number of studies reported that effector proteins from various phytopathogens target the host UPS to increase the pathogens' virulence. Recent reviews have reported numerous effectors manipulating the UPS and have highlighted its major role in the fate of plant–microbe interactions [9,13]. However, even though this cellular process is now considered as a key ETP during plant immunity, the purposes of its manipulation, its regulation, and possible effects on other pathways is still poorly understood. In this section, we describe some relevant examples of effectors targeting the UPS, classifying them based on their means of action in order to draw a proper view of their functionality, and the outcome of such manipulation on the plant's immune system. Based on their modes of action in manipulating the UPS system, we identified three major groups of effectors: degraders, stabilizers, and suppressors. Based on this new classification, we discuss the current understanding of this ETP, the contradictory aspects of recent findings, limitations of current approaches, and possible effects on other pathways.

The Degraders: How to Induce Host-specific Protein Degradation?

Initial findings in the effector biology field have been centered around effector molecules that degrade their targets by mimicking eukaryotic proteins. The effectors AvrPphB and AvrRpt2 were the first proteases found to cleave and degrade their targets – the PBS1 kinase and the enigmatic RIN4 protein – to activate the ETP [16]. Recently, AvrRpt2 was shown to employ the N-degron pathway to degrade host proteins from the nitrate-induced (NOI) domain family [17]. Later studies revealed that effector proteins directly hijack the UPS by displaying E3 ligase activity in order to

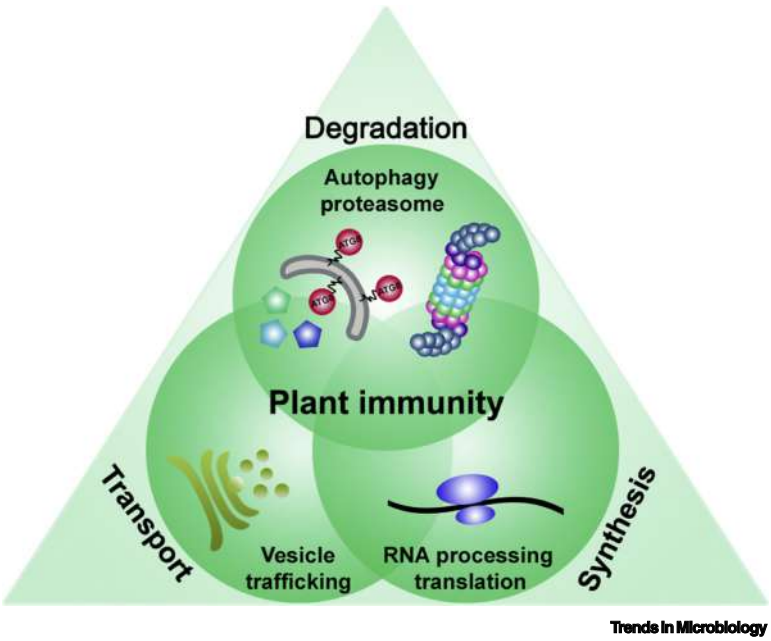

Figure 1. The Protein Synthesis-Transport-Degradation Triangle. Protein synthesis (including RNA processing and translation), transport, and degradation via proteasome and autophagy pathways are tightly interconnected processes targeted by diverse plant pathogens as they are implicated in plant immunity.

ubiquitinate targets and degrade it via the 26S proteasome [13]. The well characterized bacterial effector AvrPtoB was one of the first effectors to act as an E3 ligase in the plant cell, interacting with multiple host E2 enzymes, thus inducing the degradation of multiple host defense-related proteins such as CERK1, BAK1, FLS2, and the master regulator of salicylic signaling, NPR1 [18–22]. Other examples of effectors exhibiting E3 ligase activity can be found. Notably, some effectors harbor an F-box domain that functions within host SKP1-CULLIN-F-box (SCF) complexes. The GALA effector family from *Ralstonia solanacearum*, the *Xanthomonas campestris* effector XopI, and the *Agrobacterium tumefaciens* VirF effector were shown to act in SCF ligase complexes, the latter degrading host transcription factors to dampen defense responses [9,23,24]. However, the identification of known domains that unravel the potential function of effectors is a rare scenario. On the bright side, this brings the huge potential for the discovery of novel domains and features of effector proteins once their enzymatic function is characterized. The effector XopL from *Xanthomonas campestris* pv. *vesicatoria* (*Xcv*) is a perfect example of such a discovery as it contains a novel fold and thus represents a new class of E3 ligases with no structural homology to any known E3 ligase [25]. Even though mimicking E3 ligases or proteases seems to be the most direct way to induce host protein degradation, some effectors have evolved different mechanisms to exploit the host ubiquitination machinery. Indeed, effectors such as HopBB1 from *Pseudomonas syringae* or HaRxL44 from *Hyaloperonospora arabidopsidis* have been shown to interact and induce degradation of the transcription factors TCP14 and Med19a, respectively, probably acting as adaptors between the substrates and E3 ligases [26,27]. Other effectors alter post-translational modifications of host targets to trigger their degradation. For instance, HopZ1a from *P. syringae* acetylates JAZ1 to activate jasmonic acid (JA) signaling, and XopD from *Xcv* de-sumoylates tomato ERF4 to suppress the ethylene response. Both effectors destabilize their targets, thereby promoting pathogen growth [28,29]. Finally, another interesting mechanism has been reported for the phytoplasma effector SAP54 which can act as an adaptor between MADS-box transcription factors and the ubiquitin-binding proteins RAD23C and RAD23D. These proteins are known to shuttle substrates to the proteasome, and hence SAP54 exploits this interaction to induce target degradation via the 26S proteasome [30]. Because the bacterial effector HopM1 was shown to interact with RAD23, it is likely that HopM1 utilizes a similar mechanism to promote the proteasome-dependent degradation of AtMIN7, a host ADP ribosylation factor guanine nucleotide-exchange factor (ARF-GEF) [31].

The Stabilizers: How to Keep Host Proteins Away from Degradation?

Another strategy of pathogen effectors hijacking the proteasome system is to protect target proteins from degradation. For this purpose, multiple effectors have been reported to interfere with the host ubiquitination system. Viral effectors, such as β-C1 from *Cotton leaf curl multan virus,* or p25 from *Beet necrotic yellow vein virus*, can disturb the formation of SCF E3 ligase complexes and hence promote disease [32,33]. Other microbial effectors interact with plant E3 ligases and suppress their activity. For example, AvrPiz-t from *Magnaporthe oryzae* has been shown to inhibit E3 ligase activity of APIP6 by mediating its proteasomal degradation [34], while *Xanthomonas oryzae* pv. *oryzae* effector XopP suppresses E3 ligase activity of OsPUB44 via an unknown mechanism [35]. In contrast to this mechanism, *Phytophthora infestans* utilizes effector Avr3a to stabilize host E3 ligase CMPG1 for increased virulence [36]. As for the induction of target degradation, stabilization does not imply a direct action of the effectors on E3 ligases. Indeed, other effectors have been found to preserve their target from degradation by direct interaction. For instance, Tin2 from *Ustilago maydis,* is reported to interact with ZmTTK1 and masks its phospho-degron motif, thereby preventing its proteasomal degradation [37]. In a more direct approach, *Turnip yellow mosaic virus* (TYMV) evolved a specific ubiquitin hydrolase, TYMVpro, that contributes to viral infectivity [38]. In addition to ubiquitination, sumoylation of target proteins can affect the stability

of the modified protein [39]. The first evidence that pathogens target sumoylation was provided by the functional characterization of sumo protease XopD from *Xanthomonas campestris* [40]. Although $XopD_{Xcc8004}$ shares a high level of homology with $XopD_{Xcv}$ they possess opposing effects. $XopD_{Xcv}$ acts as a sumo protease to induce its substrate degradation, while $XopD_{Xcc8004}$ stabilizes the DELLA protein, RGA, interacting with it and inhibiting its gibberellic acid-induced proteasome-dependent degradation [41].

The Suppressors: How to Perturb Host Proteasome Complexes?

The most direct way to interfere with proteasome-dependent protein degradation is to target the proteasome complex itself. The bacterial toxin SylA from *P. syringae* was one of the first virulence factors found to directly bind to subunits of the 20S proteasome, and to act as an irreversible proteasome inhibitor [42,43]. It must be noted that SylA is not a classical microbial effector protein as it is a product of a mixed nonribosomal peptide/polypeptide synthetase [42]. As well as those of bacteria, viral effectors are also known to directly target the host proteasome complex. The RNA silencing suppressor HCPro from various potyviruses, is able to interact with different 20S core particle proteasome subunits, and to inhibit proteasome activity [44,45]. As the 20S protease complex shows RNAse activity, HCPro acts as a silencing suppressor via the 20S proteasome [46]. The first bacterial effectors identified as directly targeting the proteasome were XopJ from *Xcv*, and the closely related HopZ4 from *P. syringae* pv. *lachrymans*. Both effectors dampen proteasome activity by interaction with the proteasome subunit RPT6 [47–49]. A systematic screen of the effector repertoire of the model organism *P. syringae* pv. *tomato* DC3000 (*Pst*) revealed multiple effectors acting as putative inhibitors of the proteasome [50] and blocking SA signaling. Notably, the effector protein HopM1 was found to be the most potent proteasome inactivator, associating with proteasome subunits, E3 ligases, and other UPS-related components *in vivo* [50] (Table S1 in the supplemental information online). It is interesting to note that HopM1, in addition to its inhibitor function, is also a 'degrader', mediating the proteasome-dependent degradation of the ARF-GEF protein, AtMIN7 (see 'degraders' in the previous section).

As we reported in the first section, many effectors manipulate the UPS to degrade or stabilize host target proteins. This function implies that there are functional proteasome complexes in the host cells. However, recent advances have shown that pathogens can also induce inhibition of these complexes during infection. For instance, effectors with E3 ligase activity require a functional proteasome to degrade their targets. However, even though ubiquitination is well characterized as post-translational modification, leading to target degradation via the 26S proteasome, its role in cellular pathways is much more diverse [51]. Many studies elucidating E3 ligase effectors concentrate on the proteasome pathway, neglecting the fact that the ubiquitin code defined by various ubiquitin linkage types results in different target fates [51]. For instance, effector protein AvrPtoB degrades Fen kinase via the proteasome [52] while it stimulates degradation of CERK1 through vacuolar degradation [20]. Novel insights into E2–E3 pairings showed that bacterial effector AvrPtoB interacts with distinct E2 ligases to mediate substrate ubiquitination, which may explain the involvement of different degradation pathways [53,54]. Unraveling the possible linkage types created by these specific E2–E3 ligase pairs is required to determine the fate of the host target. All in all, this aspect highlights the point that effectors showing E3 ligase properties should be also considered as potentially modulating target activity, rather than inducing target degradation. Therefore, systematic analysis of ubiquitin chain types might help to elucidate the function of E3 ligase effectors on a potential host target.

Intriguingly, while manipulating the host ubiquitin system should permit action on specific targets, inhibiting proteasome complexes appears to impact the host cell at a broader level and hence

seems to be contradictory to the action of pathogens that induce host protein degradation during infection. However, thinking on a broader scale, and looking at plant–microbe interaction as a highly dynamic molecular exchange, all results reported previously might fit into a single model. Indeed, the effectors are known to act within different locations in the host cell, as well as the host UPS, and can be delivered at different time points by the pathogens during infection. It is therefore essential to study the compartmentalization of effector action as well as host UPS functions. How do plasma membrane-localized effectors degrade their host targets or suppress proteasome function while the proteasome is diffusely spread throughout both the cytoplasm and the nucleus [55]? Therefore, we hypothesize that the localization of the proteasome is highly dynamic during plant–microbe interaction. For instance, during neurodegenerative diseases, proteasomes are recruited to inclusion bodies [56]. Proteasomes were also shown to be tethered to the ER membrane as part of their role in endoplasmic-reticulum-associated degradation (ERAD) [57]. Recently, a plasma membrane-localized form of the 20S core particle (CP) of the proteasome was described in mammalian neurons, exclusively degrading ribosome-associated nascent polypeptides [57,58]. These examples display how dynamically proteasome localization changes under different stress conditions. Whether such dynamic changes occur during pathogen infection, and how this will impact the function of effectors, has to be studied in the future to solve the contradictory actions of effectors. This is why we propose to change our approaches, looking at the UPS as a highly dynamic pathway acting at several time points, and in several cell compartments. To investigate these questions we suggest looking at the behavior of the effectors according to the kinetics of infection, utilizing techniques such as single-cell RNA sequencing [59], or cell-type-specific CRISPR/Cas9 [60] in order to get a proper view on the effectors' dynamic action on the host UPS during infection. These broader approaches might permit us to finally put all our current knowledge into a single model of how pathogens impact the host UPS.

Autophagy, a Target of a Wide Array of Effectors

In addition to the proteasome, autophagy is another major degradation process, recently emerging as one of the most exciting topics in protein homeostasis research in plants. Over the past few years many efforts have been made to unravel how autophagy functions on a molecular level, and which processes are tightly associated with this degradation mechanism. This has created a surge in activity to identify pathogens and their molecular weapons targeting this process in order to understand the role of autophagy in plant immunity. Utilization of these microbial effectors to study autophagy is a perfect example of how we can mechanistically reveal the role of autophagy components not only in plant defense but also in other cellular pathways.

Autophagy Inhibitors: How to Escape Xenophagy in Plants

Viral pathogens have developed an array of functions in order to mediate autophagic responses in the host cell, so as to prevent the degradation of viral components. The *Barley stripe mosaic virus* (BSMV) γb protein was shown to target autophagy components in order to alter function. Indeed, Yang *et al*. have shown that γb disrupts the ATG8-ATG7 interaction, essential for ATG8 lipidation [61]. The disruption of autophagy by viral proteins goes hand in hand with the use of autophagy by the host cell to target viral proteins or particles for degradation. The selective autophagy adapter NBR1 has been identified as playing a predominant role in the targeting of viral components for degradation. For example, *Cauliflower mosaic virus* (CaMV) capsid and P4 proteins have been shown to be targeted by NBR1, as well as the *Turnip mosaic virus* (TuMV) HCPro [62,63]. These examples highlight the power of using effectors as tools to unravel novel functions of the autophagy pathway. Before these findings, understanding of the functions of NBR1 remained restricted to its ability to degrade aggregated proteins during heat stress [64], and were largely not understood. TuMV protein, VPg, and 6K2 have also been shown to block NBR1-mediated degradation of HCPro [62]. The importance of having autophagy inhibitors or

limiters for intracellular pathogens clearly appears when considering the use of the autophagy pathway as a bona fide major player in the plant cell's immune system. The plant cell appears to have a number of factors, in addition to NBR1, promoting the targeting of foreign intracellular compounds. Plant autophagy machinery in *Nicotiana benthamiana* has been shown to target the β-C1 protein of the *Cotton leaf curl multan virus* (CLCuMuV) via its interaction with NbATG8f [65]. Another autophagy core component targeting viral factors is ATG6. This component mediates the degradation of a TuMV RNA-dependent RNA polymerase called Nib [66].

Autophagy also appears to be suppressed by necrotrophic pathogens in the triggering of disease [12]. Central autophagy components were shown to be essential in limiting the systemic spread of necrotic lesions during infection by the necrotrophic pathogen *Alternaria brassicicola* [67]. The importance of autophagy for resistance to necrotrophic pathogens has also been demonstrated by Li *et al*. [68], whereby BCL-2-associated athanogene 6 (BAG6) cleavage is necessary for autophagy induction, resulting in the resistance of *A. thaliana* to *Botrytis cinerea*. Although no effectors from necrotrophic pathogens have yet been identified as perturbing the autophagy pathway, the converging evidence showing the participation of the host's autophagic machinery in resistance suggests the existence of effectors targeting this pathway, in these pathogens. Necrotrophic pathogens appear to immensely gain in terms of virulence in the absence of a functioning autophagy pathway in their hosts [69]. Therefore, it is reasonable to hypothesize that they could potentially possess effectors that would target this pathway. This untapped potential of biological tools for the dissection of the plant autophagy pathway is hugely promising and should be further explored.

Autophagy Hijackers: Pathogens Exploit Autophagic Components for Their Own Good

RNA plant viruses have a strong interest in limiting the activity of their host's RNA-silencing machinery in order to promote viral particle accumulation. Certain viruses have been shown to hijack their host's autophagic pathway in order to perturb RNA-silencing factors. For example, VPg of the *Turnip mosaic virus* (TuMV) has been identified as interacting with host RNA-silencing-associated factors, such as suppressor of gene-silencing 3 (SGS3), and RNA-dependent RNA polymerase 6 (RDR6), to induce their degradation [70]. The VPg-associated degradation of the two latter factors was shown to be limited by proteolysis-inhibiting drugs such as MG132 and 3-MA, thereby demonstrating the implication of the 20S proteasome and the autophagic pathway, respectively, in the degradation of the host factors [70]. Targeting the degradation of the RNA-silencing-associated host factor Argonaute 1 (AGO1) by the polerovirus protein P0 is also mediated by the autophagy pathway [71,72]. A very direct way to hijack the autophagy machinery was developed by *P. infestans.* Here, the oomycete evolved the effector PexRD54 which mimics a selective autophagy adaptor to outcompete selective the autophagy adapter, JOKA2 (ortholog of NBR1), to increase susceptibility [73]. Later studies revealed that this antagonistic interaction takes place at the host–pathogen interface [74]. For certain pathogens, the activation or enhancement of autophagic flux appears to play a role in their infection strategy. In plant–bacteria interactions, *Pst* activates autophagy and enhances the autophagic turnover of the proteasome megacomplex (proteaphagy) in the model plant *A. thaliana* for the benefit of infection [75]. *Pst* activates autophagy via the action of the type III effector (T3E), HopM1, which triggers proteaphagy in *A. thaliana* [75]. In contrast to this probacterial effect, the NBR1-mediated selective autophagy pathway is activated during infection to counteract HopM1-dependent disease progression [76]. This is another example of how pathogens subvert the immunity function of autophagy in the host–pathogen arms race.

Increasing research on the autophagy pathway and the discovery of selective autophagy receptors created a boom in the study of the role of autophagy in plant immunity. For years it was believed

that autophagy was a central player in ETI-associated cell death. However, recent research has demonstrated that pathogens target autophagy to impair host cellular pathways in plants, or to escape their own elimination. One major theme that occurs in the interaction of plants and microbes is the contrast of effects on, and of, the autophagy pathway [11]. Many pathogens seem to activate autophagy and also the NBR1-dependent selective autophagy pathway. Given the role of NBR1 in degrading viral proteins or suppressing HopM1-dependent water-soaking and lesion formation [62,73,75] it is not surprising that pathogens have developed means to block this pathway. Intriguingly, for *Pst,* it remains still elusive how the pathogen would overcome the effect of NBR1. On the one hand, it might be that overall autophagy, including the proteaphagy pathway, overrules the NBR1-mediated suppression of disease progression. On the other hand, the proteasome might not be the only target degraded by *Pst*-triggered autophagy. This could explain how NBR1 function is neutralized. Nevertheless, it still remains enigmatic why pathogens would activate autophagy if it is also a central player in plant immunity. One possible explanation might be that there are different selective autophagy pathways involved during plant–microbe interaction and hence inactivating the whole autophagy machinery might not be beneficial for pathogens. It appears that pathogen-triggered autophagy suppresses disease-associated senescence, thereby prolonging the lifespan of viruses as well as bacterial pathogens [63,75]. This is also consistent with previous findings that plants with constitutively activated autophagy display increased fitness [77]. Given the classical role of autophagy as a housekeeper and recycler, it is also possible that either autophagy is activated by pathogens to obtain nutrients or infection creates a starvation response which would force the host cell to induce autophagy.

However, it might still be difficult to discriminate whether autophagy was first formalized as a defense function, later hijacked by microbes, or whether pathogens modulate its function directly, in a specific manner. Direct roles of microbial or parasitic effectors in autophagy are limited to *Phytophthora* PexRD54 [72], the animal pathogenic bacterium *Legionella*, which delivers RavZ effector to inhibit lipidation of ATG8 [78], or *Plasmodium* UIS3, which sequesters host LC3 to block autophagy [79]. Consequently, there must be an effort to identify more effectors directly targeting the autophagy pathway to mechanistically understand how autophagy is modulated. Even though it is now well established that autophagy is modulated by microbes, we are still far from identifying and understanding the degradation landscape (the 'degradome'). Over the past few years, many selective autophagy adaptors have been identified in plants [80], while the specific targets they recognize, and eventually degrade, have not. New techniques, such as TurboID [81], cell-type specific systems for modulation of protein degradation, and a focus on the possible functional specialization of degradation signals such as ATG8 isoforms, might help us to decipher the degradome.

Is the Targeting of Protein Degradation Pathways a Strategy to Force the Interplay between Different Cellular Pathways?

For years, research has concentrated on single immune components, such as surface-localized receptors, and resistance genes that are integral parts of plant immunity. Effectors have long been studied in regard to their direct interactions with these single immune components and in regard to their partial molecular activities on host components. These approaches, while essential to understanding the molecular functions of effectors, have nevertheless left us unable to ultimately grasp the host's complex molecular signaling feedback mechanisms that may alter the final effects of a given effector, and/or of the synergistic effects of effectors acting in conjunction with each other. What is becoming more and more evident is that the host's cellular machinery is finely regulated by complex crosstalk and feedback loops between different organelles and molecular pathways (e.g., the proteasome/autophagy-secretion-translation) and perturbing one of these elements will likely have an impact on the others. To visualize how effectors mediate

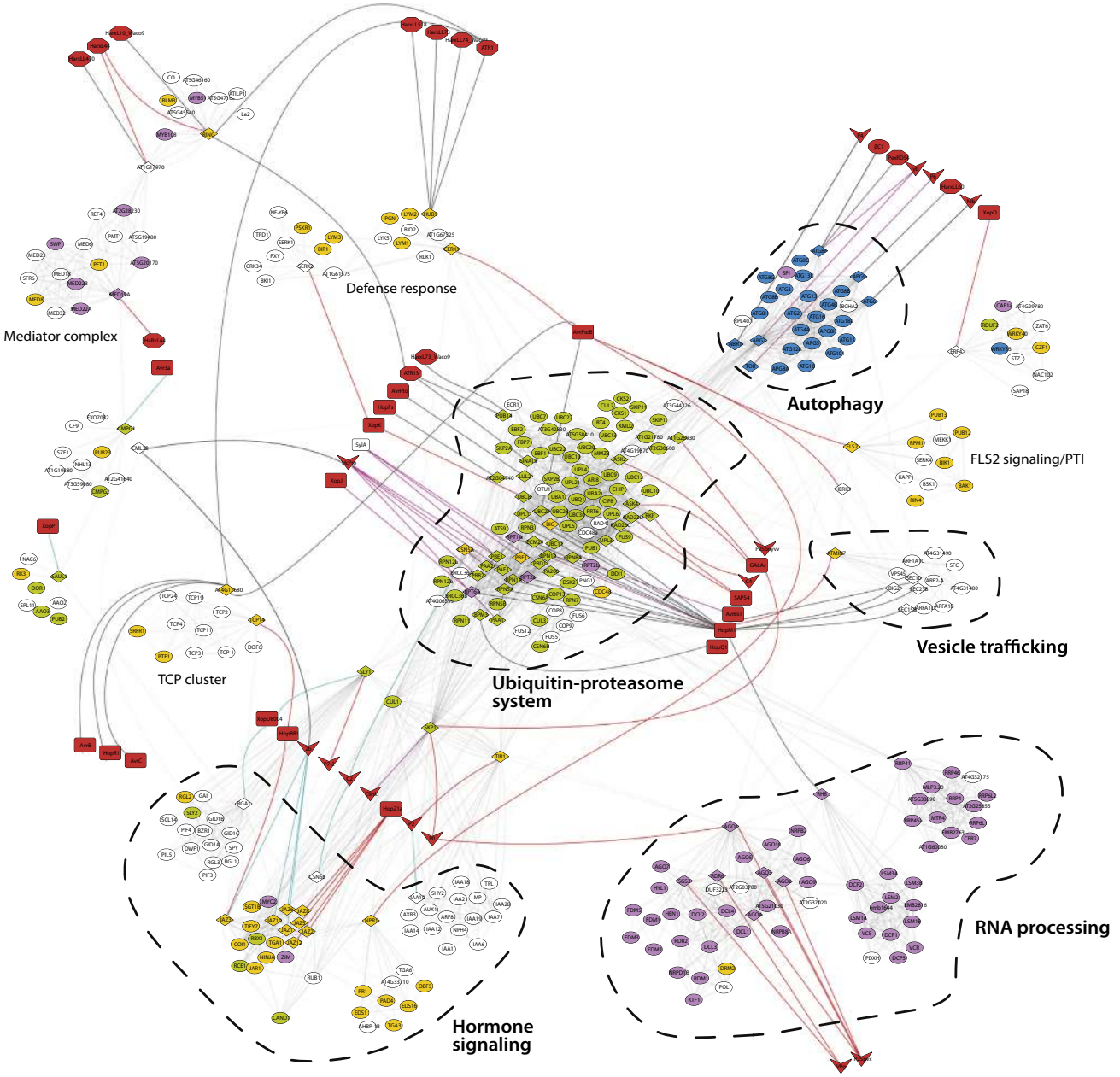

(See figure legend at the bottom of the next page.)

possible crosstalk between different ETPs we generated a network of effectors targeting proteolytic degradation pathways based on existing interactions (Table S1 in the supplemental information online) and coexpression data using the STRING database [82] (Figure 2). It must be noted that the modeling of the network is based on the *A. thaliana* database; thus, some effector targets are not represented because no relevant homologs could be found. The network analysis revealed that, in addition to the proteasome and autophagy pathways, we obtained other clusters including hormone-associated pathways, vesicle trafficking, and components of RNA processing and/or translation (e.g., P-bodies), tightly connected to the protein degradation pathways. As the UPS is linked to the regulation of phytohormone signaling, and effectors target this process to subvert hormone responses [83], it is not surprising to find salicylic acid- and jasmonic-acid-hormone-associated clusters in our network. Moreover, as previously described, there is a huge interplay between autophagy and the proteasome pathway [75]. The identification of the *Pst* effector HopM1 triggering this connection opened up the possibility that we have many other 'hidden' effectors, such as XopJ or SylA, here in the network, and that these might induce the proteaphagy/autophagy pathway. In future, it might also be interesting to test how effectors modulating autophagy (especially viral effectors) might impact the proteasome pathway, as there might be compensatory effects on the degradation pathways.

Given the endomembrane localization and role of HopM1 to mediate the degradation/and or interaction with components of the secretory pathway [31,50], HopM1 might mediate the crosstalk between proteasome, autophagy, and endomembrane pathways. In the network, the secretory pathway is tightly linked to the autophagy and proteasome cluster (Figure 2). Indeed, increasing evidence points to a link between the endomembrane and autophagy systems [84]. HopM1 is targeted to the *trans*-Golgi-network/early endosomes (TGN/EE), and triggers the proteasome-dependent degradation of AtMIN7, a TGN/EE-localized ADP ribosylation factor–guanine nucleotide exchange factor involved in vesicle trafficking [31]. Although not shown, it is believed that HopM1-induced degradation of AtMIN7 impairs secretion and endocytic recycling to dampen plant immunity. Taking into account the new finding that HopM1 suppresses proteasome activity by inducing autophagy [75], it will be intriguing to identify the mechanism of how HopM1 activates autophagy. It is tempting to speculate that HopM1 triggers autophagy activation via AtMIN7 at the trans-golgi-network (TGN). Could a loss of a TGN component and impaired vesicle trafficking lead to enhanced autophagic turnover? In animals, components of the secretory pathway, such as syntaxins, have been described to participate in the autophagy pathway [85,86]. Thus, it is possible that HopM1 interaction partners localized in the endomembrane system function in the autophagy pathway.

Intriguingly, we can also detect overlaps with both degradation pathways and RNA processing, suggesting that effectors acting on protein degradation might impact directly or indirectly these pathways (Figure 2). A recent study revealed how a proteasome subunit is implicated in post-transcriptional gene silencing (PTGS) by interaction with RNA quality components (RCQ), repressing their function [87]. Looking at the network, and considering the newly established link between the proteasome and PTGS/RQC, it is conceivable that certain effectors targeting the proteasome affect PTGS or RNA quality control. Impacting RNA processing will also likely

Figure 2. Protein Interaction Network Representing Microbial Effectors Targeting Protein Degradation Pathways. An interaction and coexpression map of plant proteins involved in protein degradation targeted by effectors targets. The proteins have been selected based on the literature and implemented in the STRING database. This first network has been kept as the core network. Ten additional interactors have been extracted from the STRING database for proteins being not part of a cluster. All the tables extracted (the 'core' network and all the ten additional interactors) have been merged to build the network using Cytoscape. Gene ontology enrichment on biological processes has been performed on all the proteins, and only the annotation related to the ubiquitin-proteasome system (UPS), autophagy, defense response, or RNA processing is shown. The classification of major functional pathways is highlighted. The strength of interaction between plant proteins is indicated by the transparency level of the lines (greater transparency indicates weaker association). The four major targeted pathways are enclosed by dashed lines. See Table S1 in the supplemental information online for the full list of interactors.

influence protein translation, as mRNA translation is stalled in RNA processing bodies [88]. This might be another example of how the very same effector, by interfering with one pathway, affects other cellular processes.

Concluding Remarks

Overall, this network, based on known interactors of the UPS and autophagy pathway targeting effectors, emphasizes the idea that effectors might have a broader impact on host cellular pathways, and a better understanding of effector biology will necessarily have to take into account the illustrated crosstalk in Figure 1. It is therefore necessary to look beyond the classical one-to-one pairing of effectors and target proteins and/or pathways. We are suggesting the idea that effectors targeting plant proteostasis will have a broader impact on the host cell. Suppressing or activating distinct degradation machineries will have an impact on other cellular machineries such as protein transport and/or translation, and we therefore propose a model in which effector proteins affect the triangle model of protein synthesis, transport, and degradation (Figure 1). It is by deciphering and taking into account the relationships between host-regulated pathways – such as proteasomal-activation and proteasome-associated protein degradation, autophagic flux, and protein trafficking pathways – that we will decrypt the interactive effects of pathogen-associated effectors on the host cell. This will be the next level of effector biology and will require implementing systems biology approaches to understand the complexity of the potential crosstalk and networks (see Outstanding Questions).

Outstanding Questions

What is the pathogen-induced or repressed 'degradome' during plant–microbe interactions?

How does the impact on proteolytic degradation change if we look beyond binary interactions?

How do effectors from one pathogen with contrasting functions work together to manipulate the very same process?

Are there nondegradative roles of E3 ligase effector proteins based on the ubiquitin code?

What are the localization dynamics of the proteasome during plant–microbe interactions?

How much do cell-type-specific immune responses and effector delivery change the impact on the autophagy and proteasome pathways?

How do pathogens manipulating one pathway of the protein synthesis-transport-degradation triangle influence the other ones?

Acknowledgments

We apologize to the authors whose work we were not able to cite due to space constraints. We thank Tom Denyer for critical reading of the manuscript, discussions, and comments. This work was supported by an Emmy Noether Fellowship GZ: UE 188/2-1 from the Deutsche Forschungsgemeinschaft (DFG) and through the Collaborative Research Council 1101 (SFB1101).

Supplemental Information

Supplemental information associated with this article can be found online at https://doi.org/10.1016/j.tim.2020.02.010.

References

1. Jones, J.D. and Dangl, J.L. (2006) The plant immune system. *Nature* 444, 323–329
2. Pritchard, L. and Birch, P.R. (2014) The zigzag model of plant-microbe interactions: is it time to move on? *Mol. Plant Pathol.* 15, 865–870
3. Couto, D. and Zipfel, C. (2016) Regulation of pattern recognition receptor signalling in plants. *Nat. Rev. Immunol.* 16, 537–552
4. Albert, I. *et al.* (2019) Surface sensor systems in plant immunity. *Plant Physiol.* Published online December 10, 2019. http://doi.org/10.1104/pp.19.01299
5. Khan, M. *et al.* (2016) Of guards, decoys, baits and traps: pathogen perception in plants by type III effector sensors. *Curr. Opin. Microbiol.* 29, 49–55
6. Win, J. *et al.* (2012) Effector biology of plant-associated organisms: concepts and perspectives. *Cold Spring Harb. Symp. Quant. Biol.* 77, 235–247
7. Mukhtar, M.S. *et al.* (2011) Independently evolved virulence effectors converge onto hubs in a plant immune system network. *Science* 333, 596–601
8. Wessling, R. *et al.* (2014) Convergent targeting of a common host protein-network by pathogen effectors from three kingdoms of life. *Cell Host Microbe* 16, 364–375
9. Üstün, S. and Börnke, F. (2014) Interactions of *Xanthomonas* type-III effector proteins with the plant ubiquitin and ubiquitin-like pathways. *Front. Plant Sci.* 5, 736
10. González-Fuente, M. *et al.* (2019) EffectorK, a comprehensive resource to mine for pathogen effector targets in the *Arabidopsis* proteome. *bioRxiv*. Published online December 16, 2019. https://doi.org/10.1101/2019.12.16.878074
11. Leary, A.Y. *et al.* (2019) Contrasting and emerging roles of autophagy in plant immunity. *Curr. Opin. Plant Biol.* 52, 46–53
12. Üstün, S. *et al.* (2017) Autophagy as a mediator of life and death in plants. *Curr. Opin. Plant Biol.* 40, 122–130
13. Banfield, M.J. (2015) Perturbation of host ubiquitin systems by plant pathogen/pest effector proteins. *Cell. Microbiol.* 17, 18–25
14. Vierstra, R.D. (2009) The ubiquitin-26S proteasome system at the nexus of plant biology. *Nat. Rev. Mol. Cell Biol.* 10, 385–397
15. Marshall, R.S. and Vierstra, R.D. (2018) Autophagy: The master of bulk and selective recycling. *Annu. Rev. Plant Biol.* 69, 173–208
16. Chisholm, S.T. *et al.* (2005) Molecular characterization of proteolytic cleavage sites of the *Pseudomonas syringae* effector AvrRpt2. *Proc. Natl. Acad. Sci. U. S. A.* 102, 2087–2092
17. Goslin, K. *et al.* (2019) Differential N-end rule degradation of RIN4/NOI fragments generated by the AvrRpt2 effector protease. *Plant Physiol.* 180, 2272–2289
18. Abramovitch, R.B. *et al.* (2006) Type III effector AvrPtoB requires intrinsic E3 ubiquitin ligase activity to suppress plant cell death and immunity. *Proc. Natl. Acad. Sci. U. S. A.* 103, 2851–2856
19. Chen, H. *et al.* (2017) A bacterial type III effector targets the master regulator of salicylic acid signaling, NPR1, to subvert plant immunity. *Cell Host Microbe* 22, e7
20. Gimenez-Ibanez, S. *et al.* (2009) AvrPtoB targets the LysM receptor kinase CERK1 to promote bacterial virulence on plants. *Curr. Biol.* 19, 423–429
21. Gohre, V. *et al.* (2008) Plant pattern-recognition receptor FLS2 is directed for degradation by the bacterial ubiquitin ligase AvrPtoB. *Curr. Biol.* 18, 1824–1832
22. Cheng, W. *et al.* (2011) Structural analysis of *Pseudomonas syringae* AvrPtoB bound to host BAK1 reveals two similar kinase-interacting domains in a type III Effector. *Cell Host Microbe* 10, 616–626

23. Lacroix, B. and Citovsky, V. (2015) Nopaline-type Ti plasmid of *Agrobacterium* encodes a VirF-like functional F-box protein. *Sci. Rep.* 5, 16610
24. Remigi, P. *et al.* (2011) Functional diversification of the GALA type III effector family contributes to *Ralstonia solanacearum* adaptation on different plant hosts. *New Phytol.* 192, 976–987
25. Singer, A.U. *et al.* (2013) A pathogen type III effector with a novel E3 ubiquitin ligase architecture. *PLoS Pathog.* 9, e1003121
26. Caillaud, M.C. *et al.* (2012) Characterization of the membraneas-sociated HaRxL17 Hpa effector candidate. *Plant Signal. Behav.* 7, 145–149
27. Yang, L. *et al.* (2017) *Pseudomonas syringae* type III effector HopBB1 promotes host transcriptional repressor degradation to regulate phytohormone responses and virulence. *Cell Host Microbe* 21, 156–168
28. Jiang, S. *et al.* (2013) Bacterial effector activates jasmonate signaling by directly targeting JAZ transcriptional repressors. *PLoS Pathog.* 9, e1003715
29. Kim, J.G. *et al.* (2013) *Xanthomonas* type III effector XopD desumoylates tomato transcription factor SlERF4 to suppress ethylene responses and promote pathogen growth. *Cell Host Microbe* 13, 143–154
30. MacLean, A.M. *et al.* (2014) Phytoplasma effector SAP54 hijacks plant reproduction by degrading MADS-box proteins and promotes insect colonization in a RAD23-dependent manner. *PLoS Biol.* 12, e1001835
31. Nomura, K. *et al.* (2006) A bacterial virulence protein suppresses host innate immunity to cause plant disease. *Science* 313 220–203
32. Thiel, H. *et al.* (2012) The P25 pathogenicity factor of Beet necrotic yellow vein virus targets the sugar beet 26S proteasome involved in the induction of a hypersensitive resistance response via interaction with an F-box protein. *Mol. Plant-Microbe Interact.* 25, 1058–1072
33. Jia, Q. *et al.* (2016) CLCuMuB betaC1 subverts ubiquitination by interacting with NbSKP1s to enhance geminivirus infection in *Nicotiana benthamiana*. *PLoS Pathog.* 12, e1005668
34. Park, C.H. *et al.* (2012) The *Magnaporthe oryzae* effector AvrPiz-t targets the RING E3 ubiquitin ligase APIP6 to suppress pathogen-associated molecular pattern-triggered immunity in rice. *Plant Cell* 24, 4748–4762
35. Ishikawa, K. *et al.* (2014) Bacterial effector modulation of host E3 ligase activity suppresses PAMP-triggered immunity in rice. *Nat. Commun.* 5, 5430
36. Bos, J.I. *et al.* (2010) *Phytophthora infestans* effector AVR3a is essential for virulence and manipulates plant immunity by stabilizing host E3 ligase CMPG1. *Proc. Natl. Acad. Sci. U. S. A.* 107, 9909–9914
37. Tanaka, S. *et al.* (2014) A secreted *Ustilago maydis* effector promotes virulence by targeting anthocyanin biosynthesis in maize. *eLife* 3, e01355
38. Lombardi, C. *et al.* (2013) A compact viral processing proteinase/ ubiquitin hydrolase from the OTU family. *PLoS Pathog.* 9, e1003560
39. Vierstra, R.D. (2012) The expanding universe of ubiquitin and ubiquitin-like modifiers. *Plant Physiol.* 160, 2–14
40. Hotson, A. *et al.* (2003) *Xanthomonas* type III effector XopD targets SUMO-conjugated proteins in planta. *Mol. Microbiol.* 50, 377–389
41. Tan, L. *et al.* (2014) The *Xanthomonas campestris* effector protein XopDXcc8004 triggers plant disease tolerance by targeting DELLA proteins. *New Phytol.* 204, 595–608
42. Groll, M. *et al.* (2008) A plant pathogen virulence factor inhibits the eukaryotic proteasome by a novel mechanism. *Nature* 452, 755–758
43. Misas-Villamil, J.C. *et al.* (2013) *Pseudomonas syringae* pv. *syringae* uses proteasome inhibitor syringolin A to colonize from wound infection sites. *PLoS Pathog.* 9, e1003281
44. Jin, Y. *et al.* (2007) HC-Pro protein of potato virus Y can interact with three *Arabidopsis* 20S proteasome subunits in planta. *J. Virol.* 81, 12881–12888
45. Sahana, N. *et al.* (2012) Inhibition of the host proteasome facilitates papaya ringspot virus accumulation and proteosomal catalytic activity is modulated by viral factor HcPro. *PLoS One* 7, e52546
46. Ballut, L. *et al.* (2005) HcPro, a multifunctional protein encoded by a plant RNA virus, targets the 20S proteasome and affects its enzymic activities. *J. Gen. Virol.* 86, 2595–2603
47. Üstün, S. *et al.* (2013) The *Xanthomonas campestris* type III effector XopJ targets the host cell proteasome to suppress salicylic-acid mediated plant defence. *PLoS Pathog.* 9, e1003427
48. Üstün, S. and Börnke, F. (2015) The *Xanthomonas campestris* type III effector XopJ proteolytically degrades proteasome subunit RPT6. *Plant Physiol.* 168, 107–119
49. Üstün, S. *et al.* (2014) HopZ4 from *Pseudomonas syringae*, a member of the HopZ type III effector family from the YopJ superfamily, inhibits the proteasome in plants. *Mol. Plant-Microbe Interact.* 27, 611–623
50. Üstün, S. *et al.* (2016) The proteasome acts as a hub for plant immunity and is targeted by *Pseudomonas* type III effectors. *Plant Physiol.* 172, 1941–1958
51. Kwon, Y.T. and Ciechanover, A. (2017) The ubiquitin code in the ubiquitin-proteasome system and autophagy. *Trends Biochem. Sci.* 42, 873–886
52. Rosebrock, T.R. *et al.* (2007) A bacterial E3 ubiquitin ligase targets a host protein kinase to disrupt plant immunity. *Nature* 448, 370–374
53. Kowarschik, K. *et al.* (2018) UbiGate: a synthetic biology toolbox to analyse ubiquitination. *New Phytol.* 217, 1749–1763
54. Turek, I. *et al.* (2018) Multi-tiered pairing selectivity between E2 ubiquitin-conjugating enzymes and E3 ligases. *J. Biol. Chem.* 293, 16324–16336
55. Marshall, R.S. and Vierstra, R.D. (2019) Dynamic regulation of the 26S proteasome: from synthesis to degradation. *Front. Mol. Biosci.* 6, 40
56. Livneh, I. *et al.* (2016) The life cycle of the 26S proteasome: from birth, through regulation and function, and onto its death. *Cell Res.* 26, 869–885
57. Ramachandran, K.V. *et al.* (2018) Activity-dependent degradation of the nascentome by the neuronal membrane proteasome. *Mol. Cell* 71, e6
58. Ramachandran, K.V. and Margolis, S.S. (2017) A mammalian nervous-system-specific plasma membrane proteasome complex that modulates neuronal function. *Nat. Struct. Mol. Biol.* 24, 419–430
59. Denyer, T. *et al.* (2019) Spatiotemporal developmental trajectories in the *Arabidopsis* root revealed using high-throughput single-cell RNA sequencing. *Dev. Cell* 48, e5
60. Decaestecker, W. *et al.* (2019) CRISPR-TSKO: A technique for efficient mutagenesis in specific cell types, tissues, or organs in *Arabidopsis*. *Plant Cell* 31, 2868–2887
61. Yang, M. *et al.* (2018) Barley stripe mosaic virus gammab protein subverts autophagy to promote viral infection by disrupting the ATG7–ATG8 interaction. *Plant Cell* 30, 1582–1595
62. Hafren, A. *et al.* (2018) Turnip mosaic virus counteracts selective autophagy of the viral silencing suppressor HCpro. *Plant Physiol.* 176, 649–662
63. Hafren, A. *et al.* (2017) Selective autophagy limits cauliflower mosaic virus infection by NBR1-mediated targeting of viral capsid protein and particles. *Proc. Natl. Acad. Sci. U. S. A.* 114, E2026–E2035
64. Zhou, J. *et al.* (2013) NBR1-mediated selective autophagy targets insoluble ubiquitinated protein aggregates in plant stress responses. *PLoS Genet.* 9, e1003196
65. Haxim, Y. *et al.* (2017) Autophagy functions as an antiviral mechanism against geminiviruses in plants. *eLife* 6, e23897
66. Li, F. *et al.* (2018) Beclin1 restricts RNA virus infection in plants through suppression and degradation of the viral polymerase. *Nat. Commun.* 9, 1268
67. Lenz, H.D. *et al.* (2011) Autophagy differentially controls plant basal immunity to biotrophic and necrotrophic pathogens. *Plant J.* 66, 818–830
68. Li, Y. *et al.* (2016) Aspartyl protease-mediated cleavage of BAG6 is necessary for autophagy and fungal resistance in plants. *Plant Cell* 28, 233–247
69. Kabbage, M. *et al.* (2013) Cell death control: the interplay of apoptosis and autophagy in the pathogenicity of *Sclerotinia sclerotiorum*. *PLoS Pathog.* 9, e1003287

70. Cheng, X. and Wang, A. (2017) The potyvirus silencing suppressor protein VPg mediates degradation of SGS3 via ubiquitination and autophagy pathways. *J. Virol.* 91, e01478-16
71. Derrien, B. *et al.* (2012) Degradation of the antiviral component ARGONAUTE1 by the autophagy pathway. *Proc. Natl. Acad. Sci. U. S. A.* 109, 15942–15946
72. Michaeli, S. *et al.* (2019) The viral F-box protein P0 induces an ER-derived autophagy degradation pathway for the clearance of membrane-bound AGO1. *Proc. Natl. Acad. Sci. U. S. A.* 116, 22872–22883
73. Dagdas, Y.F. *et al.* (2016) An effector of the Irish potato famine pathogen antagonizes a host autophagy cargo receptor. *eLife* 5, e10856
74. Dagdas, Y.F. *et al.* (2018) Host autophagy machinery is diverted to the pathogen interface to mediate focal defense responses against the Irish potato famine pathogen. *eLife* 7, e37476
75. Üstün, S. *et al.* (2018) Bacteria exploit autophagy for proteasome degradation and enhanced virulence in plants. *Plant Cell* 30, 668–685
76. Üstün, S. and Hofius, D. (2018) Anti- and pro-microbial roles of autophagy in plant-bacteria interactions. *Autophagy* 14, 1465–1466
77. Minina, E.A. *et al.* (2018) Transcriptional stimulation of rate-limiting components of the autophagic pathway improves plant fitness. *J. Exp. Bot.* 69, 1415–1432
78. Choy, A. *et al.* (2012) The *Legionella* effector RavZ inhibits host autophagy through irreversible Atg8 deconjugation. *Science* 338, 1072–1076
79. Real, E. *et al.* (2018) *Plasmodium* UIS3 sequesters host LC3 to avoid elimination by autophagy in hepatocytes. *Nat. Microbiol.* 3, 17–25
80. Marshall, R.S. *et al.* (2019) ATG8-binding UIM proteins define a new class of autophagy adaptors and receptors. *Cell* 177, e24
81. Zhang, Y. *et al.* (2019) TurboID-based proximity labeling reveals that UBR7 is a regulator of N NLR immune receptor-mediated immunity. *Nat. Commun.* 10, 3252
82. Jensen, L.J. *et al.* (2009) STRING 8 – a global view on proteins and their functional interactions in 630 organisms. *Nucleic Acids Res.* 37, D412–D416
83. Kazan, K. and Lyons, R. (2014) Intervention of phytohormone pathways by pathogen effectors. *Plant Cell* 26, 2285–2309
84. Zeng, Y. *et al.* (2019) The interplay between endomembranes and autophagy in plants. *Curr. Opin. Plant Biol.* 52, 14–22
85. Mizushima, N. *et al.* (2019) YKT6 as a second SNARE protein of mammalian autophagosomes. *Autophagy* 15, 176–177
86. Kumar, S. *et al.* (2019) Phosphorylation of syntaxin 17 by TBK1 controls autophagy initiation. *Dev. Cell* 49, e6
87. Kim, M.H. *et al.* (2019) Proteasome subunit RPT2a promotes PTGS through repressing RNA quality control in *Arabidopsis*. *Nat. Plants* 5, 1273–1282
88. Decker, C.J. and Parker, R. (2012) P-bodies and stress granules: possible roles in the control of translation and mRNA degradation. *Cold Spring Harb. Perspect. Biol.* 4, a012286
89. Stephani, M. and Dagdas, Y. (2020) Plant selective autophagy – still an uncharted territory with a lot of hidden gems. *J. Mol. Biol.* 432, 63–79

b. Selective Autophagy: Adding Precision to Plant Immunity

Scientific contributions: Scientific ideas 10%, Transcriptomic Analysis and Database mining 90%.

Details about writing contributions: Minor help on the writing of the entire manuscript. Writing of the legend section for Figure 2 and 3.

Citation: Leong JX, Langin G, Üstün S. Selective autophagy: adding precision in plant immunity. Essays Biochem. 2022 Aug 5;66(2):189-206. doi: 10.1042/EBC20210063. PMID: 35635102; PMCID: PMC9400066.

Essays in Biochemistry (2022) **66** 189–206
https://doi.org/10.1042/EBC20210063

PORTLAND PRESS

Review Article

Selective autophagy: adding precision in plant immunity

Jia Xuan Leong[1], Gautier Langin[1] and Suayib Üstün[1,2]

[1]University of Tübingen, Center for Plant Molecular Biology (ZMBP), 72076 Tübingen, Germany; [2]Faculty of Biology & Biotechnology, Ruhr-University Bochum, 44780 Bochum, Germany

Correspondence: Suayib Üstün (suayb.uestuen@rub.de)

Plant immunity is antagonized by pathogenic effectors during interactions with bacteria, viruses or oomycetes. These effectors target core plant processes to promote infection. One such core plant process is autophagy, a conserved proteolytic pathway involved in ensuring cellular homeostasis. It involves the formation of autophagosomes around proteins destined for autophagic degradation. Many cellular components from organelles, aggregates, inactive or misfolded proteins have been found to be degraded via autophagy. Increasing evidence points to a high degree of specificity during the targeting of these components, strengthening the idea of selective autophagy. Selective autophagy receptors bridge the gap between target proteins and the forming autophagosome. To achieve this, the receptors are able to recognize specifically their target proteins in a ubiquitin-dependent or -independent manner, and to bind to ATG8 via canonical or non-canonical ATG8-interacting motifs. Some receptors have also been shown to require oligomerization to achieve their function in autophagic degradation. We summarize the recent advances in the role of selective autophagy in plant immunity and highlight NBR1 as a key player. However, not many selective autophagy receptors, especially those functioning in immunity, have been characterized in plants. We propose an *in silico* approach to identify novel receptors, by screening the *Arabidopsis* proteome for proteins containing features theoretically needed for a selective autophagy receptor. To corroborate these data, the transcript levels of these proteins during immune response are also investigated using public databases. We further highlight the novel perspectives and applications introduced by immunity-related selective autophagy studies, demonstrating its importance in research.

Introduction

Plant immunity centers around the plant-pathogen interface, where an intriguing arms race occurs at the molecular level. Plants defend themselves against pathogens using their innate immunity, where broad resistance to pathogens is conferred by pathogen-associated-molecular-pattern (PAMP)-triggered immunity (PTI), which involves recognition of conserved molecules shared by pathogens by surface-localized pattern-recognition receptors (PRRs) [1–3]. For a successful infection, plant pathogens such as bacteria, fungi or oomycetes colonize the plant extracellular space and secrete effector proteins into the host cell cytoplasm, which then target essential pathways in the plant [2,4,5]. Plant viruses are rather obligate intracellular parasites, but likewise utilize effectors for manipulating host processes from within the plant cell, and to facilitate cell-to-cell movement [6–8]. Effectors have been shown to target key plant processes such as PTI signaling, cytoskeleton localization and endocytic trafficking, in a process termed "effector-targeted pathways (ETP)" [4]. Effectors can in turn be recognized by nucleotide-binding leucine-rich repeat receptors (NLRs), which guard host immune components and induce effector-triggered immunity (ETI) [1–3].

As cellular processes are mediated to a great extent by proteins, plant proteostasis i.e. the homeostasis of the plant proteome is an important factor to consider in immunity. Proteostasis is the dynamic and

Received: 15 March 2022
Revised: 06 May 2022
Accepted: 17 May 2022

Version of Record published:
05 August 2022

Essays in Biochemistry (2022) **66** 189–206
https://doi.org/10.1042/EBC20210063

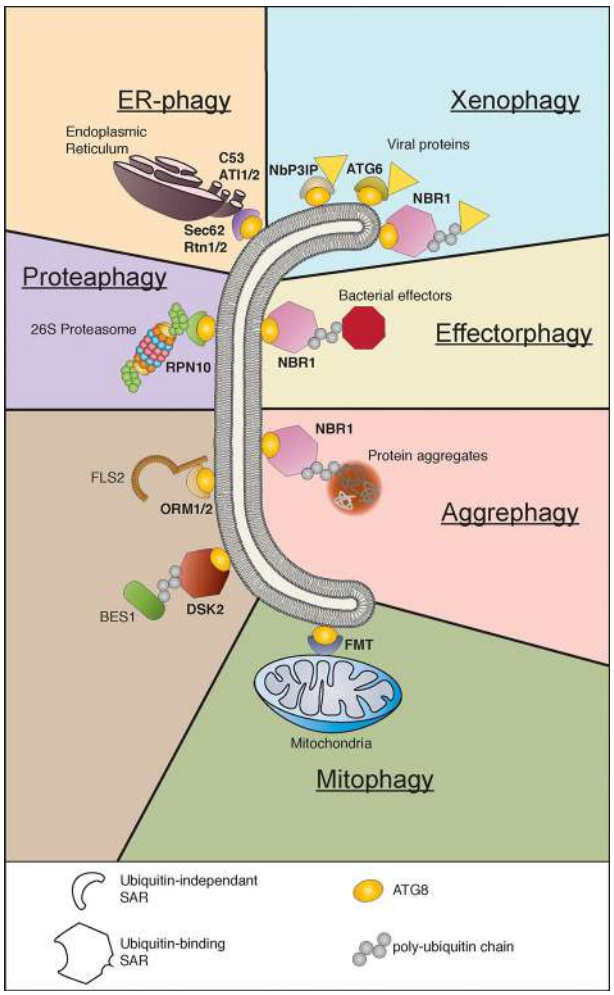

Figure 1. Selective autophagy is involved in the degradation of cellular and pathogenic components

Selective autophagy receptors (SARs) bring their substrate to the nascent autophagosome ATG8 interaction. Substrate binding can be ubiquitin-dependent or -independent. The cargo for xenophagy and effectorphagy includes viral proteins and bacterial effectors. Protein aggregates are targeted in aggrephagy. Organelles such as endoplasmic reticulum (ER), proteasome, and mitochondria are the cargo for ER-phagy, proteaphagy and mitophagy respectively. Specific proteins such as FLS2 and BES1 have also been found to be targeted by SARs. Examples were highlighted based on data availability on ubiquitin-binding and AIM/LIR/UIM-containing. For a comprehensive review on receptors and their substrates see [19,20,25].

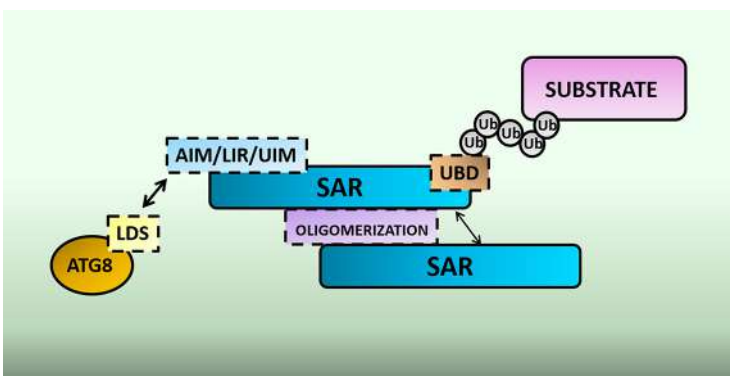

Figure 2. Domain organization of selective autophagy receptors (SAR)

SARs can have ubiquitin-binding domains (UBD) that aids in substrate recognition. ATG8-, LC3- or ubiquitin- interacting motif (AIM/LIR/UIM) of the SAR contacts the LC3 docking site (LDS) on ATG8. Some SARs also contain domains that promote oligomerization.

constant interplay between protein synthesis and degradation, which can be influenced by factors such as protein translation, folding, localization, post-translational modifications, proteasome and autophagic activity [9]. A major hub where effectors converge for ETP are the main protein degradation pathways, autophagy and the ubiquitin–proteasome system (UPS) [5]. Both proteolytic pathways have been shown to be essential, where knockouts of some genes involved in these processes result in severe growth defects, especially under nutrient limiting conditions [10,11]. Autophagy also functions directly in immunity to limit infection [7,8,12]. It follows that targeting of autophagy and UPS pathways through ETP could be highly effective in perturbing host cell during infection, and indeed many examples of this has been described, as reviewed in Langin et al. [5].

General autophagy

Macroautophagy (henceforth autophagy) is essential for cellular homeostasis through intracellular constituent recycling and mediates degradation of large protein complexes, insoluble protein aggregates and dysfunctional organelles [11]. The mechanism behind autophagy is generally conserved in eukaryotes and involves the coordinated action of around 40 autophagy-related (ATG) genes to direct formation of the autophagosome, a double-membraned vesicle that envelops cytosolic material such as proteins and organelles destined for degradation [11,13,14]. In brief, during plant autophagy, ATG1 and ATG13 take in signals from Target of Rapamycin (TOR) kinase which is influenced by both developmental and nutritional signals, although it is to note that TOR-independence exists for oxidative or ER stress-related autophagy [15]. During TOR-dependent autophagy, TOR blocks autophagy by phosphorylating ATG13, which prevents its association with ATG1. Upon nutrient deficiency or other TOR-inactivating conditions, ATG13 is rapidly dephosphorylated which results in ATG1 binding. Additional hypo-and hyperphosphorylation events allow the assembly of the ATG1, ATG13 and the accessory subunits ATG11 and ATG101. The active ATG1 kinase complex then promotes the ATG9-mediated delivery of lipids and membrane sources derived from the ER to the developing phagophore. Nucleation and expansion of the phagophore also involves the VPS34 lipid kinase, which generates PI3P on the phagophore membrane. In parallel, a ubiquitin-like conjugation system (ATG5/ATG12/ATG16) drives the conjugation of ATG8 to PE, which decorates the autophagosome membrane. The autophagosome is further sealed by recruitment of SH3 domain-containing protein 2 (SH3P2) that stimulates phagophore curvature. Mature autophagosomes are delivered to the lytic vacuole for degradation by vacuolar hydrolases.

Many steps in this pathway have been shown to be modulated during plant–pathogen interactions, with excellent reviews summarizing the known examples [5,7,12]. Effectors from plant pathogens were also shown to target different components of the host autophagic machinery, strengthening the idea that autophagy is a key cellular process in immunity [16]. Autophagy has been shown play both pro- and anti-pathogen roles [7,8,12]. Thus, there must be a high degree of regulation behind plant-pathogen interactions. In this review, we focus on protein degradation via selective autophagy, and its role in adding specificity to plant immunity.

Selective autophagy

Our early understanding of autophagy characterized it as a non-specific "bulk" process, where cell cytoplasmic contents are "randomly" engulfed and degraded. Although it was already suggested then that autophagy displays selectivity toward cargo [17], only with the characterization of selective autophagy receptors (SARs, abbreviation not to be confused with systemic acquired resistance) there is strong proof of substrate specificity in autophagy [18]. Receptors have been identified for the selective autophagy of many cellular components across a range of eukaryotic organisms, for example proteasomes (proteaphagy), endoplasmic reticulum (ER-phagy), intracellular pathogens (xenophagy), protein aggregates (aggrephagy) and mitochondria (mitophagy) [19–22] (Figure 1). Particularly relevant to immunity, xenophagy of intracellular bacteria, viruses, protozoa and fungi have been well-described in mammalian systems, whereas for plants most research is directed at xenophagy of viruses [7,8,23,24]. Research on receptors and their identified substrates have been well-summarized for plants [20,25] and for the yeast model system [19]. Thus, in this review, we rather summarize common patterns behind domain organization of SARs and highlight recent advances in plant research regarding selective autophagy and immunity.

The selective autophagy receptor

One component underlying the mechanism of action behind selective autophagy is the receptor, and the study of these SARs has been a substantial driving force behind our understanding of selective autophagy. Despite the wide range of targets and functions, there are nonetheless common patterns that can be established in the mechanism of selective autophagy. In principle, SARs should be able to achieve two tasks. First—to recognize its substrate, either directly or via polyubiquitin chains on the substrate, and second—be able to bring the bound substrate to the

Essays in Biochemistry (2022) **66** 189–206
https://doi.org/10.1042/EBC20210063

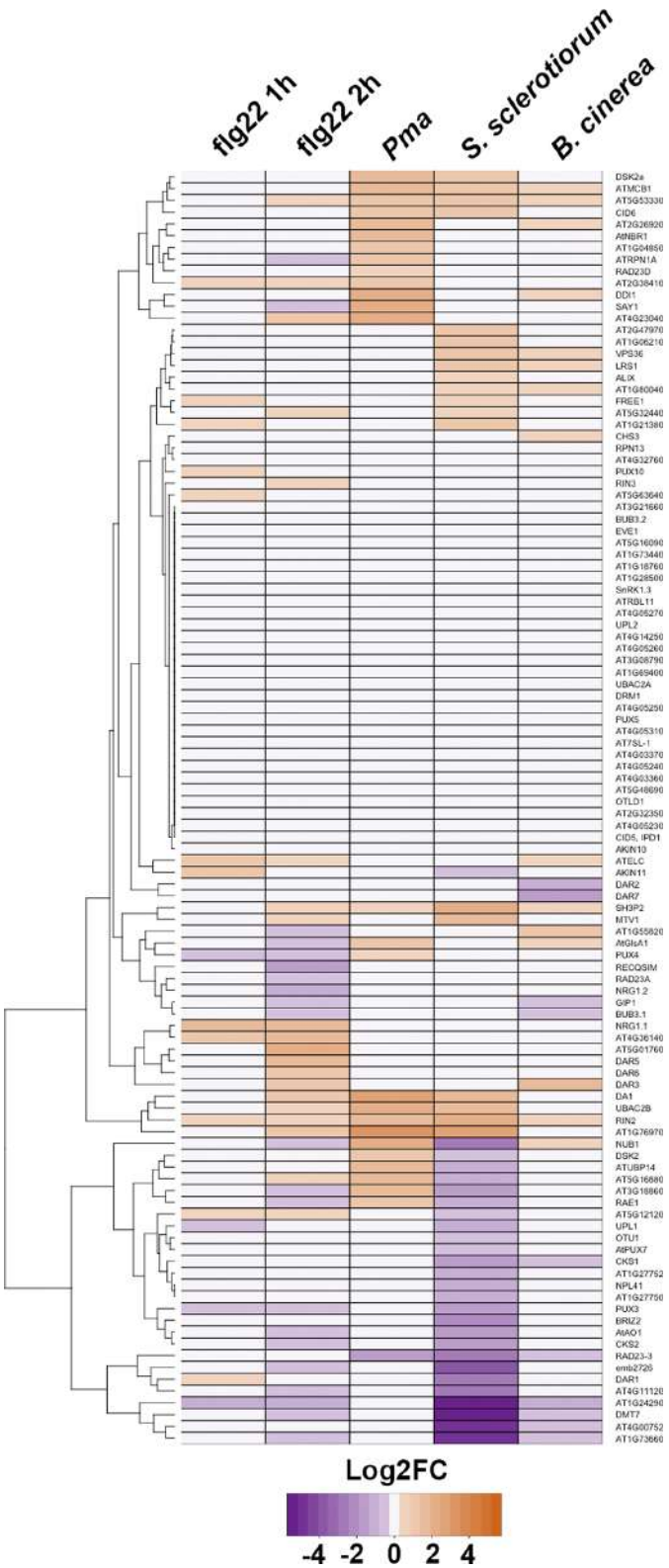

Figure 3. Differential gene expression of candidate SARs during immune responses represented in a heatmap

Expression values are represented as Log2FC, and the color key is indicated at the bottom. The dendrogram on the left clusters together genes with similar expression pattern. Columns correspond to the different dataset extracted from the public online database (http://ipf.sustech.edu.cn/pub/athrna/) as following: flg22 1h (PRJNA491484); flg22 2h (PRJNA429781); *P. syringae* pv. *maculicola* (Pma) (PRJNA390966); *S. sclerotiorum* (PRJNA418121) and *B. cinerea* (PRJNA276444).

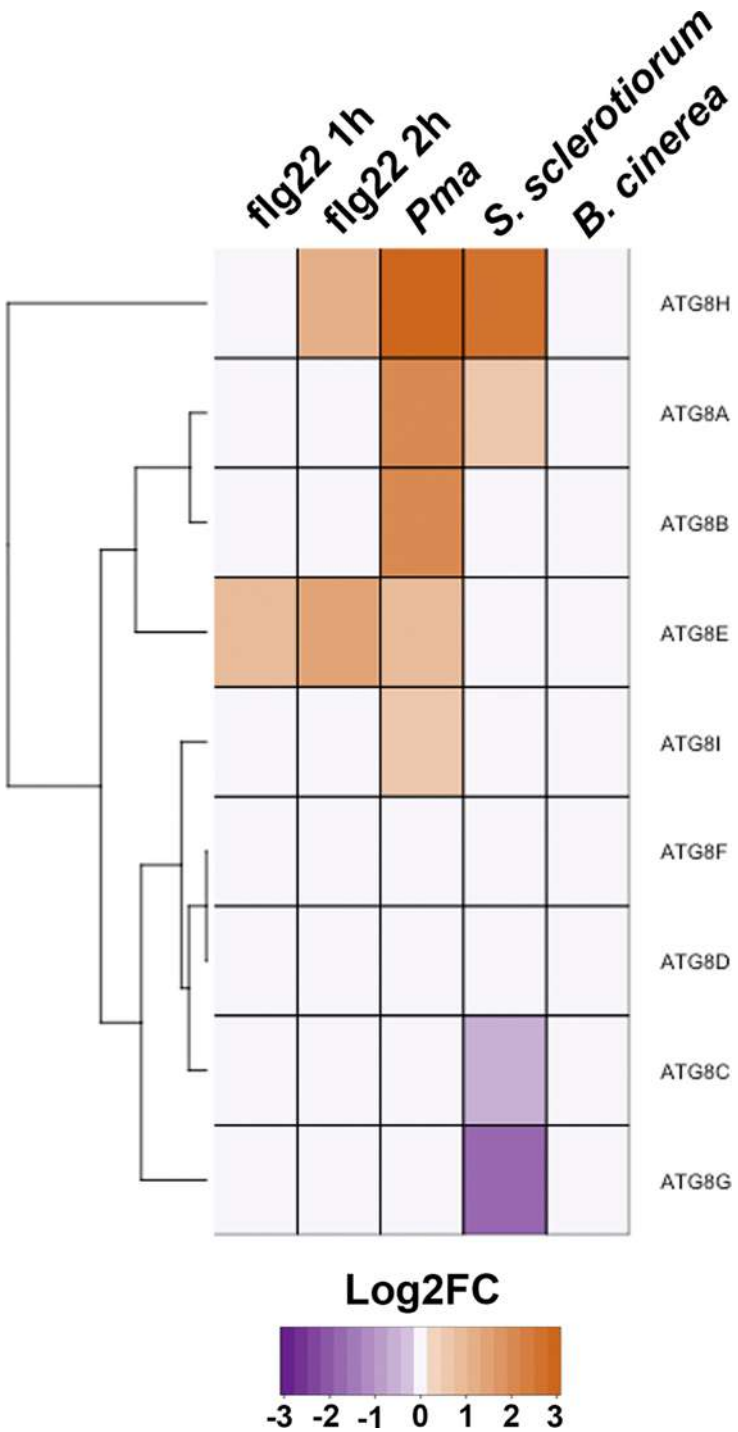

Figure 4. Differential gene expression of ATG8 isoforms during immune responses represented in a heatmap

Expression values are represented as Log2FC, and the color key is indicated at the bottom. The dendrogram on the left clusters together isoforms with similar expression pattern. Columns correspond to the different dataset extracted from the public online database (http://ipf.sustech.edu.cn/pub/athrna/) as following: flg22 1h (PRJNA491484); flg22 2h (PRJNA429781); *P. syringae* pv. *maculicola* (Pma) (PRJNA390966); *S. sclerotiorum* (PRJNA418121) and *B. cinerea* (PRJNA276444).

Essays in Biochemistry (2022) **66** 189–206
https://doi.org/10.1042/EBC20210063

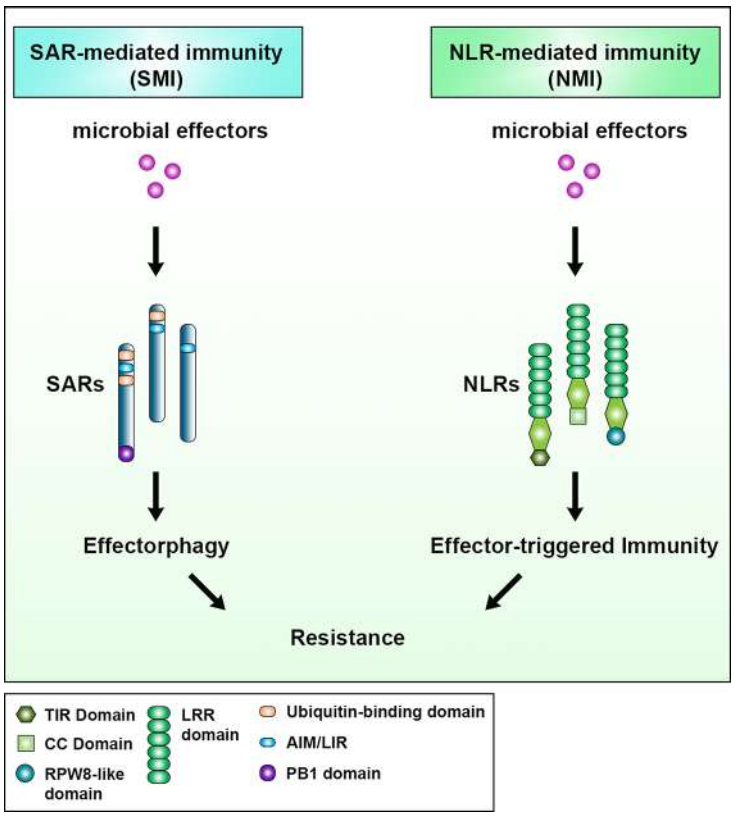

Figure 5. Parallels between SAR-mediated immunity (SMI) and NLR-mediated immunity (NMI)
Both pathways depend on recognition of microbial effectors by receptors. SARs and NLRs are different by structure and domain organization. Both receptors inactivate the effector function either by inducing cell death (NMI) or by degrading the effector via autophagy (SMI) and leading to effector-triggered immunity.

autophagy machinery by binding ATG8, for example via ATG8-interacting motifs (AIMs), LC3-interacting motifs (LIR) or ubiquitin-interacting motifs (UIM) [19,20,25–27] (Figure 2).

Ubiquitin-dependent substrate recognition

Many SARs recognize polyubiquitinated substrates, and contain ubiquitin-binding domains for the recognition of their target substrate [26]. The post-translational modification ubiquitination, also known as ubiquitylation, is described as "eat me" signal due to its role in targeting proteins toward degradative processes [28]. Ubiquitin is conjugated on a lysine residue of a target protein based on the enzymatic cascade of ubiquitin-activating (E1), ubiquitin-conjugating (E2) and ubiquitin-ligase (E3) enzymes [29]. The presence of internal lysine residues allows further conjugation of ubiquitin with itself to form polyubiquitinated chains which mark proteins for degradation [28], although targeting toward non-degradative processes such as the regulation of protein interactions and signal transduction also possible [29,30]. Domains known to bind ubiquitin include UBA (ubiquitin associated), UIM (ubiquitin-interacting motif), CUE (coupling of ubiquitin conjugation to endoplasmic reticulum degradation), TOM (target of Myb) and more as reviewed in [31].

One well-characterized plant SAR is NEIGHBOR OF BRCA1 gene 1 (NBR1), also known as Joka2 in solanaceous plants, which is a homolog of mammalian NBR1 and functionally similar to p62 [32,33]. NBR1 contains two UBA domains, but it was shown that only the C-terminal UBA domain of *A. thaliana* NBR1 could bind ubiquitin, and is thought to be involved in recognition of ubiquitinated targets for selective autophagy [32].

DOMINANT SUPPRESSOR OF KAR 2 (DSK2) is another SAR which acts as a ubiquitin receptor for BRI1-EMS SUPRESSOR 1 (BES1), the master regulator of the brassinosteroid (BR) pathway. Degradation of BES1 by DSK2 requires its UBA domain that can bind polyubiquitin chains, and AIM motif [34].

Similarly, proteasome subunit RPN10 which directs the 26S proteasome towards selective autophagy can bind both ubiquitin and ATG8 [35]. Additionally some proteasome subunits were found to be ubiquitinated thus strengthening RPN10 as a ubiquitin-dependent SAR [35,36].

Considering the role of ubiquitination as a degradation signal and the ubiquitin-binding ability of some SARs, many selective autophagy targets likely undergo ubiquitination. In fact, ubiquitinated proteins are observed to hyper-accumulate in *nbr1* or *atg5* mutants upon infection conditions shown to induce autophagy [37]. Thus, we hypothesize there are additional SARs with ubiquitin binding ability, and investigate this in more detail below.

Ubiquitin-independent substrate recognition

In plant-pathogen interactions, there is evolutionary pressure on the host side to recognize pathogenic components, and on the pathogen side to escape this recognition. Indirect substrate recognition via ubiquitination is intuitively an effective strategy in which xenophagy-related SARs can participate in the xenophagy of a wide range of molecules, from viral capsids to oomycete and bacterial effectors. However, there are exceptions where substrate recognition is still achieved independently of ubiquitin association.

The turnip mosaic virus (TuMV) subunit P4 is recognized by the *A. thaliana* NBR1, and this interaction is still observed with a truncated NBR1 variant missing its UBA domain, suggesting for ubiquitin-independence in the interaction [38].

A study from our lab showed that a bacterial effector XopL is recognized by NBR1 through both ubiquitin-dependent and independent mechanisms. We show through co-immunoprecipitation that XopL interacted with full-length NBR1 and UBA deletion mutants, but a higher molecular weight species hypothesized to be ubiquitinated XopL, only interacted with NBR1 when a functional UBA domain is present [39].

Both these examples of ubiquitin-independence during NBR1-mediated xenophagy are intriguing as NBR1 is the only xenophagy receptor identified so far in plants. Are there more similar examples to be discovered, and if so how would NBR1 recognize the diverse effectors and viral subunits that could be present within the host cell? Are there some conserved features such as structure, that can drive the recognition of these foreign molecules by xenophagy receptors? Indeed, this could be a possibility, given that plant ER-phagy receptors ATG8-interacting proteins 1 and 2 (ATI1/2) share structural similarity with other ER-phagy receptors, where their AIM is located at the end of long, intrinsically disordered cytosolic regions [40]. The structure to function relationship is proposed as the disordered domain could bridge the membrane of the rough ER to ATG8 on phagophores or endolysosomes [40].

Although not shown to be a SAR, exocyst subunit Exo70B2 was found to interact with ATG8 via two AIMs, and is subject to autophagic transport to the vacuole upon treatment with defense-related compounds salicylic acid (SA) and benzothiadiazole (BTH) or immunogenic peptide flg22 [41]. We speculate that Exo70B2 could function as a SAR, directing cargo toward autophagic degradation. Interestingly, Exo70B2 is phosphorylated by the immunity-related kinase MPK3 that enhances its interaction with ATG8 [41]. Thus, if Exo70B2 acts as a SAR, this phosphorylation could present a novel way in which SARs are regulated.

Although not related to immunity, plant mitophagy receptor, FRIENDLY (FMT) does not have UBA domain yet mediates the recycling of damaged mitochondria in Arabidopsis [42]. Furthermore, plant ER-phagy receptors ATI1/2, Sec62, C53, reticulon proteins 1 and 2 (Rtn1/2) and degrade specific proteins in the ER during proteotoxic stress [43–45] or dark-induced starvation [46]. These proteins do not have any predicted ubiquitin-binding functions, thus future work should confirm their ubiquitin-independence and characterize the mechanism.

For mammalian systems as well, under specific conditions receptors link their cargo to autophagosomes during mitophagy, pexophagy, and virophagy in a ubiquitin-independent manner [47]. Thus, is entirely possible that there are more examples of ubiquitin-independent selective autophagy involved in immunity.

Motifs for ATG8 interaction

Once a target substrate is bound, the subsequent role of a SAR is to bring its bound substrate to the autophagic machinery, usually the nascent autophagosome. To achieve this, canonical ATG8-interacting motif (AIM), otherwise known as LC3-interacting region (LIR), or the non-canonical ubiquitin-interacting motif (UIM) on a SAR is crucial, since the autophagosome is decorated with ATG8 proteins to facilitate this specific binding [48,49]. Mechanistically, this binding between the SAR and ATG8 occurs as the AIM/LIR contacts a hydrophobic patch on ATG8 known as the LIR docking site (LDS) [50,51].

Plant NBR1 has a canonical AIM facilitating its interaction with ATG8 on autophagosomes [32,33]. Svenning et al. additionally showed that AtNBR1 during co-expression with AtATG8 or human GABARAPL2, required its AIM to be recognized as an autophagic substrate in HeLa cells [32].

Essays in Biochemistry (2022) **66** 189–206
https://doi.org/10.1042/EBC20210063

Many other SARs have been found to contain AIMs which are crucial for their function in selective autophagy, for example as mentioned above DSK2, RPN10 and potentially Exo70B2 [34,35,41].

RPN10 was additionally shown to have a UIM, which is a non-canonical motif for ATG8 interaction named for its similarity to existing UIM [35,52]. The authors further screened known ATG8-binding proteins for UIM, and identified three PUX proteins, thus raising the possibility that novel SARs with UIM are yet to be characterized [52].

The importance of the AIM in autophagy has inspired tools for AIM prediction to aid in discovery of novel autophagy targets [53,54]. This has potential in aiding in the identification of novel SARs, and will be discussed below.

Oligomerization

Oligomerization of SARs have been shown to be especially important during selective autophagy of aggregates [55,56]. This is because protein aggregates are present as biomolecular condensates, which are membraneless assemblies where certain cellular components such as biopolymers are concentrated [57]. Domains such as Phox and Bem1p (PB1) are present on some SARs which enable their oligomerization [58]. It is rather intuitive that SARs involved in aggrephagy would oligomerize, so that they more easily localize into condensates where their targets reside. Indeed, this idea holds true when we consider the receptors Dsk2 and Cue2, which play a role in both proteasome- and autophagy-dependent protein degradation [59]. Lu and colleagues designed artificial ubiquitin- and Atg8-binding receptors, with or without the ability to oligomerize, and found that only oligomeric receptors could function in aggrephagy. Although direct evidence was not shown, a previous study suggest that Joka2 aggregates contain its multimeric form, and that in the nucleus and cytoplasm it is in a monomeric form [60].

The ubiquitin-binding domains of SARs can also contribute to their oligomerization. For example, a PB1 domain is present on plant NBR1, which allows it to form oligomers with other molecules of itself, but this oligomerization is also partially dependent on its UBA domains [32,60]. In a similar way, human p62 is the main driver of ubiquitin condensate formation, but NBR1 also promotes the p62 condensation through its PB1 and UBA domains [61].

SAR oligomerization may have wider implications beyond aggrephagy, and may function generally in promoting the interaction with ATG8. It was shown that oligomerization of mammalian p62 has an important role in stabilizing the binding to LC3 on the autophagosome membrane [55,56]. Furthermore, the DIX domain of Dishevelled (Dvl) mediates its self-oligomerization, which is ultimately required for interaction with LC3 [62]. There is also increasing evidence that autophagosome formation during autophagy involves liquid-liquid phase separation, which can be promoted by the oligomerization of SARs [63].

Recent advances in selective autophagy in the context of plant immunity

Plant–viral interactions

The pro-plant role of xenophagy during plant–viral interactions is well-characterized. The SAR NBR1 functions in the targeted degradation of viral particles and proteins. For example, cauliflower mosaic virus (CaMV) capsid and P4 proteins, and Turnip mosaic virus (TuMV) HcPro have been shown to be removed by NBR1 [37,38]. In turn, TuMV evolved viral proteins VPg and 6K2 to counteract NBR1-driven host xenophagy by blocking the degradation of HcPro [64]. More recently, it has been reported that nuclear autophagy degrades geminivirus nuclear protein C1 to restrict viral infection in solanaceous plants [65]. In the present study, viral protein C1 harbors an AIM which facilitates its interaction with ATG8, leading to its degradation via autophagy in the cytoplasm. Considering that AIM-containing proteins can act as autophagy adaptors or receptors it is tempting to speculate whether C1, similar to *Phytophtora infestans* effector PexRD54 elaborated on below, functions to target nuclear proteins upon viral infection.

A recent study identified that autophagy core component ATG6/Beclin1 might act as a SAR, as it mediates the degradation of a TuMV RNA-dependent RNA polymerase Nlb to restrict virus infection [66]. ATG6/Beclin1 was also shown to be involved in autophagy-like protein degradation of tobacco calmodulin-like protein rgs-CaM which bound to viral RNA silencing suppressor proteins, thus enhancing host antiviral RNAi [67]. Additionally, Jiang et al. identified a new cargo receptor NbP3IP with a previously unknown function, which specifically interacts with the P3 protein (VSR) of Rice stripe virus (RSV) and NbATG8f. These interactions mediate the selective degradation of the P3 protein and limit RSV infection [68].

Pro-viral effects of selective autophagy have also been described. P0 from Turnip yellows virus (TuYV) was found to manipulate selective autophagy for the degradation of ARGONAUTE1 (AGO1), exploiting ATI1 and ATI2 mediate the delivery of host AGO1 from the ER to the vacuole, ultimately down-regulating host antiviral RNA silencing [69].

Although the majority of the studies identified how SARs contribute to plant–virus interactions, further mechanistic details, such as oligomerization state of the SAR or whether substrate recognition is mediated by ubiquitin, remain still elusive.

Plant–bacterial interactions

During interactions with bacteria, plant autophagy can also function in a pro-plant or pro-bacterial manner. FLAGELLIN-SENSING 2 (FLS2), a receptor kinase which recognizes bacterial flagellin, was found to be degraded by selective autophagy [70]. Orosomucoid (ORM) proteins ORM1 and 2 act as SARs in the degradation of non-activated FLS2, which ensures sufficient amounts of activated FLS2 for signaling [70]. The pathway is hijacked for pro-pathogen effects, for example during *Pseudomonas syringae* infection, where it was found that a T3E HopM1 causes the targeted degradation of the host proteasome by inducing proteaphagy, which could involve the proteaphagy receptor RPN10 since *Pst* bacterial growth was elevated in the *rpn10* mutant [37].

As viruses are the only described intracellular pathogens in plants, we propose that xenophagy includes degradation of viruses, "virophagy" and of effectors, "effectorphagy". During effectorphagy, bacterial effectors are recognized in the plant cell and degraded via the autophagy pathway, for example as in Leong et al. [39]. The study showed that NBR1/Joka2 interacts with and causes the autophagic degradation of a *Xanthomonas campestris* pv. *vesicatoria (Xcv)* effector XopL which are present in aggregates, providing a link between aggrephagy in immunity [39]. This is a novel example in plants of selective autophagy targeting bacterial effectors, and there is a possibility that NBR1 is involved in degradation of other bacterial effectors. Evidence for this include increased bacterial growth and disease progression of *Pseudomonas syringae* pathovar *tomato* DC3000 *(Pst)* in the *nbr1* mutant compared with WT, which indicates for a role of NBR1 in *Pst* infection [37]. The same study further shows that overexpression of NBR1 reduces water soaking caused by HopM1. Both of these results led the authors to speculate that NBR1 is involved in the degradation of other *Pst* effectors.

Plant–oomycete interactions

Phytophtora infestans, the causal pathogen of potato late blight, was shown to secrete an effector PexRD54 which, via its AIM motif, associates with ATG8CL to antagonize Joka2, ultimately enhancing oomycete virulence [71]. Further studies showed that this interaction between oomycete effector and host SAR takes place at the extrahaustorial membrane (EHM), where defense-related Rab8a-vesicles labelled with Joka2 and ATG8CL accumulated [72,73]. Apart from providing more insight to the role of autophagy during plant–oomycete interactions, the authors additionally developed a tool for autophagy suppression. The AIM from PexRD54 was used to create an AIM peptide, which was shown to compete with ATG8-binding and thus blocks autophagy progression. The peptide has already been applied in competition assays to reinforce AIM-dependent ATG8 interactions identified in an immunoprecipitation coupled to mass spectrometry (IP-MS) screen [43]. It was also used to block autophagy by transient expression in *Nicotiana benthamiana*, as it is more specific to autophagy compared with other tools such as Concanamycin A which inhibits vacuolar degradation [39]. In summary, this highlights that studying the role of autophagy in the context of plant–microbe interaction may result in the discovery of novel tools to study the pathway in more detail.

Novel perspectives on plant immunity introduced by selective autophagy research

Identification of new receptors

We have established that SARs mediate substrate specificity during selective autophagy. Identifying and characterization of new SARs related to immunity can help advance our understanding of plant–pathogen interactions. We propose to identify new plant immunity-related SARs by mining the *Arabidopsis* database for proteins that bind to ubiquitin and/or ATG8, and further investigate these candidates by looking into their gene expression during infection using publicly available data.

Ubiquitin-binding proteins were identified based on the presence of characterized ubiquitin-binding domains (INTERPRO/PFAM/SMART) or with the Gene Ontology annotation "ubiquitin-binding" (GO:0043130). From these 106 ubiquitin-binding proteins, we further cross-checked previously published screens for ATG8-interacting proteins [52,53]. We identified 25 ubiquitin-binding proteins that was also found in Marshall et al.'s UIM-interaction dataset [52], and 15 that were found in Jacomin et al.'s LIR prediction for *A. thaliana* proteome [53], with 5 proteins found in both datasets (Table 1). Among the identified receptors include the known SARs NBR1/Joka2, RPN10 and DSK2 with both ubiquitin-binding and ATG8-interacting abilities (Table 1).

Essays in Biochemistry (2022) **66** 189–206
https://doi.org/10.1042/EBC20210063

Table 1 Ubiquitin-binding proteins identified based on presence of ubiquitin-binding domains or Gene Ontology annotation

Entry	Entry.name	Protein.names	Gene. names	Length	Agi_ Code	UBQ. binding. Prediction	ATG8_ Y2H	iLIR. pre-dic-tion
Q9SIV2	PSD2A_ARATH	26S proteasome non-ATPase regulatory subunit 2 homolog A (26S proteasome regulatory subunit RPN1a) (AtRPN1a) (26S proteasome regulatory subunit S2 homolog A)	RPN1A	891	AT2G20580	GO		
Q9ZT95	R7SL1_ARATH	Ubiquitin domain-containing protein 7SL RNA1 (At7SL-1)	7SL1	275	AT4G02970	GO		
Q9ZQZ6	R7SL2_ARATH	Ubiquitin domain-containing protein 7SL RNA2 (At7SL-2) (Protein ETERNALLY VEGETATIVE PHASE 1)	EVE1	263	AT4G03350	GO		
Q9ZQZ4	Q9ZQZ4_ARATH	Putative ubiquitin-like protein (Ubiquitin family protein) (Uncharacterized protein AT4g03370)	At4g03370	295	AT4G03370	GO		+
Q9XIP2	OTU6_ARATH	OVARIAN TUMOR DOMAIN-containing deubiquitinating enzyme 6 (OTU domain-containing protein 6) (EC 3.4.19.12) (Deubiquitinating enzyme OTU6) (Otubain-like deubiquitinase 1)	OTU6	505	AT2G27350	UBA		
Q9SZD6	PETS_ARATH	Polyprotein of EF-Ts, chloroplastic (150 kDa pro-protein) (Protein EMBRYO DEFECTIVE 2726) [Cleaved into: Plastid-specific ribosomal protein-7, chloroplastic; Elongation factor Ts, chloroplastic (EF-Ts)]	PETs	953	AT4G29060	UBA-like		
Q9SUG6	PUX3_ARATH	Plant UBX domain-containing protein 3 (PUX3) (CDC48-interacting UBX-domain protein 3)	PUX3	302	AT4G22150	UBX	+	
Q9SSD3	Q9SSD3_ARATH	F18B13.13 protein (Ubiquitin system component Cue) (Uncharacterized protein At1g80040)	At1g80040	248	AT1G80040	CUE		+
Q9SJJ5	CKS2_ARATH	Cyclin-dependent kinases regulatory subunit 2	CKS2	83	AT2G27970	GO		
Q9SB64	NBR1_ARATH	Protein NBR1 homolog (AtNBR1) (At4g24690)	NBR1	704	AT4G24690	UBA	+	
Q9M9U7	Q9M9U7_ARATH	At1g18760 (F6A14.13 protein) (Zinc finger, C3HC4 type (RING finger) family protein)	At1g18760	224	AT1G18760	UIM		
Q9M548	DRM2_ARATH	DNA (cytosine-5)-methyltransferase DRM2 (EC 2.1.1.37) (Protein DOMAINS REARRANGED METHYLASE 2)	DRM2	626	AT5G14620	UBA		
Q9M0X2	Q9M0X2_ARATH	Ubiquitin-like superfamily protein	At4g05230	206	AT4G05230	GO		
Q9M0X1	Q9M0X1_ARATH	Ubiquitin-like superfamily protein	At4g05240	197	AT4G05240	GO		
Q9M0X0	Q9M0X0_ARATH	Ubiquitin-like superfamily protein	At4g05250	318	AT4G05250	GO		
Q9M0W9	Q9M0W9_ARATH	Ubiquitin-like superfamily protein (Uncharacterized protein AT4g05260)	At4g05260	259	AT4G05260	GO		
Q9M0W8	Q9M0W8_ARATH	Ubiquitin-like superfamily protein (Uncharacterized protein AT4g05270)	At4g05270	129	AT4G05270	GO		
Q9M0W4	Q9M0W4_ARATH	Ubiquitin-like superfamily protein	At4g05310	415	AT4G05310	GO		
Q9M0N1	PUX10_ARATH	Plant UBX domain-containing protein 10 (PUX10)	PUX10	480	AT4G10790	UBA/UBX	+	
Q9LYE5	CID5_ARATH	Polyadenylate-binding protein-interacting protein 5 (PABP-interacting protein 5) (Poly(A)-binding protein-interacting protein 5) (PAM2-containing protein CID5) (Protein CTC-INTERACTING DOMAIN 5) (Protein INCREASED POLYPLOIDY LEVEL IN DARKNESS 1)	CID5	155	AT5G11440	CUE		
Q9LYC2	NPL41_ARATH	NPL4-like protein 1	At3g63000	413	AT3G63000	NPL4		
Q9LXE5	DRM1L_ARATH	DNA (cytosine-5)-methyltransferase DRM1 (EC 2.1.1.37) (Protein DOMAINS REARRANGED METHYLASE 1)	DRM1	624	AT5G15380	UBA		
Q9LVR6	DAR3_ARATH	Protein DA1-related 3	DAR3	450	AT5G66640	DA1-like		
Q9LPL6	TOL3_ARATH	TOM1-like protein 3	TOL3	506	AT1G21380	VHS-GAT		+
Q9LNC6	TOL2_ARATH	TOM1-like protein 2	TOL2	383	AT1G06210	VHS-GAT		+
Q9LJN8	BUB31_ARATH	Mitotic checkpoint protein BUB3.1 (Protein BUDDING UNINHIBITED BY BENZYMIDAZOL 3.1)	BUB3.1	340	AT3G19590	WD40		
Q9LHS5	Q9LHS5_ARATH	Cell division related protein-like (DnaJ and myb-like DNA-binding domain-containing protein)	At5g06110	663	AT5G06110	UBD		

Continued over

Table 1 Ubiquitin-binding proteins identified based on presence of ubiquitin-binding domains or Gene Ontology annotation (Continued)

Entry	Entry.name	Protein.names	Gene. names	Length	Agi_ Code	UBQ. binding. Prediction	ATG8_ Y2H	iLIR. pre-dic-tion
Q9LHN3	Q9LHN3_ARATH	AT3g18860/MCB22_3 (Transducin family protein / WD-40 repeat family protein)		760	AT3G18860	WD40/PFU/ PUL	+	+
Q9LHG8	ELC_ARATH	Protein ELC (AtELC) (ESCRT-I complex subunit VPS23 homolog 1) (Protein VACUOLAR PROTEIN SORTING 23A) (Vacuolar protein-sorting-associated protein 23 homolog 1)	ELC	398	AT3G12400	UEV		
Q9LFL3	TOL1_ARATH	TOM1-like protein 1	TOL1	407	AT5G16880	VHS-GAT		
Q9LET3	RBL20_ARATH	Rhomboid-like protein 20 (AtRBL20)	RBL20	293	AT3G56740	UBA		
Q9FMQ0	Q9FMQ0_ARATH	AT5g12120/MXC9_8 (At5g12120) (Ubiquitin-associated/translation elongation factor EF1B protein) (Uncharacterized protein At5g12120)	MXC9.8	619	AT5G12120	UBA		+
Q9FLZ3	KIN12_ARATH	SNF1-related protein kinase catalytic subunit alpha KIN12 (AKIN12) (EC 2.7.11.1) (AKIN alpha-3) (AKINalpha3) (SNF1-related kinase 1.3) (SnRK1.3)	KIN12	494	AT5G39440	UBA		
Q9FKZ1	DRL42_ARATH	Probable disease resistance protein At5g66900	At5g66900	809	AT5G66900	GO		
Q9FKZ0	DRL43_ARATH	Probable disease resistance protein At5g66910	At5g66910	815	AT5G66910	GO		
Q9FKN7	DAR4_ARATH	Protein DA1-related 4 (Protein CHILLING SENSITIVE 3)	DAR4	1613	AT5G17890	DA1-like		
Q9FJX9	DAR7_ARATH	Protein DA1-related 7	DAR7	560	AT5G66610	UIM	+	
Q9FJX8	DAR6_ARATH	Protein DA1-related 6	DAR6	644	AT5G66620	UIM	+	
Q9FFQ0	TOL5_ARATH	TOM1-like protein 5	TOL5	447	AT5G63640	VHS-GAT		
Q9FF81	VPS36_ARATH	Vacuolar protein sorting-associated protein 36 (AtVPS36) (ESCRT-II complex subunit VPS36)	VPS36	440	AT5G04920	VPS36		
Q9FDZ8	Q9FDZ8_ARATH	At1g73440 (Calmodulin-like protein) (Uncharacterized protein T9L24.51)	T9L24.51	254	AT1G73440	UIM	+	
Q9C9Y1	TOL8_ARATH	TOM1-like protein 8	TOL8	607	AT3G08790	VHS		
Q9C9U5	SIS8_ARATH	Probable serine/threonine-protein kinase SIS8 (EC 2.7.11.1) (MAPKK kinase SIS8) (Protein SUGAR INSENSITIVE 8)	SIS8	1030	AT1G73660	UIM	+	
Q9C701	BUB32_ARATH	Mitotic checkpoint protein BUB3.2 (Protein BUDDING UNINHIBITED BY BENZYMIDAZOL 3.2)	BUB3.2	339	AT1G49910	WD40		
Q9C5H4	MTV1_ARATH	Protein MODIFIED TRANSPORT TO THE VACUOLE 1	MTV1	690	AT3G16270	VHS-GAT		
Q9C5G7	PUX13_ARATH	Plant UBX domain-containing protein 13 (PUX13)	PUX13	525	AT4G23040	UBA/UBX	+	
Q9ASS2	FREE1_ARATH	Protein FREE1 (FYVE domain protein required for endosomal sorting 1) (FYVE domain-containing protein 1)	FREE1	601	AT1G20110	Experimentally proven	+	
Q94JZ8	PUX7_ARATH	Plant UBX domain-containing protein 7 (PUX7)	PUX7	468	AT1G14570	UIM/UBA/UBX	+	
Q93ZS6	Q93ZS6_ARATH	AT3g05090/T12H1_5 (Transducin/WD40 repeat-like superfamily protein) (Uncharacterized protein At3g05090)	LRS1	753	AT3G05090	WD40		
Q8W4Q5	RIN3_ARATH	E3 ubiquitin protein ligase RIN3 (EC 2.3.2.27) (RING-type E3 ubiquitin transferase RIN3) (RPM1-interacting protein 3)	RIN3	577	AT5G51450	CUE		
Q8W4F0	DAR1_ARATH	Protein DA1-related 1	DAR1	553	AT4G36860	UIM/DA1	+	
Q8VZS6	GIP1_ARATH	GBF-interacting protein 1	GIP1	567	AT3G13222	UBA-like		
Q8VYC8	RIN2_ARATH	E3 ubiquitin protein ligase RIN2 (EC 2.3.2.27) (AMF receptor-like protein 1A) (RING-type E3 ubiquitin transferase RIN2) (RPM1-interacting protein 2)	RIN2	578	AT4G25230	CUE		
Q8VWF1	SH3P2_ARATH	SH3 domain-containing protein 2 (AtSH3P2)	SH3P2	368	AT4G34660	SH3	+	
Q8RWY8	Q8RWY8_ARATH	Nucleic acid binding protein (Uncharacterized protein At1g27750)	At1g27750	1075	AT1G27750	GO		+
Q8RWU7	PUX4_ARATH	Plant UBX domain-containing protein 4 (PUX4) (CDC48-interacting UBX-domain protein 4)	PUX4	303	AT4G04210	UBX	+	

Continued over

Essays in Biochemistry (2022) **66** 189–206
https://doi.org/10.1042/EBC20210063

Table 1 Ubiquitin-binding proteins identified based on presence of ubiquitin-binding domains or Gene Ontology annotation (Continued)

Entry	Entry.name	Protein.names	Gene. names	Length	Agi_ Code	UBQ. binding. Prediction	ATG8_ Y2H	iLIR. pre-dic-tion
Q8LG98	OTU1_ARATH	OVARIAN TUMOR DOMAIN-containing deubiquitinating enzyme 1 (OTU domain-containing protein 1) (EC 3.4.19.12) (Deubiquitinating enzyme OTU1)	OTU1	306	AT1G28120	GO		
Q8LG11	Q8LG11_ARATH	Proline-rich cell wall protein-like (Ubiquitin-associated/translation elongation factor EF1B protein)	At5g53330	221	AT5G53330	UBA		
Q8L860	TOL9_ARATH	TOM1-like protein 9	TOL9	675	AT4G32760	VHS-GAT		+
Q8L6Y1	UBP14_ARATH	Ubiquitin carboxyl-terminal hydrolase 14 (EC 3.4.19.12) (Deubiquitinating enzyme 14) (AtUBP14) (TITAN-6 protein) (Ubiquitin thioesterase 14) (Ubiquitin-specific-processing protease 14)	UBP14	797	AT3G20630	UBA		
Q8H0T4	UPL2_ARATH	E3 ubiquitin-protein ligase UPL2 (Ubiquitin-protein ligase 2) (EC 2.3.2.26) (HECT-type E3 ubiquitin transferase UPL2)	UPL2	3658	AT1G70320	UIM/UBA	+	+
Q8GY23	UPL1_ARATH	E3 ubiquitin-protein ligase UPL1 (Ubiquitin-protein ligase 1) (EC 2.3.2.26) (HECT-type E3 ubiquitin transferase UPL1)	UPL1	3681	AT1G55860	UIM/UBA	+	+
Q84WJ0	DAR5_ARATH	Protein DA1-related 5	DAR5	702	AT5G66630	DA1-like		
Q84L33	RD23B_ARATH	Ubiquitin receptor RAD23b (AtRAD23b) (Putative DNA repair protein RAD23-1) (RAD23-like protein 1) (AtRAD23-1)	RAD23B	371	AT1G79650	UBA		+
Q84L32	RD23A_ARATH	Probable ubiquitin receptor RAD23a (AtRAD23a) (Putative DNA repair protein RAD23-2) (RAD23-like protein 2) (AtRAD23-2)	RAD23A	368	AT1G16190	UBA		+
Q84L31	RD23C_ARATH	Ubiquitin receptor RAD23c (AtRAD23c) (Putative DNA repair protein RAD23-3) (RAD23-like protein 3) (AtRAD23-3)	RAD23C	419	AT3G02540	UBA		
Q84L30	RD23D_ARATH	Ubiquitin receptor RAD23d (AtRAD23d) (Putative DNA repair protein RAD23-4) (RAD23-like protein 4) (AtRAD23-4)	RAD23D	378	AT5G38470	UBA		
Q7Y175	PUX5_ARATH	Plant UBX domain-containing protein 5 (PUX5)	PUX5	421	AT4G15410	UBA/UBX	+	
Q6NQK0	TOL4_ARATH	TOM1-like protein 4	TOL4	446	AT1G76970	VHS-GAT		
Q6NQH9	CID6_ARATH	Polyadenylate-binding protein-interacting protein 6 (PABP-interacting protein 6) (Poly(A)-binding protein-interacting protein 6) (PAM2-containing protein CID6) (Protein CTC-INTERACTING DOMAIN 6)	CID6	175	AT5G25540	CUE		
Q5XF75	EFTS_ARATH	Elongation factor Ts, mitochondrial (EF-Ts) (EF-TsMt)	EFTS	395	AT4G11120	UBA-like		
Q4V3D3	PUX9_ARATH	Plant UBX domain-containing protein 9 (PUX9)	PUX9	469	AT4G00752	UIM/UBA-like/ UBX	+	
Q38997	KIN10_ARATH	SNF1-related protein kinase catalytic subunit alpha KIN10 (AKIN10) (EC 2.7.11.1) (AKIN alpha-2) (AKINalpha2) (SNF1-related kinase 1.1) (SnRK1.1)	KIN10	512	AT3G01090	UBA		
Q38942	RAE1_ARATH	Protein RAE1 (RNA export factor 1)	RAE1	349	AT1G80670	WD40		
Q0WSN2	DAR2_ARATH	Protein DA1-related 2 (Protein LATERAL ROOT DEVELOPMENT 3)	DAR2	528	AT2G39830	UIM	+	
Q0WL28	Q0WL28_ARATH	Ubiquitin system component Cue protein (Uncharacterized protein At1g27750)	At1g27752	656	AT1G27752	CUE		+
P92958	KIN11_ARATH	SNF1-related protein kinase catalytic subunit alpha KIN11 (AKIN11) (EC 2.7.11.1) (AKIN alpha-1) (AKINalpha1) (SNF1-related kinase 1.2) (SnRK1.2)	KIN11	512	AT3G29160	UBA		
P55034	PSMD4_ARATH	26S proteasome non-ATPase regulatory subunit 4 homolog (26S proteasome regulatory subunit RPN10) (AtRPN10) (26S proteasome regulatory subunit S5A homolog) (Multiubiquitin chain-binding protein 1) (AtMCB1)	RPN10	386	AT4G38630	UIM	+	

Continued over

Table 1 Ubiquitin-binding proteins identified based on presence of ubiquitin-binding domains or Gene Ontology annotation (Continued)

Entry	Entry.name	Protein.names	Gene. names	Length	Agi_ Code	UBQ. binding. Prediction	ATG8_ Y2H	iLIR. pre-dic-tion
P0DKI4	PUX14_ARATH	Putative plant UBX domain-containing protein 14 (PUX14)	PUX14	417	AT4G14250	UBX	+	
P0C7Q8	DA1_ARATH	Protein DA1 (Protein SUPPRESSOR OF LARGE SEED AND ORGAN PHENOTYPES OF DA1-1 1)	DA1	532	AT1G19270	UIM	+	
O82264	NPL42_ARATH	NPL4-like protein 2	At2g47970	413	AT2G47970	UBQ-like/MPN		
O81015	O81015_ARATH	At2g26920 (Ubiquitin-associated/translation elongation factor EF1B protein) (Uncharacterized protein At2g26920)	At2g26920	646	AT2G26920	UBA		+
O80996	BRIZ2_ARATH	BRAP2 RING ZnF UBP domain-containing protein 2 (EC 2.3.2.27)	BRIZ2	479	AT2G26000	Znf_UBP-like		
O80910	TOL6_ARATH	TOM1-like protein 6	TOL6	671	AT2G38410	VHS-GAT		
O65506	O65506_ARATH	Disease resistance protein (TIR-NBS-LRR class) (Putative disease resistance protein)	At4g36140	1607	AT4G36140	GO		
O48726	RPN13_ARATH	26S proteasome regulatory subunit RPN13 (AtRPN13) (26S proteasome non-ATPase regulatory subunit 13)	RPN13	300	AT2G26590	PH		
O48696	O48696_ARATH	AAA-type ATPase family protein (F3I6.23 protein)	At1g24290	525	AT1G24290	UBA		
O23249	CKS1_ARATH	Cyclin-dependent kinases regulatory subunit 1 (CKS1-At)	CKS1	87	AT2G27960	GO		
F4KED5	F4KED5_ARATH	Ubiquitin system component Cue protein	At5g32440	265	AT5G32440	CUE		
F4KCN6	F4KCN6_ARATH	Ubiquitin receptor RAD23 (DNA repair protein RAD23)	At5g16090	171	AT5G16090	UBA		
F4KAU9	TOL7_ARATH	TOM1-like protein 7	TOL7	542	AT5G01760	VHS-GAT		
F4JPR7	PUX8_ARATH	Plant UBX domain-containing protein 8 (PUX8) (Ara4-interacting protein) (Suppressor of ARA4-induced defect of ypt1) (SAY1)	PUX8	564	AT4G11740	UIM/UBA-like/UBX	+	+
F4JI85	F4JI85_ARATH	Ubiquitin family protein	At4g03360	322	AT4G03360	GO		
F4IXN6	PUX6_ARATH	Plant UBX domain-containing protein 6 (PUX6)	PUX6	435	AT3G21660	UBX	+	+
F4ITP6	F4ITP6_ARATH	Ubiquitin-like superfamily protein	At2g32350	242	AT2G32350	GO		
F4I241	BUB33_ARATH	Mitotic checkpoint protein BUB3.3 (Protein BUDDING UNINHIBITED BY BENZYMIDAZOL 3.3)	BUB3.3	314	AT1G69400	WD40		
F4HXZ1	BRO1_ARATH	Vacuolar-sorting protein BRO1 (BRO domain-containing protein 1) (AtBRO1)	BRO1	846	AT1G15130	BRO1		
A4FVR1	GIP1L_ARATH	GBF-interacting protein 1-like (Protein GIP1-like)	GIP1L	575	AT1G55820	UBA-like		
A0A1P8AW60	A0A1P8AW60_ARATH	Ubiquitin-associated (UBA)/TS-N domain-containing protein	At1g04850	324	AT1G04850	UBA		
Q9SII9	DSK2A_ARATH	Ubiquitin domain-containing protein DSK2a	DSK2A	538	AT2G17190	UBA	+	
Q9SII8	DSK2B_ARATH	Ubiquitin domain-containing protein DSK2b	DSK2B	551	AT2G17200	UBA		
Q8RXQ2	RBL18_ARATH	Rhomboid-like protein 18, AtRBL18	RBL18	287	AT2G41160	UBA		
Q9FT69	RQSIM_ARATH	ATP-dependent DNA helicase Q-like SIM, EC 3.6.4.12†(RecQ-like protein SIM, AtRecQsim, Similar to RecQ protein)	RECQSIM	858	AT5G27680	UBA		
Q500V3	Q500V3_ARATH	At2g12550 (Ubiquitin-associated (UBA)/TS-N domain-containing protein)	NUB1	562	AT2G12550	UBA		
Q8LB17	RBL15_ARATH	Rhomboid-like protein 15, AtRBL15, EC 3.4.21.-	RBL15	403	AT3G58460	UBA		
Q1EBV4	DDI1_ARATH	Protein DNA-DAMAGE INDUCIBLE 1, EC 3.4.23.-	DDI1	414	AT3G13235	UBA		

The list of proteins were cross-checked with previously published screens for ATG8-interacting proteins conducted by Marshall et al. [52] and Jacomin et al. [53] and indicated if they were found in these screens.

Expression level of candidate receptors were then analyzed using data available from public *Arabidopsis* RNAseq libraries [74]. In brief, five representative datasets were used for the analysis based on following criteria: (1) Dataset contains only one treatment. (2) There are at least three biological replicates in control and treated conditions. (3) Datasets are non-redundant. FPKM values for each gene and replicate were extracted from the five datasets, and subsequent Log2 Fold-change (Log2FC) and false discovery rate (FDR) for each gene comparing treated samples

Essays in Biochemistry (2022) **66** 189–206
https://doi.org/10.1042/EBC20210063

to control samples were assessed using Rstudio software (https://www.rstudio.com/). Only, genes with FDR < 0.05 were considered statistically significant. Log2FC of statistically significant genes are displayed as a heatmap with a dendrogram representing genes sorting based on expression pattern similarity from the different dataset (Figure 3).

As NBR1 is well-characterized, we first investigated the data on NBR1 presented by the heatmap. Notably, expression of NBR1 displayed a high positive log fold change during infection with P. *syringae* pv. *maculicola (Pma)* but showed no significant expression differences during flg22 treatment or *Sclerotinia sclerotiorum* and *Botrytis cinerea* infection (Figure 3).

We draw focus to the proteins which display expression patterns evidently different from NBR1, as they could be novel immune-related SARs with specialized functions different from the well-characterized NBR1. For example, the subset of proteins ATMCB1, VPS36, LRS1, SH3P2 and RIN2 were up-regulated during infection with *S. sclerotiorum* and *B. cinerea*, and could be novel ubiquitin- and/or AIM- binding receptors with functions in immunity. In contrast, there is a high negative log fold change in the expression of proteins AT1G24290, DMT7, ATG4G00752, and AT1G73660 during *S. sclerotiorum* and *B. cinerea* infection (Figure 3). This indicates for a possibility that these proteins could be targeted during infection, perhaps because they as well play a role in immunity.

S. sclerotiorum and *B. cinerea* are necrotrophic in contrast with the hemibiotrophic *P. syringae*. Past studies have shown autophagy plays different roles during immunity against biotrophic and necrotrophic pathogens, due in part to its cross-talk with salicylic-acid signalling which mediates resistance against biotrophic pathogens [75]. It is therefore plausible that these putative SARs which respond specifically to necrotrophic pathogens could mediate resistance in a novel manner.

We have identified here many ubiquitin- and/or ATG8- binding receptors with significant expression differences upon flg22 treatment or pathogen challenge. Further investigation should be directed at validating the role of these proteins as SARs, and characterizing how they mediate pathogen interactions and immune responses. The molecular mechanisms that drive their substrate recognition and interaction with autophagic machinery should also be studied so we gain more insight into these interactions.

ATG8 isoforms

We have discussed in depth how SARs can promote the specificity of substrate degradation via autophagy. On the other hand, recent research has shown that different ATG8 isoforms can also add specificity to autophagy. This was already hinted at in earlier publications where Arabidopsis NBR1 showed different levels of interaction with different members from the ATG8 family of proteins [32]. A study into potato ATG8 isoforms showed that the isoforms display differential gene expression under a range of conditions, and interact with distinct sets of proteins with varying degrees of overlap, which suggests some degree of functional specialization of the isoforms [76]. In addition, a yeast-two-hybrid screen revealed differential preference of *A. thaliana* ATG8 isoforms to associate with the UIM [52]. In an immunity context, Leong et al. found that in *N. benthamiana* transcript levels of *NbATG8-2* increased earlier than that of *NbATG8-1* during *Xcv* infection [39]. *P. infestans* effector PexRD54 also showed a preference for ATG8CL over ATG8IL [72].

To strengthen the idea that ATG8 isoforms add specificity during autophagic responses in immunity, we analyzed publicly available data on the gene expression of *A. thaliana* ATG8 isoforms during responses to immunogenic peptide flg22 and pathogens *Pma*, *B. cinerea*, and *S. sclerotiorum* (Figure 4). The analysis method and datasets used are the same as above for identification of putative novel SARs. We found differential gene expression patterns of the ATG8 isoforms during these conditions. Notably, the ATG8 isoforms show different expression patterns compared to each other and under different pathogenic contexts. As previously mentioned, potato ATG8 isoforms show differential gene expression and interact with distinct subsets of proteins, which suggests functionalization [76]. We build upon this hypothesis and apply it to our analysis of *A. thaliana* ATG8 isoforms, and suggest that the differential expression patterns in ATG8 isoforms strengthen the idea that the isoforms have specific functions. Some ATG8 isoforms could be grouped according to the similarity in which they behave. For example, *ATG8B, ATG8E*, and *ATG8I* were up-regulated during *Pma* infection and but did not show significant log fold change during *S. sclerotiorum* or *B. cinerea* infection. *ATG8A* and *ATG8H* responded to both hemibiotrophic *Pma* and necrotrophic *S. sclerotiorum*. In contrast, *ATG8C* and *ATG8G* displayed negative log fold change during infection with *S. sclerotiorum*. These patterns, where a subset of isoforms could specifically respond to the different pathogenic contexts, are similar to the patterns presented by putative ubiquitin- and/or ATG8- binding proteins analyzed above. This strongly supports a scenario where receptor and ATG8 works together to add specificity during immunity.

Spatiotemporal control

Studies in selective autophagy and immunity have also revealed the importance of spatiotemporal regulation in cellular processes. Infection and autophagy are dynamic processes involving many players which constantly display changes in expression, localization, and stability. Dagdas et al. showed that during *P. infestans* infection, the effector PexRD54 caused a diversion of Joka2-ATG8CL defense-related vesicles to haustoria [72]. Leong et al. further showed that the protein accumulation of NBR1 occurs earlier than its increase in transcription [39]. In the same study, it was also shown that knockdown of NBR1 expression via virus-induced gene silencing (VIGS) reduced *Xcv* growth at 3 days-post-inoculation (dpi) compared with WT but not at 6dpi, thus indicating for a role in selective autophagy during the earlier steps of infection [39].

Conclusions

Selective autophagy research has contributed much to our understanding of plant–pathogen interactions. During infection, autophagy is targeted by pathogens due to its central role in plant homeostasis but can also function in clearing pathogenic components and reducing infection. The SARs mediate selective autophagy, and studying these receptors gives us more mechanistic insight into how selective autophagy interacts with immunity. We have highlighted many excellent studies which have shed more light on the role of selective autophagy during immunity. There are nevertheless still many questions to answer, giving great potential for further investigation.

In a classical immunity concept of the "zig-zag" model, gene-for-gene resistance is mediated by cell surface PRRs and cytoplasmic NLRs, which recognize pathogenic components in an extracellular and intracellular manner respectively [1,3]. In this review, we have highlighted the role of SARs in recognizing pathogenic components and their downstream effects within the cell. We draw parallels between NLRs-mediated immunity (NMI) and the role of immune-related SARs reviewed here, and propose that SARs can confer immunity to pathogens through SAR-mediated immunity (SMI) which results in effectorphagy (Figure 5). In both scenarios, effectors and/or their downstream effects are recognized by intracellular proteins with various features leading to effector-triggered immunity (ETI). In fact, Deretic et al. proposed, in the context of mammalian SARs, that they could represent a new paradigm in innate immunity as a new class of PRRs [77]. We support this view, and further emphasize the mechanistic details behind SAR function–how substrate recognition can be both ubiquitin-dependent and -independent, and how SARs directly bridge their substrate to the autophagosome thus immediately targeting them for degradation. This allows SARs to recognize a wide range of pathogenic effectors that are more directly involved in modulation of cellular processes.

Summary

- Due to its central role in ensuring plant cellular homeostasis, autophagy is targeted by plant pathogens during infection
- Selective autophagy has been found to play pro-plant or pro-pathogen roles during immunity
- Similarities can be found across selective autophagy receptor domain organization and function
- Selective autophagy receptors are emerging as key players in plant interaction with bacteria, viruses, and oomycetes.
- The interplay between selective autophagy and pathogenic effectors can present new perspectives on the molecular mechanisms behind plant–pathogen interactions

Competing Interests

The authors declare that there are no competing interests associated with the manuscript.

Funding

This project has received funding from the European Research Council (ERC) under the European Union's Horizon 2020 research and innovation programme [grant number 948996, DIVERSIPHAGY] and Emmy Noether Fellowship GZ: UE188/2-1 from the Deutsche Forschungsgemeinschaft.

Essays in Biochemistry (2022) **66** 189–206
https://doi.org/10.1042/EBC20210063

Author Contribution

J.X.L. and S.Ü. wrote the manuscript. J.X.L. S.Ü. and G.L designed figures. G.L. performed *in silico* analysis to identify novel SARs.

Acknowledgements

We thank all members of the Üstün Lab for fruitful discussions.

Abbreviations

CaMV, cauliflower mosaic virus; ETI, effector-triggered immunity; NMI, NLR-mediated immunity; PAMP, pathogen-associated-molecular-pattern; PRR, pattern-recognition receptor; PTI, PAMP-triggered immunity; SAR, selective autophagy receptor; SMI, SAR-mediated immunity; TuMV, Turnip mosaic virus; TuYV, Turnip yellows virus; VIGS, virus-induced gene silencing.

References

1 Jones, J.D.G. and Dangl, J.L. (2006) The plant immune system. *Nature* **444**, 323–329, https://doi.org/10.1038/nature05286
2 Dodds, P.N. and Rathjen, J.P. (2010) Plant immunity: Towards an integrated view of plant-pathogen interactions. *Nat. Rev. Genet.* **11**, 539–548, https://doi.org/10.1038/nrg2812
3 Pok, B., Ngou, M., Ding, P. and Jones, J.D. (2022) Thirty years of resistance: Zig-zag through the plant immune system. *Plant Cell* **34** (5), 1447–1478, https://doi.org/10.1093/plcell/koac041
4 Win, J., Chaparro-Garcia, A., Belhaj, K., Saunders, D.G.O., Yoshida, K., Dong, S. et al. (2012) Effector biology of plant-associated organisms: concepts and perspectives. *Cold Spring Harb. Symp. Quant. Biol.* **77**, 235–247, https://doi.org/10.1101/sqb.2012.77.015933
5 Langin, G., Gouguet, P. and Üstün, S. (2020) Microbial effector proteins - a journey through the proteolytic landscape. *Trends Microbiol.* **28**, 523–535, https://doi.org/10.1016/j.tim.2020.02.010
6 Laliberté, J.F. and Sanfaçon, H. (2010) Cellular remodeling during plant virus infection. *Ann. Rev.* **48**, 69–91
7 Yang, M., Ismayil, A. and Liu, Y. (2020) Autophagy in plant-virus interactions. *Ann. Rev.* **7**, 403–419
8 Kushwaha, N.K., Hafrén, A. and Hofius, D. (2019) Autophagy-virus interplay in plants: from antiviral recognition to proviral manipulation. *Mol. Plant Pathol.* **20**, 1211–1216, https://doi.org/10.1111/mpp.12852
9 Harper, J.W. and Bennett, E.J. (2016) Proteome complexity and the forces that drive proteome imbalance. *Nature* **537**, 328–338, https://doi.org/10.1038/nature19947
10 Guiboileau, A., Avila-Ospina, L., Yoshimoto, K., Soulay, F., Azzopardi, M., Marmagne, A. et al. (2013) Physiological and metabolic consequences of autophagy deficiency for the management of nitrogen and protein resources in Arabidopsis leaves depending on nitrate availability. *New Phytol.* **199**, 683–694, https://doi.org/10.1111/nph.12307
11 Marshall, R.S. and Vierstra, R.D. (2018) Autophagy: the master of bulk and selective recycling. *Annu. Rev. Plant Biol.* **69**, 173–208, https://doi.org/10.1146/annurev-arplant-042817-040606
12 Üstün, S. and Hofius, D. (2018) Anti- and pro-microbial roles of autophagy in plant-bacteria interactions. *Autophagy* **14**, 1465–1466, https://doi.org/10.1080/15548627.2018.1475817
13 He, C. and Klionsky, D.J. (2009) Regulation mechanisms and signaling pathways of autophagy. *Annu. Rev. Genet.* **43**, 67–93, https://doi.org/10.1146/annurev-genet-102808-114910
14 Lamb, C.A., Yoshimori, T. and Tooze, S.A. (2013) The autophagosome: Origins unknown, biogenesis complex. *Nat. Rev. Mol. Cell Biol.* **14**, 759–774, https://doi.org/10.1038/nrm3696
15 Pu, Y., Luo, X. and Bassham, D.C. (2017) Tor-dependent and -independent pathways regulate autophagy in arabidopsis thaliana. *Front. Plant Sci.* **8**, 1204, https://doi.org/10.3389/fpls.2017.01204
16 Lal, N.K., Thanasuwat, B., Huang, P.-jui, Cavanaugh, K.A., Carter, A., Michelmore, R.W. et al. (2020) Phytopathogen effectors use multiple mechanisms to manipulate plant autophagy. *Cell Host Microbe* **28**, 558–571, https://doi.org/10.1016/j.chom.2020.07.010
17 De Duve, C. and Wattiaux, R. (1966) Functions of lysosomes. *Annu. Rev. Physiol.* **28**, 435–492, https://doi.org/10.1146/annurev.ph.28.030166.002251
18 Kirkin, V. (2020) History of the selective autophagy research: how did it begin and where does it stand today? *J. Mol. Biol.* **432**, 3–27, https://doi.org/10.1016/j.jmb.2019.05.010
19 Kirkin, V. and Rogov, V.V. (2019) A diversity of selective autophagy receptors determines the specificity of the autophagy pathway. *Mol. Cell, Cell Press* **76**, 268–285, https://doi.org/10.1016/j.molcel.2019.09.005
20 Luo, S., Li, X., Zhang, Y., Fu, Y., Fan, B., Zhu, C. et al. (2021) Cargo recognition and function of selective autophagy receptors in plants. *Int. J. Mol. Sci.* **22**, 1013, https://doi.org/10.3390/ijms22031013
21 Ding, X., Zhang, X. and Otegui, M.S. (2018) Plant autophagy: new flavors on the menu. *Curr. Opin. Plant Biol.* **46**, 113–121, https://doi.org/10.1016/j.pbi.2018.09.004
22 Gatica, D., Lahiri, V. and Klionsky, D.J. (2018) Cargo recognition and degradation by selective autophagy. *Nat. Cell Biol.* **20**, 233–242, https://doi.org/10.1038/s41556-018-0037-z
23 Levine, B., Mizushima, N. and Virgin, H.W. (2011) Autophagy in immunity and inflammation. *Nature* **469**, 323–335, https://doi.org/10.1038/nature09782

24 Evans, R.J., Sundaramurthy, V. and Frickel, E.M. (2018) The interplay of host autophagy and eukaryotic pathogens. *Front. Cell Dev. Biol.* **6**, 118, https://doi.org/10.3389/fcell.2018.00118
25 Stephani, M. and Dagdas, Y. (2020) Plant selective autophagy—still an uncharted territory with a lot of hidden gems. *J. Mol. Biol.* **432**, 63–79, https://doi.org/10.1016/j.jmb.2019.06.028
26 Lamark, T. and Johansen, T. (2021) Mechanisms of selective autophagy. *Ann. Rev.* **37**, 143–169
27 Zaffagnini, G. and Martens, S. (2016) Mechanisms of selective autophagy. *J. Mol. Biol.* **428**, 1714–1724, https://doi.org/10.1016/j.jmb.2016.02.004
28 Kwon, Y.T. and Ciechanover, A. (2017) The ubiquitin code in the ubiquitin-proteasome system and autophagy. *Trends Biochem. Sci* **42**, 873–886, https://doi.org/10.1016/j.tibs.2017.09.002
29 Komander, D. and Rape, M. (2012) The ubiquitin code. *Ann. Rev.* **81**, 203–229
30 Oh, E., Akopian, D. and Rape, M. (2018) Principles of ubiquitin-dependent signaling. *Annu. Rev. Cell Dev. Biol.* **34**, 137–162, https://doi.org/10.1146/annurev-cellbio-100617-062802
31 Hurley, J.H., Lee, S. and Prag, G. (2006) Ubiquitin-binding domains. *Biochem. J.* **399**, 361–372, https://doi.org/10.1042/BJ20061138
32 Svenning, S., Lamark, T., Krause, K. and Johansen, T. (2011) Plant NBR1 is a selective autophagy substrate and a functional hybrid of the mammalian autophagic adapters NBR1 and p62/SQSTM1. *Autophagy* **7**, 993–1010, https://doi.org/10.4161/auto.7.9.16389
33 Zientara-Rytter, K., Lukomska, J., Moniuszko, G., Gwozdecki, R., Surowiecki, P., Lewandowska, M. et al. (2011) Identification and functional analysis of Joka2, a tobacco member of the family of selective autophagy cargo receptors. *Autophagy* **7**, 1145, https://doi.org/10.4161/auto.7.10.16617
34 Nolan, T.M., Brennan, B., Yang, M., Chen, J., Zhang, M., Li, Z. et al. (2017) Selective autophagy of BES1 mediated by DSK2 balances plant growth and survival. *Dev. Cell* **41**, 33–46, https://doi.org/10.1016/j.devcel.2017.03.013
35 Marshall, R.S., Li, F., Gemperline, D.C., Book, A.J. and Vierstra, R.D. (2015) Autophagic degradation of the 26S proteasome is mediated by the dual ATG8/ubiquitin receptor RPN10 in Arabidopsis. *Mol. Cell* **58**, 1053–1066, https://doi.org/10.1016/j.molcel.2015.04.023
36 Book, A.J., Gladman, N.P., Lee, S.S., Scalf, M., Smith, L.M. and Vierstra, R.D. (2010) Affinity purification of the Arabidopsis 26 S proteasome reveals a diverse array of plant proteolytic complexes. *J. Biol. Chem.* **285**, 25554–25569, https://doi.org/10.1074/jbc.M110.136622
37 Üstün, S., Hafrén, A., Liu, Q., Marshall, R.S., Minina, E.A., Bozhkov, P.V. et al. (2018) Bacteria exploit autophagy for proteasome degradation and enhanced virulence in plants. *Plant Cell* **30**, 668–685, https://doi.org/10.1105/tpc.17.00815
38 Hafrén, A., Macia, J.L., Love, A.J., Milner, J.J., Drucker, M. and Hofius, D. (2017) Selective autophagy limits cauliflower mosaic virus infection by NBR1-mediated targeting of viral capsid protein and particles. *Proc. Natl. Acad. Sci. U. S. A.* **114**, E2026–E2035, https://doi.org/10.1073/pnas.1610687114
39 Leong, J.X., Raffeiner, M., Spinti, D., Langin, G., Franz-Wachtel, M., Guzman, A.R. et al. (2021) A bacterial effector counteracts host autophagy by promoting degradation of an autophagy component. *EMBO*, accepted 05.2022
40 Molinari, M. (2021) ER-phagy responses in yeast, plants, and mammalian cells and their crosstalk with UPR and ERAD. *Dev. Cell, Cell Press* **56**, 949–966, https://doi.org/10.1016/j.devcel.2021.03.005
41 Brillada, C., Teh, O.K., Ditengou, F.A., Lee, C.W., Klecker, T., Saeed, B. et al. (2021) Exocyst subunit Exo70B2 is linked to immune signaling and autophagy. *Plant Cell* **33**, 404–419, https://doi.org/10.1093/plcell/koaa022
42 Ma, J., Liang, Z., Zhao, J., Wang, P., Ma, W., Mai, K.K. et al. (2021) Friendly mediates membrane depolarization-induced mitophagy in Arabidopsis. *Curr. Biol.* **31**, 1931–1944, https://doi.org/10.1016/j.cub.2021.02.034
43 Stephani, M., Picchianti, L., Gajic, A., Beveridge, R., Skarwan, E., de Medina Hernandez, V.S. et al. (2020) A cross-kingdom conserved er-phagy receptor maintains endoplasmic reticulum homeostasis during stress. *eLife* **9**, 1–105, https://doi.org/10.7554/eLife.58396
44 Zhang, X., Ding, X., Marshall, R.S., Paez-Valencia, J., Lacey, P., Vierstra, R.D. et al. (2020) Reticulon proteins modulate autophagy of the endoplasmic reticulum in maize endosperm. *Elife* **9**, e51918, https://doi.org/10.7554/eLife.51918
45 Hu, S., Ye, H., Cui, Y. and Jiang, L. (2020) AtSec62 is critical for plant development and is involved in ER-phagy in Arabidopsis thaliana. *J. Integr. Plant Biol.* **62**, 181–200, https://doi.org/10.1111/jipb.12872
46 Wu, J., Michaeli, S., Picchianti, L., Dagdas, Y., Galili, G. and Peled-Zehavi, H. (2021) ATI1 (ATG8-interacting protein 1) and ATI2 define a plant starvation-induced reticulophagy pathway and serve as MSBP1/MAPR5 cargo receptors. *Autophagy* **17**, 3375–3388, https://doi.org/10.1080/15548627.2021.1872886
47 Khaminets, A., Behl, C. and Dikic, I. (2016) Ubiquitin-dependent and independent signals in selective autophagy. *Trends Cell Biol.* **26**, 6–16, https://doi.org/10.1016/j.tcb.2015.08.010
48 Noda, N.N., Ohsumi, Y. and Inagaki, F. (2010) Atg8-family interacting motif crucial for selective autophagy. *FEBS Lett.* **584**, 1379–1385, https://doi.org/10.1016/j.febslet.2010.01.018
49 Birgisdottir, Å.B., Lamark, T. and Johansen, T. (2013) The LIR motif - crucial for selective autophagy. *J. Cell Sci.* **126**, 3237–3247, https://doi.org/10.1242/jcs.126128
50 Liu, W., Liu, Z., Mo, Z., Guo, S., Liu, Y. and Xie, Q. (2021) ATG8-interacting motif: evolution and function in selective autophagy of targeting biological processes. *Front. Plant Sci.* **12**, 2671, https://doi.org/10.3389/fpls.2021.783881
51 Wirth, M., Zhang, W., Razi, M., Nyoni, L., Joshi, D., O'Reilly, N. et al. (2019) Molecular determinants regulating selective binding of autophagy adapters and receptors to ATG8 proteins. *Nat. Commun.* **10**, 1–18, https://doi.org/10.1038/s41467-019-10059-6
52 Marshall, R.S., Hua, Z., Mali, S., Mcloughlin, F. and Vierstra, R.D. (2019) ATG8-binding UIM proteins define a new class of autophagy adaptors and receptors. *Cell* **177**, 766–781, https://doi.org/10.1016/j.cell.2019.02.009
53 Jacomin, A.C., Samavedam, S., Promponas, V. and Nezis, I.P. (2016) iLIR database: a web resource for LIR motif-containing proteins in eukaryotes. *Autophagy* **12**, 1945–1953, https://doi.org/10.1080/15548627.2016.1207016

Essays in Biochemistry (2022) **66** 189–206
https://doi.org/10.1042/EBC20210063

54 Xie, Q., Tzfadia, O., Levy, M., Weithorn, E., Peled-Zehavi, H., Van Parys, T. et al. (2016) hfAIM: a reliable bioinformatics approach for in silico genome-wide identification of autophagy-associated Atg8-interacting motifs in various organisms. *Autophagy* **12**, 876, https://doi.org/10.1080/15548627.2016.1147668
55 Wurzer, B., Zaffagnini, G., Fracchiolla, D., Turco, E., Abert, C., Romanov, J. et al. (2015) Oligomerization of p62 allows for selection of ubiquitinated cargo andisolation membrane during selective autophagy. *eLife* **4**, e08941, https://doi.org/10.7554/eLife.08941
56 Chen, W., Shen, T., Wang, L. and Lu, K. (2021) Oligomerization of selective autophagy receptors for the targeting and degradation of protein aggregates. *Cells* **10**, 1989, https://doi.org/10.3390/cells10081989
57 Alberti, S. and Hyman, A.A. (2021) Biomolecular condensates at the nexus of cellular stress, protein aggregation disease and ageing. *Nat. Rev. Mol. Cell Biol.* **22**, 196–213, https://doi.org/10.1038/s41580-020-00326-6
58 Sumimoto, H., Kamakura, S. and Ito, T. (2007) Structure and function of the PB1 domain, a protein interaction module conserved in animals, fungi, amoebas, and plants. *Sci. STKE* **401**, re6
59 Lu, K., Den Brave, F. and Jentsch, S. (2017) Receptor oligomerization guides pathway choice between proteasomal and autophagic degradation. *Nat. Cell Biol.* **19**, 732–739, https://doi.org/10.1038/ncb3531
60 Zientara-Rytter, K. and Sirko, A. (2014) Significant role of PB1 and UBA domains in multimerization of Joka2, a selective autophagy cargo receptor from tobacco. *Front. Plant Sci.* **5**, 13, https://doi.org/10.3389/fpls.2014.00013
61 Turco, E., Savova, A., Gere, F., Ferrari, L., Romanov, J., Schuschnig, M. et al. (2021) Reconstitution defines the roles of p62, NBR1 and TAX1BP1 in ubiquitin condensate formation and autophagy initiation. *Nat. Commun.* **12**, 1–16, https://doi.org/10.1038/s41467-021-25572-w
62 Gao, C., Cao, W., Bao, L., Zuo, W., Xie, G., Cai, T. et al. (2010) Autophagy negatively regulates Wnt signalling by promoting Dishevelled degradation. *Nat. Cell Biol.* **12**, 781–790, https://doi.org/10.1038/ncb2082
63 Fujioka, Y. and Noda, N.N. (2021) Biomolecular condensates in autophagy regulation. *Curr. Opin. Cell Biol.* **69**, 23–29, https://doi.org/10.1016/j.ceb.2020.12.011
64 Hafrén, A., Üstün, S., Hochmuth, A., Svenning, S., Johansen, T. and Hofius, D. (2018) Turnip mosaic virus counteracts selective autophagy of the viral silencing suppressor HCpro. *Plant Physiol.* **176**, 649–662, https://doi.org/10.1104/pp.17.01198
65 Li, F., Zhang, M., Zhang, C. and Zhou, X. (2020) Nuclear autophagy degrades a geminivirus nuclear protein to restrict viral infection in solanaceous plants. *New Phytol.* **225**, 1746–1761, https://doi.org/10.1111/nph.16268
66 Li, F., Zhang, C., Li, Y., Wu, G., Hou, X., Zhou, X. et al. (2018) Beclin1 restricts RNA virus infection in plants through suppression and degradation of the viral polymerase. *Nat. Commun.* **9**, 1–17
67 Nakahara, K.S., Masuta, C., Yamada, S., Shimura, H., Kashihara, Y., Wada, T.S. et al. (2012) Tobacco calmodulin-like protein provides secondary defense by binding to and directing degradation of virus RNA silencing suppressors. *Proc. Natl. Acad. Sci. U. S. A.* **109**, 10113–10118, https://doi.org/10.1073/pnas.1201628109
68 Jiang, L., Lu, Y., Zheng, X., Yang, X., Chen, Y., Zhang, T. et al. (2021) The plant protein NbP3IP directs degradation of Rice stripe virus p3 silencing suppressor protein to limit virus infection through interaction with the autophagy-related protein NbATG8. *New Phytol.* **229**, 1036–1051, https://doi.org/10.1111/nph.16917
69 Michaeli, S., Clavel, M., Lechner, E., Viotti, C., Wu, J., Dubois, M. et al. (2019) The viral F-box protein P0 induces an ER-derived autophagy degradation pathway for the clearance of membrane-bound AGO1. *Proc. Natl. Acad. Sci. U. S. A.* **116**, 22872–22883, https://doi.org/10.1073/pnas.1912222116
70 Yang, F., Kimberlin, A.N., Elowsky, C.G., Liu, Y., Gonzalez-Solis, A., Cahoon, E.B. et al. (2019) A plant immune receptor degraded by selective autophagy. *Mol. Plant* **12**, 113–123, https://doi.org/10.1016/j.molp.2018.11.011
71 Dagdas, Y.F., Beihaj, K., Maqbool, A., Chaparro-Garcia, A., Pandey, P., Petre, B. et al. (2016) An effector of the irish potato famine pathogen antagonizes a host autophagy cargo receptor. *eLife* **5**, e10856, https://doi.org/10.7554/eLife.10856
72 Dagdas, Y.F., Pandey, P., Tumtas, Y., Sanguankiattichai, N., Belhaj, K., Duggan, C. et al. (2018) Host autophagy machinery is diverted to the pathogen interface to mediate focal defense responses against the irish potato famine pathogen. *eLife* **7**, e37476, https://doi.org/10.7554/eLife.37476
73 Pandey, P., Leary, A.Y., Tumtas, Y., Savage, Z., Dagvadorj, B., Duggan, C. et al. (2021) An oomycete effector subverts host vesicle trafficking to channel starvation-induced autophagy to the pathogen interface. *eLife* **10**, e65285, https://doi.org/10.7554/eLife.65285
74 Zhang, H., Zhang, F., Yu, Y., Feng, L., Jia, J., Liu, B. et al. (2020) A comprehensive online database for exploring ∼20,000 public Arabidopsis RNA-Seq Libraries. *Mol. Plant* **13**, 1231–1233, https://doi.org/10.1016/j.molp.2020.08.001
75 Lenz, H.D., Haller, E., Melzer, E., Kober, K., Wurster, K., Stahl, M. et al. (2011) Autophagy differentially controls plant basal immunity to biotrophic and necrotrophic pathogens. *Plant J.* **66**, 818–830, https://doi.org/10.1111/j.1365-313X.2011.04546.x
76 Zess, E.K., Jensen, C., Cruz-Mireles, N., De la Concepcion, J.C., Sklenar, J. et al. (2019) N-terminal β-strand underpins biochemical specialization of an ATG8 isoform. *PLoS Biol.* **17**, e3000373, https://doi.org/10.1371/journal.pbio.3000373
77 Deretic, V. (2012) Autophagy as an innate immunity paradigm: expanding the scope and repertoire of pattern recognition receptors. *Curr. Opin. Immunol.* **24**, 21–31, https://doi.org/10.1016/j.coi.2011.10.006

c. A bacterial effector counteracts host autophagy by promoting degradation of an autophagy component

Scientific contributions: Scientific ideas 0%, Data generation 5%, Paper Writing 5%.

Details about writing contributions: Minor help on the writing of the entire manuscript. Writing of the legend section for Figure 5C and Figure S19. Writing of Material and Methods section “FRET-FLIM measurement” and “Phylogenetic analysis” under SÜ supervision.

Citation: Leong JX, Raffeiner M, Spinti D, Langin G, Franz-Wachtel M, Guzman AR, Kim JG, Pandey P, Minina AE, Macek B, Hafrén A, Bozkurt TO, Mudgett MB, Börnke F, Hofius D, Üstün S. A bacterial effector counteracts host autophagy by promoting degradation of an autophagy component. EMBO J. 2022 Jul 4;41(13):e110352. doi: 10.15252/embj.2021110352. Epub 2022 May 27. PMID: 35620914; PMCID: PMC9251887.

Article

SOURCE DATA | TRANSPARENT PROCESS | OPEN ACCESS

THE EMBO JOURNAL

A bacterial effector counteracts host autophagy by promoting degradation of an autophagy component

Jia Xuan Leong[1], Margot Raffeiner[2], Daniela Spinti[2], Gautier Langin[1], Mirita Franz-Wachtel[3], Andrew R Guzman[4], Jung-Gun Kim[4], Pooja Pandey[5], Alyona E Minina[6], Boris Macek[3], Anders Hafren[7], Tolga O Bozkurt[5], Mary Beth Mudgett[4], Frederik Börnke[2,8], Daniel Hofius[7] & Suayib Üstün[1,9,*]

Abstract

Beyond its role in cellular homeostasis, autophagy plays anti- and promicrobial roles in host–microbe interactions, both in animals and plants. One prominent role of antimicrobial autophagy is to degrade intracellular pathogens or microbial molecules, in a process termed xenophagy. Consequently, microbes evolved mechanisms to hijack or modulate autophagy to escape elimination. Although well-described in animals, the extent to which xenophagy contributes to plant–bacteria interactions remains unknown. Here, we provide evidence that *Xanthomonas campestris* pv. *vesicatoria (Xcv)* suppresses host autophagy by utilizing type-III effector XopL. XopL interacts with and degrades the autophagy component SH3P2 via its E3 ligase activity to promote infection. Intriguingly, XopL is targeted for degradation by defense-related selective autophagy mediated by NBR1/Joka2, revealing a complex antagonistic interplay between XopL and the host autophagy machinery. Our results implicate plant antimicrobial autophagy in the depletion of a bacterial virulence factor and unravel an unprecedented pathogen strategy to counteract defense-related autophagy in plant–bacteria interactions.

Keywords autophagy; effectors; immunity; ubiquitination; xenophagy

Subject Categories Microbiology, Virology & Host Pathogen Interaction; Plant Biology

DOI 10.15252/embj.2021110352 | Received 3 December 2021 | Revised 15 April 2022 | Accepted 21 April 2022 | Published online 27 May 2022

The EMBO Journal (2022) 41: e110352

Introduction

Eukaryotic cells react dynamically to external and internal stimuli by adjusting their proteome. This requires a stringent regulation of protein homeostasis, which is achieved in large part by regulated protein degradation. Cellular degradation machineries including the proteasome and autophagy maintain protein homeostasis by recycling unwanted or dysfunctional proteins (Pohl & Dikic, 2019). While the proteasome degrades short-lived proteins or misfolded proteins, autophagy can remove larger protein complexes, insoluble aggregates, entire organelles, and pathogens (Marshall & Vierstra, 2018). Under normal conditions, both degradation pathways are critical for cellular housekeeping functions, while under stress conditions they facilitate the reorganization of the proteome to adapt to a changing environment (Marshall & Vierstra, 2018).

Regulated proteolytic degradation by proteasome has been identified as an essential component of immunity influencing the outcome of host–microbe interactions across kingdoms (Hu & Sun, 2016; Adams & Spoel, 2018). In recent years, autophagy has also emerged as a central player in immunity and disease in humans and plants (Levine *et al*, 2011; Üstün *et al*, 2017; Germic *et al*, 2019; Leary *et al*, 2019; Yang & Klionsky, 2020). In mammals, autophagy has various connections to several diseases, regulating cell death and innate immunity (Germic *et al*, 2019; Yang & Klionsky, 2020). Dual roles have also been ascribed to autophagy in host–bacteria interactions (Mostowy, 2013). While some bacterial pathogens recruit the autophagy machinery in order to create a replicative niche (probacterial autophagy), antibacterial autophagy removes bacterial intruders to limit pathogen infection (Huang & Brumell, 2014). The

1 Center for Plant Molecular Biology (ZMBP), University of Tübingen, Tübingen, Germany
2 Leibniz-Institute of Vegetable and Ornamental Crops (IGZ), Großbeeren, Germany
3 Interfaculty Institute for Cell Biology, Department of Quantitative Proteomics, University of Tübingen, Tübingen, Germany
4 Department of Biology, Stanford University, Stanford, CA, USA
5 Department of Life Sciences, Imperial College London, London, UK
6 Department of Molecular Sciences, Uppsala BioCenter, Swedish University of Agricultural Sciences and Linnean Center for Plant Biology, Uppsala, Sweden
7 Department of Plant Biology, Uppsala BioCenter, Swedish University of Agricultural Sciences and Linnean Center for Plant Biology, Uppsala, Sweden
8 Institute of Biochemistry and Biology, University of Potsdam, Potsdam, Germany
9 Faculty of Biology & Biotechnology, Ruhr-University Bochum, Bochum, Germany
*Corresponding author. Tel: +49 07071 29 76149; E-mail: suayb.uestuen@rub.de

elimination of bacteria is a selective autophagy response, termed xenophagy (Gomes & Dikic, 2014). In this process, bacterial pathogens such as *Salmonella* and *Shigella* are degraded by autophagy through a ubiquitin-dependent mechanism (Dupont *et al*, 2009; van Wijk *et al*, 2012). This demonstrates that autophagy is not only a largely unspecific ("bulk") catabolic and recycling process, as increasing evidence now indicates that autophagy also acts as a selective mechanism to degrade protein aggregates, organelles, and pathogens. Selectivity is mediated by autophagy receptors, of which p62 and NBR1 play key roles in controlling pathogenic infection in mammals (Gomes & Dikic, 2014). Both autophagy receptors can bind to ubiquitinated bacteria, and degrade them, through their ability to bind autophagosome-associated ATG8 proteins (Gomes & Dikic, 2014).

It is known that type-III effector (T3E) proteins of plant pathogenic bacteria are present in the host cell while bacteria reside in the extracellular space. These effectors are able to manipulate host defense responses for the benefit of the pathogen (Khan *et al*, 2018). Very recently, it has been shown that microbial effectors perturb or hijack degradation machineries to attenuate plant immune reactions (Banfield, 2015; Langin *et al*, 2020). For instance, *Pst* activates autophagy via the action of the T3E HopM1 to degrade the proteasome and suppress its function in a process termed proteaphagy (Üstün *et al*, 2016, 2018). Although this process can be categorized as a pro-bacterial role of autophagy, NBR1-mediated antibacterial autophagy seems to restrict lesion formation and pathogenicity of *Pst* (Üstün & Hofius, 2018). The dual role of autophagy in plant–bacteria interactions is further confirmed by findings that certain effectors are also able to suppress autophagy responses, although the understanding of the exact molecular mechanisms is still very limited (Lal *et al*, 2020). In addition, plant NBR1, which is also referred to as Joka2 in solanaceous species, is able to restrict the growth and disease progression of the plant pathogenic oomycete *Phytophthora infestans* (Dagdas *et al*, 2016, 2018). Recently, plant NBR1-mediated xenophagy was described to remove intracellular viral proteins (Hafren *et al*, 2017, 2018). These studies demonstrated that, similar to that in mammals, plant NBR1 participates in xenophagy by degrading viral proteins. Given the fact that plant pathogenic bacteria reside in the extracellular space and the presence of T3Es inside the host cell, it is not known whether NBR1-mediated xenophagy might play a role in plant–microbe interactions by targeting intracellular T3Es.

Like *Pst*, *Xanthomonas campestris* pv. *vesicatoria* (*Xcv*) is another well-studied hemibiotrophic bacterium, causing disease in tomato and pepper plants (Timilsina *et al*, 2020). Mounting evidence has been established that *Xcv* and its T3Es exploit plant ubiquitin- and ubiquitin-like pathways (Üstün & Börnke, 2014; Büttner, 2016). While the role of the proteasome system in *Xanthomonas* infections is well understood, little is known about how autophagy shapes the outcome of *Xanthomonas*–host interactions. Recent findings in the cassava- *Xanthomonas axonopodis* pv. *manihotis* (*Xam*) model suggests that autophagy has an antibacterial role (Yan *et al*, 2017; Zeng *et al*, 2018). However, our current understanding of how T3Es might modulate and regulate this response is very limited. Are there similar mechanisms operating in pro- and antibacterial roles across different pathogenic bacteria? Do plants utilize xenophagy as an antibacterial mechanism to degrade pathogenic components in plant–bacteria interactions?

To address these questions, we performed a mechanistic analysis of the interplay of plant defense-related autophagy and *Xcv* pathogenesis. Here, we provide evidence that *Xcv* blocks autophagy via bacterial effector E3 ligase XopL. T3E XopL degrades autophagy component SH3P2 in a proteasome-dependent manner to suppress autophagic degradation. In turn, the NBR1/Joka2-selective autophagy pathway of the host recognizes XopL and leads to its degradation by the autophagy pathway. Thus, the capacity of XopL to dampen autophagy responses via the degradation of SH3P2 allows its partial escape from autophagic turnover in order to act as a virulence factor in *Xcv*–host interactions.

Results

Xanthomonas blocks autophagy in an effector-dependent manner to promote pathogenicity

Given the prominent role of autophagy in host–microbe interactions, we investigated autophagic response after *Xanthomonas* infection. To this end, we used the model plant *Nicotiana benthamiana*, since methods such as agrobacterium-mediated transient expression, virus-induced gene silencing (VIGS), and autophagy activity reporter assays are well-established and reproducible. Assays were conducted with an *Xcv* strain harboring a deletion in the T3E XopQ (*Xcv ΔxopQ*), which is a host range determinant in *Nicotiana* species (Adlung *et al*, 2016), thus restoring the full virulence of *Xcv* in *Nicotiana benthamiana* in the absence of XopQ.

First, we monitored autophagosome formation using RFP-ATG8g, which is a structural component of autophagosomes and is widely used to label these structures (Üstün *et al*, 2018). We infected *N. benthamiana* plants transiently expressing RFP-ATG8g with *Xcv ΔxopQ* and monitored autophagosomal structures during Concanamycin A (ConA) treatment. ConA is an inhibitor of vacuolar acidification that blocks autophagic body degradation (Svenning *et al*, 2011; Minina *et al*, 2018), thus impairing the late steps of autophagic degradation. In the absence of ConA, *Xcv ΔxopQ* induced a massive accumulation of autophagosome-like structures, which could not be further enhanced by the presence of ConA (Fig 1A). This suggests that *Xcv* blocks autophagic degradation *in planta*. To provide additional evidence that these structures are indeed autophagosomes, we imaged *N. benthamiana* plants, which were silenced using VIGS for *ATG7*, a crucial component of the autophagy pathway, and transiently expressing GFP-ATG8e, and found that the structures that accumulated under Xcv infection after 6 hpi or AZD8055 treatment, a compound known to induce autophagy (Marshall & Vierstra, 2018), no longer accumulating (Appendix Fig S1A). The induction of autophagosome formation and suppression of autophagic degradation prompted us to investigate host autophagy by immunoblotting for endogenous ATG8 and Joka2 in *N. benthamiana* (Svenning *et al*, 2011; Dagdas *et al*, 2016). We also used the previously described autophagy suppressor AIMp, a small peptide sequence derived from the *Phytophthora* PexRD54 effector (Pandey *et al*, 2021), as a positive control for autophagy suppression. The AIM peptide inhibits autophagosome biogenesis by occupying the binding pockets on ATG8 that mediate the docking of host autophagy adaptors such as Joka2 (Pandey *et al*, 2021). Joka2 protein abundance increased during infection, to a small extent 1-day

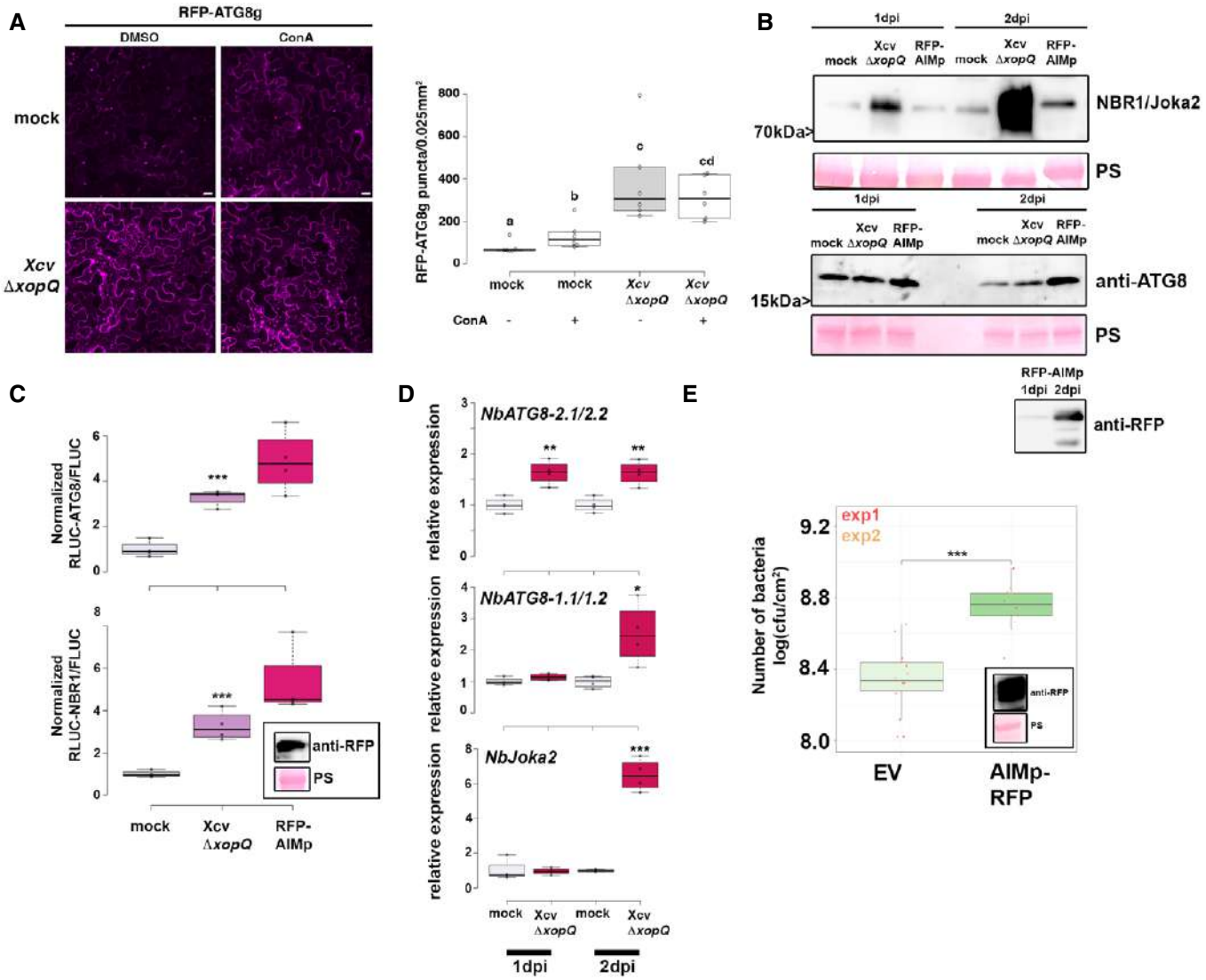

Figure 1. Xanthomonas blocks autophagy to enhance its pathogenicity.

A RFP-ATG8g-labeled autophagosomes were quantified from plant syringe infected with mock or Xcv *ΔxopQ* (oD_{600} = 0.2) at 2 dpi in the presence or absence of ConA (bars = 20 μm). Puncta were calculated from z-stacks (15) of $n = 6$ individuals using ImageJ. Central band of boxplots represents the median, the bottom and the top represent the 25th and 75th percentiles, and whiskers extend to at most 1.5 times the interquartile range. Different letters indicate statistically different groups ($P < 0.05$) as determined by one-way ANOVA. The experiment was repeated twice with similar results.

B Immunoblot analysis of NBR1 and ATG8 protein levels in Xcv *ΔxopQ* or mock-infected *N. benthamiana* plants at 1 and 2 dpi. Agrobacterium-mediated transient expression of AIMp-RFP serves as a control for autophagy suppression. Ponceau staining (PS) served as a loading control. The experiment was repeated three times with similar results.

C RLUC-ATG8a or RLUC-NBR1 constructs were coexpressed with internal control FLUC in *N. benthamiana*. *Xcv ΔxopQ* was co-infiltrated with Agrobacteria containing the luciferase reporter constructs. Coexpression of RFP-AIMp serves as a control for autophagy inhibition. Expression of the latter was confirmed with western blot (inset). *Renilla* (RLUC) and *Firefly* (FLUC) luciferase activities were simultaneously measured in leaf extracts at 48 h postinfiltration using the dual-luciferase system ($n = 4$). Middle horizontal bars of boxplots represent the median, the bottom and top represent the 25th and 75th percentiles, and whiskers extend to at most 1.5 times the interquartile range. Statistical significance (***$P < 0.001$) was revealed by the Student's *t*-test. The experiment was repeated more than 3 times with similar results.

D RT-qPCR analysis of *NbATG8-1.1/1.2*, *NbATG8-2.1/2.2*, and *NbJoka2* transcript levels upon the challenge of *N. benthamiana* plants with Xcv *ΔxopQ* for 1 and 2 dpi compared with mock-infected plants. Values represent the expression relative to mock control of respective timepoint and were normalized to *actin*. Values are biological replicates ($n = 4$). Middle horizontal bars of boxplots represent the median, the bottom and top represent the 25th and 75th percentiles, and whiskers extend to at most 1.5 times the interquartile range. Statistical significance (*$P < 0.05$, **$P < 0.01$, ***$P < 0.001$) was revealed by the Student's *t*-test.

E Bacterial density in leaves of *N. benthamiana* infected with *Xcv* in the presence or absence of autophagy suppressor AIMp-RFP. Leaves were syringe infiltrated with OD_{600} = 0.0004, and colony-forming units were counted at 6 dpi. Compared with empty vector control (EV), AIMp-expressing plants ($n = 6$) harbor significantly more bacteria. Bacterial growth was repeated with the same result in 12 plants over two independent experiments. Red and yellow data points indicate independent repeats of the experiment. Middle horizontal bars of boxplots represent the median, the bottom and top represent the 25th and 75th percentiles, and whiskers extend to at most 1.5 times the interquartile range. Statistical significance (***$P < 0.001$) was revealed by the Student's *t*-test. Expression of RFP-AIMp was verified at 6 dpi with an anti-RFP blot (inset).

Source data are available online for this figure.

postinoculation (dpi), and to a greater extent at 2 dpi, while ATG8 protein levels only slightly increased at 2 dpi (Fig 1B). Protein accumulation seen during immunoblotting could be attributed to increased transcription and/or decreased degradation. Thus, to uncouple these effects we utilized a quantitative autophagy assay to measure autophagic degradation during infection. This assay is based on Agrobacterium-mediated transient expression of 35S promoter-driven *Renilla* luciferase (RLUC) fused to ATG8a (RLUC-ATG8a) or NBR1 (RLUC-NBR1), together with free *Firefly* luciferase (FLUC), which serves as an internal control for expression as it is not degraded with autophagy (Üstün *et al*, 2018; Dauphinee *et al*, 2019). The autophagy reporter assay revealed that *Xcv ΔxopQ* infection led to a significant increase in RLUC-ATG8a/FLUC and RLUC-NBR1/FLUC ratios, suggesting reduced autophagic turnover after 2 dpi (Fig 1C, Appendix Fig S1B). Another indicator of impaired autophagy is the increased gene expression of the autophagic markers (Minina *et al*, 2018). Transcript levels of *Joka2*, *NbATG8-2.1/2*, and *NbATG8-1.1/1.2* were significantly higher compared to that of mock infection at 2 dpi (Fig 1D), with *NbATG8-2.1/2.2* showing an earlier increase than the two other genes and suggesting at a differential response of NbATG8 isoforms during *Xcv* infection. Taken together with previous results, accumulation of Joka2 protein levels at 1 dpi, which was observed earlier than its induced gene expression at 2 dpi, and reduced autophagic turnover after 6 hpi using the autophagy reporter assay (Appendix Fig S1B) strongly suggest that *Xcv* dampens autophagic flux. To assess the biological relevance of suppressed autophagic degradation during *Xcv* infection, we determined bacterial growth in *N. benthamiana roq1* plants, which carry a mutation in *Recognition of XopQ 1 (Roq1)* that recognizes the effector XopQ to activate resistance to *Xcv* (Schultink *et al*, 2017; Gantner *et al*, 2019). In these plants, we transiently expressed RFP-AIMp as an autophagy suppressor. At 6 dpi, *Xcv* growth was significantly elevated in *roq1* plants transiently expressing RFP-AIMp compared with empty vector (EV) control (Fig 1E). The same trend was observed when *ATG7* was silenced in *N. benthamiana*, as *ATG7* silencing rendered plants more susceptible to *Xcv* Δ*xopQ* at 6 dpi (Appendix Fig S2A). Silencing was done using VIGS verified via qRT-PCR (Appendix Fig S2B).

Because T3Es were previously shown to modulate proteasome function and autophagy (Üstün *et al*, 2013, 2016, 2018), we analyzed host autophagy response to a nonpathogenic type-III secretion system (T3SS) mutant *Xcv ΔhrcN*, which is unable to drive secretion of T3Es (Lorenz & Büttner, 2009). In contrast to *Xcv ΔxopQ*, the T3SS-deficient mutant *Xcv ΔhrcN* did not alter the protein abundance of ATG8 and Joka2 (Appendix Fig S3A), nor RLUC-ATG8a/FLUC or RLUC-NBR1/FLUC ratio (Appendix Fig S3B) or transcript abundance of autophagy marker genes *NbJoka2* and *NbATG8-1.1/1.2* (Appendix Fig S3C). Together, these data support the model that *Xcv* blocks autophagy in a T3E-dependent manner to promote virulence.

T3E XopL suppresses autophagy

To address which T3E(s) might manipulate autophagy, we screened for *Xcv* effectors XopJ, XopD, and XopL, which have known functions in modulating proteolytic degradation pathways (Kim *et al*, 2013; Singer *et al*, 2013; Üstün & Börnke, 2014, 2015; Üstün *et al*, 2015) and XopS, which has not been described to modulate degradation machineries. To this end, we used the quantitative dual-luciferase autophagy reporter assay. Transient expression of XopL, a previously characterized E3 ligase (Singer *et al*, 2013), and XopJ, an effector previously shown to inhibit host proteasome, led to a significant increase in RLUC-ATG8a/FLUC and RLUC-NBR1/FLUC ratio (Fig 2A and Appendix Fig S4A), which was consistent across multiple experiments. In contrast, transient expression of XopD and XopS had no evident effect on autophagic degradation (Appendix Fig S4A). We chose to study XopL further, as XopJ was previously shown to inhibit host proteasome (Üstün *et al*, 2013), which may result in modulation of autophagy as shown by the effect of treatment with a proteasome inhibitor MG132 (Appendix Fig S4B). Performing immunoblot analysis of ATG8 protein levels in *N. benthamiana* leaves, we found that transient expression of XopL resulted in an accumulation of NBR1 and ATG8 proteins at 2 dpi (Fig 2B). While this was also consistent with elevated gene expression of ATG8, NBR1/Joka2 expression was only induced at 1 dpi but not 2 dpi upon XopL expression (Appendix Fig S4C). Transient expression of the autophagy inhibitor AIMp showed similar expression trends (Appendix Fig S4C). Treatment with ConA revealed that ATG8 levels could not be further enhanced when XopL was expressed (Fig 2C), providing strong evidence that XopL inhibits autophagic turnover. We note that XopL accumulates under ConA treatment (Fig 2C), which suggests that XopL is also subject to autophagic degradation.

To validate that XopL also acts as an autophagy suppressor during *Xcv* infection we constructed a *xopL* deletion mutant in *Xcv* WT and *Xcv ΔxopQ* backgrounds. *Xcv ΔxopL* displayed reduced growth and symptom development upon infection of tomato plants and the same, but to a lesser extent, was observed for *Xcv ΔxopL* in *N. benthamiana* (Appendix Fig S5A–E), demonstrating that XopL has a role during infection. Monitoring autophagosome-like structures in leaves transiently expressing GFP-ATG8e revealed that tissue infected with *Xcv ΔxopL* induced fewer GFP-ATG8e puncta than *Xcv* in the absence of ConA (Figs 2D and Appendix Fig S6A). The addition of ConA increased GFP-ATG8e puncta in leaves infected with *Xcv ΔxopL* but not in *Xcv*, indicating that XopL has a role in dampening autophagy during infection (Fig 2D). By analyzing ATG8 and NBR1 protein levels, we also verified that XopL partially contributes to ATG8 and NBR1/Joka2 accumulation (Fig 2E), supporting the notion that XopL suppresses autophagic degradation. We confirmed this when we monitored RFP-Joka2 in transiently expressing *N. benthamiana roq1* plants after Xcv infection. Infection with *Xcv* resulted in an induction of NBR1/Joka2 bodies in comparison to *Xcv ΔxopL* infected leaves (Appendix Fig S6B). Utilizing the quantitative dual-luciferase autophagy assay, we show that *Xcv ΔxopQ ΔxopL* was unable to suppress autophagy to levels observed in tissues infected with *Xcv ΔxopQ* levels, both at 2 dpi (Fig 2F), indicating that XopL has a major impact on autophagy during infection. However, *Xcv ΔxopQ ΔxopL* still leads to an increase in both RLUC-ATG8a/FLUC and RLUC-NBR1/FLUC ratios, suggesting that *Xcv* possesses another T3E with a redundant function.

To analyze whether XopL has similar functions in other plant species, we generated transgenic *Arabidopsis thaliana* lines expressing GFP-XopL under the UBQ10 promoter. Similar to the results we obtained in *N. benthamiana*, GFP-XopL transgenic *A. thaliana* plants showed increased NBR1 protein abundance in the absence and presence of ConA treatment (Appendix Fig S7A), suggesting a

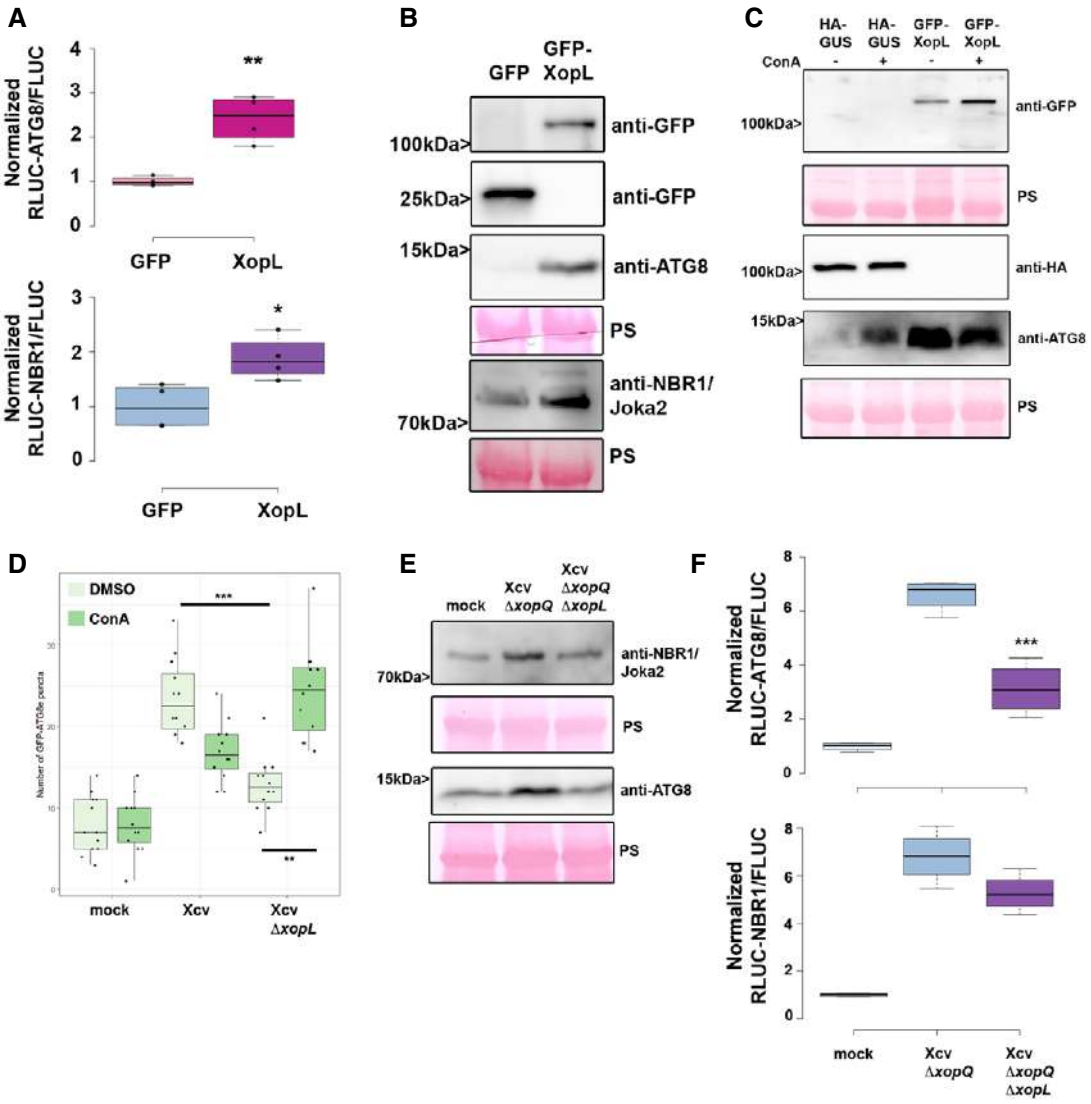

Figure 2. Xanthomonas T3E XopL is suppressing autophagy.

A RLUC-ATG8a or RLUC-NBR1 constructs were coexpressed with internal control FLUC in *N. benthamiana*. XopL or GFP constructs were co-infiltrated. RLUC and FLUC signals were simultaneously measured in leaf extracts at 48 h postinfiltration using the dual-luciferase system. Values represent the ratio of RLUC-ATG8a and FLUC activities to the mean of control ($n = 4$). Middle horizontal bars of boxplots represent the median, the bottom and top represent the 25th and 75th percentiles, and whiskers extend to at most 1.5 times the interquartile range. Statistical significance ($P < 0.01$) was shown by the Student's *t*-test. The experiment was repeated more than 3 times with similar results.

B Immunoblot analysis of NBR1 and ATG8 protein levels in *N. benthamiana* plants transiently expressing GFP-XopL or GFP control at 2 dpi verified with an anti-GFP antibody (the same blot was split for visualization purpose). Ponceau staining (PS) served as a loading control. The experiment was repeated at least three times with similar results.

C Immunoblot analysis of ATG8 protein levels in *N. benthamiana* plants transiently expressing XopL or GUS control at 2 dpi after ConA or DMSO treatment. Expression of GFP-XopL was verified with an anti-GFP antibody, while expression of GUS-HA was confirmed with an anti-HA antibody. Ponceau staining (PS) served as a loading control. The experiment was repeated twice with similar results.

D GFP-ATG8g-labeled autophagosomes were quantified from plants infected with *Xcv* or *Xcv ΔxopL* at 2 dpi in the presence or absence of ConA. Puncta were calculated from z-stacks (15) of $n = 12$ individuals using ImageJ. Middle horizontal bars of boxplots represent the median, the bottom and top represent the 25th and 75th percentiles, and whiskers extend to at most 1.5 times the interquartile range. Statistical significance (**$P < 0.01$, ***$P < 0.001$) was determined by one-way ANOVA. The experiment was repeated twice with similar results.

E Immunoblot analysis of NBR1 and ATG8 protein levels in Xcv *ΔxopQ*, Xcv *ΔxopQ ΔxopL*, or mock-infected *N. benthamiana* plants at 2 dpi. Ponceau staining (PS) served as a loading control. The experiment was repeated twice with similar results.

F RLUC-ATG8a or RLUC-NBR1 constructs were coexpressed with internal control FLUC in *N. benthamiana. Xcv ΔxopQ and Xcv ΔxopQ ΔxopL* were co-infiltrated with Agrobacteria containing the respective constructs. RLUC and FLUC activities were simultaneously measured in leaf extracts at 48 h postinfiltration using the dual-luciferase system. Values represent the ratio of RLUC-ATG8a and FLUC activities ($n = 4$). Middle horizontal bars of boxplots represent the median, the bottom and top represent the 25th and 75th percentiles, and whiskers extend to at most 1.5 times the interquartile range. Statistical significance comparing *Xcv ΔxopQ and Xcv ΔxopQ ΔxopL* values (***$P < 0.001$) was revealed by the Student's *t*-test. The experiment was repeated 3 times with similar results.

Source data are available online for this figure.

block of NBR1 turnover. The early senescence phenotype of transgenic lines expressing XopL (Appendix Fig S7B) and elevated gene expression of *ATG8a* and *NBR1* is indicative of altered autophagy activity (Appendix Fig S7D). Imaging with confocal microscopy revealed that GFP-XopL localizes to punctate structures in *A. thaliana* leaf epidermal cells (Appendix Fig S7C).

XopL interacts with and degrades the autophagy component SH3P2 contributing to Xcv virulence during infection

Previously, XopL was characterized as belonging to a novel class of E3 ligases and is capable of suppressing plant defense responses. There are no known plant targets of XopL (Singer *et al*, 2013), so we carried out a yeast two-hybrid (Y2H) screen using a cDNA library from tobacco (*Nicotiana tabacum*) to investigate whether XopL directly targets autophagy components to act as an autophagy suppressor. Our previous interactions studies indicate that the tobacco cDNA library is sufficient to identify host targets of *Xcv* T3Es that are conserved across different plant species, such as pepper, tomato, and *A. thaliana* (Üstün *et al*, 2013, 2014; Albers *et al*, 2019). One cDNA identified in the Y2H screening for XopL-interacting proteins encoded a homologue of *A. thaliana* SH3P2, which has an amino acid identity of 74% to the *N. tabacum* homologue (Appendix Fig S8A). Homologues are also present in *Nicotiana benthamiana* (NbSH3P2a and NbSH3P2b, 98% identity) and tomato (SlSH3P2, 96% to NtSH3P2) (Appendix Fig S8A and B). Direct interaction assays in yeast revealed that XopL is able to interact with SH3P2 from *N. tabacum* and *N. benthamiana* (Fig 3A and Appendix Fig S8C). SH3P2 from *A. thaliana* was previously identified as a novel autophagy component that interacts with ATG8 and binds to phosphatidylinositol 3-phosphate (PI3P) to regulate autophagosome formation, having also a potential role in late events of autophagosome biogenesis (Zhuang *et al*, 2013; Zhuang & Jiang, 2014). SH3P2 was also found to play a role in the recognition of ubiquitinated membrane proteins, and in targeting them to the endosomal sorting complexes required for transport (ESCRT) machinery (Nagel *et al*, 2017). We next sought to determine whether the interaction between XopL and SH3P2 occurs *in planta*. Due to expression problems of tobacco SH3P2 and also due to their high identity, we conducted further interaction studies with AtSH3P2. Using bimolecular fluorescence complementation (BiFC) and *in vivo* co-immunoprecipitation (co-IP), we found that XopL and AtSH3P2 interact in the plant cell, in small punctate structures resembling autophagosomes, and also in larger structures (Fig 3B and C; Movie EV1). Additional *in vitro* co-IP data, using *E. coli* produced recombinant MBP-XopL and GST-*At*SH3P2, suggests that XopL and SH3P2 might directly interact with each other (Appendix Fig S8D). Given the fact that SH3P2 from *A. thaliana* interacts with ATG8 and XopL localizes in puncta within plant cells (Zhuang *et al*, 2013; Erickson *et al*, 2018), we assessed whether XopL colocalizes with autophagosomes *in planta*. We were able to identify that transient expression of GFP-XopL in *N. benthamiana* with the autophagosome markers RFP-ATG8e and SH3P2-RFP resulted in colocalization (Fig 3D). SH3P2 also colocalized with ATG8e upon transient coexpression in *N. benthamiana* (Fig 3D). This further supports the idea that XopL is functioning in the autophagy pathway by associating with these components *in planta*. Since XopL possesses E3 ligase activity, we next sought to investigate whether XopL might destabilize SH3P2 via ubiquitination, and thereby block autophagic degradation. Indeed, *in planta* transient coexpression of GFP-XopL and AtSH3P2-GFP resulted in a reduction in the latter's protein abundance in *N. benthamiana* (Fig 3E). This was not due to mere overexpression of T3E XopL, as protein levels of Histone H3 were unchanged in the presence of XopL (Appendix Fig S8E). In order to investigate whether XopL can promote the destabilization of SH3P2 during bacterial infection, *N. benthamiana* plants expressing SH3P2-GFP or SH3P2-HA were infected with *Xcv* WT or *Xcv ΔxopL*. When SH3P2 levels were monitored by immunoblotting at 2 dpi, leaves infected with *Xcv ΔxopL* showed a stronger SH3P2 signal than those infected with mock or *Xcv* WT (Appendix Fig S8F). This indicates XopL degrades SH3P2 during *Xcv* infection.

Previously, downregulation of SH3P2 in *A. thaliana* has been shown to reduce autophagic activity (Zhuang *et al*, 2013). However, the role of SH3P2 is still controversial, as another study identified that SH3P2 functions in clathrin-mediated endocytosis without having any obvious effects on dark-induced autophagy (Nagel *et al*, 2017). To shed light on the enigmatic and versatile function of SH3P2, we used VIGS in *N. benthamiana* targeting both endogenous isoforms *NbSH3P2a* and *b*. Silencing had no obvious phenotypic effect on plants, and silencing efficiency was assessed by qPCR (Appendix Fig S9A and B). Subsequent immunoblot analysis revealed that in comparison to the pTRV2-GFP control, SH3P2 VIGS plants displayed an accumulation of ATG8 protein levels, similar results to that reported by Zhuang *et al,* 2013 (Appendix Fig S9C). To corroborate this finding, we transiently expressed GFP-ATG8e in control and silenced plants and monitored autophagosome formation upon AZD8055 treatment, a TOR inhibitor, and autophagy activator. The number of autophagosomes increased upon AZD8055 treatment in both plants but was significantly less in SH3P2 VIGS plants when treated with ConA (Appendix Fig S9D). This indicates that downregulation of SH3P2 in *N. benthamiana* impairs the maturation of autophagosomes and hence autophagic degradation. Indeed, using confocal microscopy and GFP-ATG8e labeling, we observed aberrant autophagosomal structures in VIGS SH3P2 plants, which might explain why autophagy is not entirely functional anymore. These data suggest that SH3P2 might be required during later steps of autophagosome formation, as autophagosomal structures seem to be normal during autophagy induction with AZD8055. VIGS in *N. benthamiana roq1* plants and subsequent bacterial growth measurements with *Xcv* and *Xcv ΔxopL* revealed that pTRV2-*SH3P2* plants are more susceptible to *Xcv* and display slightly enhanced symptom development (Fig 3F Appendix Fig S9E). Essentially, partially reduced growth of *Xcv ΔxopL* was rescued in SH3P2-silenced plants strengthening our findings that XopL acts on *SH3P2* to suppress host autophagy and promote disease.

XopL mediates proteasomal degradation of SH3P2 via its E3 ligase activity

Our results so far suggest that XopL might manipulate autophagy by interacting with and degrading the autophagy component SH3P2. Previous research on SH3P2 revealed that RNAi-mediated downregulation of AtSH3P2 affects the autophagy pathway (Zhuang *et al*, 2013). To understand how SH3P2 is degraded by XopL we analyzed the degradation mechanisms in more detail. Firstly, degradation of AtSH3P2 by XopL was dependent on a functional proteasome, as

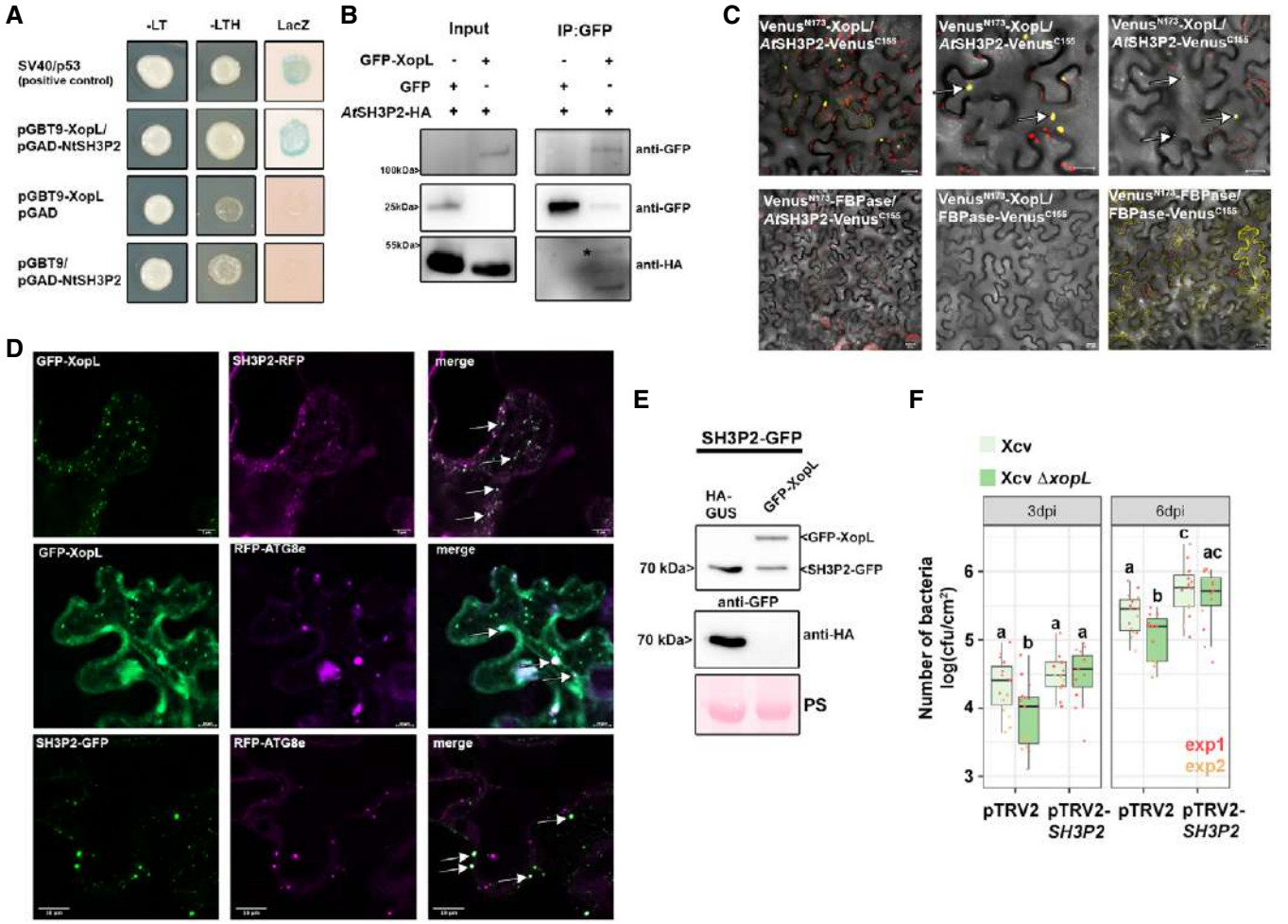

Figure 3. XopL interacts with and degrades SH3P2 and boosts *Xcv* virulence.

A Interaction of XopL with SH3P2 in yeast two-hybrid assays. XopL fused to the GAL4 DNA-binding domain was expressed in combination with SH3P2 fused to the GAL4 activation domain (AD) in yeast strain Y190. Cells were grown on selective media before a LacZ filter assay was performed. pSV40/p53 served as a positive control, while the empty AD or BD vector served as a negative control. NtSH3P2 = *Nicotiana tabacum* SH3P2. –LT = yeast growth on medium without Leu and Trp, –HLT = yeast growth on medium lacking His, Leu, and Trp, indicating expression of the HIS3 reporter gene. LacZ—activity of the lacZ reporter gene.

B Coimmunoprecipitation of GFP-XopL with AtSH3P2-HA. GFP-XopL or GFP was transiently coexpressed with AtSH3P2-HA in leaves of *N. benthamiana*. After 48 h, total proteins (Input) were subjected to immunoprecipitation (IP) with GFP-Trap beads, followed by immunoblot analysis using either anti-GFP or anti-HA antibodies. GFP blot was split for visualization purpose. AtSH3P2 = *Arabidopsis thaliana* SH3P2. Two repetitions with similar results have been conducted.

C Visualization of protein interactions *in planta* by the bimolecular fluorescence complementation assay. Yellow fluorescent protein (YFP) confocal microscopy images show *Nicotiana benthamiana* leaf epidermal cells transiently expressing Venus^{N173}-XopL in combination with AtSH3P2-Venus^{C155}. A positive control showing the dimerization of fructose-1,6-bisphosphatase (FBPase) within the cytosol. White arrows indicate the reconstitution of YFP fluorescence. The red structures indicate autofluorescence of chloroplasts. The combination of Venus^{N173}-XopL with FBPase-Venus^{C155} or Venus^{N173}-FBPase with AtSH3P2-Venus^{C155} does not induce YFP fluorescence and serves as negative controls. Bars = 20 μm.

D Colocalization analysis of GFP-XopL with SH3P2-RFP, RFP-ATG8e, and RFP-ATG8g in *N. benthamiana* leaves. Imaging was performed 2 days after transient expression and images represent single confocal planes from abaxial epidermal cells (scale bars = 20 μm and 10 μm, lower panel). White arrows indicate the colocalization of GFP and RFP signals. The experiment was repeated twice with similar results.

E Total proteins were extracted at 48 hpi with *A. tumefaciens* harboring the respective GFP-XopL, HA-XopL, and SH3P2-GFP expression constructs. SH3P2-GFP protein levels (lower band) were detected using an anti-GFP antibody. Expression of the XopL was verified using an anti-HA or anti-GFP antibody. Expression of GUS-HA served as a control. Ponceau S staining serves as a loading control. The experiment was repeated three times with similar results.

F Growth of Xcv *and* Xcv *ΔxopL* strains in *roq1 N. benthamiana* plants silenced for SH3P2 (pTRV2-*SH3P2*) compared with control plants (pTRV2). Leaves were dip-inoculated with a bacteria suspension at OD_{600} = 0.2, and bacteria were quantified at 3 and 6 dpi. Experimental repeats are indicated by data points in red (n = 8) and yellow (n = 6) data points. Middle horizontal bars of boxplots represent the median, the bottom and top represent the 25th and 75th percentiles, and whiskers extend to at most 1.5 times the interquartile range. Different letters indicate statistically significant differences (P < 0.05) as determined by one-way ANOVA.

Source data are available online for this figure.

chemical inhibition of the proteasome with MG132 partially restored AtSH3P2-GFP protein levels (Fig 4A). Additionally, we identified that SH3P2 undergoes proteasomal degradation also in the absence of XopL, as its abundance increases during proteasome inhibition (Appendix Fig S10A). Changes in SH3P2 protein levels in the presence of XopL were due to post-transcriptional events, as gene

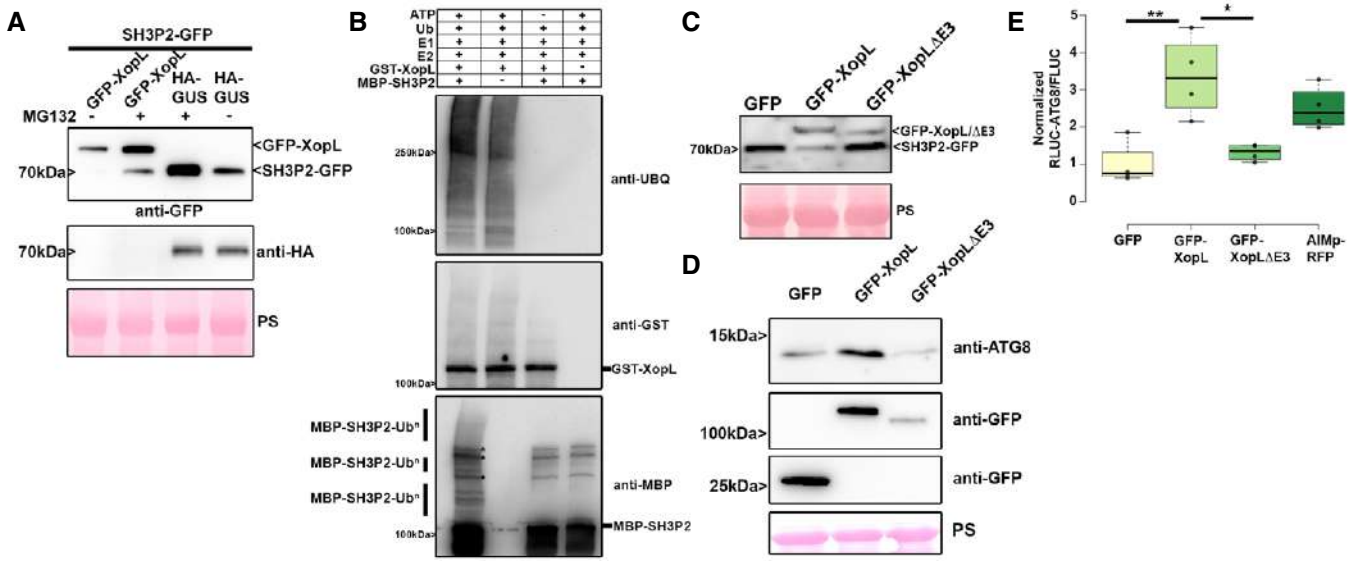

Figure 4. XopL mediates the proteasome degradation of SH3P2 via its E3 ligase activity.

A SH3P2-GFP was transiently coexpressed together with GUS-HA and GFP-XopL in *N. benthamiana* using agroinfiltration. At 42 hpi, 200 μM MG132 was infiltrated into *A. tumefaciens*-inoculated leaves, and leaf material was collected at 48 hpi. Expression of SH3P2-GFP (lower band) and GFP-XopL (upper band) was detected using an anti-GFP antibody. GUS-HA expression was confirmed with an anti-HA antibody. Ponceau S staining serves as a loading control. The experiment was repeated three times with similar results.

B *In vitro* ubiquitination assay reveals ubiquitination of SH3P2 by XopL. GST-XopL and MBP-SH3P2 were tested using the *Arabidopsis* His-AtUBA1 and His-AtUBC8. Lanes 2–4 are negative controls. Proteins were separated by SDS–PAGE and detected by immunoblotting using the indicated antibodies. Asterisks indicate bands that are not ubiquitinated and present in controls. The experiment was repeated twice with similar results.

C SH3P2-GFP was transiently coexpressed together with GFP, GFP-XopL, and GFP-XopL ΔE3 in *N. benthamiana* using agroinfiltration. GFP protein levels were detected with an anti-GFP antibody. Ponceau S staining serves as a loading control. The experiment was repeated three times with similar results.

D Immunoblot analysis of ATG8 protein levels in *N. benthamiana* plants transiently expressing GFP-XopL, GFP-XopL ΔE3, or GFP control at 2 dpi. Expression of binary constructs was verified with an anti-GFP antibody. GFP blot was split for visualization purpose. Ponceau staining (PS) served as a loading control. The experiment was repeated twice with similar results.

E RLUC-ATG8a constructs were coexpressed with internal control FLUC in *N. benthamiana*. GFP-XopL, GFP-XopL ΔE3, or GFP control were co-infiltrated together with RLUC/FLUC mixture. *Renilla* and *Firefly* luciferase activities were simultaneously measured in leaf extracts at 48 hpi using the dual-luciferase system. Values represent the ratio of RLUC-ATG8a and FLUC activities ($n = 4$). Middle horizontal bars of boxplots represent the median, the bottom and top represent the 25th and 75th percentiles, and whiskers extend to at most 1.5 times the interquartile range. Statistical significance (*$P < 0.5$, **$P < 0.01$) was revealed by the Student's *t*-test. The experiment was repeated 3 times.

Source data are available online for this figure.

expression of SH3P2 is rather induced upon transient expression of XopL in *N. benthamiana* (Appendix Fig S10B). To assess whether the proteasome-mediated degradation of SH3P2 was directly mediated by XopL and its E3 ligase activity, we performed an *in vitro* ubiquitination assay. In the presence of all required components of the E1-E2-E3 system, we observed that GST-XopL ubiquitinated MBP-AtSH3P2, which is indicated by a laddering pattern, leading to larger sized molecular species of MBP-AtSH3P2, when probed with the anti-MBP antibody (Fig 4B). To address whether E3 ligase activity of XopL is crucial in the SH3P2-dependent modulation of host autophagy, we employed the triple point mutant of $XopL_{H584A\ L585A\ G586E}$ (hereafter referred to as XopL ΔE3), lacking E3 ligase activity (Singer *et al*, 2013; Erickson *et al*, 2018). Transient coexpression revealed that XopL requires its E3 ligase activity to trigger the degradation of AtSH3P2 in *N. benthamiana* (Fig 4C). This was not due to an altered localization of XopL ΔE3, as it still colocalizes with AtSH3P2 upon transient expression in *N. benthamiana* (Appendix Fig S11A). In addition, XopL ΔE3 was also unable to ubiquitinate SH3P2 in an *in vitro* ubiquitination assay (Fig S11B). Consistent with its inability to degrade SH3P2 *in planta*, XopL ΔE3 did not lead to an increase in ATG8 protein levels and suppression of autophagy responses in the quantitative luciferase autophagy assay (Fig 4D and E). Protein expression for the luciferase autophagy assay was verified via immunoblot (Appendix Fig S11C). XopLΔE3 is also more unstable than XopL WT, suggesting that its E3 ligase activity is crucial to maintaining its stability, likely through its function in subverting autophagy (Fig 4F). Taken together, our findings support the notion that the E3 ligase activity of XopL and its ability to directly ubiquitinate and degrade AtSH3P2 promote suppression of autophagy.

NBR1/Joka2-mediated selective autophagy degrades ubiquitinated XopL

While we investigated the effect of *Xcv* and its T3E XopL on host autophagy, we noticed that NBR1/Joka2 responds at both transcript and protein levels during infection (Fig 1B and D). We also observed that XopL protein accumulated under ConA treatment (Fig 2C, Appendix Fig S5A), hinting that it was subject to autophagic degradation. Previous studies imply that NBR1/Joka2

mediates xenophagy by degrading viral particles and that Joka2 is required for immunity against bacteria and *Phytophthora* (Dagdas *et al*, 2016; Hafren *et al*, 2018; Üstün *et al*, 2018). However, the role of NBR1-mediated xenophagy in plant–*Phytophthora* and plant–bacteria interactions remains unknown. Plant NBR1 is a hybrid of the mammalian autophagy adaptors NBR1 and p62/SQSTM1 (Svenning *et al*, 2011). The latter was shown to mediate xenophagy of *Mycobacterium tuberculosis* (Mtb) by binding to the Mtb ubiquitin-binding protein Rv1468c and ubiquitin-coated *Salmonella enterica* in human cells (Zheng *et al*, 2009; Chai *et al*, 2019).

To corroborate our previous finding that XopL accumulates when autophagy is perturbed, we coexpressed GFP-XopL with autophagy inhibitor AIMp-RFP in *N. benthamiana leaves*. Immunoblot analysis revealed that indeed XopL also accumulates in the presence of autophagy inhibitor AIMp (Fig 5A). As NBR1/Joka2 bodies were substantially induced during *Xcv* infection (Appendix Fig S6), and block of autophagic degradation using ConA caused accumulation of GFP-XopL in vacuoles of *A. thaliana* (Appendix Fig S12), we decided to examine whether XopL and NBR1/Joka2 associate *in planta*. Intriguingly, we discovered that XopL colocalizes with NBR1/Joka2 in puncta (Fig 5B). The association of both proteins was determined using Förster resonance energy transfer by fluorescence lifetime imaging microscopy (FRET-FLIM). Only in the presence of RFP-XopL a significant reduction of 0.1 ns in the lifetime of the donor Joka2 was observed in comparison to coexpression of RFP or donor alone (Fig 5C). This reduction in a lifetime is similar to what was achieved with the positive control GFP-Joka2/RFP-ATG8e. These findings prompted us to investigate whether XopL might be targeted by NBR1/Joka2 for autophagic degradation, similar to insoluble ubiquitinated protein aggregates (Zhou *et al*, 2013). Performing co-IP experiments with GFP-XopL, we discovered that XopL associates with NBR1/Joka2 *in planta* (Fig 5D), confirming the results of our FRET-FLIM and colocalization studies. To address whether E3 ligase activity of XopL is required for interaction, we employed XopL ΔE3, lacking E3 ligase activity. Co-IP experiments revealed that XopL ΔE3 was also able to pull down NBR1/Joka2 after transient expression in *N. benthamiana* (Fig 5E). This suggests that NBR1/Joka2 may not mediate the degradation of a complex containing XopL and its ubiquitinated target protein(s), but rather targets XopL for autophagic degradation. Given the fact that XopL is degraded by autophagy and associates with NBR1/Joka2, we next analyzed the stability of XopL in Joka2-silenced *N. benthamiana* plants. Silencing of NBR1/Joka2 was confirmed by qPCR (Appendix Fig S13A). Indeed, we could observe an increase in GFP-XopL protein abundance (Fig 5F), but not for GFP (Appendix Fig S13B), in pTRV2-Joka2 plants, arguing for a direct participation of NBR1/Joka2 in XopL turnover. To assess whether this might impact the pathogenicity of *Xcv* we performed bacterial growth assays using the pTRV2-Joka2 plants. Increased growth at 3 dpi of *Xcv ΔxopQ* in *N. benthamiana* plants silenced for *Joka2* strengthened our finding that Joka2 is having antibacterial effects on *Xcv* early on during infection (Fig 5G). As NBR1/Joka2 or p62 recognize their cargos by their ability to bind ubiquitinated substrates, we hypothesized that XopL might be ubiquitinated *in planta*. To test this, we transiently

Figure 5. XopL is ubiquitinated in planta and degraded by NBR1-mediated selective autophagy.

A GFP-XopL was coexpressed with GFP or AIMp-RFP. Proteins were separated by SDS–PAGE and detected by immunoblotting using the indicated antibodies. GFP blot was split for visualization purpose. Ponceau staining (PS) served as a loading control. The experiment was repeated three times with similar results.

B Colocalization of RFP-XopL with GFP-Joka2 in *N. benthamiana* leaves. Imaging was performed 2 days after transient expression, and images represent single confocal planes from abaxial epidermal cells (bars = 20 μm). The experiment was repeated twice with similar results.

C FRET-FLIM measurements of GFP-Joka2 and RFP-XopL in *N. benthamiana* leaves. The freeRFP construct served as a negative control and RFP-ATG8E (n = 9) as a positive control. Scattered points show individual data points, and color indicates biological repeats. The lifetime (in ns) of GFP-Joka2 (donor, n = 41) was significantly reduced in the presence of RFP-XopL (n = 40) but not in the presence of freeRFP (n = 35). Middle horizontal bars of boxplots represent the median, the bottom and top represent the 25th and 75th percentiles, and whiskers extend to at most 1.5 times the interquartile range. Significant differences were calculated using the Wilcoxon rank-sum test, with significantly different groups denoted by different letters. The experiment was repeated three times with similar results.

D Immunoprecipitation (IP) of GFP-XopL reveals the association with NBR1. Immunoblots of input and IP samples from *N. benthamiana* plants transiently expressing GFP or GFP-XopL were probed with anti-GFP and anti-NBR1 antibodies. GFP blot was split for visualization purpose.

E Immunoprecipitation (IP) of GFP-XopL and GFP-XopL ΔE3 reveals association with NBR1. Immunoblots of input and IP samples from *N. benthamiana* plants transiently expressing GFP, GFP-XopL, and GFP-XopL ΔE3 were probed with anti-GFP and anti-NBR1 antibodies. GFP blot was split for visualization purpose.

F GFP-XopL was transiently expressed in pTRV2, pTRV2-Joka2, and *N. benthamiana* WT plants. Expression of binary constructs was verified with an anti-GFP antibody. Joka2 silencing was verified using an anti-NBR1 antibody. Ponceau staining (PS) served as a loading control. The experiment was repeated twice with similar results.

G Growth of Xcv *ΔxopQ* in *N. benthamiana* plants silenced for *Joka2* (pTRV2-Joka2) compared with control plants (pTRV2). Leaves were dip-inoculated with a bacteria suspension at OD_{600} = 0.2, and bacteria were quantified at 3 and 6 dpi. Red, blue, and green data points represent repeats of the experiments. Middle horizontal bars of boxplots represent the median, the bottom and top represent the 25th and 75th percentiles, and whiskers extend to at most 1.5 times the interquartile range. Significant differences were calculated using the Student's t-test and are indicated by $^{**}P < 0.01$. The experiment was repeated three times with similar trends.

H GFP-XopL and GFP-XopL ΔE3 were transiently expressed in *N. benthamiana*. RFP-AIMp was co-infiltrated to stabilize both XopL variants. Samples were taken at 48 hpi, and total proteins (Input) were subjected to immunoprecipitation (IP) with GFP-Trap beads, followed by immunoblot analysis of the precipitates using either anti-GFP or anti-ubiquitin antibodies. GFP served as a negative control. RFP-AIMp expression was verified by an anti-RFP antibody. GFP blot was split for visualization purpose. Asterisk indicates the GFP-XopL full-length protein. The experiment was repeated three times with similar results.

I GFP-XopL was transiently expressed in *N. benthamiana*. Samples were taken at 48 hpi, and total proteins (Input) were subjected to immunoprecipitation (IP) with the ubiquitin pan selector, followed by immunoblot analysis of the precipitates using either anti-GFP or anti-ubiquitin antibodies. GFP served as a control. Asterisk indicates the GFP-XopL full-length protein. GFP blot was split for visualization purpose. The experiment was repeated two times with similar results.

J Immunoblot analysis GFP-XopL and GFP-$XopL_{K191A}$ at 1 and 2 dpi using an anti-GFP antibody. Ponceau staining (PS) served as a loading control. The experiment was repeated three times with similar results.

K HA-XopL and GFP-Joka2 and their variants were transiently expressed in *N. benthamiana*. Samples were taken at 48 hpi, and total proteins (Input) were subjected to immunoprecipitation (IP) with GFP-Trap beads, followed by immunoblot analysis of the precipitates using anti-GFP, anti-ubiquitin, and anti-NBR1 antibodies. GFP served as a control.

Source data are available online for this figure.

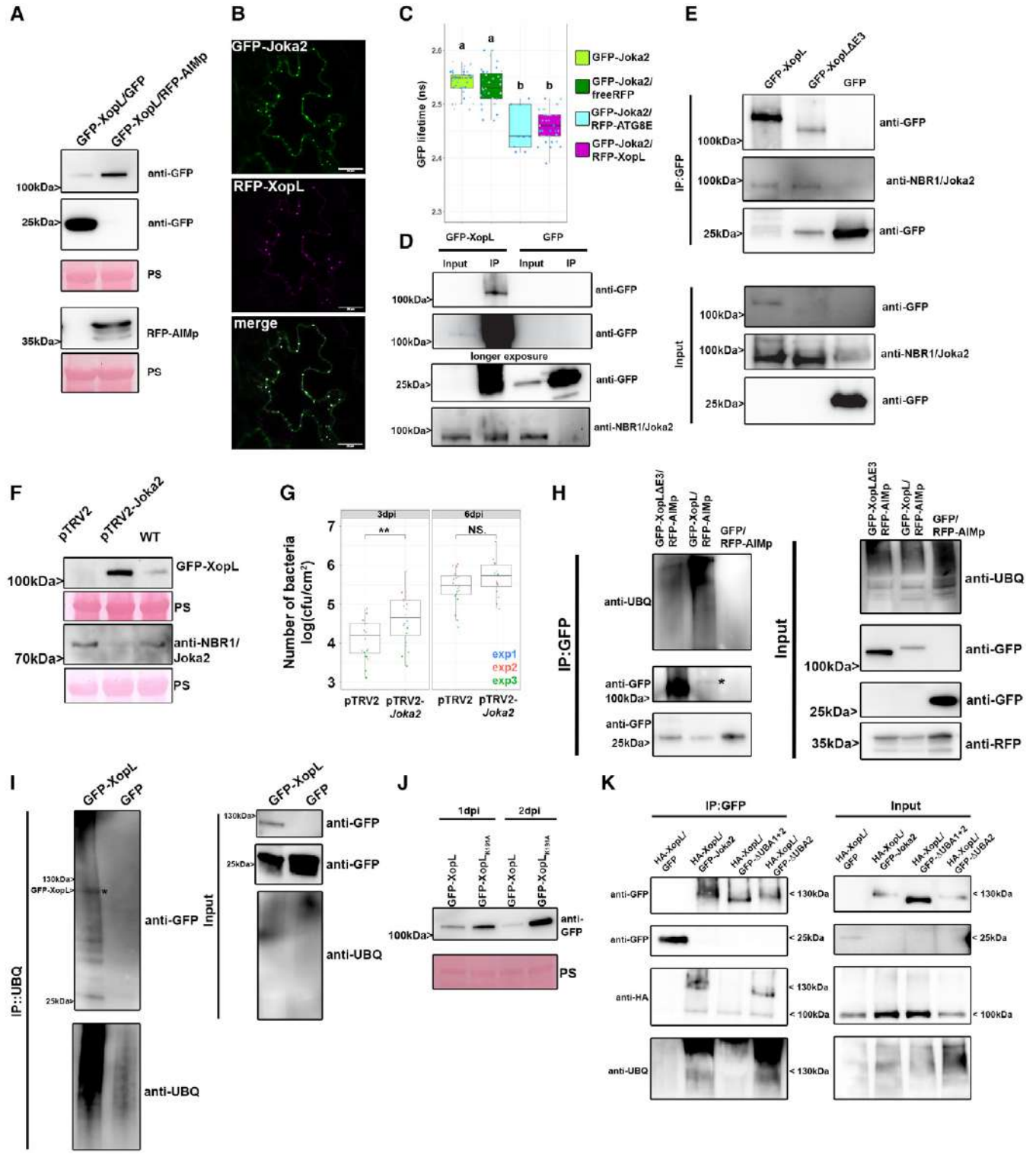

Figure 5.

expressed GFP-XopL in *N. benthamiana* leaves and then immunoprecipitated GFP-XopL from leaf protein extracts. Ubiquitinated GFP-XopL was detected using immunoblotting. GFP-XopL, but not the GFP control, displayed polyubiquitination *in planta*, while GFP-XopL ΔE3 showed reduced polyubiquitination (Fig 5H). To further confirm the ubiquitination of XopL, we purified total ubiquitinated proteins using the ubiquitin pan selector, which is based on a high-affinity single-domain antibody that is covalently immobilized on cross-linked agarose beads. We detected a smear of high molecular weight bands including the full-length XopL protein (Fig 5I), which

was strongly enhanced when we coexpressed with AIMp but absent in the GFP control (Appendix Fig S14).

To identify ubiquitinated residues within the XopL protein, we immunoprecipitated GFP-XopL from *N. benthamiana* leaves transiently expressing GFP-XopL and performed mass spectrometry (MS) analysis. *In planta*, MS analysis revealed one potential ubiquitination site at lysine 191 (K191) in the N-terminal part of XopL (Appendix Fig S15A). For plant E3 ligases such as PUB22, it has been reported that its stability is dependent on its autoubiquitination activity (Furlan *et al*, 2017). Using MBP-XopL in an *in vitro* ubiquitination assay we confirmed self-ubiquitination (Appendix Fig S15B), indicated by the presence of higher molecular weight bands probing with an anti-MBP antibody. Performing LC-MS/MS we did detect the same ubiquitination (K191) site identified *in planta* when we analyzed *in vitro* ubiquitination samples containing GST-XopL (Appendix Fig S15C). Additionally, an *in vitro* self-ubiquitination assay comparing XopL WT to its K191A mutant counterpart shows that K191A displays less intensity on its high molecular weight smear, suggesting that K191A is less ubiquitinated in this assay (Appendix Fig S16A). This strongly argues for K191A being an autoubiquitination site of XopL. This is strengthened by our findings showing that the mutation of lysine 191 to alanine (K191A) rendered the XopL K191A more stable than WT XopL (Fig 5J) without altering its subcellular localization (Appendix Fig S16B). Changes in XopL vs. K191A protein levels were due to post-transcriptional events, as gene expression of XopL and XopL K191A are similar upon transient expression in *N. benthamiana* (Appendix Fig S16C) but did not abolish ubiquitination of XopL and association with autophagic machinery as shown by co-IP with NBR1/Joka2 (Appendix Fig S16D and E). However, we cannot rule out trans-ubiquitination by plant E3 ligases, as XopL ΔE3 still interacts with NBR1 and is still ubiquitinated in *planta*. Immunoblot analysis also suggests that XopL ΔE3 is less able to block autophagy, as it is more unstable compared with XopL WT (Appendix Fig S17A) and is also degraded by autophagy (Appendix Fig S17B). This might indicate the presence of additional ubiquitination sites in XopL. Taken together, our results suggest that XopL is ubiquitinated *in planta* and subjected to NBR1/Joka2-dependent selective autophagy.

To assess whether ubiquitinated XopL is recognized by NBR1/Joka2 we performed co-IP experiments with different NBR1/Joka2 variants lacking one or both UBA domains that are required to bind to polyubiquitin chains (Svenning *et al*, 2011). ΔUBA2 is likely able to still bind polyubiquitin chains due to the presence of the UBA1 domain, whereas ΔUBA1+2 is unable to bind polyubiquitin chains. All Joka2 variants co-immunoprecipitate full-length HA-XopL, indicating that the XopL-Joka2 interaction can be ubiquitin-independent (Fig 5K). However, we also detected a higher molecular weight band of HA-XopL, which could be an indication of polyubiquitinated XopL. The presence of this higher Mw smear seems to be dependent on a functional UBA domain, as it is only observed during interaction with Joka2 WT and its ΔUBA2 mutant (Fig 5K). Our results indicate that ubiquitin-dependent and ubiquitin-independent mechanisms drive the interaction of XopL and Joka2.

Discussion

Here, by studying *Xanthomonas*–host interactions, we revealed a complex multi-layered regulatory role of autophagy in plant immunity. We demonstrate that *Xanthomonas* can subvert plant autophagy, which is achieved by the T3E XopL. Through its E3 ligase activity, XopL can ubiquitinate and degrade SH3P2, an autophagy component functioning in autophagosome biogenesis. This in turn dampens autophagy to boost the virulence of Xanthomonas. However, the same T3E is targeted by NBR1/Joka2-triggered selective autophagy/xenophagy, which constitutes a novel form of plant defense mechanism (Appendix Fig S18A and B). The mutual targeting of pathogen effector XopL and plant protein SH3P2 unveils how different layers of regulation contribute to autophagy pathway specificity during host–bacteria interactions.

Autophagy in host–immune interactions

In animals, several pathogenic bacteria have been identified to modulate the autophagy pathway to their own benefit (Huan & Brummel, 2014). Many intracellular animal pathogenic bacteria can be eliminated by autophagy, while others (such as *Shigella*, *Yersinia*, and *Listeria*) are able to exploit autophagy to increase their pathogenicity (Huang & Brumell, 2014). In plants, several studies have highlighted that pathogens manipulate the autophagy pathway (Leary *et al*, 2019). More specifically, the plant pathogenic bacterium *Pseudomonas syringae* pv. *tomato* (*Pst*) has been shown to utilize effectors to modulate autophagic degradation (Üstün *et al*, 2016, 2018). With *Xcv*, we have identified another plant pathogenic bacterium that modulates autophagy, similar to *Pst*, in an effector-dependent manner. Although both pathogens have the same habitat and hemibiotrophic lifestyle, they act in different ways on the autophagy pathway. For *Xcv* inhibition of the autophagy pathway is crucial to maintain pathogenicity while *Pst* activates it for its own benefit (Üstün *et al*, 2018). Previously, it has been reasoned that autophagy activation might be essential to maintain plant viability and lifespan (Hafren *et al*, 2018). However, autophagy may not be required for this during *Xcv* infection, as it has been shown that T3Es XopD and XopJ are able to prolong the biotrophic phase by other mechanisms (Kim *et al*, 2008; Üstün *et al*, 2013). As such, autophagy is dispensable for the virulence of *Xcv* and actively dampened to boost virulence and partially prevent xenophagy of XopL. Within the realm of xenophagy, the degradation of effectors by autophagy can be considered as a form of "effectorphagy." Perturbation of general autophagy is achieved by degrading SH3P2 through the action of T3E XopL. SH3P2 was first identified as a novel autophagy component, stimulating autophagosome formation during nitrogen starvation and BTH-triggered immune responses (Zhuang *et al*, 2013). Later studies also showed that SH3P2 plays a key role in membrane tubulation during cell plate formation (Ahn *et al*, 2017) and clathrin-mediated endosomal sorting and degradation, with no effect on dark-induced autophagy (Nagel *et al*, 2017). Our findings that silencing of SH3P2 from *N. benthamiana* impairs autophagy and somewhat promotes pathogenicity sheds further light on its diverse functions. However, the effects of XopL on SH3P2 and increasing virulence of *Xcv* might not only be attributed to its function in autophagy. Because endocytic trafficking also plays a major role in plant immunity (Gu *et al*, 2017), it is likely that XopL has a function beyond autophagy to impair plant defense mechanisms. This is also supported by the fact that XopL can reduce PTI responses (Singer *et al*, 2013), which is not due to its function in autophagy, as autophagy deficiency has no impact on PTI responses

(Lenz *et al*, 2011). Previously, XopL was also shown to impact stromule formation by localizing to microtubules (Erickson *et al*, 2018), which was shown only for the XopL version lacking E3 ligase activity. Although we do not see any microtubule localization of the XopL ΔE3 version, XopL might affect stromule formation as they are thought to be recognized by autophagic membranes prior to autophagic degradation (Marshall & Vierstra, 2018).

Role of xenophagy in immunity

One of the best-studied selective autophagy receptors across kingdoms is NBR1/p62 that plays a central role in xenophagy and degradation of protein aggregates (Kirkin *et al*, 2009; Svenning *et al*, 2011). Its role in plant immune responses has been shown by the involvement of NBR1/Joka2-mediated selective autophagy in restricting pathogen growth or disease progression during *P. infestans* or *Pst* infection (Dagdas *et al*, 2016; Üstün *et al*, 2018). In animals, p62, the counterpart of plant NBR1, functions to mediate xenophagy, which has been also described for NBR1 in plants in a plant–virus infection context but not for other plant pathogens (Hafren *et al*, 2017, 2018). Our analysis provides the first evidence that like viral proteins, bacterial effector XopL constitutes a target of NBR1-mediated selective autophagy. This sheds light on previous findings about the role of NBR1/Joka2 in plant immunity and makes it a central hub in plant–microbe interactions. Consequently, XopL developed the ability to suppress autophagy, to boost the virulence of Xcv but does XopL suppress autophagy to an extent to escape its own degradation? Indeed, treating plants with ConA or expressing AIMp still stabilize XopL protein levels, indicating that the effect of XopL on the autophagy pathway is either very specific or not sufficient to shut down the pathway completely. It is also possible that XopL is degraded by other additional mechanisms such as endocytosis or proteasome-mediated degradation as it is most likely ubiquitinated by plant E3 ligases. In line with our observations on the autophagy pathway is that the ability of XopL to suppress the autophagy is still less than the recently discovered autophagy inhibitor AIMp (Pandey *et al*, 2021). This is also in line with the fact that loss of SH3P2 is only partially suppressing autophagy formation (Zhuang *et al*, 2013) while silencing of ATG7 or expression of AIMp result in a complete block of autophagy. Currently, we also do not know whether SH3P2 might only affect a subset of ATG8 isoforms to facilitate autophagosome formation. Thus, it might be also possible that the NBR1/Joka2-selective autophagy pathway might involve ATG8 isoforms that do not require SH3P2.

To date, it has not been reported that bacterial effectors in animals and plants are removed by selective autophagy as an antimicrobial response. Interestingly, the *Salmonella* effector SseL, which inhibits selective autophagy to abolish p62-dependent degradation of *Salmonella*, was also found to interact with p62 (Mesquita *et al*, 2012). This might suggest the possibility that SseL might also have been an autophagy target before it acquired its function to block this pathway via its deubiquitinase activity (Mesquita *et al*, 2012). We hypothesize that NBR1/p62 might have evolved to have a function in antibacterial autophagy by triggering xenophagy of bacterial molecules as an alternative strategy to degrade entire intracellular bacteria. This may have happened for the function of NBR1 in plants, as fungal and oomycete pathogens and Gram-negative bacteria reside in the extracellular space. Animal pathogens also occupy the extracellular space, before entering the host cell. In the case of *Salmonella*, it first needs to inject bacterial effectors via its SPI-1 T3SS to establish internalization and its replication niche (Lou *et al*, 2019). It is therefore tempting to speculate that these effectors may be targeted by selective autophagy mechanisms as an early defense mechanism of the immune system. Similar to XopL, several of the SPI-1 T3Es can mimic E3 ligases and/or are ubiquitinated in the host cell (Kubori & Galan, 2003), making them potential targets for NBR1/p62-mediated selective autophagy. Indeed, T3Es SopA and SopE have been reported to be degraded through the proteasome (Kubori & Galan, 2003; Zhang *et al*, 2005). A possible degradation by autophagy was not investigated in these studies. Our results also suggest that XopL is targeted by a host E3 ligase for degradation as the XopL variant lacking E3 ligase activity is still ubiquitinated *in planta* although to a lesser extent. Several E3 ligases have been implicated in plant–microbe interactions, which opens up the possibility that they may target microbial proteins (Furlan *et al*, 2012). Although the recognition of XopL by NBR1/Joka2 seems to be partially ubiquitin-dependent another pool of XopL associates with NBR1/Joka2 in a ubiquitin-independent manner. Similar ubiquitin-independent mechanisms have been reported previously for plant–virus interactions (Hafren *et al*, 2017). Future studies will identify the specificity of this mechanism.

Although plant pathogenic bacteria possess T3Es that are implicated in the host ubiquitin system, to date there is no evidence that they might be ubiquitinated in the host. In addition, we identified that XopL undergoes self-ubiquitination. In this scenario, it is tempting to speculate whether the self-ubiquitination activity of XopL attracts it to the autophagy pathway. Although the biological significance of K191 remains elusive, it might still have regulatory functions. To date, the self-ubiquitination of E3 ligases has been assigned as a mechanism of self-regulation through which their activity is controlled (Furlan *et al*, 2017). In the case of bacterial T3Es that mimic E3 ligases, it might be a strategy to trick degradation systems. Other post-translational modifications of T3Es such as phosphorylation of AvrPtoB have been found to be crucial for its virulence function (Lei *et al*, 2020), which might be also the case for the ubiquitination of XopL. Our results suggest that ubiquitinated XopL is targeted for autophagic degradation that might be indeed a strategy to recruit different autophagy components. Indeed, we can find high conservation of K191 in several other XopL-like T3Es across different Xanthomonas species (Appendix Fig S19A and B), which would be in favor of the proposed hijacking hypothesis. However, the fact that the K191 variant is still ubiquitinated *in planta* and associates with NBR1, and other autophagy components are not in favor of this hypothesis. The discovery of other alternative ubiquitination sites in XopL will help us to unravel why XopL undergoes self-ubiquitination and how this might contribute to its virulence.

Taken together, we provide a primary example where a bacterial effector subverts host autophagy to downregulate host immunity, and the autophagic machinery in turn targets the same bacterial effector for degradation. Thus, this reveals a complex multi-layered role of autophagy particularly in the context of immunity and disease. Additionally, XopL possesses self-ubiquitination activity, which some evidence we have uncovered here suggest that this functions to hijack the host autophagy system.

Material and Methods

Plant material and growth conditions

Wild-type plants were *Arabidopsis thaliana* ecotype Columbia (Col-0) and *Nicotiana benthamiana*. *Arabidopsis* plants were grown on soil under short-day conditions (8/16 h light/dark cycles) in a growth chamber or for maintenance and crossings under long-day conditions (16/8 h light/ dark cycles) in a growth room with the light intensity of 150 μE, 21°C, and 70% relative humidity, respectively. *N. benthamiana* plants were grown under long-day conditions 16/8 h light/dark cycles, 21°C, and 70% relative humidity.

Plasmid construction

For transient expression experiments, the coding region of XopL, AtSH3P2, or SlJoka2 were cloned into pENTR/D-TOPO and subsequently recombined into pUBN-DEST-GFP or RFP (Grefen *et al*, 2010), pGWB614/5 (Nakagawa *et al*, 2007), pMAlc2, pDEST15. The RFP-ATG8E/G, GFP-ATG8e, RFP-NBR1, RLUC-ATG8, RLUC-NBR1, XopD-GFP, XopJ-GFP, pTRV2-Joka2, pTRV2-ATG7 constructs were described previously (Üstün *et al*, 2013, 2018). All binary plasmids were transformed into Agrobacterium tumefaciens strain C58C1 and infiltration of *N. benthamiana* was done at the four-to six-leaf stage. Stable *Arabidopsis* transformation was performed using the floral dip method (Clough & Bent, 1998).

Transient expression in *Nicotiana benthamiana* by agrobacterium-mediated leaf infiltration

Transient expression was performed as described previously (Üstün *et al*, 2018).

Immunoprecipitation

GFP pull-down assays were performed as previously described (Üstün *et al*, 2018). Pulldown of ubiquitinated proteins was performed according to the manufacturer's instructions (NanoTag Biotechnologies).

In vitro pull-down

In vitro pull-down was performed as previously described (Üstün *et al*, 2013).

Dual-luciferase assay

A dual-luciferase assay was performed as described previously (Üstün *et al*, 2018).

Virus-induced gene silencing

VIGS was performed as described previously (Üstün *et al*, 2013).

Bacterial growth conditions

Agrobacterium tumefaciens, Agrobacteria strain C58C1 was grown in LB Hi-Salt (10 g/l sodium chloride, 10 g/l tryptone, 5 g/l yeast extract) with 100 μg/ml rifampicin at 28°C. The cultures were supplemented with the appropriate antibiotics for those harboring plasmids. Xcv strain 85-10 was grown in NYG media (0.5% peptone, 0.3% yeast extract, 2% glycerol) with 100 μg/ml rifampicin at 28°C.

Construction of Xcv Δ*xopL* and Δ*xopQ* null mutants

To construct Xcv 85-10 *xopL* and *xopQ* deletion mutants, the 1.7-kb upstream and downstream regions of the xopL or xopQ gene were PCR amplified using Xcv 85-10 genomic DNA as a template and cloned into pLVC18 linearized with EcoRI (New England Biolabs) using Gibson assembly. The plasmid was introduced into Xcv 85-10 by triparental mating. Xcv transconjugants were analyzed by PCR to confirm that homologous recombination occurred at the xopL or XopQ locus.

Constructs for Xcv Δ*xopL* complementation analysis

To construct the xopL gene with a 0.3-kb promoter region in a broad host range vector, the 0.3-kb promoter-xopL gene was PCR amplified using Xcv 85-10 genomic DNA as a template and cloned into pBBR1MCS-2 (Kovach *et al*, 1995) linearized with EcoRV (New England Biolabs) using Gibson assembly. The plasmid was introduced into Xcv 85-10 Δ*xopL* by triparental mating.

Bacterial infection

Xcv carrying a deletion mutation of XopQ (Xcv *ΔxopQ*), or of HrcN (Xcv Δ*hrcN*), or of both XopQ and XopL (Xcv *ΔxopQ ΔxopL*) were used to infect wild-type *N. benthamiana*. Xcv were grown overnight in NYG with appropriate antibiotics at 28°C with shaking. Bacteria were diluted to OD_{600} = 0.2 for dual-luciferase assays, immunoblot analysis of NBR1, ATG8, or confocal microscopy of autophagosomal structures. For in planta growth curves using syringe infiltration, Xcv strains were inoculated at OD_{600} = 0.0004, and for dip-inoculation OD_{600} = 0.2 was used.

Tomato growth condition and bacterial growth assay

Tomato (*Solanum lycopersicum*) cv. VF36 was grown in greenhouse (22–28°C, 50–70% RH, 16 h light). For bacterial growth assays, leaflets were dipped in a 2×10^8 CFU/ml suspension of Xcv 85-10 strains in 10 mM $MgCl_2$ with 0.025% (v/v) silwet L-77 (Helena Chemical Company) for 30 s. Plants were then placed in plastic chambers at high humidity (> 95%) for 24 h. For each strain analyzed, four-leaf disks (0.5 cm^2) per treatment per timepoint were ground in 10 mM $MgCl_2$ and diluted and spotted onto NYGA plates in triplicate to determine bacterial load. Three biological replicates (i.e., three plants) were used, and the experiment was repeated at least three times.

Confocal microscopy

Live-cell images were acquired from abaxial leaf epidermal cells using a Zeiss LSM780 and LSM880 microscope. Excitation/emission parameters for GFP and RFP were 488 nm/490 to 552 nm and 561 nm/569 to 652 nm, respectively, and sequential scanning mode

was used for colocalization of both fluorophores. Confocal images with ImageJ (version 2.00) software. Quantification of ATG8-labeled autophagosomal structures was done on z-stacks that were converted to eight-bit grayscale and then counted for ATG8 puncta either manually or by the Particle Analyzer function of ImageJ.

FRET-FLIM measurement

FRET-FLIM was performed on an SP8 confocal laser scanning microscope (CLSM) (Leica Microsystems GMBH) with LAS AF and SymPhoTime 64 software using a 63d7/1.20 water immersion objective. FLIM measurements were performed with a 470 nm pulsed laser (LDH-P-C-470) with the 40 MHz repetition rate and a reduced speed yielding, with an image resolution of 256 × 256, a pixel dwell time of ~10 µs. Max count rate was set to ~15,000 cps. Measurements were stopped, when the brightest pixel had a photon count of 1,000. The corresponding emission was detected with a Leica HyD SMD detector from 500 nm to 530 nm by time-correlated single-photon counting using a Timeharp260 module (PicoQuant, Berlin). The calculation of GFP lifetime was performed by iterative reconvolution, i.e., the instrument response function was convolved with exponential test functions to minimize the error with regard to the original TCSPC histograms in an iterative process. For measurements of GFP-JOKA2 protein aggregates, ROIs were drawn manually on SymphoTime64 software around the aggregates to analyze the GFP lifetime in these structures.

Immunoblot analysis

Proteins were extracted in 100 mM Tris (pH 7.5) containing 2% SDS, boiled for 10 min in SDS loading buffer, and cleared by centrifugation. The protein extracts were then separated by SDS–PAGE, transferred to PVDF membranes (Biorad), blocked with 5% skimmed milk in PBS, and incubated with primary antibodies anti-NBR1 (Agrisera), anti-ATG8 (Agrisera), anti-ubiquitin (Agrisera), anti-GFP (SantaCruz), anti-RFP (Chromotek), anti-HA (Sigma Aldrich) primary antibodies using 1:2000 dilutions in PBS containing 0.1% Tween 20. This was followed by incubation with horseradish peroxidase-conjugated secondary antibodies diluted 1:10,000 in PBS containing 0.1% Tween 20. The immunoreaction was developed using an ECL Prime Kit (GE Healthcare) and detected with Amersham Imager 680 blot and gel imager.

In vitro ubiquitination assay

Recombinant proteins were expressed in *E. coli* BL21(DE3) and purified by affinity chromatography using amylose resin (New England Biolabs). Recombinant His-UBA1 and His-UBC8 were purified using Ni-Ted resin (Macherey-Nagel). Purified proteins were used for *in vitro* ubiquitination assays. Each reaction of 30 ml final volume contained 25 mM Tris–HCl, pH 7.5, 5 mM $MgCl_2$, 50 mM KCl, 2 mM ATP, 0.6 mM DTT, 2 µg ubiquitin, 200 ng E1 His-*At*UBA1, 1.2 µg E2 His-*At*UBC8, 2 µg of E3s, and 0.3 µg of MBP-*At*SH3P2. Samples were incubated for 1 h at 30°C, and the reaction was stopped by adding SDS loading buffer and incubated for 10 min at 68°C. Samples were separated by SDS–PAGE electrophoresis using 4–15% Mini-PROTEAN® TGX™ Precast Protein Gels (BioRad) followed by detection of the ubiquitinated substrate by immunoblotting using anti-MBP (New England Biolabs), anti-GST and anti-ubiquitin (Santa Cruz Biotechnology) antibodies.

NanoLC-MS/MS analysis and data processing

Proteins were purified on a NuPAGE 12% gel (Invitrogen) and Coomassie-stained gel pieces were digested in-gel with trypsin as described previously (Borchert *et al*, 2010) with a small modification: chloroacetamide was used instead of iodoacetamide for carbamidomethylation of cysteine residues to prevent the formation of lysine modifications isobaric to two glycine residues left on ubiquitinylated lysine after tryptic digestion. After desalting using C18 Stage tips peptide mixtures were run on an Easy-nLC 1200 system coupled to a Q Exactive HF-X mass spectrometer (both Thermo Fisher Scientific) as described elsewhere (Kliza *et al*, 2017) with slight modifications: the peptide mixtures were separated using a 87-min segmented gradient from 10-33-50-90% of HPLC solvent B (80% acetonitrile in 0.1% formic acid) in HPLC solvent A (0.1% formic acid) at a flow rate of 200 nl/min. The seven most intense precursor ions were sequentially fragmented in each scan cycle using higher energy collisional dissociation (HCD) fragmentation. In all measurements, sequenced precursor masses were excluded from further selection for 30 s. The target values were 105 charges for MS/MS fragmentation and 3 × 106 charges for the MS scan.

Acquired MS spectra were processed with MaxQuant software package version 1.5.2.8 with an integrated Andromeda search engine. Database search was performed against a *Nicotiana benthamiana* database containing 74,802 protein entries, the sequences of XopL from *Xanthomonas campestris* pv. *vesicatoria*, and 285 commonly observed contaminants. Endoprotease trypsin was defined as a protease with a maximum of two missed cleavages. Oxidation of methionine, phosphorylation of serine, threonine, and tyrosine, GlyGly dipeptide on lysine residues, and N-terminal acetylation were specified as variable modifications. Carbamidomethylation on cysteine was set as a fixed modification. Initial maximum allowed mass tolerance was set to 4.5 parts per million (ppm) for precursor ions and 20 ppm for fragment ions. Peptide, protein, and modification site identifications were reported at a false discovery rate (FDR) of 0.01, estimated by the target-decoy approach (Elias and Gygi). The iBAQ (Intensity Based Absolute Quantification) and LFQ (Label-Free Quantification) algorithms were enabled, as was the "match between runs" option (Schwanhausser *et al*, 2011).

RNA extraction and RT-qPCR

RNA was extracted from 4 leaf disks according to manufacturer instructions using the GeneMATRIX Universal RNA Purification Kit (Roboklon) with on-column DNase I digestion.

RNA integrity was checked by loading on 1% agarose gel and separating by electrophoresis. RNA concentrations were measured using Nanodrop 2000 (Thermo Fisher), and equal amounts of RNA were used for cDNA synthesis. cDNA synthesis was performed using LunaScript™ RT SuperMix Kit (New England Biolabs) and in a standard thermocycler according to manufacturer instructions. Gene expression was measured by qPCR using MESA BLUE qPCR MasterMix Plus for SYBR® Assay No ROX (Eurogentec) and cycle quantification by Biorad CFX system.

was used for colocalization of both fluorophores. Confocal images with ImageJ (version 2.00) software. Quantification of ATG8-labeled autophagosomal structures was done on z-stacks that were converted to eight-bit grayscale and then counted for ATG8 puncta either manually or by the Particle Analyzer function of ImageJ.

FRET-FLIM measurement

FRET-FLIM was performed on an SP8 confocal laser scanning microscope (CLSM) (Leica Microsystems GMBH) with LAS AF and SymPhoTime 64 software using a 63d7/1.20 water immersion objective. FLIM measurements were performed with a 470 nm pulsed laser (LDH-P-C-470) with the 40 MHz repetition rate and a reduced speed yielding, with an image resolution of 256 × 256, a pixel dwell time of ~10 µs. Max count rate was set to ~15,000 cps. Measurements were stopped, when the brightest pixel had a photon count of 1,000. The corresponding emission was detected with a Leica HyD SMD detector from 500 nm to 530 nm by time-correlated single-photon counting using a Timeharp260 module (PicoQuant, Berlin). The calculation of GFP lifetime was performed by iterative reconvolution, i.e., the instrument response function was convolved with exponential test functions to minimize the error with regard to the original TCSPC histograms in an iterative process. For measurements of GFP-JOKA2 protein aggregates, ROIs were drawn manually on SymphoTime64 software around the aggregates to analyze the GFP lifetime in these structures.

Immunoblot analysis

Proteins were extracted in 100 mM Tris (pH 7.5) containing 2% SDS, boiled for 10 min in SDS loading buffer, and cleared by centrifugation. The protein extracts were then separated by SDS–PAGE, transferred to PVDF membranes (Biorad), blocked with 5% skimmed milk in PBS, and incubated with primary antibodies anti-NBR1 (Agrisera), anti-ATG8 (Agrisera), anti-ubiquitin (Agrisera), anti-GFP (SantaCruz), anti-RFP (Chromotek), anti-HA (Sigma Aldrich) primary antibodies using 1:2000 dilutions in PBS containing 0.1% Tween 20. This was followed by incubation with horseradish peroxidase-conjugated secondary antibodies diluted 1:10,000 in PBS containing 0.1% Tween 20. The immunoreaction was developed using an ECL Prime Kit (GE Healthcare) and detected with Amersham Imager 680 blot and gel imager.

In vitro ubiquitination assay

Recombinant proteins were expressed in *E. coli* BL21(DE3) and purified by affinity chromatography using amylose resin (New England Biolabs). Recombinant His-UBA1 and His-UBC8 were purified using Ni-Ted resin (Macherey-Nagel). Purified proteins were used for *in vitro* ubiquitination assays. Each reaction of 30 ml final volume contained 25 mM Tris–HCl, pH 7.5, 5 mM $MgCl_2$, 50 mM KCl, 2 mM ATP, 0.6 mM DTT, 2 µg ubiquitin, 200 ng E1 His-*At*UBA1, 1.2 µg E2 His-*At*UBC8, 2 µg of E3s, and 0.3 µg of MBP-*At*SH3P2. Samples were incubated for 1 h at 30°C, and the reaction was stopped by adding SDS loading buffer and incubated for 10 min at 68°C. Samples were separated by SDS–PAGE electrophoresis using 4–15% Mini-PROTEAN® TGX™ Precast Protein Gels (BioRad) followed by detection of the ubiquitinated substrate by immunoblotting using anti-MBP (New England Biolabs), anti-GST and anti-ubiquitin (Santa Cruz Biotechnology) antibodies.

NanoLC-MS/MS analysis and data processing

Proteins were purified on a NuPAGE 12% gel (Invitrogen) and Coomassie-stained gel pieces were digested in-gel with trypsin as described previously (Borchert *et al*, 2010) with a small modification: chloroacetamide was used instead of iodoacetamide for carbamidomethylation of cysteine residues to prevent the formation of lysine modifications isobaric to two glycine residues left on ubiquitinylated lysine after tryptic digestion. After desalting using C18 Stage tips peptide mixtures were run on an Easy-nLC 1200 system coupled to a Q Exactive HF-X mass spectrometer (both Thermo Fisher Scientific) as described elsewhere (Kliza *et al*, 2017) with slight modifications: the peptide mixtures were separated using a 87-min segmented gradient from 10-33-50-90% of HPLC solvent B (80% acetonitrile in 0.1% formic acid) in HPLC solvent A (0.1% formic acid) at a flow rate of 200 nl/min. The seven most intense precursor ions were sequentially fragmented in each scan cycle using higher energy collisional dissociation (HCD) fragmentation. In all measurements, sequenced precursor masses were excluded from further selection for 30 s. The target values were 105 charges for MS/MS fragmentation and 3 × 106 charges for the MS scan.

Acquired MS spectra were processed with MaxQuant software package version 1.5.2.8 with an integrated Andromeda search engine. Database search was performed against a *Nicotiana benthamiana* database containing 74,802 protein entries, the sequences of XopL from *Xanthomonas campestris* pv. *vesicatoria*, and 285 commonly observed contaminants. Endoprotease trypsin was defined as a protease with a maximum of two missed cleavages. Oxidation of methionine, phosphorylation of serine, threonine, and tyrosine, GlyGly dipeptide on lysine residues, and N-terminal acetylation were specified as variable modifications. Carbamidomethylation on cysteine was set as a fixed modification. Initial maximum allowed mass tolerance was set to 4.5 parts per million (ppm) for precursor ions and 20 ppm for fragment ions. Peptide, protein, and modification site identifications were reported at a false discovery rate (FDR) of 0.01, estimated by the target-decoy approach (Elias and Gygi). The iBAQ (Intensity Based Absolute Quantification) and LFQ (Label-Free Quantification) algorithms were enabled, as was the "match between runs" option (Schwanhausser *et al*, 2011).

RNA extraction and RT-qPCR

RNA was extracted from 4 leaf disks according to manufacturer instructions using the GeneMATRIX Universal RNA Purification Kit (Roboklon) with on-column DNase I digestion.

RNA integrity was checked by loading on 1% agarose gel and separating by electrophoresis. RNA concentrations were measured using Nanodrop 2000 (Thermo Fisher), and equal amounts of RNA were used for cDNA synthesis. cDNA synthesis was performed using LunaScript™ RT SuperMix Kit (New England Biolabs) and in a standard thermocycler according to manufacturer instructions. Gene expression was measured by qPCR using MESA BLUE qPCR MasterMix Plus for SYBR® Assay No ROX (Eurogentec) and cycle quantification by Biorad CFX system.

Büttner D (2016) Behind the lines-actions of bacterial type III effector proteins in plant cells. *FEMS Microbiol Rev* 40: 894 – 937

Chai Q, Wang X, Qiang L, Zhang Y, Ge P, Lu Z, Zhong Y, Li B, Wang J, Zhang L *et al* (2019) A *Mycobacterium tuberculosis* surface protein recruits ubiquitin to trigger host xenophagy. *Nat Commun* 10: 1973

Clough SJ, Bent AF (1998) Floral dip: a simplified method for Agrobacterium-mediated transformation of *Arabidopsis thaliana*. *Plant J* 16: 735 – 743

Dagdas YF, Belhaj K, Maqbool A, Chaparro-Garcia A, Pandey P, Petre B, Tabassum N, Cruz-Mireles N, Hughes RK, Sklenar J *et al* (2016) An effector of the Irish potato famine pathogen antagonizes a host autophagy cargo receptor. *Elife* 5: e10856

Dagdas YF, Pandey P, Tumtas Y, Sanguankiattichai N, Belhaj K, Duggan C, Leary AY, Segretin ME, Contreras MP, Savage Z *et al* (2018) Host autophagy machinery is diverted to the pathogen interface to mediate focal defense responses against the Irish potato famine pathogen. *Elife* 7: e37476

Dauphinee AN, Cardoso C, Dalman K, Ohlsson JA, Fick SB, Robert S, Hicks GR, Bozhkov PV, Minina EA (2019) Chemical screening pipeline for identification of specific plant autophagy modulators. *Plant Physiol* 181: 855 – 866

Dupont N, Lacas-Gervais S, Bertout J, Paz I, Freche B, Van Nhieu GT, van der Goot FG, Sansonetti PJ, Lafont F (2009) Shigella phagocytic vacuolar membrane remnants participate in the cellular response to pathogen invasion and are regulated by autophagy. *Cell Host Microbe* 6: 137 – 149

Erickson JL, Adlung N, Lampe C, Bonas U, Schattat MH (2018) The *Xanthomonas* effector XopL uncovers the role of microtubules in stromule extension and dynamics in *Nicotiana benthamiana*. *Plant J* 93: 856 – 870

Furlan G, Klinkenberg J, Trujillo M (2012) Regulation of plant immune receptors by ubiquitination. *Front Plant Sci* 3: 238

Furlan G, Nakagami H, Eschen-Lippold L, Jiang X, Majovsky P, Kowarschik K, Hoehenwarter W, Lee J, Trujillo M (2017) Changes in PUB22 ubiquitination modes triggered by MITOGEN-ACTIVATED PROTEIN KINASE3 dampen the immune response. *Plant Cell* 29: 726 – 745

Gantner J, Ordon J, Kretschmer C, Guerois R, Stuttmann J (2019) An EDS1-SAG101 complex is essential for TNL-mediated immunity in *Nicotiana benthamiana*. *Plant Cell* 31: 2456 – 2474

Germic N, Frangez Z, Yousefi S, Simon HU (2019) Regulation of the innate immune system by autophagy: neutrophils, eosinophils, mast cells, NK cells. *Cell Death Differ* 26: 703 – 714

Gomes LC, Dikic I (2014) Autophagy in antimicrobial immunity. *Mol Cell* 54: 224 – 233

Grefen C, Donald N, Hashimoto K, Kudla J, Schumacher K, Blatt MR (2010) A ubiquitin-10 promoter-based vector set for fluorescent protein tagging facilitates temporal stability and native protein distribution in transient and stable expression studies. *Plant J* 64: 355 – 365

Gu Y, Zavaliev R, Dong X (2017) Membrane trafficking in plant immunity. *Mol Plant* 10: 1026 – 1034

Hafren A, Macia JL, Love AJ, Milner JJ, Drucker M, Hofius D (2017) Selective autophagy limits cauliflower mosaic virus infection by NBR1-mediated targeting of viral capsid protein and particles. *Proc Natl Acad Sci USA* 114: E2026 – E2035

Hafren A, Üstün S, Hochmuth A, Svenning S, Johansen T, Hofius D (2018) Turnip mosaic virus counteracts selective autophagy of the viral silencing suppressor HCpro. *Plant Physiol* 176: 649 – 662

Hu H, Sun SC (2016) Ubiquitin signaling in immune responses. *Cell Res* 26: 457 – 483

Huang J, Brumell JH (2014) Bacteria-autophagy interplay: a battle for survival. *Nat Rev Microbiol* 12: 101 – 114

Khan M, Seto D, Subramaniam R, Desveaux D (2018) Oh, the places they'll go! A survey of phytopathogen effectors and their host targets. *Plant J* 93: 651 – 663

Kim JG, Stork W, Mudgett MB (2013) *Xanthomonas* type III effector XopD desumoylates tomato transcription factor SlERF4 to suppress ethylene responses and promote pathogen growth. *Cell Host Microbe* 13: 143 – 154

Kim JG, Taylor KW, Hotson A, Keegan M, Schmelz EA, Mudgett MB (2008) XopD SUMO protease affects host transcription, promotes pathogen growth, and delays symptom development in xanthomonas-infected tomato leaves. *Plant Cell* 20: 1915 – 1929

Kirkin V, Lamark T, Johansen T, Dikic I (2009) NBR1 cooperates with p62 in selective autophagy of ubiquitinated targets. *Autophagy* 5: 732 – 733

Kliza K, Taumer C, Pinzuti I, Franz-Wachtel M, Kunzelmann S, Stieglitz B, Macek B, Husnjak K (2017) Internally tagged ubiquitin: a tool to identify linear polyubiquitin-modified proteins by mass spectrometry. *Nat Methods* 14: 504 – 512

Kovach ME, Elzer PH, Hill DS, Robertson GT, Farris MA, Roop 2nd RM, Peterson KM (1995) Four new derivatives of the broad-host-range cloning vector pBBR1MCS, carrying different antibiotic-resistance cassettes. *Gene* 166: 175 – 176

Kubori T, Galan JE (2003) Temporal regulation of salmonella virulence effector function by proteasome-dependent protein degradation. *Cell* 115: 333 – 342

Lal NK, Thanasuwat B, Huang PJ, Cavanaugh KA, Carter A, Michelmore RW, Dinesh-Kumar SP (2020) Phytopathogen effectors use multiple mechanisms to manipulate plant autophagy. *Cell Host Microbe* 28: 558 – 571

Langin G, Gouguet P, Üstün S (2020) Microbial Effector proteins – a journey through the proteolytic landscape. *Trends Microbiol* 28: 523 – 535

Leary AY, Savage Z, Tumtas Y, Bozkurt TO (2019) Contrasting and emerging roles of autophagy in plant immunity. *Curr Opin Plant Biol* 52: 46 – 53

Lei L, Stevens DM, Coaker G (2020) Phosphorylation of the pseudomonas effector AvrPtoB by *Arabidopsis* SnRK2.8 is required for bacterial virulence. *Mol Plant* 13: 1513 – 1522

Lenz HD, Haller E, Melzer E, Kober K, Wurster K, Stahl M, Bassham DC, Vierstra RD, Parker JE, Bautor J *et al* (2011) Autophagy differentially controls plant basal immunity to biotrophic and necrotrophic pathogens. *Plant J* 66: 818 – 830

Levine B, Mizushima N, Virgin HW (2011) Autophagy in immunity and inflammation. *Nature* 469: 323 – 335

Lorenz C, Büttner D (2009) Functional characterization of the type III secretion ATPase HrcN from the plant pathogen *Xanthomonas campestris* pv. *vesicatoria*. *J Bacteriol* 191: 1414 – 1428

Lou L, Zhang P, Piao R, Wang Y (2019) Salmonella pathogenicity Island 1 (SPI-1) and its complex regulatory network. *Front Cell Infect Microbiol* 9: 270

Marshall RS, Vierstra RD (2018) Autophagy: the master of bulk and selective recycling. *Annu Rev Plant Biol* 69: 173 – 208

Mesquita FS, Thomas M, Sachse M, Santos AJ, Figueira R, Holden DW (2012) The Salmonella deubiquitinase SseL inhibits selective autophagy of cytosolic aggregates. *PLoS Pathog* 8: e1002743

Minina EA, Moschou PN, Vetukuri RR, Sanchez-Vera V, Cardoso C, Liu Q, Elander PH, Dalman K, Beganovic M, Lindberg Yilmaz J *et al* (2018) Transcriptional stimulation of rate-limiting components of the autophagic pathway improves plant fitness. *J Exp Bot* 69: 1415 – 1432

Mostowy S (2013) Autophagy and bacterial clearance: a not so clear picture. *Cell Microbiol* 15: 395 – 402

Nagel MK, Kalinowska K, Vogel K, Reynolds GD, Wu Z, Anzenberger F, Ichikawa M, Tsutsumi C, Sato MH, Kuster B *et al* (2017) *Arabidopsis* SH3P2 is an

ubiquitin-binding protein that functions together with ESCRT-I and the deubiquitylating enzyme AMSH3. *Proc Natl Acad Sci USA* 114: E7197 – E7204

Nakagawa T, Kurose T, Hino T, Tanaka K, Kawamukai M, Niwa Y, Toyooka K, Matsuoka K, Jinbo T, Kimura T (2007) Development of series of gateway binary vectors, pGWBs, for realizing efficient construction of fusion genes for plant transformation. *J Biosci Bioeng* 104: 34 – 41

Pandey P, Leary AY, Tumtas Y, Savage Z, Dagvadorj B, Duggan C, Yuen EL, Sanguankiattichai N, Tan E, Khandare V *et al* (2021) An oomycete effector subverts host vesicle trafficking to channel starvation-induced autophagy to the pathogen interface. *Elife* 10: e65285

Pohl C, Dikic I (2019) Cellular quality control by the ubiquitin-proteasome system and autophagy. *Science* 366: 818 – 822

Schultink A, Qi T, Lee A, Steinbrenner AD, Staskawicz B (2017) Roq1 mediates recognition of the *Xanthomonas* and *Pseudomonas* effector proteins XopQ and HopQ1. *Plant J* 92: 787 – 795

Schwanhausser B, Busse D, Li N, Dittmar G, Schuchhardt J, Wolf J, Chen W, Selbach M (2011) Global quantification of mammalian gene expression control. *Nature* 473: 337 – 342

Singer AU, Schulze S, Skarina T, Xu X, Cui H, Eschen-Lippold L, Egler M, Srikumar T, Raught B, Lee J *et al* (2013) A pathogen type III effector with a novel E3 ubiquitin ligase architecture. *PLoS Pathog* 9: e1003121

Svenning S, Lamark T, Krause K, Johansen T (2011) Plant NBR1 is a selective autophagy substrate and a functional hybrid of the mammalian autophagic adapters NBR1 and p62/SQSTM1. *Autophagy* 7: 993 – 1010

Timilsina S, Potnis N, Newberry EA, Liyanapathiranage P, Iruegas-Bocardo F, White FF, Goss EM, Jones JB (2020) Xanthomonas diversity, virulence and plant-pathogen interactions. *Nat Rev Microbiol* 18: 415 – 427

Üstün S, Bartetzko V, Börnke F (2013) The *Xanthomonas campestris* type III effector XopJ targets the host cell proteasome to suppress salicylic-acid mediated plant defence. *PLoS Pathog* 9: e1003427

Üstün S, Bartetzko V, Börnke F (2015) The *Xanthomonas* effector XopJ triggers a conditional hypersensitive response upon treatment of N. benthamiana leaves with salicylic acid. *Front Plant Sci* 6: 599

Üstün S, Börnke F (2014) Interactions of *Xanthomonas* type-III effector proteins with the plant ubiquitin and ubiquitin-like pathways. *Front Plant Sci* 5: 736

Üstün S, Börnke F (2015) The *Xanthomonas campestris* type III effector XopJ proteolytically degrades proteasome subunit RPT6. *Plant Physiol* 168: 107 – 119

Üstün S, Hafren A, Hofius D (2017) Autophagy as a mediator of life and death in plants. *Curr Opin Plant Biol* 40: 122 – 130

Üstün S, Hafren A, Liu Q, Marshall RS, Minina EA, Bozhkov PV, Vierstra RD, Hofius D (2018) Bacteria exploit autophagy for proteasome degradation and enhanced virulence in plants. *Plant Cell* 30: 668 – 685

Üstün S, Hofius D (2018) Anti- and pro-microbial roles of autophagy in plant-bacteria interactions. *Autophagy* 14: 1465 – 1466

Üstün S, Konig P, Guttman DS, Börnke F (2014) HopZ4 from *Pseudomonas syringae*, a member of the HopZ type III effector family from the YopJ superfamily, inhibits the proteasome in plants. *Mol Plant Microbe Interact* 27: 611 – 623

Üstün S, Sheikh A, Gimenez-Ibanez S, Jones A, Ntoukakis V, Börnke F (2016) The proteasome acts as a hub for plant immunity and is targeted by *Pseudomonas* type III effectors. *Plant Physiol* 172: 1941 – 1958

van Wijk SJ, Fiskin E, Putyrski M, Pampaloni F, Hou J, Wild P, Kensche T, Grecco HE, Bastiaens P, Dikic I (2012) Fluorescence-based sensors to monitor localization and functions of linear and K63-linked ubiquitin chains in cells. *Mol Cell* 47: 797 – 809

Yan Y, Wang P, He C, Shi H (2017) MeWRKY20 and its interacting and activating autophagy-related protein 8 (MeATG8) regulate plant disease resistance in cassava. *Biochem Biophys Res Commun* 494: 20 – 26

Yang Y, Klionsky DJ (2020) Autophagy and disease: unanswered questions. *Cell Death Differ* 27: 858 – 871

Zeng H, Xie Y, Liu G, Lin D, He C, Shi H (2018) Molecular identification of GAPDHs in cassava highlights the antagonism of MeGAPCs and MeATG8s in plant disease resistance against cassava bacterial blight. *Plant Mol Biol* 97: 201 – 214

Zhang Y, Higashide W, Dai S, Sherman DM, Zhou D (2005) Recognition and ubiquitination of Salmonella type III effector SopA by a ubiquitin E3 ligase, HsRMA1. *J Biol Chem* 280: 38682 – 38688

Zheng YT, Shahnazari S, Brech A, Lamark T, Johansen T, Brumell JH (2009) The adaptor protein p62/SQSTM1 targets invading bacteria to the autophagy pathway. *J Immunol* 183: 5909 – 5916

Zhou J, Wang J, Cheng Y, Chi YJ, Fan B, Yu JQ, Chen Z (2013) NBR1-mediated selective autophagy targets insoluble ubiquitinated protein aggregates in plant stress responses. *PLoS Genet* 9: e1003196

Zhuang X, Jiang L (2014) Autophagosome biogenesis in plants: roles of SH3P2. *Autophagy* 10: 704 – 705

Zhuang X, Wang H, Lam SK, Gao C, Wang X, Cai Y, Jiang L (2013) A BAR-domain protein SH3P2, which binds to phosphatidylinositol 3-phosphate and ATG8, regulates autophagosome formation in *Arabidopsis*. *Plant Cell* 25: 4596 – 4615

III. The Proteasome Complex at the Centre of Plant Immunity

This chapter is based on the publication “The Plant Ubiquitin–Proteasome System as a Target for Microbial Manipulation”, published in 2023. In this manuscript, we provide an extensive description of the state of art of knowledge regarding the role of the UPS in Plant immunity. While the previous chapter focused on the targeting of host proteolytic pathways by pathogenic organisms, here we also describe the role of the UPS in regulating host defense response to infection. It highlights the striking importance of this pathway in regulation of immunity from pathogen perception to defense onset and being concomitantly heavily hijacked by various pathogens. Taken together it reflects the ambivalent role of the 26S proteasome complex acting in pro- and anti-defense context as well as pro- and anti-pathogen proliferation. It shows that the 26S Proteasome complex can be seen as a multi-faceted degradation hub which therefore requires precise regulation in time and space to mediates the desired modulation on cellular proteostasis.

a. The Plant Ubiquitin–Proteasome System as a Target for Microbial Manipulation

Scientific contributions: Scientific ideas 50%, Figure representation 100%.

Details about writing contributions: Writing of the entire manuscript in collaboration with MGF and under supervision of SÜ.

Citation: Langin G, González-Fuente M, Üstün S. The Plant Ubiquitin-Proteasome System as a Target for Microbial Manipulation. Annu Rev Phytopathol. 2023 Sep 5; 61:351-375. doi: 10.1146/annurev-phyto-021622-110443. Epub 2023 May 30. PMID: 37253695.

ANNUAL REVIEWS

Annual Review of Phytopathology

The Plant Ubiquitin–Proteasome System as a Target for Microbial Manipulation

Gautier Langin,[1,2,*] Manuel González-Fuente,[2,*] and Suayib Üstün[2]

[1]Centre for Plant Molecular Biology (ZMBP), University of Tübingen, Tübingen, Germany; email: suayb.uestuen@rub.de

[2]Faculty of Biology and Biotechnology, Ruhr-University Bochum, Bochum, Germany

Annu. Rev. Phytopathol. 2023. 61:351–75

First published as a Review in Advance on May 30, 2023

The *Annual Review of Phytopathology* is online at phyto.annualreviews.org

https://doi.org/10.1146/annurev-phyto-021622-110443

*These authors contributed equally to this work.

Keywords

ubiquitin–proteasome system, plant immunity, pathogens, effectors, ubiquitination, proteostasis

Abstract

The plant immune system perceives pathogens to trigger defense responses. In turn, pathogens secrete effector molecules to subvert these defense responses. The initiation and maintenance of defense responses involve not only de novo synthesis of regulatory proteins and enzymes but also their regulated degradation. The latter is achieved through protein degradation pathways such as the ubiquitin–proteasome system (UPS). The UPS regulates all stages of immunity, from the perception of the pathogen to the execution of the response, and, therefore, constitutes an ideal candidate for microbial manipulation of the host. Pathogen effector molecules interfere with the plant UPS through several mechanisms. This includes hijacking general UPS functions or perturbing its ability to degrade specific targets. In this review, we describe how the UPS regulates different immunity-related processes and how pathogens subvert this to promote disease.

1. INTRODUCTION

To prevent outbreaks of diseases caused by phytopathogens, plants have developed a complex evolutionarily driven multilayered immune system (56). The first layer of this immune system depends on the recognition of conserved microbial molecules, termed pathogen-associated molecular patterns (PAMPs), by cell surface pattern-recognition receptors (PRRs) (24). This first layer of defense is known as PAMP-triggered immunity (PTI) (56). Adapted plant pathogens are able to overcome these PTI responses by delivering effector proteins into the host cells, where they manipulate the host cell machinery for the benefit of the pathogen (60). In turn, plants have evolved a second potentiated layer of defense that is driven by the recognition of these effectors by intracellular receptors (93). This second layer is referred to as effector-triggered immunity (ETI) (56). Recognition of microbial molecules by immune receptors activates downstream defense reactions via hormone signaling and transcriptional reprogramming, which lead to the secretion of antimicrobial compounds and/or programmed cell death (PCD) to counteract the invasion (8, 21). This so-called zig-zag model involves a complex interplay among many cellular processes and for years served as a framework to study plant–microbe interactions at the molecular level (92). This requires a high degree of proteomic plasticity involving both the synthesis and turnover of regulatory proteins (98). Therefore, it is not surprising that protein degradation pathways such as the ubiquitin–proteasome system (UPS) have been identified as major coordinators of plant immunity and determine the outcome of plant–microbe interactions (66).

The UPS is a highly conserved pathway involved in the degradation of up to 80% of eukaryotic proteins (22). Poly-ubiquitination of target proteins is a prerequisite for recycling proteins through the UPS (22). To this end, an enzymatic cascade involving ubiquitin-activating (E1), ubiquitin-conjugating (E2), and ubiquitin-ligase (E3) enzymes is required (135). In the first step, activated ubiquitin binds to an E1 and is then transferred to an E2. This E2 carries the activated ubiquitin to the E3, which in turn facilitates the transfer of the ubiquitin from the E2 to a lysine residue of the target protein. After several rounds of the E1→E2→E3 cascade, the substrate protein bears one or multiple ubiquitin chains that are then recognized by the 26S proteasome for its subsequent degradation (135). The 26S proteasome is a 2.5-MDa ATP-dependent protease complex composed of a 20S core protease (CP) and one or two 19S regulatory particles (RPs), each of which contains a lid and a base subunit (83). The CP is a broad-spectrum ATP- and ubiquitin-independent protease complex harboring peptidase activity (83). The assembly of these two subcomplexes leads to the formation of a capped cylindric megacomplex that is able to recognize, unfold, and degrade ubiquitinated proteins. Substrate recognition is followed by deubiquitination and unfolding by lid RP subunits (83). The linearized target protein is processed through the base RP subunits and delivered to the CP core particles. Here, the CP peptidases cleave a broad array of polypeptides, with the β1, β2, and β5 active sites providing trypsin-like, chymotrypsin-like, and caspase-like cleavage properties, respectively. The RP subcomplex is responsible for recognizing ubiquitinated target proteins and opening the channel of the CP to later insert the unfolded substrate into the CP chamber for degradation (83). Since the discovery of ubiquitin more than 50 years ago, the UPS has gained prominence as one of the most ubiquitous, versatile, and efficient regulators of many different cellular processes in eukaryotes (135, 144). For instance, the *Arabidopsis* genome encodes more than 1,600 genes (>6% of the total genome) involved in UPS-related functions. Most of these genes (>1,400) encode putative E3s (25). The diversification of E3s in plants is essential to ensure substrate specificity and provides the UPS with huge flexibility in reacting to different environmental changes. In plants, E3s can be classified into four main types: really interesting new gene (RING); Cullin–RING ligases (CRLs); homologous to the E6-AP carboxyl terminus (HECT); and plant U-box (PUB) proteins. RING,

HECT, and PUB E3s act as monomeric proteins, whereas CRLs form multimeric complexes (12). In plants, the UPS pathway, and particularly E3s, has been shown to be involved in responses to many internal and external stimuli (25, 112). Characterization of E3s involved in plant immunity has led to historical milestones in the understanding of defense mechanisms. However, recent studies highlighted that other UPS components such as E1, E2, and the 26S proteasome complex itself are also required to mount effective plant defense reactions. Owing to this prominent role in plant immunity, pathogens have evolved strategies to manipulate the UPS to their own advantage. In this review, we first describe the different ways in which the UPS regulates plant immunity. We then detail the different mechanisms that plant pathogens have evolved to interfere with the UPS in their effort to subvert plant defenses and trigger disease.

2. THE UBIQUITIN–PROTEASOME SYSTEM REGULATES ALL STAGES OF PLANT IMMUNITY

The UPS is involved in the regulation of many developmental and stress response processes, including plant immunity. UPS regulation of plant immunity affects all stages, from pathogen perception to execution of the different defense responses.

2.1. The Ubiquitin–Proteasome System Degrades Key Immune Components

Upon pathogen perception, plant immune components undergo degradation by the UPS. In the following sections, we summarize key findings about how immune receptors and other defense components are degraded by the UPS.

2.1.1. Immune receptors. Pathogen recognition is the first step in plant immune responses. This recognition occurs at two levels: PAMP perception by cell-surface PRRs and effector recognition by intracellular receptors. Examples of both types of immune receptors have been reported as targets of UPS-mediated degradation (**Figure 1*a***).

Pattern-recognition receptors and associated proteins. PRRs encode receptor kinases and receptor-like proteins located mostly at the plasma membrane, where they recognize conserved PAMPs (161). Given their importance in initiating plant defense responses, their controlled turnover is a key regulatory process in which the UPS is heavily involved. *Arabidopsis* flagellin-sensitive 2 (FLS2), probably the best-characterized PRR, recognizes flg22, a peptide derived from the bacterial flagellin. Upon flg22 recognition, FLS2 associates with its coreceptor BRI1-associated receptor kinase 1 (BAK1) following multiple phosphorylation events mediated by their respective kinase domains (24). After this recognition, FLS2 undergoes a rapid turnover that has been associated with the UPS, as chemical inhibition of proteasomal degradation with MG132 stabilizes FLS2 protein levels (77). Additionally, FLS2 also undergoes ubiquitination by the E3 pair PUB12 and 13 (77, 89). Although ubiquitination of FLS2 has not yet been clearly associated with proteasomal degradation, it cannot be ruled out that it does play a role through yet unknown mechanisms. Among the first downstream components of the phosphorylation signaling cascade activated by FLS2 we find *Botrytis*-induced kinase 1 (BIK1). BIK1 directly associates with the FLS2/BAK1 complex, becomes phosphorylated by them, and transduces the signal to additional intracellular downstream components (89). BIK1 is also targeted for proteasomal degradation upon ubiquitination mediated by yet another PUB pair, PUB25 and 26 (136). A more recent report also identified PUB4 as responsible for ubiquitin-mediated proteasomal degradation of BIK1 (153). Interestingly, when it comes to BIK1 phosphorylation, contrasting roles have been described. Although BIK1 phosphorylation by the FLS2–BAK1 complex positively regulates BIK1 activity, calcium-dependent protein kinase 28 (CPK28)-mediated phosphorylation of BIK1

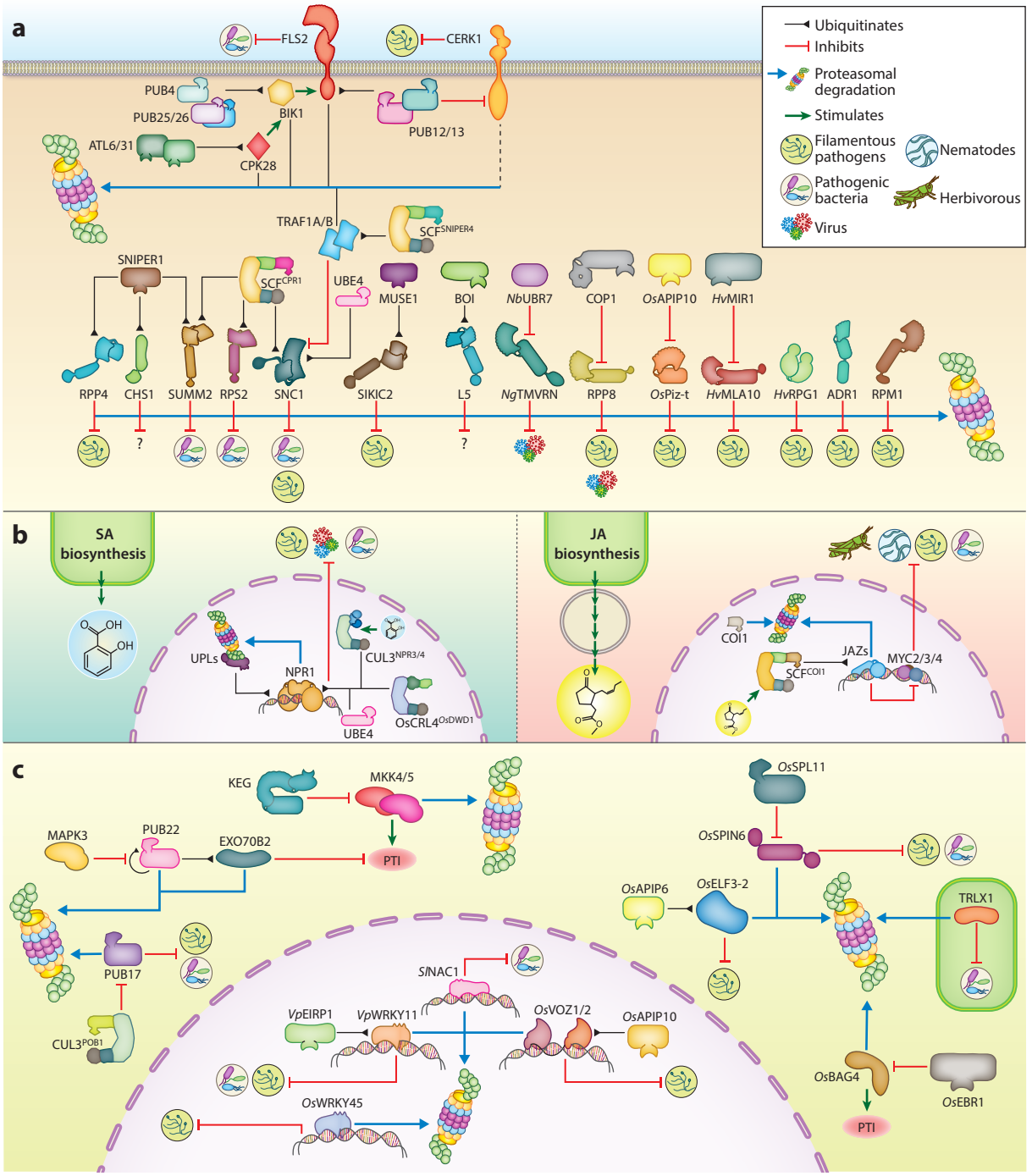

(Caption appears on following page)

Figure 1 (*Figure appears on preceding page*)

The 26S proteasome is a master regulator of immune component turnover from early to later immune signaling. (*a*) Proteasomal degradation mediates regulation of multiple immune receptors, including cell surface pattern recognition receptors and intracellular nucleotide-binding leucine-rich repeat receptors in a wide range of species. (*b*) Defense hormone-dependent transcriptional reprogramming against pathogens is fine-tuned in the nucleus by the 26S proteasome. (*c*) The 26S proteasome coordinates later immune signals through regulation of a broad range of proteins involved in signal transduction and transcriptional response. Abbreviations: JA, jasmonic acid; JAZs, jasmonate ZIM domain proteins; PTI, PAMP-triggered immunity; SA, salicylic acid; UPLs, ubiquitin-protein ligases.

negatively impacts its activity (89). CPK28 itself is another target of proteasomal degradation mediated by ubiquitination via the RING domain E3 pair *Arabidopsis* toxicos en levadura 6/31 (ATL6 and 31) (75).

Another well-known PRR is *Arabidopsis* chitin elicitor receptor kinase 1 (CERK1). CERK1 recognizes chitin, a conserved PAMP from fungal cell walls, to induce the correspondent downstream immune signaling via phosphorylation of PBL27 (24). Similar to FLS2, CERK1 protein levels are also stabilized upon chemical inhibition of proteasomal degradation (38). PUB12 regulates the CERK1–PBL27 complex. Both PUB12 and PUB13 are able to interact with CERK1, and, additionally, PUB12 negatively regulates CERK1 stability (145). Intriguingly, CERK1 has also been shown to be subjected to ectodomain shedding (101). This is a mechanism better characterized in animals, in which upon proteolytical cleavage, the extracellular domain of a receptor is released into the extracellular matrix, whereas the intracellular domain is internalized and ultimately undergoes proteasomal degradation (62). Monocot PRRs such as rice SPL11 cell-death suppressor 2 (OsSDS2) have also been found to be targeted by the UPS (32). Altogether, these reports demonstrate how the UPS acts as a central regulator of early immune signaling pathways and highlight the eminent role of plant E3s in this process.

Intracellular immune receptors. Intracellular immune receptors play key roles in resistance to adapted pathogens. Most of them encode nucleotide-binding leucine-rich repeat (NLR) proteins. NLR-mediated immunity usually leads to PCD, also called hypersensitive response (HR) in these cases (21). For this reason, it is vital for the survival of the plant to control the basal activity of these proteins and avoid autoimmunity. This is mediated by the UPS, as evidenced by multiple reports identifying NLR proteins from *Arabidopsis* (17, 30, 42, 48, 71, 73, 80, 109, 141), *Nicotiana benthamiana* (156), rice (100), and barley (95, 139) targeted for proteasomal degradation (**Figure 1*a***).

Altogether, these reports highlight the importance of the UPS in the regulation of both PTI and ETI responses in multiple plant species against a wide variety of pathogens. Interestingly, the UPS can act as both a positive and negative regulator of immune responses, evidencing the complexity and versatility of the system.

2.1.2. Defense-related hormone signaling components. Perception of plant pathogens results in a massive reprogramming of various cellular processes to orchestrate appropriate defense responses. An important part of this reprogramming occurs at the transcriptional level and involves hormone signaling. Interestingly, hormone-induced transcriptional reprogramming in plants is tightly linked to proteasomal degradation (**Figure 1*b***). This applies to the two main hormones involved in immunity: salicylic acid (SA) and jasmonic acid (JA).

Salicylic acid. SA is the key hormone implicated in defense responses against biotrophic pathogens. SA-mediated defense responses are regulated by the master transcriptional regulator non-expresser of PR genes 1 (NPR1) (8). NPR1 protein levels are tightly controlled by SA perception via the $CRL3^{NPR3/NRP4}$ receptor complex (34, 117). Under basal conditions, the UPS targets NPR1 for degradation via $CRL3^{NPR3}$-mediated ubiquitination. Upon early SA

accumulation, NPR3 is inhibited, leading to NPR1 stabilization. In turn, NPR4 acts as a sort of guardrail by being activated to induce NPR1 degradation upon SA overaccumulation (34). A recent study has expanded the importance of NPR1 ubiquitination for its activity. It has been shown that primary CRL3 ubiquitination of NPR1 increases its activity, but it is also the first step for the subsequent UBE4-mediated ubiquitin chain elongation, ultimately leading to NPR1 degradation (115). Moreover, the recent discovery of two HECT E3s, ubiquitin-protein ligase 3/4 (UPL3 and 4), as modifiers of NPR1 adds an extra layer of complexity to the ubiquitin-mediated control of NPR1 turnover (140). Rice OsNPR1 is also targeted for degradation by the UPS via the CRL4 complex (18), indicating either an alternative degradation mechanism for NPR1 or evolutionary divergence between different plant lineages.

Jasmonic acid. JA mediates defense responses against necrotrophic pathogens. JA signaling relies on transcriptional repression that is mainly mediated by the jasmonate ZIM domain protein (JAZ) family. JAZ proteins are negative regulators of the transcription factors (TFs) MYC2, 3, and 4 (33). Upon pathogen perception, JA accumulation is perceived in the nucleus by the SCF^{COI1} complex, which triggers the ubiquitination/degradation of the JAZ repressor and ultimately derepresses the abovementioned MYCs (125, 147). In turn, COI1 is also a target of proteasomal degradation, evidencing contrasting roles of the UPS in JA signaling (146).

2.1.3. Downstream immune components. Plant immunity relies on a complex molecular network that integrates the abovementioned external (e.g., pathogen perception) and internal signals (e.g., hormones) to orchestrate the correspondent appropriate defense responses. For this, it is essential to regulate the abundance and activity of the proteins involved in these processes. This regulation occurs largely thanks to post-translational modifications (PTMs) such as phosphorylation, acetylation, SUMOylation, and ubiquitination. Ubiquitination is a way for the UPS to monitor the stability of the targets (**Figure 1*c***).

E3 ubiquitin ligases. Based on the previously mentioned reports, the importance of E3s in regulating plant immunity is evident. Interestingly, some of the E3s involved in immunity also undergo proteasomal degradation. This applies mostly to E3s from the PUB family. PUB22 dimerization and autoubiquitination lead to PUB22's degradation in basal conditions and are prevented upon infection through phosphorylation by mitogen-activated protein kinase 3 (MAPK3) (35). This stabilization allows PUB22 to ubiquitinate its substrate, the exocyst subunit EXO70B2, which is required for the attenuation of PAMP-induced signaling (118). PUB17 regulates HR and is involved in resistance against the oomycete *Phytophthora infestans* and RPM1- and RPS4-mediated resistance against *Pseudomonas syringae* (46, 149). PUB17 is targeted to the UPS upon ubiquitination by the POZ–BTB-containing protein 1 (POB1) component of the CRL3 E3 complex (97). The involvement in immunity of PUB17 orthologs has been reported for many other plant species such as tobacco, cotton, and potato, evidencing PUB17 as an important conserved immune hub in many plant lineages against a wide variety of pathogens (85, 103).

Signaling and other immune-related proteins. Phosphorylation is a key PTM ruling signaling pathways, including defense-related pathways. For instance, MAPK cascades are core components of PTI signaling (24). A recent study showed that the E3 KEEP ON GOING (KEG) mediates ubiquitination and subsequent degradation of MAPK kinase 4 and 5 (MKK4 and 5) (37). Interestingly, KEG seems to be degraded upon fungal infection, supporting its role as the negative regulator of immunity (45). Other important signaling proteins are GTPases and associated proteins. For instance, rice Rho GTPase-activating protein SPL11-interacting protein 6 (*Os*SPIN6) is a key regulator of antifungal and bacterial HR (74). *Os*SPIN6 turnover is controlled by ubiquitination/proteasomal degradation mediated by the rice PUB13 ortholog *Os*SPL11 (74). Also

involved in rice responses against fungi, the circadian clock regulator *Os*ELF3–2 is a UPS target upon *Os*APIP6-mediated ubiquitination (94). Rice cell death regulator BCL2-associated anthogen 4 (*Os*BAG4) confers broad-spectrum resistance and is targeted to the proteasome upon ubiquitination by enhanced blight and blast resistance 1 (*Os*EBR1) in the basal condition to avoid autoimmunity (152). Organelle signaling is also involved in immunity. For example, the homeostasis of chloroplastic TRX-like 1 (TRXL1) mediated by both the UPS and the intrachloroplastic degradation machinery is involved in defense against *P. syringae* (99).

Transcription factors. An important part of the plant defense responses is controlled at the transcriptional level by several TFs. Therefore, TFs are also targets of UPS during regulation of immunity. A prominent family of such TFs is the plant-specific WRKY family. Many different WRKY family members have been reported as targets of proteasomal degradation in several plant species. For instance, rice WRKY45, involved in the defense against *Magnaporthe grisae*, is subjected to proteasomal degradation in basal conditions (84, 110, 111). In wild grape, the E3 *Erysiphe necator*-induced RING finger protein 1 (*Vp*EIRP1) confers increased resistance against bacterial and fungal pathogens mediating the proteasomal degradation of *Vp*WRKY11 (154). Pepper WRKY40, an ortholog of *Arabidopsis* WRKY40 known to be a negative regulator of PTI, is also degraded by the proteasome to regulate stomatal immunity against the bacterium *Xanthomonas euvesicatoria* (104). Another important family of plant-specific transcription factors is the NAC family. For instance, tomato NAC1, a positive regulator of defense against *P. syringae*, is also targeted by the UPS (86). Recently, rice vascular plant one-zinc-finger 1 and 2 (VOZ1 and 2) have also been found to be degraded upon ubiquitination by the E3 *Os*APIP10 to regulate Piz-t-mediated immunity. Interestingly, *Os*APIP10 also mediates the ubiquitination/degradation of Piz-t itself, making it a major coordinator of rice PTI/ETI responses (100, 137).

Altogether, this evidences the importance of proteasomal degradation of immune-related proteins as a mechanism of regulation in plant immunity. This regulation occurs at all stages, from perception to execution, and allows finely tuned effective defense responses. It is noteworthy that many E3s such as the abovementioned PUB13 or *Os*APIP10 present multiple targets. This guarantees a huge degree of versatility to react to changing environmental conditions, which could explain their evolutionary expansion in the plant lineage. However, it also shows how vulnerable the UPS and its components are toward perturbations by factors that can manipulate these processes, making the UPS an ideal target for plant pathogens.

2.2. The Ubiquitin–Proteasome System Is Also Directly Involved in Plant Immunity

The UPS's ability to regulate plant immunity goes beyond the degradation of immune-related proteins as components of the UPS itself and upstream regulators of its assembly and/or activity are also involved in regulating defense responses (**Figure 2*a***).

2.2.1. Roles of the 26S proteasome complex in immunity. The 26S proteasome complex is the heart of the UPS. Although proteasome subunits have been historically considered housekeeping genes, mounting evidence supports a very dynamic regulation at the transcription, translation, and post-translational levels (83). How the proteasome assembly and functioning are regulated and what additional proteasome-independent functions the individual subunits might have remain elusive.

Proteasome subunits and their function in plant immunity. A general trend among plants upon pathogen perception is the induction of transcription and/or translation of proteasomal subunits to increase their abundance and accessibility; e.g., fungal elicitation induces *Arabidopsis* PBB1

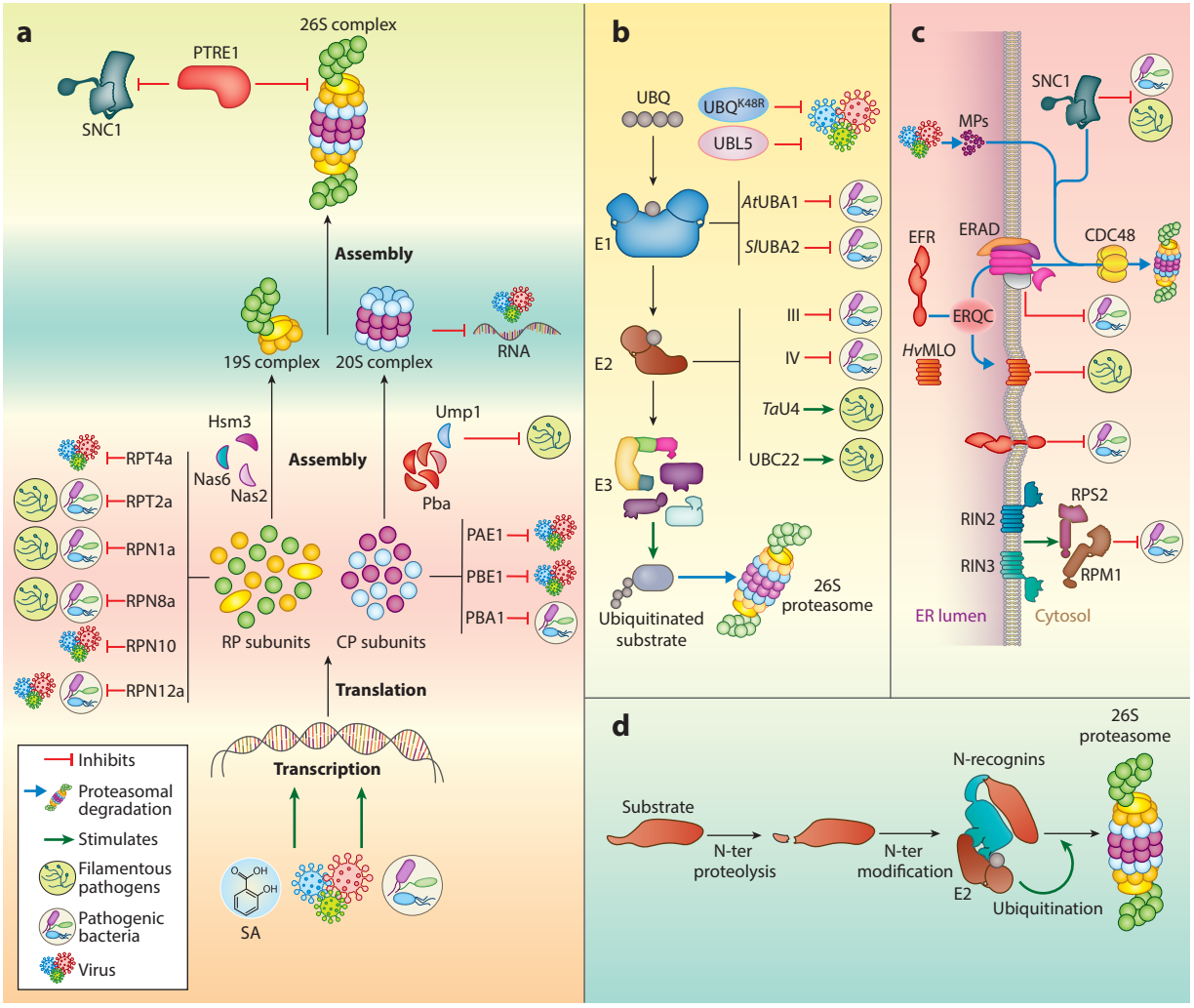

Figure 2

Different ubiquitin–proteasome system (UPS) components are directly involved in plant immunity. (*a*) The 26S proteasome formation requires successive steps of transcription/translation of individual subunits and generation of the 19S regulatory particle (RP) and 20S core particle (CP) complexes and their assembly. All these steps are involved in plant immunity. (*b*) Early components of the ubiquitination machinery are involved in plant immunity. Ubiquitin moieties, E1 activating enzyme, and E2 conjugating enzyme are all involved in plant defense with contrasting roles at several levels. (*c*) The UPS branch endoplasmic reticulum quality control (ERQC) involves ER-resident components to monitor multiple immune-related proteins. ERQC mediates protein subcellular sorting through ER-associated degradation (ERAD). Other ERAD-related components are also involved in cytosolic protein turnover and immune signaling. (*d*) The N-degron pathway, another branch of the UPS, depends on specific post-translational modification of the N-termini of substrate proteins. This modification is recognized by specific E3 ligases for subsequent ubiquitination and proteasomal degradation. Abbreviations: EFR, EF-Tu receptor; MPs, movement proteins; SA, salicylic acid.

accumulation (69), viral infection increases pepper *RPN7* transcription (67), *P. syringae* induces accumulation of PBA1 and RPT2, and SA induces tobacco *RPT6* gene expression (128, 131). Over the years, many studies have genetically investigated the role of proteasomal subunits in immunity. For instance, it was shown that mutating subunits *PBA1*, *RPN1a*, and *RPN8* in *Arabidopsis* result

in increased susceptibility to *P. syringae* and powdery mildew (151). Additionally, silencing *RPT6* abolishes XopJ–SA-induced cell death (129). Proteasome mutants deficient in *RPT2a* display altered NLR stability, reduced systemic acquired resistance (SAR), and increased susceptibility to *P. syringae* (20, 133). Similarly, several mutants of proteasomal subunits also show increased susceptibility to *cauliflower mosaic virus* (CaMV) infection (113). Interestingly, the tomato *RPT4a* is involved in resistance against *tomato leaf curl New Delhi virus* in a proteolytic-independent manner but through viral DNA binding and host RNA polymerase II inhibition (108).

The holoenzyme and its regulation. The assembly of the different proteasomal subunits and subcomplexes requires the coordinated action of several players, some of which have been shown to be directly involved in immunity. For instance, the rice regulators of the 26S proteasome assembly OsUMP1 mediate non-race-specific resistance against *Magnaporthe oryzae* by modulating the H_2O_2 levels (47). Moreover, proteasome regulator 1 (PTRE1) is involved in the degradation of the NLR suppressor of npr1–1 constitutive 1 (SNC1) (126). The proteasomal subcomplexes themselves can also affect immunity prior to assembly. Extracted sunflower 20S complexes were shown to possess endonuclease activity and degrade viral RNA from *tobacco mosaic virus* and *lettuce mosaic virus* (LMV) (3).

2.2.2. Roles of other components and branches of the ubiquitin–proteasome system in immunity. The prominent role of E3s as drivers of target specificity has already been discussed in previous sections. However, ubiquitin-mediated degradation also requires upstream E1 and E2 enzymes to activate and transfer the ubiquitin moiety (**Figure 2*b***). A mutation in one of the two *Arabidopsis* E1 enzymes, ubiquitin-activating enzyme 1 (UBA1), results in increased susceptibility to *P. syringae* (40). In contrast, in tomato it is only UBA2 and not UBA1 that, upon silencing, causes increased susceptibility against the same pathogen, evidencing species-specific differences (159). In the same study, several E2s were found to also contribute to resistance against *P. syringae* (159). Several E2s from *N. benthamiana* have also been described as positive regulators of immunity. In contrast, other E2 enzymes have been described as negative regulators of immunity (158). This is the case of wheat TaU4 or *Arabidopsis* ubiquitin-conjugating enzyme 22 (UBC22) (87, 138). The ubiquitin molecule itself is also important, as overexpression of a variant unable to make K48 linkages results in enhanced tolerance to a viral infection and overaccumulation of the canonical defense marker protein pathogenesis-related 1 (PR1) (5). Furthermore, ubiquitin-like peptide 5 (UBL5) is also a positive regulator of defense against viruses in *N. benthamiana* and rice (10). Finally, the UPL E3 ligases have been identified as novel upstream regulators of the proteasome. The UPLs have been described to be associated with the proteasome to promote its processivity and involved in plant immune responses (36). This is confirmed by a recent study that identified a ubiquitin-ligase relay that involves the UPL3 and UPL4 E3 ligases to promote processive degradation of SA master regulator NPR1 (140).

A specific branch of the UPS occurs at the endoplasmic reticulum (ER), where protein translation and subcellular sorting occur. This UPS branch is called ER quality control (ERQC) and relies on specific ER-associated E2–E3 enzymes that mediate proteasomal degradation of ER-resident proteins through ER-associated degradation (ERAD) (13) (**Figure 2*c***). In plants, ERAD has been widely studied in the context of the brassinosteroid (BR) receptor BR-insensitive 1 (BRI1) quality control (119). However, it has been proposed that ERAD is also involved in degradation of immune receptors such as the *Arabidopsis* EF-Tu receptor (EFR) or barley *Mildew Locus O* (MLO) (70, 90). Additional ERQC components such as *Arabidopsis* E3s RING2 and 3 and the CDC48 retro-translocase complex, as well as several tomato ER-resident E2s, are also involved in different immune responses (23, 59, 159).

Another UPS branch involved in immunity is the N-degron pathway. This pathway relies on the proteolytic cleavage and modification of the N-termini of substrate proteins that make them accessible to specific E3 ligases for subsequent degradation (29) (**Figure 2*d***). The involvement of this pathway in immunity is evidenced by SNC1, whose N-terminal methionine can be targeted by two acetyl transferases antagonistically regulating its stability (143). Additionally, mutation on certain components of the N-degron pathway such as *arginine transferase 1* and *2* (*ATE1* and *2*) or the E3 *proteolysis 1* and *6* (*PRT1* and *6*) show contrasting roles in tolerance/susceptibility to different pathogens (27, 43, 127, 134).

In this section, we have reviewed the complex and multifaceted involvement of the UPS in the regulation of plant immunity. Over the years, it has become quite clear that the UPS is a major immune hub, involved in all stages of plant defenses against all kinds of pathogens across most plant species. This involvement is, however, complex, as different reports show contrasting contributions to defenses depending on the path system, condition, or component studied. This implies an underlying yet unknown regulatory network that determines the outcome of plant–pathogen interactions.

3. PLANT PATHOGENS TARGET THE UBIQUITIN–PROTEASOME SYSTEM FOR THEIR OWN BENEFIT

Given the conservation and importance of the UPS in fine-tuning the plant defense response, it constitutes an ideal target for microbial manipulation. Targeting the proteasome and its components is a very efficient way to subvert cellular processes, as pathogens only need to hit one particular pathway to manipulate and disrupt the entire host system. Creating a chaotic environment in the host benefits the pathogen, as the host cannot react to invading intruders anymore. Thus, during the course of evolution, pathogens gained sophisticated strategies to indirectly and directly target the host UPS. To date, various plant pathogens, from viruses and bacteria to oomycetes, fungi, and nematodes, use different means to manipulate the UPS for their own benefit. In this section, we discuss various examples of how diverse plant pathogens employ different mechanisms to exploit the host UPS to dampen plant immune responses and create a favorable environment for their multiplication.

3.1. Bacteria

To overcome plant defense responses, plant-pathogenic bacteria have acquired a highly conserved type III secretion system (T3SS) to inject so-called type III effectors (T3Es) into the host cell. These T3Es are targeted to many cellular compartments and act as important determinants to promote disease progression by dampening various plant immune reactions (60). Although for many years research was focused on their function to suppress PTI and ETI responses, growing evidence suggests that T3Es target more central processes such as the UPS to subvert cellular processes in the host system (66, 105) (**Figure 3*a***). Initial findings in the effector biology field have been focused on effectors mimicking host eukaryotic proteins. Among the most studied effector proteins is AvrPtoB from *P. syringae*, which displays E3 ligase activity in planta (1). Its E3 ligase function is essential to ubiquitinate and degrade host targets via the 26S proteasome, making AvrPtoB the first effector to hijack the UPS to facilitate its virulence function during bacterial infection. The bacterial effector AvrPtoB was shown to interact with several E2 ligases in the host cell to enable the degradation of various PRRs such as CERK1, FLS2, and other PRR-associated proteins such as BAK1 and BIK1 (16, 38, 39). It is a primary example of how an effector hijacks and tricks host cellular systems by targeting the housekeeping recycling machinery of PRRs to subvert plant defense responses. Many other host targets have been identified

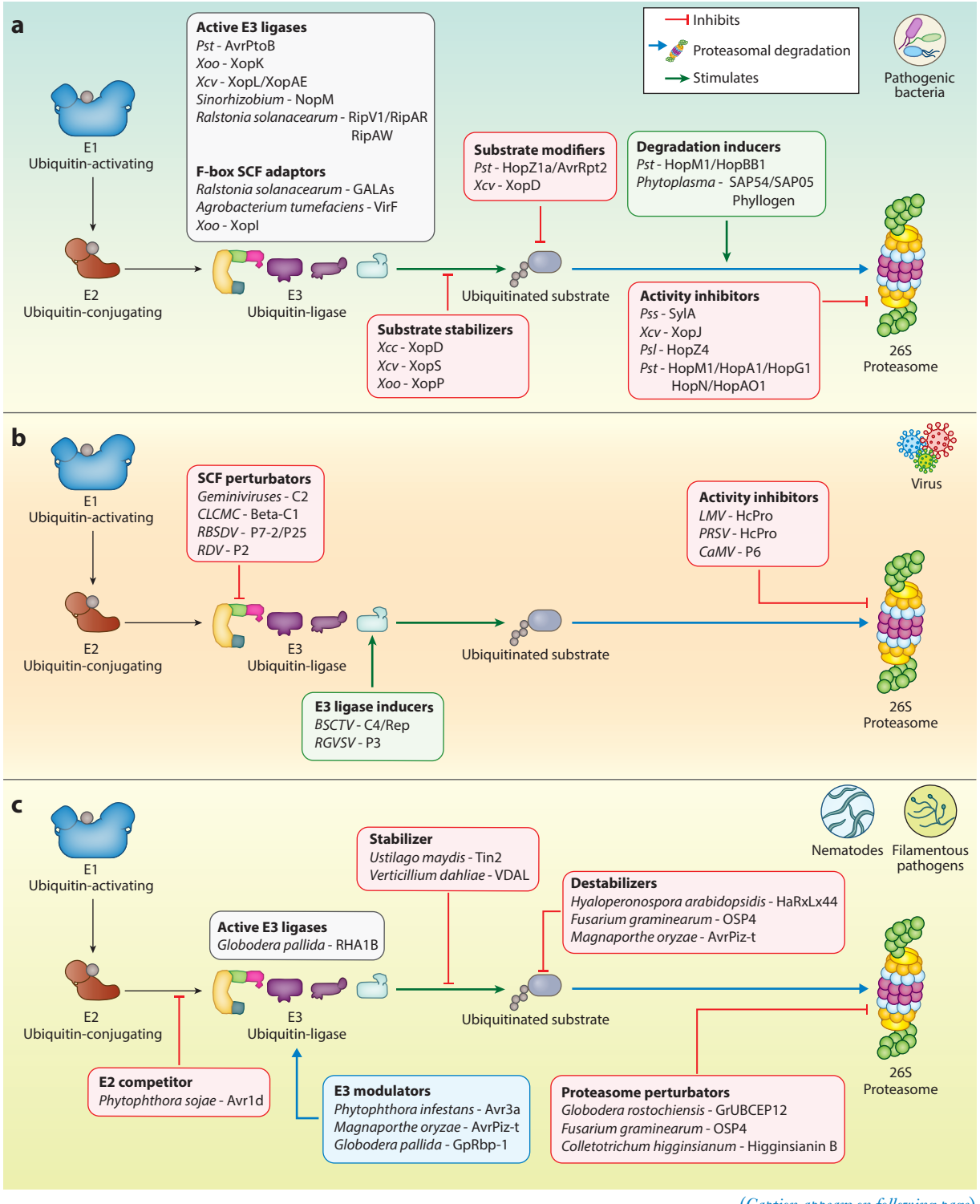

(Caption appears on following page)

Figure 3 (*Figure appears on preceding page*)

Plant pathogens deploy diverse mechanisms to exploit the ubiquitin–proteasome system (UPS) to promote disease. Each pathogenic molecule and the species of origin are grouped in boxes based on their modes of action. (*a*) Bacteria use different effector proteins to either degrade or stabilize host targets through different mechanisms. (*b*) Viruses target Skp1-cullin 1-F-box (SCF) complexes, E3 ligases, and the 26S proteasome to modulate the degradation of substrate proteins. (*c*) Eukaryotic pathogens alter the UPS at various steps, including competition with host E2s, modulation of E3 activities, destabilization of effector targets, and perturbation of the 26S proteasome.

that are targeted by AvrPtoB for degradation, of which SA master regulator NPR1 plays one of the most central roles in plant immunity (11). To guarantee a functional SA signaling, NPR1 is constitutively degraded in the nucleus by the 26S proteasome. The T3E AvrPtoB exploits this feature by targeting NPR1 in an SA-dependent manner. Association of both proteins results in a degradation of NPR1, which most likely takes place in the cytoplasm before its delivery into the nucleus. As such, AvrPtoB is not only able to dampen SA-mediated defense responses but also attenuate PTI and SAR reactions. The T3E AvrPtoB is not the only bacterial E3 ligase targeting PTI by degrading PRRs or master regulators of plant immunity. Another T3E that targets a PRR is the E3 ligase XopK from *Xanthomonas oryzae*. XopK interacts and ubiquitinates rice *Os*SERK2 to degrade it via the 26S proteasome (102). Removal of *Os*SERK2 enables the efficient inhibition of multiple PRR signaling pathways, thus providing an attractive target to promote virulence.

Although AvrPtoB is structurally homologous to RING E3s, other identified T3Es lack similarities to known eukaryotic E3 enzymes. Among them there is a family of bacterial E3s containing a novel E3 ligase (NEL) domain. At the structural level, most proteins belonging to the NEL family have an N-terminal domain with leucine-rich repeats (LRRs). The C-terminal region harbors the NEL domain with a catalytic cysteine residue required for the formation of E3–ubiquitin intermediates and E2–ubiquitin complex formation. Although T3Es belonging to the NEL family were first discovered in animal pathogens, later studies revealed that they are also present in plant-associated *Sinorhizobium*, *Ralstonia*, and *Xanthomonas* (7). This is the case of *X. euvesicatoria* XopL. The crystal structure of its C-terminal domain revealed a novel fold, termed XL-box, displaying E3 ligase activity in vitro, whereas the N-terminal region harbors an LRR domain that is necessary to suppress PTI in plants (114). However, its C-terminal domain lacks cysteine residues that are present in other NEL family members. Further studies revealed that XopL associates with the autophagy component SH3P2 to dampen host autophagy (68). Specifically, XopL ubiquitinates SH3P2 in vitro and in planta, which results in proteasome-dependent degradation of SH3P2. The elimination of SH3P2 perturbs autophagic degradation, which is beneficial for the proliferation of *Xanthomonas* in plants. Interestingly, XopL also undergoes autoubiquitination in planta, which may result in its autophagic degradation, termed effectorphagy. This constitutes another example of the evolutionary arms race between plants and pathogens, in which XopL may have acquired its function to degrade SH3P2 to prevent its own removal to exhibit its virulence function in the host system. Alongside XopL, XopAE from the same *Xanthomonas* species has been identified to share structural and functional similarities with XopL harboring an XL-box with E3 ligase activity and dampening PTI responses (68). XopAE plant targets, however, remain elusive. In addition, the E3 ligase function of XopL seems to be conserved across different *Xanthomonas* species. Rice pathogen *X. oryzae* pv. *oryzae* injects XopL to degrade ferredoxin in a proteasome-dependent manner to cause cell death (79). Other *Xanthomonas* species such as *Xanthomonas axonopodis* pv. *punicae* or *Xanthomonas campestris* pv. *campestris* possess XopL homologs that display major virulence function, although their targets remain to be identified (116, 148). NopM from *Sinorhizobium* exhibits E3 ligase activity and is phosphorylated by MAPKs (142). Further studies are required to unveil its targets in the host system as well as how its E3 ligase activity acts during the interaction with host plants. Other NEL members, including RipV1, RipAR, and RipAW, are described in

Ralstonia solanacearum. All these T3Es have been shown to suppress plant PTI reactions in an E3-activity-dependent manner, although their targets remain unknown (15, 91).

Although mimicking E3 ligase activity is a very efficient way for a T3E to degrade host proteins, it is not the only way to achieve the removal of immune-related components. Several plant-pathogenic bacteria have evolved F-box effector proteins that can act as adaptors in the Skp1-cullin 1-F-box (SCF) E3 ligase complex. The RipG T3E family from *R. solanacearum* associates with the host SCF complex and is hypothesized to act as E3s (2). In a similar way, VirF from *Agrobacterium tumefaciens* and, more recently, XopI from *X. oryzae* were shown to act in the SCF complex to mediate the degradation of the transcription factor VIRE2-interacting protein 1 (VIP1) and the rice thioredoxin OsTrxh2, respectively, to subvert plant resistance (51, 64).

Although this seems to be another direct way to target host proteins to the proteasome, some T3Es have been suggested to serve as adaptors between E3 ligases without displaying any known features of F-box proteins or other UPS components. One of the first examples of how an effector leads to the destabilization and degradation of its target is HopM1 from *P. syringae*. HopM1 is able to promote disease by inducing the proteasomal degradation of HopM1 interactor 7 (AtMIN7), a host ADP ribosylation factor guanine nucleotide exchange factor (96). As *At*MIN7 was previously shown to be involved in vesicle trafficking and recycling of auxin efflux transporters (121), it was suggested that HopM1-mediated degradation of *At*MIN7 is suppressing secretion to the benefit of the bacteria. It has now been revealed that HopM1 and AvrE establish an aqueous environment by hijacking abscisic acid signaling and are largely independent of *At*MIN7 (106). Future studies may reveal the immunity-related function of *At*MIN7 degradation. Another example of a T3E promoting degradation of its host target is HopBB1 from *P. syringae*. HopBB1 was identified to promote the degradation of the TF TCP14 by targeting it to the SCF^{COI} complex. With this, HopBB1 modulates phytohormone responses and virulence (150). In a similar manner, SAP54 from phytoplasmas, which are phloem-inhabiting bacteria, hijacks RAD23, a ubiquitin-binding protein and proteasome-shuttle factor, to degrade MADS-box TFs from *Arabidopsis* via the 26S proteasome to promote insect colonization (81). Another study identified that phyllogen, an effector from phytoplasmas, induces the degradation of floral MADS-box TFs (MTFs) via RAD23 shuttle proteins. Interestingly, these findings suggest that phyllogen is functionally mimicking ubiquitin, as MTF–phyllogen–RAD23 complex formation was ubiquitin independent (61, 82). Along this line, another phytoplasma effector, SAP05, was recently described to mediate ubiquitin-independent degradation of *Arabidopsis* TFs SQUAMOSA promoter-binding protein-like (SPL) and GATA to induce symptoms. Degradation of both TFs was achieved by direct interaction of SAP05 with the ubiquitin receptor RPN10, a subunit of the 26S proteasome (49). Most of the mentioned examples involve the proteasome shuttle factor RAD23 and how effectors hijack its function to degrade their targets. Although not shown, HopM1 could also deploy a similar strategy to induce the proteasome-dependent removal of AtMIN7, as it was initially identified to interact with RAD23.

Other examples of ubiquitin-independent degradation of host target proteins involve T3Es with specific enzymatic functions that destabilize their substrates by PTMs. For instance, *Pseudomonas* HopZ1a acts as an acetyltransferase on JAZ repressors to activate JA signaling, which in turn suppresses SA defense responses. Acetylation of JAZ proteins leads to their destabilization and degradation by the UPS (53). Apart from acetylation, SUMOylation also plays a major role in destabilization or stabilization. XopD from *Xanthomonas* exhibits SUMO-protease activity on tomato ethylene responsive factor 4 (ERF4), resulting in its proteasomal degradation. Destabilization of proteins not only includes the modulation of PTMs but can also appear via the N-degron pathway. The first T3E described to hijack this pathway is AvrRpt2 from *P. syringae*, a cysteine protease that degrades host proteins containing a nitrate-induced domain (41).

The manipulation mechanisms we have described so far rely on the degradation of host targets. However, sometimes the opposite is required, as stabilization of negative regulators of immunity could ultimately end in subversion of plant defenses as well. For instance, *Xanthomonas* XopD is able to inhibit the degradation of the DELLA protein repressor of GA (RGA) to promote disease (120). In a similar way, a recent study characterized the role of *X. euvesicatoria* XopS in preventing the proteasomal degradation of pepper TF WRKY40 (104). XopS is a major virulence factor of *X. euvesicatoria* that prevents stomatal closure to promote disease progression. This is dependent on the stabilization of WRKY40, a negative regulator of PTI. XopS interacts with and inhibits the degradation of WRKY40 via a yet unknown mechanism to reduce downstream defense gene expression and alter phytohormone cross talk. Although in the case of XopS the mode of action is yet not understood, another *Xanthomonas* effector, XopP from *X. oryzae* pv. *oryzae*, has been identified to specifically inhibit the E3 ligase activity of *Os*PUB44, a positive regulator of immune responses, to suppress PTI in rice (50).

Although targeting E3 ubiquitin activity or PTMs indirectly affects the proteasomal degradation, there is also a very direct way to inhibit the proteasome: by targeting the proteasome itself. The bacterial toxin syringolin A (SylA) was the first virulence factor described to directly bind to subunits of the 20S proteasome and, thereby, act as an irreversible proteasome inhibitor (44). Direct inhibition of the proteasome by SylA has many positive effects on *P. syringae*: It (*a*) results in a block of SA signaling in adjacent tissues, (*b*) increases the bacterial motility, and (*c*) suppresses immune responses at the local infection site (88). Despite its important virulence function, SylA is not widely distributed in *Pseudomonas* or other plant-pathogenic bacteria (4). Nevertheless, plant-pathogenic bacteria have evolved T3Es that can directly target the 26S proteasome to alter its function. A primary example is XopJ from *X. euvesicatoria*. XopJ directly interacts with the proteasomal subunit RPT6 (130). This interaction results in reduced proteasome activity and suppression of SA-mediated plant defenses. Subsequent studies have revealed that XopJ displays protease activity to degrade RPT6, which hampers the proteasome function. A following study revealed that a closely related *P. syringae* ortholog of XopJ, HopZ4, also interacts with RPT6 and suppresses proteasome activity (132).

Although *P. syringae* pv. *tomato* lacks SylA, it still suppresses proteasome activity in a T3E-dependent manner. Several T3Es from *P. syringae* pv. *tomato* such as HopA1, HopG1, HopN, HopAO1, and HopM1 hamper proteasome activity (133). The latter was additionally shown to associate with several proteasome subunits and HECT UPL E3 ligases in planta (133). Given the function of the UPL E3 as regulators of proteasome function, it is possible that HopM1 suppresses proteasome activity in a direct manner by interfering with their function (140). However, subsequent studies revealed that HopM1 removes proteasome subunits by activating a selective autophagy mechanism termed proteaphagy (131).

3.2. Viruses

Viruses are versatile, intracellular, obligate pathogens with a biotrophic lifestyle, as they lack their own replication machinery and thus require host cellular pathways to colonize their hosts. In contrast to bacteria, viruses are intracellular pathogens and associate with various host cellular compartments that they can reprogram for their own benefit. Emerging evidence suggests that the plant UPS plays an important role during plant–virus interactions: On one hand, the UPS can impair viral pathogenesis; on the other hand, viruses evolved strategies to exploit the UPS (31). Although viral genomes are very small and encode only a few proteins, they can act on multiple targets to generate a very flexible and versatile response to the plant defense machinery. Viruses employ different strategies to manipulate the host UPS, including the direct targeting of the

proteasome, influencing the expression of UPS components and their activities, or perturbing the degradation of host proteins (**Figure 3*b***). Viral effector HcPro, a known gene silencing suppressor, from LMV and *papaya ring spot virus* (PRSV) directly interacts with the catalytic subunits of the 20S proteasome to inhibit the 20S endonuclease and proteasome activity, respectively (3, 107). Inhibition of the 20S activity resulted in enhanced viral accumulation and, therefore, can be considered a proviral mechanism. Similar to HcPro from LMV and PRSV, HcPro from *potato virus x* directly associates with subunits of the 20S proteasome, albeit the nature of this interaction has yet to be determined (55).

Although no viral effectors have been identified that directly degrade host proteins, some viral proteins have been shown to induce endogenous E3 gene expression. For instance, the C4 protein from *beet severe curly top virus* (BSCTV) induces the transcription of related to KPC1 (RKP) in *Arabidopsis*. RKP targets the cell-cycle inhibitor kinase inhibitor protein (KIP)-related protein 2, which was shown to be beneficial for viral replication (65). Another viral protein from BSCTV, Rep, was found to transcriptionally induce variant in methylation 5 (*VIM5*) to induce the transcription of the viral proteins C2 and C3 (14). Similarly, the P3 protein from *rice grassy stunt virus* (RGSV) has been described to induce the transcription of *Os*P3IP1 in rice. *Os*P3IP1 ubiquitinates nuclear RNA polymerase D1a (*Os*NRPD1a), the largest subunit of plant-specific RNA polymerase IV, for proteasomal degradation (155). However, not only E3 ligases and their activities are crucial for viral replication and fitness. Recently, it has been shown that CaMV requires the proteasome for robust infection. CaMV induces proteasome activity in an SA-dependent manner to support systemic viral accumulation and plant fitness. Interestingly, the viral protein P6 attenuates proteasome activity induced by SA during CaMV infection, which may act as a counteracting measure in the proteasome–virus interaction (113). These apparently conflicting findings emphasize the complexity of the intimate interplay between viruses and the UPS pathway.

A more direct way for viruses to perturb E3 ligase activity in the host is to target SCF complexes, which seem to be target hubs for viral proteins. Several viral proteins target these complexes to promote viral replication in different ways. For instance, C2 proteins from geminiviruses subvert ubiquitination by compromising CSN activity, which in turn perturbs the function of SCF complexes and inhibits JA signaling (76). Other viral effectors such as βC1 from *cotton leaf curly multan virus* have been described to interfere with SCF complex formation. Here, βC1 inhibits the association between *Nb*SKP1 and *Nb*CUL1 to disturb JA and gibberellin signaling (57). Other viral proteins interacting with the SCF complex are P7-2 and P25 from *rice black-streaked dwarf virus*, which interacts with eight S-phase kinase-associated protein 1 (SKP1) proteins, a core subunit of the SCF complex (123, 124). Exploiting the SCF complex likely affects degradation of host proteins and thus constitutes an attractive target for viral proteins. In support of this, P2 protein from the *rice dwarf virus* blocks association between *Os*IAA10 and the F-box *Os*TIR1 to dampen *Os*IAA10 proteasomal degradation (54). Another viral protein 2b from *cucumber mosaic virus* (CMV) inhibits JA signaling by preventing the degradation of JAZ repressors to enhance aphid-mediated viral transmission (160).

3.3. Oomycetes, Fungi, Nematodes, and Insects

Similar to bacteria, eukaryotic pathogens such as oomycetes, fungi, nematodes, and insects also exploit their effector arsenals to subvert the host defenses. However, owing to their higher complexity, fewer examples have been characterized. Nevertheless, there is enough current evidence supporting the ability of eukaryotic pathogens to infer the proper functioning of the plant UPS (**Figure 3*c***). For instance, there are several effectors from eukaryotic pathogens that target host proteins for proteasomal degradation to carry out their virulence function. This is the case of the effector HaR×L×44 from the biotrophic oomycete *Hyaloperonospora arabidopsidis*, which interacts

and destabilizes mediator complex 19A (MED19A) in a proteasome-dependent manner (9). MED19A is a subunit of the mediator complex, responsible for the interaction between transcriptional regulators and RNA polymerase II. By doing this, *H. arabidopsidis* tilts the SA–JA antagonistic balance toward the latter, making the plant more susceptible to biotrophic pathogens. The fungal effector AvrPiz-t from *M. oryzae* itself is targeted by the plant proteasome upon ubiquitination by the rice E3 ligases *Os*APIP6 and *Os*APIP10 (100). Interestingly, by doing so, AvrPiz-t targets these E3 ligases to proteasomal degradation as well in a sort of kamikaze move, which, in turn, dampens the rice basal defenses. Similarly, *Zymoseptoria tritici* effector *Zt*SSP2 has been recently shown to interact with the E3 ligase *Ta*E3UBQ, a positive regulator of wheat immunity. However, the influence of the *Zt*SSP2–*Ta*E3UBQ interaction on *Zt*SSP2 and *Ta*E3UBQ stability and activity remains to be discovered (58). Fungal effector orphan secreted protein 24 (OSP24) from *Fusarium graminearum* also induces the proteasomal degradation of the wheat protein *Ta*SNRK1a by competing with the host kinase stabilizer *Fusarium* resistance orphan gene (*Ta*FROG) (52). Another mentioned strategy to trigger host protein degradation is mimicking plant E3 ligases. This strategy could potentially be developed more easily in the case of eukaryotic pathogens compared to bacteria considering their closer phylogenetic relationship to plants. This strategy is deployed by the potato cyst nematode *Globodera pallida*. *G. pallida* effector RHA1B is an active RING E3 ligase that can interact with multiple host E2 enzymes (63). RHA1B possesses a double virulence function, inhibiting both PTI and ETI in E3-independent and E3-dependant manners, respectively. It has been hypothesized that this strategy could also be deployed by gall-forming insects, as suggested by the expansion of secreted RING E3 ligases in *Daktulosphaira vitifoliae* (157).

In addition to targeting positive regulators of immunity for degradation, eukaryotic pathogen effectors can exert their virulence functions also by doing the opposite: stabilizing negative regulators of immunity. This is the case of the oomycete effector Avr3a from *P. infestans*. Avr3a inhibits the proteasomal degradation of the PUB E3 ligase CYS, MET, PRO, and GLY protein 1 (CMPG1), perturbing CMPG1-mediated defensive PCD (6). Fungal effector Tin2 from *Ustilago maydis* stabilizes maize TIN2-targeting kinase 1 (ZmTTK1) by masking its ubiquitin–proteasome degradation motif, ultimately rewiring metabolic fluxes toward the synthesis of anthocyanins instead of defensive tissue lignification (122). Another strategy for stabilization of host targets is to outcompete for the interaction with the correspondent E3 ligase(s). This is, for instance, the case of the fungal effector VDAL from *Verticillium dahliae*, whose interaction with the host PUB25 and PUB26 E3 ligases prevents their association with its native target, MYB6, to possibly expand the biotrophic phase of infection (78).

Besides degrading or stabilizing UPS targets, eukaryotic pathogens can also affect the normal functioning of the UPS in a more direct manner by targeting regulatory processes of proteasomal assembly or activity. For example, the effector ubiquitin carboxyl extension protein 12 (GrUBCEP12) from the yellow potato cyst nematode *Globodera rostochiensis* prevents the expression of the proteasomal subunit encoding gene *RPN2* and, upon proteolytic activation, blocks PTI responses (19). The enzymatic activity of the proteasome can also be targeted by pathogen molecules. For instance, the fungal toxin higginsianin B from *Colletotrichum higginsianum* is a potent inhibitor of the chymotrypsin- and caspase-like proteasomal activities. This inhibition ultimately leads to JAZ stabilization and impaired JA signaling to the benefit of the pathogen (26). There is also evidence of a nematode effector, GpRbp-1 from *G. pallida*, that interacts with a nuclear proteasome-associated HECT E3 ligase UPL3 (28). Although the outcome of this interaction remains to be characterized, it has been reported that the HECT-containing ubiquitin-protein ligases (UPLs) are regulators of the proteasome and plant immunity (36, 140). The E1→E2→E3 cascade can also be targeted by pathogen effectors in their effort to subvert plant defenses. This is the case for the oomycete *Phytophthora sojae* effector Avr1d, which acts as

an E2 competitor occupying the E2 binding site of the soy E3 ligase GmPUB13 and ultimately promoting *P. sojae* proliferation (72). Altogether, these data show how general and important is the manipulation of the UPS and UPS-related proteins among all kinds of plant pathogens.

4. CONCLUDING REMARKS AND PERSPECTIVES

Emerging evidence suggests that the UPS is a key pillar of the plant immune system. The UPS governs the turnover of many immune-related components and hence constitutes a vulnerable target for pathogens. As such, diverse plant pathogens employ sophisticated strategies to manipulate the UPS and combat plant immune reactions. Pathogen effectors can induce or block the degradation of target proteins involved in immune reactions. In this context, effectors can serve as tools to dissect how the UPS is involved in plant–pathogen interactions. Current knowledge implies that the UPS acts as a double-edged sword: on one hand, the UPS is required to maintain efficient plant defense responses; on the other hand, pathogens require its proper function to promote pathogenicity. In addition, different effectors from the same pathogen can display contrasting functions, which could be partially explained by their distinct spatiotemporal modes of action. Taking these observations into consideration, it is evident that we are only scratching the surface of this complex interplay. To gain a better understanding, it will be crucial to decipher the fine-tuning of the proteasome and its components on every level: from transcription and translation to the assembly of the proteasome and its associated components. We will thereby decipher the complexity of the interplay between microbes and the UPS.

5. OUTSTANDING QUESTIONS

Recent findings on the plant UPS, its cross talk with plant immunity, and how it is targeted by plant microbes have advanced our understanding in this field. However, many open questions remain unanswered and need to be addressed in the future to fully decipher the complex interplay between the UPS and microbes:

- How do microbial effectors with contrasting or additive functions on the UPS influence each other?
- Do microbes directly target the regulation of the proteasome complex to impact plant immune reactions and host cellular pathways?
- Are there different proteasome complexes with alternative functions induced during microbial infection?
- What role does cell-type specificity play in the interaction of microbes with the UPS?
- How can we strengthen the host UPS to avoid its targeting by microbes?
- How are organelle- or compartment-specific associated degradation systems influenced by microbes?
- How is the UPS altered if we look beyond binary interactions?

DISCLOSURE STATEMENT

The authors are not aware of any affiliations, memberships, funding, or financial holdings that might be perceived as affecting the objectivity of this review.

ACKNOWLEDGMENTS

We apologize to the authors whose work we were not able to cite due to space constraints. S.Ü. was supported by an Emmy Noether Fellowship GZ: UE 188/2-1 from the Deutsche

Forschungsgemeinschaft (DFG). G.L. was supported by the Collaborative Research Centre 1101 (SFB1101). M.G.F. was supported by the Walter Benjamin Program of the DFG (GO 3479/1-1).

LITERATURE CITED

1. Abramovitch RB, Janjusevic R, Stebbins CE, Martin GB, Lindow SE. 2006. Type III effector AvrPtoB requires intrinsic E3 ubiquitin ligase activity to suppress plant cell death and immunity. *PNAS* 103(8):2851–56
2. Angot A, Peeters N, Lechner E, Vailleau F, Baud C, et al. 2006. *Ralstonia solanacearum* requires F-box-like domain-containing type III effectors to promote disease on several host plants. *PNAS* 103(39):14620–25
3. Ballut L, Petit F, Le Gall O, Candresse T, Schmid P, et al. 2003. Biochemical identification of proteasome-associated endonuclease activity in sunflower. *Biochim. Biophys. Acta* 1645(1):30–39
4. Baltrus DA, Nishimura MT, Romanchuk A, Chang JH, Mukhtar MS, et al. 2011. Dynamic evolution of pathogenicity revealed by sequencing and comparative genomics of 19 *Pseudomonas syringae* isolates. *PLOS Pathog.* 7(7):e1002132
5. Becker F, Buschfeld E, Schell J, Bachmair A. 1993. Altered response to viral infection by tobacco plants perturbed in ubiquitin system. *Plant J.* 3(6):875–81
6. Bos JIB, Armstrong MR, Gilroy EM, Boevink PC, Hein I, et al. 2010. *Phytophthora infestans* effector AVR3a is essential for virulence and manipulates plant immunity by stabilizing host E3 ligase CMPG1. *PNAS* 107(21):9909–14
7. Bullones-Bolaños A, Bernal-Bayard J, Ramos-Morales F. 2022. The NEL family of bacterial E3 ubiquitin ligases. *Int. J. Mol. Sci.* 23(14):7725
8. Bürger M, Chory J. 2019. Stressed out about hormones: how plants orchestrate immunity. *Cell Host Microbe* 26(2):163–72
9. Caillaud MC, Asai S, Rallapalli G, Piquerez S, Fabro G, Jones JDG. 2013. A downy mildew effector attenuates salicylic acid-triggered immunity in *Arabidopsis* by interacting with the host mediator complex. *PLOS Biol.* 11(12):e1001732
10. Chen B, Lin L, Lu Y, Peng J, Zheng H, et al. 2020. Ubiquitin-like protein 5 interacts with the silencing suppressor p3 of rice stripe virus and mediates its degradation through the 26S proteasome pathway. *PLOS Pathog.* 16(8):e1008780
11. Chen H, Chen J, Li M, Chang M, Xu K, et al. 2017. A bacterial type III effector targets the master regulator of salicylic acid signaling, NPR1, to subvert plant immunity. *Cell Host Microbe* 22(6):777–88.e7
12. Chen L, Hellmann H. 2013. Plant E3 ligases: flexible enzymes in a sessile world. *Mol. Plant* 6(5):1388–404
13. Chen Q, Zhong Y, Wu Y, Liu L, Wang P, et al. 2016. HRD1-mediated ERAD tuning of ER-bound E2 is conserved between plants and mammals. *Nat. Plants* 2:16094
14. Chen ZQ, Zhao JH, Chen Q, Zhang ZH, Li J, et al. 2020. DNA geminivirus infection induces an imprinted E3 ligase gene to epigenetically activate viral gene transcription. *Plant Cell* 32(10):3256–72
15. Cheng D, Zhou D, Wang Y, Wang B, He Q, et al. 2021. *Ralstonia solanacearum* type III effector RipV2 encoding a novel E3 ubiquitin ligase (NEL) is required for full virulence by suppressing plant PAMP-triggered immunity. *Biochem. Biophys. Res. Commun.* 550:120–26
16. Cheng W, Munkvold KR, Gao H, Mathieu J, Schwizer S, et al. 2011. Structural analysis of *Pseudomonas syringae* AvrPtoB bound to host BAK1 reveals two similar kinase-interacting domains in a type III effector. *Cell Host Microbe* 10(6):616–26
17. Cheng YT, Li Y, Huang S, Huang Y, Dong X, et al. 2011. Stability of plant immune-receptor resistance proteins is controlled by SKP1-CULLIN1-F-box (SCF)-mediated protein degradation. *PNAS* 108(35):14694–99
18. Choi C, Im JH, Lee J, Il Kwon S, Kim W-Y, et al. 2022. OsDWD1 E3 ligase-mediated OsNPR1 degradation suppresses basal defense in rice. *Plant J.* 112(4):966–81
19. Chronis D, Chen S, Lu S, Hewezi T, Carpenter SCD, et al. 2013. A ubiquitin carboxyl extension protein secreted from a plant-parasitic nematode *Globodera rostochiensis* is cleaved in planta to promote plant parasitism. *Plant J.* 74(2):185–96

20. Chung K, Tasaka M. 2011. RPT2a, a 26S proteasome AAA-ATPase, is directly involved in *Arabidopsis* CC-NBS-LRR protein uni-1D-induced signaling pathways. *Plant Cell Physiol.* 52(9):1657–64
21. Coll NS, Epple P, Dangl JL. 2011. Programmed cell death in the plant immune system. *Cell Death Differ.* 18(8):1247–56
22. Collins GA, Goldberg AL. 2017. The logic of the 26S proteasome. *Cell* 169(5):792–806
23. Copeland C, Woloshen V, Huang Y, Li X. 2016. AtCDC48A is involved in the turnover of an NLR immune receptor. *Plant J.* 88(2):294–305
24. Couto D, Zipfel C. 2016. Regulation of pattern recognition receptor signalling in plants. *Nat. Rev. Immunol.* 16(9):537–52
25. Craig A, Ewan R, Mesmar J, Gudipati V, Sadanandom A. 2009. E3 ubiquitin ligases and plant innate immunity. *J. Exp. Bot.* 60(4):1123–32
26. Dallery JF, Zimmer M, Halder V, Suliman M, Pigné S, et al. 2020. Inhibition of jasmonate-mediated plant defences by the fungal metabolite higginsianin B. *J. Exp. Bot.* 71(10):2910–21
27. de Marchi R, Sorel M, Mooney B, Fudal I, Goslin K, et al. 2016. The N-end rule pathway regulates pathogen responses in plants. *Sci. Rep.* 6(1):26020
28. Diaz-Granados A, Sterken MG, Overmars H, Ariaans R, Holterman M, et al. 2020. The effector GpRbp- 1 of *Globodera pallida* targets a nuclear HECT E3 ubiquitin ligase to modulate gene expression in the host. *Mol. Plant Pathol.* 21(1):66–82
29. Dissmeyer N. 2019. Conditional protein function via N-degron pathway-mediated proteostasis in stress physiology. *Annu. Rev. Plant. Biol.* 70:83–117
30. Dong OX, Ao K, Xu F, Johnson KCM, Wu Y, et al. 2018. Individual components of paired typical NLR immune receptors are regulated by distinct E3 ligases. *Nat Plants* 4(9):699–710
31. Dubiella U, Serrano I. 2021. The ubiquitin proteasome system as a double agent in plant-virus interactions. *Plants* 10(5):4–7
32. Fan J, Bai P, Ning Y, Wang J, Shi X, et al. 2018. The monocot-specific receptor-like kinase SDS2 controls cell death and immunity in rice. *Cell Host Microbe* 23(4):498–510.e5
33. Fernández-Calvo P, Chini A, Fernández-Barbero G, Chico JM, Gimenez-Ibanez S, et al. 2011. The *Arabidopsis* bHLH transcription factors MYC3 and MYC4 are targets of JAZ repressors and act additively with MYC2 in the activation of jasmonate responses. *Plant Cell* 23(2):701–15
34. Fu ZQ, Yan S, Saleh A, Wang W, Ruble J, et al. 2012. NPR3 and NPR4 are receptors for the immune signal salicylic acid in plants. *Nature* 486(7402):228–32
35. Furlan G, Nakagami H, Eschen-Lippold L, Jiang X, Majovsky P, et al. 2017. Changes in PUB22 ubiquitination modes triggered by MITOGEN-ACTIVATED PROTEIN KINASE3 dampen the immune response. *Plant Cell* 29(4):726–45
36. Furniss JJ, Grey H, Wang Z, Nomoto M, Jackson L, et al. 2018. Proteasome-associated HECT-type ubiquitin ligase activity is required for plant immunity. *PLOS Pathog.* 14(11):e1007447
37. Gao C, Sun P, Wang W, Tang D. 2021. *Arabidopsis* E3 ligase KEG associates with and ubiquitinates MKK4 and MKK5 to regulate plant immunity. *J Integr. Plant Biol.* 63(2):327–39
38. Gimenez-Ibanez S, Hann DR, Ntoukakis V, Petutschnig E, Lipka V, Rathjen JP. 2009. AvrPtoB targets the LysM receptor kinase CERK1 to promote bacterial virulence on plants. *Curr. Biol.* 19(5):423–29
39. Göhre V, Spallek T, Häweker H, Mersmann S, Mentzel T, et al. 2008. Plant pattern-recognition receptor FLS2 is directed for degradation by the bacterial ubiquitin ligase AvrPtoB. *Curr. Biol.* 18(23):1824–32
40. Goritschnig S, Zhang Y, Li X. 2007. The ubiquitin pathway is required for innate immunity in *Arabidopsis*. *Plant J.* 49(3):540–51
41. Goslin K, Eschen-Lippold L, Naumann C, Linster E, Sorel M, et al. 2019. Differential N-end rule degradation of RIN4/NOI fragments generated by the AvrRpt2 effector protease. *Plant Physiol.* 180(4):2272–89
42. Gou M, Shi Z, Zhu Y, Bao Z, Wang G, Hua J. 2012. The F-box protein CPR1/CPR30 negatively regulates R protein SNC1 accumulation. *Plant J.* 69(3):411–20
43. Gravot A, Richard G, Lime T, Lemarié S, Jubault M, et al. 2016. Hypoxia response in *Arabidopsis* roots infected by *Plasmodiophora brassicae* supports the development of clubroot. *BMC Plant Biol.* 16(1):251

44. Groll M, Schellenberg B, Bachmann AS, Archer CR, Huber R, et al. 2008. A plant pathogen virulence factor inhibits the eukaryotic proteasome by a novel mechanism. *Nature* 452(7188):755–58
45. Gu Y, Innes RW. 2012. The KEEP ON GOING protein of *Arabidopsis* regulates intracellular protein trafficking and is degraded during fungal infection. *Plant Cell* 24(11):4717–30
46. He Q, McLellan H, Boevink PC, Sadanandom A, Xie C, et al. 2015. U-box E3 ubiquitin ligase PUB17 acts in the nucleus to promote specific immune pathways triggered by *Phytophthora infestans*. *J. Exp. Bot.* 66(11):3189–99
47. Hu X-H, Fan J, Wu J-L, Shen S, He J-X, et al. 2021. Proteasome maturation factor UMP1 confers broad-spectrum disease resistance by modulating H_2O_2 accumulation in rice. bioRxiv 433750. **https://doi.org/10.1101/2021.03.03.433750**
48. Huang J, Wu X, Gao Z. 2021. The RING-type protein BOI negatively regulates the protein level of a CC-NBS-LRR in *Arabidopsis*. *Biochem. Biophys. Res. Commun.* 578:104–9
49. Huang W, MacLean AM, Sugio A, Maqbool A, Busscher M, et al. 2021. Parasitic modulation of host development by ubiquitin-independent protein degradation. *Cell* 184(20):5201–14.e12
50. Ishikawa K, Yamaguchi K, Sakamoto K, Yoshimura S, Inoue K, et al. 2014. Bacterial effector modulation of host E3 ligase activity suppresses PAMP-triggered immunity in rice. *Nat. Commun.* 5:5430
51. Ji H, Liu D, Zhang Z, Sun J, Han B, Li Z. 2020. A bacterial F-box effector suppresses SAR immunity through mediating the proteasomal degradation of OsTrxh2 in rice. *Plant J.* 104(4):1054–72
52. Jiang C, Hei R, Yang Y, Zhang S, Wang Q, et al. 2020. An orphan protein of *Fusarium graminearum* modulates host immunity by mediating proteasomal degradation of TaSnRK1α. *Nat. Commun.* 11(1):4382
53. Jiang S, Yao J, Ma KW, Zhou H, Song J, et al. 2013. Bacterial effector activates jasmonate signaling by directly targeting JAZ transcriptional repressors. *PLOS Pathog.* 9(10):e1003715
54. Jin L, Qin Q, Wang Y, Pu Y, Liu L, et al. 2016. Rice dwarf virus P2 protein hijacks auxin signaling by directly targeting the rice OsIAA10 protein, enhancing viral infection and disease development. *PLOS Pathog.* 12(9):e1005847
55. Jin Y, Ma D, Dong J, Jin J, Li D, et al. 2007. HC-Pro protein of Potato virus Y can interact with three *Arabidopsis* 20S proteasome subunits in planta. *J. Virol.* 81(23):12881–88
56. Jones JDG, Dangl JL. 2006. The plant immune system. *Nature* 444(7117):323–29
57. Kamal H, Minhas F, Tripathi D, Abbasi WA, Hamza M, et al. 2019. βC1, pathogenicity determinant encoded by Cotton leaf curl Multan betasatellite, interacts with calmodulin-like protein 11 (Gh-CML11) in *Gossypium hirsutum*. *PLOS ONE* 14(12):e0225876
58. Karki SJ, Reilly A, Zhou B, Mascarello M, Burke J, et al. 2021. A small secreted protein from *Zymoseptoria tritici* interacts with a wheat E3 ubiquitin ligase to promote disease. *J. Exp. Bot.* 72(2):733–46
59. Kawasaki T, Nam J, Boyes DC, Holt BF, Hubert DA, et al. 2005. A duplicated pair of *Arabidopsis* RING-finger E3 ligases contribute to the RPM1- and RPS2-mediated hypersensitive response. *Plant J.* 44(2):258–70
60. Khan M, Subramaniam R, Desveaux D. 2016. Of guards, decoys, baits and traps: pathogen perception in plants by type III effector sensors. *Curr. Opin. Microbiol.* 29:49–55
61. Kitazawa Y, Iwabuchi N, Maejima K, Sasano M, Matsumoto O, et al. 2022. A phytoplasma effector acts as a ubiquitin-like mediator between floral MADS-box proteins and proteasome shuttle proteins. *Plant Cell* 34(5):1709–23
62. Kreitman M, Noronha A, Yarden Y. 2018. Irreversible modifications of receptor tyrosine kinases. *FEBS Lett.* 592(13):2199–212
63. Kud J, Wang W, Gross R, Fan Y, Huang L, et al. 2019. The potato cyst nematode effector RHA1B is a ubiquitin ligase and uses two distinct mechanisms to suppress plant immune signaling. *PLOS Pathog.* 15(4):e1007720
64. Lacroix B, Citovsky V. 2015. Nopaline-type Ti plasmid of *Agrobacterium* encodes a VirF-like functional F-box protein. *Sci Rep.* 5:16610
65. Lai J, Chen H, Teng K, Zhao Q, Zhang Z, et al. 2009. RKP, a RING finger E3 ligase induced by BSCTV C4 protein, affects geminivirus infection by regulation of the plant cell cycle. *Plant J.* 57(5):905–17
66. Langin G, Gouguet P, Üstün S. 2020. Microbial effector proteins: a journey through the proteolytic landscape. *Trends Microbiol.* 28(7):523–35

67. Lee BJ, Kwon SJ, Kim SK, Kim KJ, Park CJ, et al. 2006. Functional study of hot pepper 26S proteasome subunit RPN7 induced by Tobacco mosaic virus from nuclear proteome analysis. *Biochem. Biophys. Res. Commun.* 351(2):405–11
68. Leong JX, Raffeiner M, Spinti D, Langin G, Franz-Wachtel M, et al. 2022. A bacterial effector counteracts host autophagy by promoting degradation of an autophagy component. *EMBO J.* 41(13):e110352
69. Lequeu J, Simon-Plas F, Fromentin J, Etienne P, Petitot AS, et al. 2005. Proteasome comprising a β1 inducible subunit acts as a negative regulator of NADPH oxidase during elicitation of plant defense reactions. *FEBS Lett.* 579(21):4879–86
70. Li J, Chu ZH, Batoux M, Nekrasov V, Roux M, et al. 2009. Specific ER quality control components required for biogenesis of the plant innate immune receptor EFR. *PNAS* 106(37):15973–78
71. Lim G-H, Hoey T, Zhu S, Clavel M, Yu K, et al. 2018. COP1, a negative regulator of photomorphogenesis, positively regulates plant disease resistance via double-stranded RNA binding proteins. *PLOS Pathog.* 14(3):e1006894
72. Lin Y, Hu Q, Zhou J, Yin W, Yao D, et al. 2021. *Phytophthora sojae* effector Avr1d functions as an E2 competitor and inhibits ubiquitination activity of GmPUB13 to facilitate infection. *PNAS* 118(10):e2018312118
73. Liu J, Huang Y, Kong L, Yu X, Feng B, et al. 2020. The malectin-like receptor-like kinase LETUM1 modulates NLR protein SUMM2 activation via MEKK2 scaffolding. *Nat. Plants* 6(9):1106–15
74. Liu J, Park CH, He F, Nagano M, Wang M, et al. 2015. The RhoGAP SPIN6 associates with SPL11 and OsRac1 and negatively regulates programmed cell death and innate immunity in rice. *PLOS Pathog.* 11(2):e1004629
75. Liu X, Zhou Y, Du M, Liang X, Fan F, et al. 2022. The calcium-dependent protein kinase CPK28 is targeted by the ubiquitin ligases ATL31 and ATL6 for proteasome-mediated degradation to fine-tune immune signaling in *Arabidopsis*. *Plant Cell* 34(1):679–97
76. Lozano-Durán R, Rosas-Díaz T, Gusmaroli G, Luna AP, Taconnat L, et al. 2011. Geminiviruses subvert ubiquitination by altering CSN-mediated derubylation of SCF E3 ligase complexes and inhibit jasmonate signaling in *Arabidopsis thaliana*. *Plant Cell* 23(3):1014–32
77. Lu D, Lin W, Gao X, Wu S, Cheng C, et al. 2011. Direct ubiquitination of pattern recognition receptor FLS2 attenuates plant innate immunity. *Science* 332(6036):1439–42
78. Ma A, Zhang D, Wang G, Wang K, Li Z, et al. 2021. *Verticillium dahliae* effector VDAL protects MYB6 from degradation by interacting with PUB25 and PUB26 E3 ligases to enhance Verticillium wilt resistance. *Plant Cell* 33(12):3675–99
79. Ma W, Xu X, Cai L, Cao Y, Haq F, et al. 2020. A *Xanthomonas oryzae* type III effector XopL causes cell death through mediating ferredoxin degradation in *Nicotiana benthamiana*. *Phytopathol. Res.* 2:16
80. Mackey D, Yun D, Nam J. 2021. Proteasome-dependent degradation of RPM1 desensitizes the RPM1-mediated hypersensitive response. *J. Plant Biol.* 64(3):217–25
81. MacLean AM, Orlovskis Z, Kowitwanich K, Zdziarska AM, Angenent GC, et al. 2014. Phytoplasma effector SAP54 hijacks plant reproduction by degrading MADS-box proteins and promotes insect colonization in a RAD23-dependent manner. *PLOS Biol.* 12(4):e1001835
82. Maejima K, Kitazawa Y, Tomomitsu T, Yusa A, Neriya Y, et al. 2015. Degradation of class E MADS-domain transcription factors in *Arabidopsis* by a phytoplasmal effector, phyllogen. *Plant Signal. Behav.* 10(8):e1042635
83. Marshall RS, Vierstra RD. 2019. Dynamic regulation of the 26S proteasome: from synthesis to degradation. *Front. Mol. Biosci.* 6:40
84. Matsushita A, Inoue H, Goto S, Nakayama A, Sugano S, et al. 2013. Nuclear ubiquitin proteasome degradation affects WRKY45 function in the rice defense program. *Plant J.* 73(2):302–13
85. McLellan H, Chen K, He Q, Wu X, Boevink PC, et al. 2020. The ubiquitin E3 ligase PUB17 positively regulates immunity by targeting a negative regulator, KH17, for degradation. *Plant Commun.* 1(4):100020
86. Miao M, Niu X, Kud J, Du X, Avila J, et al. 2016. The ubiquitin ligase SEVEN IN ABSENTIA (SINA) ubiquitinates a defense-related NAC transcription factor and is involved in defense signaling. *New Phytol.* 211(1):138–48

87. Millyard L, Lee J, Zhang C, Yates G, Sadanandom A. 2016. The ubiquitin conjugating enzyme, TaU4 regulates wheat defence against the phytopathogen *Zymoseptoria tritici*. *Sci. Rep.* 6:35683
88. Misas-Villamil JC, Kolodziejek I, Crabill E, Kaschani F, Niessen S, et al. 2013. *Pseudomonas syringae* pv. *syringae* uses proteasome inhibitor syringolin A to colonize from wound infection sites. *PLOS Pathog.* 9(3):10–16
89. Mithoe SC, Menke FL. 2018. Regulation of pattern recognition receptor signalling by phosphorylation and ubiquitination. *Curr. Opin. Plant Biol.* 45(Pt. A):162–70
90. Müller J, Piffanelli P, Devoto A, Miklis M, Elliott C, et al. 2005. Conserved ERAD-like quality control of a plant polytopic membrane protein. *Plant Cell* 17(1):149–63
91. Nakano M, Oda K, Mukaihara T. 2017. *Ralstonia solanacearum* novel E3 ubiquitin ligase (NEL) effectors RipAW and RipAR suppress pattern-triggered immunity in plants. *Microbiology* 163(7):992–1002
92. Ngou BPM, Ding P, Jones JDG. 2022. Thirty years of resistance: zig-zag through the plant immune system. *Plant Cell* 34(5):1447–78
93. Ngou BPM, Heal R, Wyler M, Schmid MW, Jones JDG. 2022. Concerted expansion and contraction of immune receptor gene repertoires in plant genomes. *Nat. Plants* 8(10):1146–52
94. Ning Y, Shi X, Wang R, Fan J, Park CH, et al. 2015. OsELF3-2, an ortholog of *Arabidopsis* ELF3, interacts with the E3 ligase APIP6 and negatively regulates immunity against *Magnaporthe oryzae* in rice. *Mol. Plant* 8(11):1679–82
95. Nirmala J, Dahl S, Steffenson BJ, Kannangara CG, von Wettstein D, et al. 2007. Proteolysis of the barley receptor-like protein kinase RPG1 by a proteasome pathway is correlated with *Rpg1*-mediated stem rust resistance. *PNAS* 104(24):10276–81
96. Nomura K, Debroy S, Lee YH, Pumplin N, Jones J, He SY. 2006. A bacterial virulence protein suppresses host innate immunity to cause plant disease. *Science* 313(5784):220–23
97. Orosa B, He Q, Mesmar J, Gilroy EM, McLellan H, et al. 2017. BTB-BACK domain protein POB1 suppresses immune cell death by targeting ubiquitin E3 ligase PUB17 for degradation. *PLOS Genet.* 13(1):e1006540
98. Orosa B, Üstün S, Calderón Villalobos LIA, Genschik P, Gibbs D, et al. 2020. Plant proteostasis—shaping the proteome: a research community aiming to understand molecular mechanisms that control protein abundance. *New Phytol.* 227(4):1028–33
99. Pant BD, Oh S, Lee HK, Nandety RS, Mysore KS. 2020. Antagonistic regulation by CPN60A and CLPC1 of TRXL1 that regulates MDH activity leading to plant disease resistance and thermotolerance. *Cell Rep.* 33(11):108515
100. Park CH, Shirsekar G, Bellizzi M, Chen S, Songkumarn P, et al. 2016. The E3 ligase APIP10 connects the effector AvrPiz-t to the NLR receptor Piz-t in rice. *PLOS Pathog.* 12(3):e1005529
101. Petutschnig EK, Stolze M, Lipka U, Kopischke M, Horlacher J, et al. 2014. A novel *Arabidopsis* CHITIN ELICITOR RECEPTOR KINASE 1 (CERK1) mutant with enhanced pathogen-induced cell death and altered receptor processing. *New Phytol.* 204(4):955–67
102. Qin J, Zhou X, Sun L, Wang K, Yang F, et al. 2018. The *Xanthomonas* effector XopK harbours E3 ubiquitin-ligase activity that is required for virulence. *New Phytol.* 220(1):219–31
103. Qin T, Liu S, Zhang Z, Sun L, He X, et al. 2019. GhCyP3 improves the resistance of cotton to *Verticillium dahliae* by inhibiting the E3 ubiquitin ligase activity of GhPUB17. *Plant Mol. Biol.* 99(4–5):379–93
104. Raffeiner M, Üstün S, Guerra T, Spinti D, Fitzner M, et al. 2022. The *Xanthomonas* type-III effector XopS stabilizes CaWRKY40a to regulate defense responses and stomatal immunity in pepper (*Capsicum annuum*). *Plant Cell* 34(5):1684–708
105. Ramachandran P, Joshi JB, Maupin-Furlow JA, Uthandi S. 2021. Bacterial effectors mimicking ubiquitin-proteasome pathway tweak plant immunity. *Microbiol. Res.* 250:126810
106. Roussin-Léveillée C, Lajeunesse G, St-Amand M, Veerapen VP, Silva-Martins G, et al. 2022. Evolutionarily conserved bacterial effectors hijack abscisic acid signaling to induce an aqueous environment in the apoplast. *Cell Host Microbe* 30(4):489–501.e4
107. Sahana N, Kaur H, Basavaraj, Tena F, Jain RK, et al. 2012. Inhibition of the host proteasome facilitates Papaya ringspot virus accumulation and proteosomal catalytic activity is modulated by viral factor HcPro. *PLOS ONE* 7(12):e52546

108. Sahu PP, Sharma N, Puranik S, Chakraborty S, Prasad M. 2016. Tomato 26S proteasome subunit RPT4a regulates ToLCNDV transcription and activates hypersensitive response in tomato. *Sci. Rep*. 6:27078
109. Saile SC, Ackermann FM, Sunil S, Keicher J, Bayless A, et al. 2021. *Arabidopsis* ADR1 helper NLR immune receptors localize and function at the plasma membrane in a phospholipid dependent manner. *New Phytol*. 232(6):2440–56
110. Shimono M, Koga H, Akagi A, Hayashi N, Goto S, et al. 2012. Rice WRKY45 plays important roles in fungal and bacterial disease resistance. *Mol. Plant Pathol.* 13(1):83–94
111. Shimono M, Sugano S, Nakayama A, Jiang CJ, Ono K, et al. 2007. Rice WRKY45 plays a crucial role in benzothiadiazole-inducible blast resistance. *Plant Cell* 19(6):2064–76
112. Shu K, Yang W. 2017. E3 ubiquitin ligases: ubiquitous actors in plant development and abiotic stress responses. *Plant Cell Physiol.* 58(9):1461–76
113. Shukla A, Üstün S, Hafrén A. 2021. Proteasome homeostasis is essential for a robust cauliflower mosaic virus infection. bioRxiv 436740. **https://doi.org/10.1101/2021.03.24.436740**
114. Singer AU, Schulze S, Skarina T, Xu X, Cui H, et al. 2013. A pathogen type III effector with a novel E3 ubiquitin ligase architecture. *PLOS Pathog*. 9(1):e1003121
115. Skelly MJ, Furniss JJ, Grey H, Wong K-W, Spoel SH. 2019. Dynamic ubiquitination determines transcriptional activity of the plant immune coactivator NPR1. *eLife* 8:e47005
116. Soni M, Mondal KK. 2018. *Xanthomonas axonopodis* pv. *punicae* uses XopL effector to suppress pomegranate immunity. *J. Integr. Plant Biol.* 60(4):341–57
117. Spoel SH, Mou Z, Tada Y, Spivey NW, Genschik P, Dong X. 2009. Proteasome-mediated turnover of the transcription coactivator NPR1 plays dual roles in regulating plant immunity. *Cell* 137(5):860–72
118. Stegmann M, Anderson RG, Ichimura K, Pecenkova T, Reuter P, et al. 2012. The ubiquitin ligase PUB22 targets a subunit of the exocyst complex required for PAMP-triggered responses in *Arabidopsis*. *Plant Cell* 24(11):4703–16
119. Su W, Liu Y, Xia Y, Hong Z, Li J. 2011. Conserved endoplasmic reticulum-associated degradation system to eliminate mutated receptor-like kinases in *Arabidopsis*. *PNAS* 108(2):870–75
120. Tan L, Rong W, Luo H, Chen Y, He C. 2014. The *Xanthomonas campestris* effector protein XopD Xcc
8004 triggers plant disease tolerance by targeting DELLA proteins. *New Phytol.* 204(3):595–608
121. Tanaka H, Kitakura S, De Rycke R, De Groodt R, Friml J. 2009. Fluorescence imaging-based screen identifies ARF GEF component of early endosomal trafficking. *Curr. Biol.* 19(5):391–97
122. Tanaka S, Brefort T, Neidig N, Djamei A, Kahnt J, et al. 2014. A secreted *Ustilago maydis* effector promotes virulence by targeting anthocyanin biosynthesis in maize. *eLife* 3:e01355
123. Tao T, Zhou CJ, Wang Q, Chen XR, Sun Q, et al. 2017. Rice black streaked dwarf virus P7-2 forms a
SCF complex through binding to *Oryza sativa* SKP1-like proteins, and interacts with GID2 involved in the gibberellin pathway. *PLOS ONE* 12(5):e0177518
124. Thiel H, Hleibieh K, Gilmer D, Varrelmann M. 2012. The P25 pathogenicity factor of Beet necrotic yellow vein virus targets the sugar beet 26s proteasome involved in the induction of a hypersensitive resistance response via interaction with an F-box protein. *Mol. Plant-Microbe Interact.* 25(8):1058–72
125. Thines B, Katsir L, Melotto M, Niu Y, Mandaokar A, et al. 2007. JAZ repressor proteins are targets of the SCFCOI1 complex during jasmonate signalling. *Nature* 448(7154):661–65
126. Thulasi Devendrakumar K, Copeland C, Li X. 2019. The proteasome regulator PTRE1 contributes to the turnover of SNC1 immune receptor. *Mol. Plant Pathol.* 20(11):1566–73
127. Till CJ, Vicente J, Zhang H, Oszvald M, Deery MJ, et al. 2019. The *Arabidopsis thaliana* N-recognin E3 ligase PROTEOLYSIS1 influences the immune response. *Plant Dir*. 3(12):e00194
128. Üstün S, Bartetzko V, Börnke F. 2013. The *Xanthomonas campestris* type III effector XopJ targets the host cell proteasome to suppress salicylic-acid mediated plant defence. *PLOS Pathog*. 9(6):e1003427
129. Üstün S, Bartetzko V, Börnke F. 2015. The *Xanthomonas* effector XopJ triggers a conditional hypersensitive response upon treatment of *N. benthamiana* leaves with salicylic acid. *Front. Plant Sci.* 6:599
130. Üstün S, Börnke F. 2015. The *Xanthomonas campestris* type III effector XopJ proteolytically degrades proteasome subunit RPT6. *Plant Physiol*. 168(1):107–19

132. Üstün S, König P, Guttman DS, Börnke F. 2014. HopZ4 from *Pseudomonas syringae*, a member of the HopZ Type III effector family from the YopJ superfamily, inhibits the proteasome in plants. *Mol. Plant-Microbe Interact.* 27(7):611–23
133. Üstün S, Sheikh A, Gimenez-Ibanez S, Jones A, Ntoukakis V, Börnke F. 2016. The proteasome acts as a hub for plant immunity and is targeted by *Pseudomonas* type III effectors. *Plant Physiol.* 172(3):1941–58
134. Vicente J, Mendiondo GM, Pauwels J, Pastor V, Izquierdo Y, et al. 2019. Distinct branches of the N-end rule pathway modulate the plant immune response. *New Phytol.* 221(2):988–1000
135. Vierstra RD. 2009. The ubiquitin-26S proteasome system at the nexus of plant biology. *Nat. Rev. Mol. Cell Biol.* 10(6):385–97
136. Wang J, Grubb LE, Wang J, Liang X, Li L, et al. 2018. A regulatory module controlling homeostasis of a plant immune kinase. *Mol. Cell* 69(3):493–504.e6
137. Wang J, Wang R, Fang H, Zhang C, Zhang F, et al. 2021. Two VOZ transcription factors link an E3 ligase and an NLR immune receptor to modulate immunity in rice. *Mol. Plant* 14(2):253–66
138. Wang S, Li Q, Zhao L, Fu S, Qin L, et al. 2020. *Arabidopsis* UBC22, an E2 able to catalyze lysine-11 specific ubiquitin linkage formation, has multiple functions in plant growth and immunity. *Plant Sci.* 297:110520
139. Wang T, Chang C, Gu C, Tang S, Xie Q, Shen Q-H. 2016. An E3 ligase affects the NLR receptor stability and immunity to powdery mildew. *Plant Physiol.* 172(4):2504–15
140. Wang Z, Orosa-Puente B, Nomoto M, Grey H, Potuschak T, et al. 2022. Proteasome-associated ubiquitin ligase relays target plant hormone-specific transcriptional activators. *Sci. Adv.* 8(42):4466
141. Wu Z, Tong M, Tian L, Zhu C, Liu X, et al. 2020. Plant E3 ligases SNIPER 1 and SNIPER 2 broadly regulate the homeostasis of sensor NLR immune receptors. *EMBO J.* 39(15):e104915
142. Xu CC, Zhang D, Hann DR, Xie ZP, Staehelin C. 2018. Biochemical properties and in planta effects of NopM, a rhizobial E3 ubiquitin ligase. *J. Biol. Chem.* 293(39):15304–15
143. Xu F, Huang Y, Li L, Gannon P, Linster E, et al. 2015. Two N-terminal acetyltransferases antagonistically regulate the stability of a nod-like receptor in *Arabidopsis*. *Plant Cell* 27(5):1547–62
144. Xu FQ, Xue HW. 2019. The ubiquitin-proteasome system in plant responses to environments. *Plant Cell Environ.* 42(10):2931–44
145. Yamaguchi K, Mezaki H, Fujiwara M, Hara Y, Kawasaki T. 2017. *Arabidopsis* ubiquitin ligase PUB12 interacts with and negatively regulates chitin elicitor receptor kinase 1 (CERK1). *PLOS ONE* 12(11):e0188886
146. Yan J, Li H, Li S, Yao R, Deng H, et al. 2013. The *Arabidopsis* F-box protein CORONATINE INSENSITIVE1 is stabilized by SCFCOI1 and degraded via the 26S proteasome pathway. *Plant Cell* 25(2):486–98
147. Yan J, Yao R, Chen L, Li S, Gu M, et al. 2018. Dynamic perception of jasmonates by the F-box protein COI1. *Mol. Plant* 11(10):1237–47
148. Yan X, Tao J, Luo HL, Tan LT, Rong W, et al. 2019. A type III effector XopLXcc8004 is vital for *Xanthomonas campestris* pathovar *campestris* to regulate plant immunity. *Res. Microbiol.* 170(3):138–46
149. Yang CW, González-Lamothe R, Ewan RA, Rowland O, Yoshioka H, et al. 2006. The E3 ubiquitin ligase activity of *Arabidopsis* PLANT U-BOX17 and its functional tobacco homolog ACRE276 are required for cell death and defense. *Plant Cell* 18(4):1084–98
150. Yang L, Teixeira PJPL, Biswas S, Finkel OM, He Y, et al. 2017. *Pseudomonas syringae* type III effector HopBB1 promotes host transcriptional repressor degradation to regulate phytohormone responses and virulence. *Cell Host Microbe* 21(2):156–68
151. Yao C, Wu Y, Nie H, Tang D. 2012. RPN1a, a 26S proteasome subunit, is required for innate immunity in *Arabidopsis*. *Plant J.* 71(6):1015–28
152. You Q, Zhai K, Yang D, Yang W, Wu J, et al. 2016. An E3 ubiquitin ligase-BAG protein module controls plant innate immunity and broad-spectrum disease resistance. *Cell Host Microbe* 20(6):758–69
153. Yu G, Derkacheva M, Rufian JS, Brillada C, Kowarschik K, et al. 2022. The *Arabidopsis* E3 ubiquitin ligase PUB4 regulates BIK1 and is targeted by a bacterial type-III effector. *EMBO J.* 41(23):e107257
154. Yu Y, Xu W, Wang J, Wang L, Yao W, et al. 2013. The Chinese wild grapevine (*Vitis pseudoreticulata*) E3 ubiquitin ligase *Erysiphe necator*-induced RING finger protein 1 (EIRP1) activates plant defense responses by inducing proteolysis of the VpWRKY11 transcription factor. *New Phytol.* 200(3):834–46

155. Zhang C, Wei Y, Xu L, Wu KC, Yang L, et al. 2020. A bunyavirus-inducible ubiquitin ligase targets RNA polymerase IV for degradation during viral pathogenesis in rice. *Mol. Plant* 13(6):836–50
156. Zhang Y, Song G, Lal NK, Nagalakshmi U, Li Y, et al. 2019. TurboID-based proximity labeling reveals that UBR7 is a regulator of N NLR immune receptor-mediated immunity. *Nat Commun*. 10(1):3252
157. Zhao C, Rispe C, Nabity PD. 2019. Secretory RING finger proteins function as effectors in a grapevine galling insect. *BMC Genom*. 20(1):923
158. Zhou B, Mural RV, Chen X, Oates ME, Connor RA, et al. 2017. A subset of ubiquitin-conjugating enzymes is essential for plant immunity. *Plant Physiol*. 173(2):1371–90
159. Zhou B, Wang C, Chen X, Zhang Y, Zeng L. 2021. Two ubiquitin-activating systems occur in plants with one playing a major role in plant immunity. bioRxiv 458739. **https://doi.org/10.1101/2021.09.02.458739**
160. Ziebell H, Murphy AM, Groen SC, Tungadi T, Westwood JH, et al. 2011. Cucumber mosaic virus and its 2b RNA silencing suppressor modify plant-aphid interactions in tobacco. *Sci. Rep.* 1:187
161. Zipfel C. 2014. Plant pattern-recognition receptors. *Trends Immunol*. 35(7):345–51

Annual Review of Phytopathology
Volume 61, 2023

Contents

Errata

An online log of corrections to *Annual Review of Phytopathology* articles may be found at http://www.annualreviews.org/errata/phyto

IV. Investigating Proteasome Complex homeostasis in Plants

This chapter includes the method publication “A Pipeline to Monitor Proteasome Homeostasis in Plants”, published in 2023. In the previous chapter we have seen that the 26S proteasome complex is involved in regulation of a very large number of molecular pathways, hence requiring precise regulation. A critical aspect in the understanding of the overall 26S proteasome role in each biological context comes from the analysis of its own homeostasis. Indeed, the regulation of the 26S proteasome homeostasis is a dynamic process involving many (if not all) the regulatory mechanisms described in Chapter I.

Here we provide a blueprint for reliable analysis of the 26S proteasome homeostasis in plants through monitoring of proteasome gene transcripts level, subunits abundance, proteolytic activity and subsequent impact on total ubiquitinome. These techniques are appliable to multiple species and, altogether, provide a global picture of the 26S proteasome status.

a. A Pipeline to Monitor Proteasome Homeostasis in Plants

Scientific contributions: Scientific ideas 50%, Data generation 100%.

Details about writing contributions: Writing of the entire manuscript under supervision of SÜ.

Citation: Langin G, Üstün S. A Pipeline to Monitor Proteasome Homeostasis in Plants. Methods Mol Biol. 2023; 2581:351-363. doi: 10.1007/978-1-0716-2784-6_25. PMID: 36413330.

Chapter 25

A Pipeline to Monitor Proteasome Homeostasis in Plants

Gautier Langin and Suayib Üstün

Abstract

The proteasome is a key component for regulation of protein turnover across kingdoms. The proteasome has been shown to be involved in or affected by various stress conditions in multiple model organisms in plants. As such, studying proteasome homeostasis is crucial to understand its participation in different cellular conditions. However, the involvement of the proteasome in many cellular processes and its interplay with other degradation pathways hamper the interpretation of experiments based on a single approach. Thus, it is crucial to formulate a framework to investigate proteasome dynamics in different model organisms including plants. Here, we describe a pipeline to monitor proteasome homeostasis using four different methods including (i) luminescent-based proteasome activity measurement, (ii) immunoblot analysis of ubiquitinated proteins, (iii) evaluation of proteasome subunit protein levels, and (iv) monitoring of the proteasome stress regulon on mRNA levels using quantitative real-time PCR (polymerase chain reaction).

Key words Proteasome activity, Bioluminescence, Immunoblot, Ubiquitin, Proteasome, Gene expression

1 Introduction

The proteasome is a eukaryotic protein complex playing a major role in the regulation of protein homeostasis, mediating degradation in the ubiquitin-proteasome system (UPS) [1]. The UPS can be divided into a two-step mechanism: (i) an enzymatic cascade mediated by E1 ubiquitin-activating enzyme, E2 ubiquitin-conjugating enzyme, and E3 ubiquitin ligase (E1-> E2-> E3) leading to posttranslational modification of target proteins with mono- and/or poly-ubiquitin and (ii) subsequent degradation of the ubiquitinated proteins by the proteasome. Throughout the last decade, the importance of the UPS in plant development, response to abiotic stress, and biotic interactions have been recurrently reported [2–4]. However, while involvement of the UPS enzymatic cascade during plant life has been extensively shown by the characterization of various E3 ligase-substrate pairs, the precise role of the

L. Maria Lois and Marco Trujillo (eds.), *Plant Proteostasis: Methods and Protocols*,
Methods in Molecular Biology, vol. 2581, https://doi.org/10.1007/978-1-0716-2784-6_25,

proteasome complex and its dynamics remain elusive. Increasing evidence have confirmed the importance of several proteasome subunits in response to several stresses [5–8].

The proteasome complex is formed by a core cylinder, the 20S complex, consisting of four rings of seven subunits each, called the core particle (CP). The two external rings are formed from α-subunits (α1–α7) and the two inner rings from β-subunits (β1–β7). Its proteolytic activity depends on subunits β1, β2, and β5, which constitute caspase-like, trypsin, and chymotrypsin proteases, respectively. The 20S CP complex is known to be dynamically regulated, notably via interaction with other proteins [9]. Indeed, the best characterized form of the complex is the 26S proteasome consisting of the 20S CP complex capped by one or two 19S regulatory particles (RP) [10]. The RP is known to mediate multiple processes such as substrate recognition, de-ubiquitination of target proteins, and regulation of the "gating" of the CP. The 20S CP complex is also proposed to form a complex with the protein PA200 (Proteasome Activator 200) which is thought to be involved in the activation of the 20S CP complex [9]. Regulation of the complex is also proposed to be mediated through posttranslational modifications [9]. While in plants such modifications of proteasome subunits are poorly characterized, a total of 207 modifications of different types have been reported to date based on MS/MS data on *A. thaliana* [4]. These data indicate that proteasome complexes may undergo a dynamic regulation depending on the posttranslational modification and stress response.

The fact that the regulation of the proteasome is highly dynamic, it is highlighted by recent reports identifying that the proteasome complex itself is degraded by autophagy [11]. It has been shown that upon chemical inhibition with MG132, the proteasome complex undergoes autophagic degradation through a mechanism termed proteaphagy [11]. In a more physiological context, proteaphagy has been shown to be triggered by carbon starvation in *A. thaliana* roots, as well as by the pathogenic bacterium *Pseudomonas syringae*, resulting in suppression of proteasome activity [12, 13]. A different mechanism of proteasome activity suppression has been suggested for the pathogenic bacterium *Xanthomonas campestris* pv. *vesicatoria* that utilizes type III effector XopJ to induce proteolytic degradation of the RP subunit RPT6 [14, 15].

Taken together, these examples illustrate multiple conditions in which proteasome homeostasis is modulated *in planta* and manipulated by pathogens. During proteotoxic stress caused by chemical or microbial modulation of proteasome activity, several hallmarks of proteasome inhibition have been reported: Chemical inhibition of the proteasome and pathogen-induced suppression of proteasome activity are often accompanied by (i) accumulation of ubiquitinated proteins, (ii) upregulation of proteasome subunit

transcript levels, and (iii) increased protein abundance of proteasome subunits [7, 13, 16, 17]. However, these hallmarks can also occur under other conditions. For instance, bacterial infection of *A. thaliana* with *P. syringae* DC3000 *ΔhrcC* (lacking type III secretion system) or flg22 treatment increases the levels of ubiquitinated proteins, although the proteasome activity is enhanced [7, 18].

These examples depict how difficult it is to conclude on proteasome complex behavior based on a single experimental proxy. Because current analysis of the proteasome complex in the plant literature often lacks complementary experiments to fully support conclusions, we propose a blueprint to monitor proteasome homeostasis in plants. This pipeline is based on robust and quick experiments suitable for multiple plants species, for example, *Arabidopsis thaliana*, *Nicotiana benthamiana*, *Solanum lycopersicum*, *Capsicum annuum*, and *Marchantia polymorpha* (*see* **Note 1**). It must be noted that using only one experimental approach is not sufficient to conclude on the status of proteasome activity and homeostasis *in planta*. Evaluating the mRNA levels of proteasome genes and abundance of corresponding subunits is necessary to assess a possible stress response of the proteasome. The proteasome is also connected with other pathways such as autophagy and unfolded protein response [19], and hence the result of each experiment can be impacted by these alternative pathways. Thus, we consider that all four experiments provide a solid foundation to conclude on the state of proteasome homeostasis *in planta*.

2 Materials

2.1 Proteasome Activity Measurement with Luminogenic Proteasome Substrate

1. Luminescent chymotrypsin-like (Suc-LLVY-aminoluciferin), trypsin-like (Z-LRR-aminoluciferin), and caspase-like (Z-nLPnLD-aminoluciferin) proteasome substrates (*see* **Note 2**).
2. Luciferin detection reagent (*see* **Note 2**).
3. Assay buffer (*see* **Note 2**).
4. Proteasome extraction buffer (PEB): 50 mM HEPES-KOH pH 7.2, 2 mM DTT, 2 mM ATP, and 0.25 M sucrose.
5. Proteasome inhibitor Bortezomib.
6. White MicroWell 96-Well plate.
7. Ultrapure water (resistivity = 18.2 MΩ.cm at 25 °C).
8. Microcentrifuge tube 1.5 mL.
9. Biopsy punch 6.0 mm (or similar, *see* **Note 3**).
10. Tissue homogenizer.
11. Refrigerated table top centrifuge for 1.5 mL tubes.
12. Luminescence plate reader.

2.2 Evaluation of Total Ubiquitinated Proteins

1. Microcentrifuge tubes 1.5 mL and 2 mL.
2. Glass beads 5 mm.
3. Biopsy punch 6.0 mm (or similar, *see* **Note 3**).
4. Protein extraction buffer: 100 mM Tris-HCl, pH 7.5, and 2% SDS.
5. Laemmli sample buffer with 2-mercaptoethanol.
6. Polyacrylamide (PA) 10% gel.
7. Tris-glycine-SDS (TGS) buffer: 25 mM Tris-base, 192 mM glycine, and 0.1% (w/v) SDS.
8. Western blotting equipment.
9. 0.2 μm PVDF (polyvinylidene difluoride) membranes and filter paper
10. Transfer buffer.
11. Tris buffered saline (TBS) buffer: 20 mM Tris-HCL, pH 7.5, and 137 mM NaCl.
12. TBS Tween (TBST) buffer: 20 mM Tris-HCL, pH 7.5, 137 mM NaCl, and 0.05% (v/v) Tween 20.
13. Blocking buffer: 5% (w/v) skim milk in TBST buffer.
14. Absolute ethanol.
15. Heat block for microcentrifuge tubes.
16. Monoclonal anti-ubiquitin HRP (anti-Ub) antibody (or similar).
17. Enhanced chemiluminescent (ECL) reagents.
18. Horizontal shaker.
19. Chemiluminescence detection apparatus.

2.3 Monitoring of Proteasome Stress Regulon mRNA Levels

1. Plant RNA extraction kit.
2. cDNA synthesis kit,
3. SYBR Green qPCR Master Mix.
4. PCR 384 well plates.
5. Adhesive Clear qPCR Seal.
6. Ultrapure water.
7. qPCR primers for proteasome subunits genes (*see* **Note 4**),
8. RNase-free glass beads 5 mm.
9. TissueLyser.
10. 2-Mercaptoethanol
11. Real-time thermocycler suitable for 384 well plate.
12. Multi-channel pipette 1–10 μL.
13. PCR clean dispenser tips 0.2 mL.
14. Multi-dispenser pipette.

2.4 Evaluation of Proteasome Subunit Protein Level

1. Microcentrifuge tubes 1.5 mL and 2 mL.
2. Glass beads 5 mm.
3. Biopsy punch 6.0 mm (or similar, *see* **Note 3**).
4. Protein extraction buffer: 100 mM Tris-HCL, pH 7.5, and 2% SDS.
5. Laemmli sample buffer with 2-mercaptoethanol.
6. Polyacrylamide (PA) 10% gel.
7. Tris-glycine-SDS (TGS) buffer: 25 mM Tris-base, 192 mM glycine, and 0.1% (w/v) SDS.
8. Western blotting equipment.
9. 0.2 μm PVDF membranes and filter paper
10. Transfer buffer.
11. Tris-buffered saline (TBS) buffer: 20 mM Tris-HCL, pH 7.5, and 137 mM NaCL.
12. TBS Tween (TBST) buffer: 20 mM Tris-HCL, pH 7.5, 137 mM NaCL, and 0.05% (v/v) Tween 20.
13. Blocking buffer: 5% (w/v) skim milk in TBST buffer.
14. Absolute ethanol.
15. Heat block for microcentrifuge tubes.
16. Polyclonal antibodies against proteasome subunits: anti-PBA1 AS19 4260, anti-RPT4a AS19 4263, and anti-RPN10 AS19 4266.
17. Polyclonal anti-rabbit HRP IgG (or similar).
18. Enhanced chemiluminescent (ECL) reagents.
19. Horizontal shaker.
20. Chemiluminescence detection apparatus.

3 Methods

3.1 Characterization of Proteasome Activity in Plants

3.1.1 Proteasome Activity Measurement with Luminogenic Proteasome Substrate

1. Harvest four leaf disks per biological replicates (*see* **Note 3**) in 1.5 mL microcentrifuge tube and flash freeze in liquid nitrogen (*see* **Note 5**).
2. Allow luciferase buffer to thaw at room temperature and cover with aluminum foil.
3. Homogenize the leaf tissue in 200 μL of cold proteasome extraction buffer (*see* **Note 3**). Make sure tissue is well ground, and keep chilled.
4. Centrifuge the tubes at 4 °C at 17,000 *g* for 10 min. The supernatant should be clear to light green.

5. Meanwhile, prepare the assay substrate solution according to provider's recommendations. For 1 mL luciferase buffer:
   - 5 µL LLVY chymotrypsin substrate
   - 10 µL LRR trypsin substrate
   - 5 µL nLPnLD caspase substrate.
6. Pipette 50 µL of the supernatant per replicate and per reactions in 96-well plate (*see* **Note 6**).
7. Incubate the plate for 15 min at room temperature in the dark.
8. For LLVY and nLPnLD, add 50 µL of assay substrate solution. For the LRR, mix 10 µL of assay substrate solution with 40 µL ultrapure water (*see* **Note 3**) per reaction. Chemical treatment on proteasome extracts can be included at this point (*see* **Note 7**).
9. Measure luminescence for 0.1 s every minute for 60 min with a plate reader *(see* **Note 8**).
10. The results should be analyzed as follows:
    (a) Identify an area of interest, where the samples of kinetic curves display linear pattern (e.g., from t_x to t_n; *see* Fig. 1a). The selected area should be common to all the samples for a given substrate (which often comprise the first half of the measurement).
    (b) Multiply the mean of all the data points from the area of interest by the slope of the linear curve in the corresponding area:

$$\text{activity} = \bar{y} * m$$

Where:

$$\bar{y} = \frac{\sum_{i=tx}^{n} yi}{n} \qquad m = \frac{y_n - y_x}{t_n - t_x}$$

activity = Sample proteasome activity in RLU.min^{-1}

n = number of timepoints in the area of interest

t_x = first timepoint

t_n = last timepoint

y_x = RLU at first timepoint

y_n = RLU at last timepoint

y_i = RLU at timepoint i

    (c) Representative results obtained for measurements in *A. thaliana*, *N. benthamiana*, and *M. polymorpha* are shown in Fig. 1. Figure 1a shows average kinetic curves for four biological replicates obtained in *A. thaliana* measuring chymotrypsin-like, trypsin-like, and caspase-like

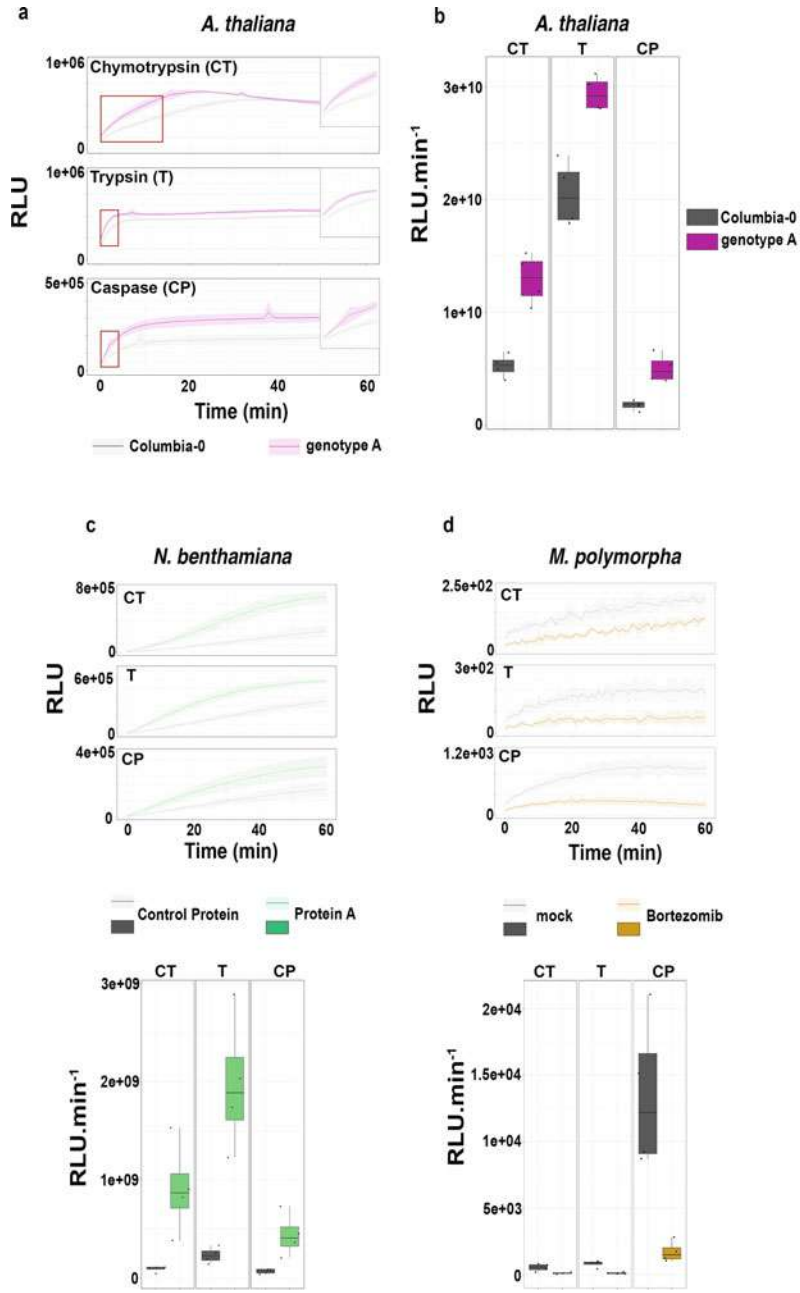

Fig. 1 Representative proteasome activity results on *A. thaliana*, *N. benthamiana*, and *M. polymorpha*. (**a**) Relative luminescence unit (RLU) kinetic obtained after measurement of different protease activities on Columbia-0 and a mutant genotype (here genotype A). The curves represent the mean RLU and the shadows the standard deviation ($n = 4$). Areas taken for calculation of proteasome activity are highlighted by a red box and shown in the upper-right corners. (**b**) Boxplots representing the proteasome activity of all three proteases in RLU.min-1 for Columbia-0 and genotype A displaying increased activity ($n = 4$). (**c**) Measurement of proteasome activity in *N. benthamiana* expressing a control protein and a protein of interest (protein A). The graphics on the left represent mean RLU kinetics with standard deviation and on right boxplots obtained after proteasome activity measurement calculation ($n = 4$). (**d)** Measurement of proteasome activity in

activities. Figure 1b shows boxplot of proteasome activities obtained for the corresponding measurement after calculation as described above. The boxplot values, expressed as $RLU.min^{-1}$, correspond to the luminescence signal released by luminogenic substrate proteasomal cleavage among time. Thus, a higher value corresponds to a higher activity of the proteasome complex in the extract. This experiment permits conclusion on the impact of genetic background, protein expression, or chemical treatment on proteasome activity of several plant species (*see* **Note 9**).

3.1.2 Evaluation of Total Ubiquitinated Proteins

1. Harvest plant tissue in 2 mL microcentrifuge tubes containing two glass beads and flash freeze in liquid nitrogen (*see* **Note 5**).
2. Grind tissue with a TissueLyser and appropriate adapter precooled at −20 °C, two times for 30 s at frequency 25/s.
3. Freeze the tube in liquid nitrogen after grinding (*see* **Note 5**).
4. On ice, add 150 μL of protein extraction buffer (*see* **Note 3**) to the tube containing the tissue powder, and vortex for 10 sec to allow sample to thaw in buffer.
5. Add 50 μL of Laemmli buffer (containing 2-mercaptoethanol) per tubes.
6. Boil sample for 10 min at 95 °C.
7. Centrifuge sample 1 min at 13000 g.
8. Pipette 150 μL of the supernatant in a new 1.5 mL microcentrifuge tube (*see* **Note 10**).
9. Prepare PA (polyacrylamide) gel(s) according to the method of choice (*see* **Note 11**). Number of samples will define number of gels to prepare and/or preparation of 10-well or 15-well gels.
10. Load 20 μL of samples per well for 10-well gels or 15 μL of samples for 15-well gels. Load 5 μL of protein ladder in one well per gels.
11. Run gel electrophoresis at 180 V for 30–40 min in TGS buffer.
12. Activate PVDF membrane in absolute ethanol and filter papers into transfer buffer.
13. Mount transfer sandwich including filter papers, PVDF membrane, and the gel in the blotting cassette.
14. Run transfer for mixed molecular weight according to the blotting equipment manufacturer's recommendations.

Fig. 1 (continued) M. polymorpha tissue vacuum infiltrated with a mock treatment or Bortezomib. Left: mean RLU kinetics with standard deviation. Right: boxplots obtained after proteasome activity measurement calculation ($n = 4$)

15. After transfer, incubate membrane for 1 h on horizontal shaker at room temperature in 6 mL blocking buffer.
16. Pipette 3 μL of anti-UBQ-HRP antibody in the blocking buffer, and incubate on a horizontal shaker for 1 h at room temperature.
17. Briefly wash the membrane with TBST, and wash three times for 5 min with TBST on a horizontal shaker at room temperature.
18. Perform a last wash with TBS for 5 min on a horizontal shaker at room temperature.
19. Prepare 500 μL of ECL according to the manufacturer's instructions.
20. Pipette 500 μL of ECL on the membrane, and make sure the solution is homogeneously distributed on the membrane.
21. Detect chemiluminescence.

3.2 Characterization of Proteasome Transcript Regulation and Protein Abundance

3.2.1 Monitoring of Proteasome Stress Regulon mRNA Levels

1. Harvest plant tissue in 2 mL microcentrifuge tubes containing two glass beads each, and flash freeze in liquid nitrogen (*see* **Note 5**).
2. Grind tissue using an appropriate adapter precooled to −20 °C, two times for 30 sec at frequency 25/s.
3. Freeze tubes in liquid nitrogen after grinding.
4. Extract RNA according to provider's recommendations.
5. Extracted RNA can be stored at −80 °C or kept at 4 °C if they are used within the next 24 h post extraction.
6. Perform cDNA synthesis with 1 μg of RNA per sample according to manufacturer's instructions.
7. Dilute five times cDNA in ultrapure water (*see* **Note 12**).
8. Prepare qPCR mix, each reaction includes the following:
   (a) 4 μL SYBR Green qPCR Master Mix
   (b) 0.12 μL Fwd Primer (10 μM) + 0.12 μL Rv Primer (10 μM)
   (c) 1.76 μL ultrapure water.
9. With multi-channel pipette, pipette 2 μL of diluted cDNA as triplicates for each qPCR mix (*see* **Note 4**).
10. With dispenser tips, add 6 μL of SYBR mix in corresponding wells to a total volume of 8 μL (SYBR mix + cDNA).
11. Seal the plate with transparent sealing.
12. Run qPCR program according to manufacturer's recommendations.

13. Export *Ct* values.
14. Calculate $\Delta\Delta Ct$ for the proteasome genes as the following:

$$\Delta\Delta Ct_{\text{pgoi}} = \frac{\Delta Ct_{\text{pgoi}}}{\Delta Ct_{\text{housekeeping}}}$$

Where:

$$\Delta Ct_{\text{pgoi}} = \frac{1}{2^{\overline{Ct}_{\text{pgoi}}}}$$

$$\Delta Ct_{\text{housekeeping}} = \frac{1}{2^{\overline{Ct}_{\text{housekeeping}}}}$$

$$\overline{Ct} = \frac{\sum_{i=1}^{n} Ct_i}{n}$$

Cti = *Ct* value for a given technical replicate

n = number of technical replicates (typically three)

pgoi = Proteasome gene of interest

houskeeping = Housekeeping gene used for the experiment

3.2.2 Evaluation of Proteasome Subunit Protein Level

1–13 Refer to Subheading 3.1.2 for the preparation and migration of two PA gels with identical sample loading.

14. After transfer of the two PA gels on two PVDF membranes, cut one membrane at the 30–35 kDa ladder band. The second membrane can be kept whole.
15. Incubate the three membranes in 6 mL of blocking buffer for 1 h on horizontal shaker at room temperature.
16. Add 3 μL of anti-PBA1 antibody (1: 2000) to the lower half membrane. Add 3 μL of anti-RPT4a antibody (1: 2000) to the upper half membrane. Add 3 μL of anti-RPN10 antibody (1: 2000) to the third membrane. Incubate all three membranes for 1 h on horizontal shaker at room temperature.
17. Briefly wash the membrane with TBST and perform three washes for 5 min with TBST on horizontal shaker at room temperature.
18. Add 6 mL of blocking buffer supplemented with 0.6 μL of anti-rabbit-HRP antibody (1:10,000) to each membrane. Incubate for 1 h on a horizontal shaker at room temperature.
19. Briefly wash the membrane with TBST and perform three washes for 5 min with TBST on horizontal shaker at room temperature.
20. Perform a last wash for 5 min with TBS on a horizontal shaker at room temperature.
21. Prepare 1 mL of ECL according to the provider's material.

22. Pipette 500 μL of ECL on the full membrane and 250 μL for each half membrane. Make sure the solution is homogeneously distributed on the membrane.
23. Detect chemiluminescence. Detection can be done with all the membranes simultaneously and each membrane individually (*see* **Note 13**).

4 Notes

1. In this chapter, we provide several protocols that are suitable for the species mentioned above. All protocols have been carried out in our lab in at least two of the species mentioned, and similar experiments have been published in the literature [14, 15, 20].
2. To ensure reliability and reproducibility of the results, we recommend using a commercial kit to perform proteasome activity measurements. In our lab, we use the following reference: Cell-Based Proteasome-Glo™ Assays.
3. In this chapter, we provide protocols done in our lab in which we harvest leaf disks of 6.0 mm. For *M. polymorpha*, we recommend 100 mg tissue for the methods described in Subheadings 3.1.1 and 3.2.1 and 50 mg tissue for those described in Subheadings 3.1.2 and 3.2.2. All the substrates and buffer volumes, as well as other parameters mentioned in this chapter, have been optimized for the mentioned amount of plant tissue. The protocols can be adapted for other amounts.
4. We recommend using four different primer pairs resulting in four qPCR mixes: one with housekeeping gene primers and three with proteasome gene primers for CP 20S (e.g., *AtPBA1*), 19S base (e.g., *AtRPT4a*), and 19S lid subunits (e.g., *AtRPN10*).
5. At this step, the sample can be stored at −80 °C until it is used.
6. The sample is also suitable for native and denaturing PA gel experiments.
7. For the first assay, we recommend performing control reactions including pharmacological proteasome inhibitors, such as Bortezomib at 1 μM to abolish proteasome activity. To a similar extend, including other chemicals or peptides to assay a putative effect on the proteasome activity is suitable with the assay.
8. Time of kinetic can be adjusted as long as the linear curve is obtained.
9. Data depicted on Fig. 1 can be interpreted as follows: On Fig. 1a and Fig. 1b, the *A. thaliana* genotype A displays increased activity for all three protease types as compared to

wild-type plants. On Fig. 1c, transient expression of protein A in *N. benthamiana* epidermal cell results in increased activities as compared to control protein. On Fig. 1d, treatment of *M. polymorpha* thalli with Bortezomib results in inhibition of proteasome activities as compared to mock treatment.

10. At this step, sample can be stored at −20 °C until used.
11. While we recommend the use of 10% acrylamide resolving phase for PA gels, these assays can be achieved with other acrylamide percentage for the resolving phase or gradient PA gels.
12. cDNA dilution can be adjusted empirically. However, we recommend using one-fifth dilution for the first measurements.
13. Sensitivity of antibodies and variation in abundance of the different proteasome subunits might make simultaneous detection of the membranes not possible.

Acknowledgments

This work was supported by an Emmy Noether Fellowship GZ: UE188/2-1 from the Deutsche Forschungsgemeinschaft (DFG, to S.Ü.) through the collaborative research council 1101 (CRC1101, to G.L.).

References

1. Vierstra RD (2009) The ubiquitin-26S proteasome system at the nexus of plant biology. Nat Rev Mol Cell Biol 10:385–397
2. Langin G, Gouguet P, Üstün S (2020) Microbial effector proteins – a journey through the proteolytic landscape. Trends Microbiol 28: 523–535
3. Xu FQ, Xue HW (2019) The ubiquitin-proteasome system in plant responses to environments. Plant Cell Environ 42:2931–2944
4. Wang H, Schippers JHM (2019) The role and regulation of autophagy and the proteasome during aging and senescence in plants. Genes (Basel) 10:267
5. Cai YM, Yu J, Ge Y et al (2018) Two proteases with caspase-3-like activity, cathepsin B and proteasome, antagonistically control ER-stress-induced programmed cell death in Arabidopsis. New Phytol 218:1143–1155
6. Han JJ, Yang X, Wang Q et al (2019) The β5 subunit is essential for intact 26S proteasome assembly to specifically promote plant autotrophic growth under salt stress. New Phytol 221: 1359–1368
7. Üstün S, Sheikh A, Gimenez-Ibanez S et al (2016) The proteasome acts as a hub for plant immunity and is targeted by pseudomonas type III effectors. Plant Physiol 172:1941–1958
8. Sakamoto T, Sotta N, Suzuki T et al (2019) The 26s proteasome is required for the maintenance of root apical meristem by modulating auxin and cytokinin responses under high-boron stress. Front Plant Sci 10:1–13
9. Marshall RS, Vierstra RD (2019) Dynamic regulation of the 26S proteasome: from synthesis to degradation. Front Mol Biosci 6:40
10. Rabl J, Smith DM, Yu Y et al (2008) Mechanism of gate opening in the 20S proteasome by the proteasomal ATPases. Mol Cell 30: 360–368
11. Marshall RS, Li F, Gemperline DC et al (2015) Autophagic degradation of the 26S proteasome is mediated by the dual ATG8/ubiquitin receptor RPN10 in Arabidopsis. Mol Cell 81: 2053
12. Marshall RS, Vierstra RD (2018) Proteasome storage granules protect proteasomes from

autophagic degradation upon carbon starvation. elife 7:1–38

13. Üstün S, Hafrén A, Liu Q et al (2018) Bacteria exploit autophagy for proteasome degradation and enhanced virulence in plants. Plant Cell 30: 668–685
14. Üstün S, Bartetzko V, Börnke F (2013) The Xanthomonas campestris type III effector XopJ targets the host cell proteasome to suppress salicylic-acid mediated plant Defence. PLoS Pathog 9:e1003427
15. Üstün S, Börnke F (2015) The Xanthomonas campestris type III effector XopJ proteolytically degrades proteasome subunit RPT6. Plant Physiol 168:107–119
16. Book AJ, Gladman NP, Lee SS et al (2010) Affinity purification of the Arabidopsis 26 S proteasome reveals a diverse array of plant proteolytic complexes. J Biol Chem 285: 25554–25569
17. Gladman NP, Marshall RS, Lee KH et al (2016) The proteasome stress regulon is controlled by a pair of NAC transcription factors in arabidopsis. Plant Cell 28:1279–1296
18. Sun HH, Fukao Y, Ishida S et al (2013) Proteomics analysis reveals a highly heterogeneous proteasome composition and the post-translational regulation of peptidase activity under pathogen signaling in plants. J Proteome Res 12:5084–5095
19. Zientara-Rytter K, Sirko A (2016) To deliver or to degrade – an interplay of the ubiquitin–-proteasome system, autophagy and vesicular transport in plants. FEBS J 283:3534–3555
20. Saint-Marcoux D, Proust H, Dolan L et al (2015) Identification of reference genes for real-time quantitative PCR experiments in the liverwort marchantia polymorpha. PLoS One 10:1–14

V. The Proteasome integrated signaling coordinates subcellular proteostasis during proteotoxic stress

In the previous chapters, we described the mechanisms required to regulate proteostasis, illustrating the importance of proteostasis during plant immunity. In addition, we discussed the dynamic aspect of proteasome regulation, providing an experimental pipeline to investigate proteasome function. Given the important role in the proteasome in various cellular processes it is crucial to understand how the proteasome is (i) regulated and (i) how the accumulation of proteasome substrates from various subcellular compartments are perceived, integrated and processed to cope with proteotoxicity.

We have addressed these questions in the manuscript “ER-anchored protein sorting controls the fate of two proteasome activators for intracellular organelle communication during proteotoxic stress”, first published in 2023, by characterization the proteasome regulatory feedback loop in plants. This mechanism relies on the degradation of the proteasome transcriptional activators by the proteasome itself, allowing maintenance of proteasome complex (Marshall and Vierstra, 2019). Here we identified that the two known plant proteasome activators, transcription factors NAC53 and NAC78, are sorted at the ER, through a mechanism we termed ER-anchored protein sorting (ERAPS). The ERAPS system is dependent on NAC53/78 ubiquitination and subsequent CDC48 recognition. CDC48 is a conserved ATPase forming hexameric complex responsible for retro-translocation of membrane bound protein into the cytosol. We show ERAPS mediates basal proteasomal turnover of both proteasome activators NAC53/78 after their extraction from the ER by CDC48. Upon proteotoxic stress, the proteasomal degradation of both TFs is dampened due to accumulation of other proteasome substrates. Through the CDC48-dependent retro-translocation, both TFs will be directed to the nucleus and activate the gene expression of proteasome subunits. Interestingly, we identified that both TFs associate with Photosynthesis associated nuclear genes (PhANGs) promoters via the same cis-element that is present in the proteasome promoters. Intriguingly, this association with PhANGs promoters leads to the downregulation of PhANGs expression while both NACs activate proteasome gene expression. While we used bacterial infection to decipher this process, we found it was not restricted to this context. Stabilization, translocation and the transcriptomic signature mediated by NAC53/78 is triggered during many stress responses. It constitutes an elaborated molecular system where the 26S proteasome complex can act as a *bona fide* signaling hub to perceive, integrate and coordinate the response to proteostasis perturbation.

In the second part of this chapter, we will provide additional results and further discuss several aspects of the mentioned manuscript. We highlight that NAC53/78 displays a complex level of specificity with promoter cis-elements and that their transcriptomic impact seems broad with a link to hormonal signaling and metabolism. We will discuss several observations regarding their subcellular dynamics that could be associated with their PTMs and how these subcellular features could make them sensors of local proteotoxicity. Finally, we will approach some uncharacterized aspects of the plant proteasome complex, speculating on the importance of proteasome gene duplication and the existence of unknown specificities behind the proteasome regulation in plants and eukaryotes.

Altogether, we propose an integrated signaling system that has evolved around the conserved 26S proteasome complex to shape cellular proteostasis.

a. ER-anchored protein sorting controls the fate of two proteasome activators for intracellular organelle communication during proteotoxic stress

Scientific contributions: Scientific ideas 50%, Figure representation 100%, Data Generation 90%, Paper Writing 50%.

Details about writing contributions: Writing of the entire manuscript under supervision of SÜ.

Citation: ER-anchored protein sorting controls the fate of two proteasome activators for intracellular organelle communication during proteotoxic stress. Gautier Langin, Margot Raffeiner, David Biermann, Mirita Franz-Wachtel, Daniela Spinti, Frederik Börnke, Boris Macek, Suayib Üstün bioRxiv 2023.12.11.571118; https://doi.org/10.1101/2023.12.11.571118

ER-anchored protein sorting controls the fate of two proteasome activators for intracellular organelle communication during proteotoxic stress

Gautier Langin[1,2], Margot Raffeiner[1], David Biermann[2], Mirita Franz-Wachtel[3], Daniela Spinti[4], Frederik Börnke[4,5], Boris Macek[3], Suayib Üstün[1,*]

[1] Faculty of Biology & Biotechnology, Ruhr-University Bochum, Bochum, Germany

[2] Center for Plant Molecular Biology (ZMBP), University of Tübingen, Tübingen, Germany

[3] Institute for Cell Biology, Department of Quantitative Proteomics, University of Tübingen, Tübingen, Germany Method section for MS/MS analysis

[4] Leibniz-Institute of Vegetable and Ornamental Crops (IGZ), Großbeeren, Germany

[5] Institute of Biochemistry and Biology, University of Potsdam, Potsdam, Germany

[*]Correspondence: suayb.uestuen@rub.de

Summary

Proteotoxic stress, characterized by the accumulation of damaged proteins, poses a significant challenge to cellular homeostasis. To mitigate proteotoxicity eukaryotes employ the proteasome that is regulated by proteasome activators, e.g. transcription factors that promote gene expression of proteasome subunits. As proteotoxicity originates in different compartments, cells need to perceive signals from various locations. Understanding which components integrate signals to address proteotoxicity is essential to develop strategies to cope with proteotoxicity but remain elusive. Here, we identify that the proteasome autoregulatory feedback loop acts as a gatekeeper to facilitate the communication between nucleus and chloroplast. We reveal that the ER-anchored protein sorting system (ERAPS) controls the proteasomal degradation or nuclear translocation of proteasome activators NAC53 and NAC78. While both transcription factors activate the proteasome gene expression, they repress photosynthesis-associated nuclear genes during proteotoxicity. Collectively, our discoveries provide a novel conceptual framework in which the proteasome autoregulatory feedback loop coordinates subcellular proteostasis.

Introduction

Protein homeostasis, hereafter proteostasis, is defined as the synthesis of proteins by translating genetic information, encoded in form of mRNA, into a sequence of amino acids and their regulated degradation. This intimate ying-yang balance between newly synthesized proteins

and protein degradation is tightly regulated in all organisms, in order to develop or respond to several environmental stimuli (Jayaraj et al., 2020; Orosa et al., 2020; Sampaio-Marques and Ludovico, 2018). Various perturbations can alter this equilibrium, leading to proteotoxic stress by disruption of normal proteostasis. This alteration can ultimately result in irreversible cellular damage due to the accumulation of aberrant proteins, an outcome known as proteotoxicity. Perturbations resulting in proteotoxic stress can range from ageing to pathological diseases such as Parkinson and Alzheimer as well as infection by pathogens (Jayaraj et al., 2020; Langin et al., 2023). The latter is a consequence of the onset and maintenance of defense responses during microbial infections and microbes' ability to manipulate proteostasis for their own benefit (Langin et al., 2023; Langin et al., 2020).

To mitigate deleterious effects due to excessive proteotoxic stress, cells employ various protein quality control machineries. Strikingly, the response to proteotoxic stress is often controlled by intricate regulatory feedback loops influenced by proteotoxic stress itself. One of the major protein quality control machineries across the tree of life is the ubiquitin-proteasome system (UPS). The ubiquitin-proteasome system controls proteostasis through selective elimination of defective proteins as well as short-lived regulatory proteins (Raffeiner et al., 2023). Selective protein degradation by the proteasome proceeds from the ligation of ubiquitin proteins to a lysine residue within specific target proteins via the concerted action of E1, E2, and E3 enzymes. The ubiquitinated target is then recognized by the 26S proteasome for degradation. The 26S proteasome itself is a conserved 2.5 MDa ATP-dependent protease complex composed of a 20S core protease (CP) capped by 19S regulatory particles (RPs), that assists in ubiquitin recognition and target protein unfolding. Recent findings highlight that the proteasome is a highly dynamic structure, as more than 40 subunits participate in forming the 26S proteasome. Changes in the subunit composition or the association of the 20S CP with other adaptors drive flexibility of the 26S proteasome which can help to cope with proteotoxic stress (Albert et al., 2020; Colberg et al., 2020; Peters et al., 2013; Tanaka et al., 2012). To guarantee this high degree of structural flexibility and to immediately react to proteotoxic stress, all the constituents of the 26S proteasome are under tight transcriptional control.

All eukaryotic kingdoms possess transcription factors (TFs) required for proteasome genes transcriptional activation (Marshall and Vierstra, 2019). Yeast utilizes the C2H2 zinc-finger TF Rpn4, mammals the bZIPs (Basic Leucine Zipper) Nrf1/2 and plants the pair of NACs (NAM, ATAF and CUC) NAC53/NAC78 as a conserved mechanism to cope with proteotoxicity

although all TFs are evolutionary distinct. In yeast and animal systems, the proteasome activators Rpn4 and Nrf1/2 have been shown to be UPS targets (Radhakrishnan et al., 2014; Sha and Goldberg, 2014; Steffen et al., 2010; Ulasov et al., 2022; Xie and Varshavsky, 2001; Xie, 2001). Rpn4 and Nrf2 are degraded in the cytosol while Nrf1, a tail-anchored (TA) protein, is subjected to endoplasmic reticulum-associated degradation (ERAD). In the context of exceeded proteasomal capacity, hereafter proteasomal stress, their degradation is impaired, leading to their stabilization and subsequent nuclear translocation for proteasome gene activation (Marshall and Vierstra, 2019). This transcriptional activation triggered by Rpn4 and Nrf1/2 is mediated through binding of, respectively, the proteasome-associated control element (PACE, [(A/G)GTGGC)]) or antioxidant response element (ARE, [(A/G)TGACTCAGC] (Baird et al., 2017; Mannhaupt et al., 1999; Shirozu et al., 2015; Xie and Varshavsky, 2001). This mechanism constitutes a negative feedback loop which allows systematic maintenance of proteasome homeostasis. In plants, NAC78 has been shown to mediate transcriptional activation of proteasome promoters through association with the proteasome regulatory cis element (PRCE, [TGGGC], (Nguyen et al., 2013). In addition, loss of the NAC53/78 TF pair rendered plants hypersensitive to proteasome inhibition due to its incapacity to activate proteasome genes expression (Gladman et al., 2016). Therefore, a similar proteasome regulatory feedback loop has been proposed in plants (Marshall and Vierstra, 2019); however, to date, no evidence supports NAC53/78 proteasomal degradation.

Given the importance of proteasomal degradation in various cellular pathways, from cell cycle to immune response (Langin et al., 2023; Ma and Liu, 2010; Wang et al., 2008; Wang et al., 2010), it appears that the autoregulatory feedback loop is a central mechanism to precisely integrate and coordinate stress responses through proteotoxic stress sensing. Indeed, a growing body of evidence suggests that localized proteotoxic stress in compartments and organelles causes the activation of respective proteasome-mediated degradation pathways to release the stress. These mechanisms include ERAD, Endosome/Golgi-associated degradation (EGAD), mitochondria-associated degradation (MAD) and chloroplast-associated degradation (CHLORAD) (Christianson and Ye, 2014; Fonseca and Carvalho, 2019; Liao et al., 2020; Ling et al., 2019). This implies a multi-layered role of the proteasome in governing subcellular proteostasis. This aspect is particularly relevant for semi-autonomous organellar nuclear-encoded proteins, as their regulation also involves cytosolic proteasomal degradation prior to organellar import (Bragoszewski et al., 2017; Hristou et al., 2020). In turn, perturbations in the turn-over of such proteins can lead to proteasomal stress. Indeed, Rpn4 is activated by mitochondrial precursor protein accumulation to likely upregulate the proteasome for removal

of precursor proteins (Kramer et al., 2021). While for Nrf1/2 similar mechanisms remain elusive, Nrf2 is activated upon mitochondrial stress and activates mitochondrial biogenesis and precursors import (Gureev et al., 2019). This places the evolutionary distinct transcription factors Rpn4, Nrf1/2 and NAC53/78 into the spotlight: Are they the main communicators between organelles and the 26S proteasome to cope with proteotoxicity? As such, proteasome activators could act as gatekeepers of the communication between the nucleus and energy-producing organelles to maintain subcellular proteostasis. While to date it remains elusive whether proteasome activators might act as such communicators, it would constitute a direct way to coordinate 26S proteasome capacity and proteasome substrates to cope with proteotoxic stress. It is also unknown how different signals from various organelles and compartments are integrated to respond to overall proteotoxic stress.

Here we demonstrate that the plant proteasome autoregulatory feedback loop, driven by the proteasome activators NAC53/78, functions as signal integrators by controlling the intracellular communication between the nucleus and the chloroplast during proteotoxic stress. We show that NAC53/78 are short-lived proteins regulated by the ERAD machinery through a mechanism we termed ER-Anchored-Protein Sorting (ERAPS). At steady-state conditions NAC53/78 are degraded via the HRD1-CDC48 axis. In contrast, proteotoxic stress caused by pathogenic infection or pharmacological drug treatments stabilizes both transcription factors, leading to their ERAPS-dependent nuclear translocation and subsequent transcriptional reprogramming. We identified that NAC53/78 coordinate the transcriptional activation of proteasome genes and repression of photosynthesis associated nuclear genes (PhANGs) through association with a conserved PRCE-like cis-element. Strikingly, we have found that the proteasome autoregulatory feedback loop is essential to maintain normal response to subcellular proteostasis perturbation. Ultimately, we identified that the transcriptional signature coordinated by NAC53/78 is a general feature in context of biotic interactions as wells as in response to various developmental cues. Taken together, our findings provide a new conceptual framework, in which an autoregulatory feedback loop shapes the response to environmental stress: the integration of signals from different organelles and the role of proteasome activators as gatekeepers of organelle communication constitutes a novel mechanism for ensuring the global surveillance of cellular proteostasis in photosynthetic tissues.

NAC53/78 are central integrators of various proteotoxic stress conditions

Proteotoxicity is triggered by a wide range of physicochemical stresses. The induced proteotoxic stress is often due to a perturbation of local subcellular proteostasis. For instance, damage in energy-producing organelles such as chloroplast and mitochondria often lead to accumulation of proteins that are not imported into these organelles (Hristou et al., 2020; Kramer et al., 2021). How such signals from different cellular compartments are integrated is still not understood. Thus, we hypothesized that proteasome activators might play a role in integrating signals from different locations. To test our hypothesis, we subjected the double mutant *nac53-1 78-1,* known to be hypersensitive towards proteasome inhibition (Gladman et al., 2016), to various treatments previously reported to induce proteotoxic stress through specific mechanisms. We inhibited the proteasome (BTZ, (Gladman et al., 2016) and the ubiquitin-dependent segregase CDC48, a central player of multiple associated-degradation pathways (CB-5083, (Li et al., 2022; Marshall et al., 2019), and induced the ER unfolded protein response (DTT, TM, (Pastor-Cantizano et al., 2020). Additionally, we targeted semi-autonomous organelles such as chloroplasts and mitochondria (Lin, Cml and MV (Li et al., 2022; Wu et al., 2019), and the cytosolic chaperone Hsp90 that is essential for the organellar import of chloroplastic/mitochondrial precursors or proteasomal degradation of these precursors (GDA, (Wu et al., 2019). Ultimately, we used pathogenic infection with the bacterial strain *Pseudomonas syringeae pv. tomato DC3000* (*Pst*), known to impact cellular proteostasis through multiple mechanism notably via direct proteasome targeting (Üstün et al., 2016) (**Figure 1A**).

Consistent with previous studies, BTZ treatment led to *nac53-1 78-1* hypersensitivity resulting in a complete growth defect. Similarly, CDC48 inhibition resulted in a strong plant growth defect (**Figure 1B**), supporting the importance of the proteasome activators in the context of general proteotoxic stress, beyond direct proteasome targeting. Consistently, we observed increased sensitivity of the double mutant to ER stress inducers DTT and TM (**Figure 1B**). Strikingly, all other treatments resulted in *nac53-1 78-1* double mutant increased tolerance compared to WT plants (**Figure 1B**). In accordance with the hypersensitivity towards proteasome inhibition, bacterial infection also increased susceptibility of the *nac53-1 78-1* compared to Col-0 plants (**Figure 1C**).

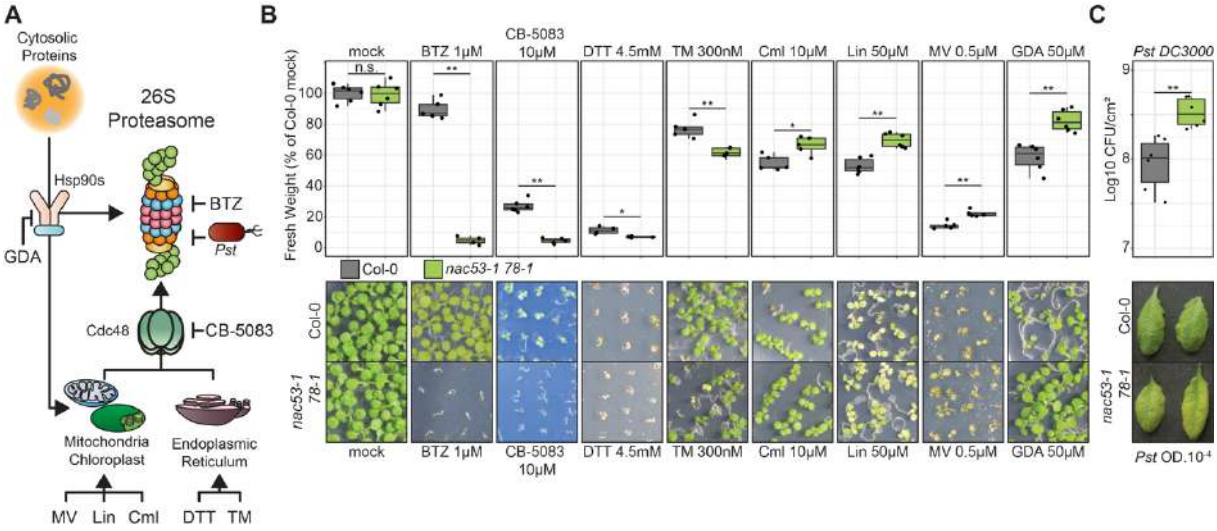

Figure 1. NAC53/78 are central integrators of various proteotoxic stress conditions.
(A) The role of the 26S Proteasome in degradation of proteins from distinct subcellular compartments. Prime site of action of the several treatments used in this study: Blunt head arrows indicate enzymatic activity suppression; pointed head arrows indicate trigger of substrate accumulation.
(B) Fresh weight of seedlings grown under the indicated treatments at 10-14 day after germination (dag). Fresh weight is expressed as a percentage of Col-0 mock conditions. Boxplots colors refer to the genotype. Statistical significance is assessed by a Wilcoxon-Mann-Whitney test (p values: n.s. > 0.05; * < 0.05; ** < 0.01). Every treatment has been repeated at least twice with similar results.
(C) Bacterial density in Log10 Colony-Forming-Unit (CFU) per leaf cm². Statistical significance is assessed by a Wilcoxon-Mann-Whitney test (p values: n.s. > 0.05; ** < 0.01). Boxplots colors refer to the genotype as in panel B. The treatment has been repeated three times with consistent results.
(B-C) Representative phenotypic pictures of Col-0 and *nac53-1 78-1* plants under several treatments are included.

Taken together this suggests that both proteasome activators are involved in general regulation of subcellular proteostasis. However, depending on the perturbation site, in the light of organellar stress, the response appears multi-layered. Overall, it suggests a precise subcellular regulation of NAC53 and NAC78 to adjust their impact on plant response to stress. But how do two transcription factors integrate different signals to have a global influence on the proteome during proteotoxic stress conditions?

NAC53/78 are part of an autoregulatory proteasome feedback loop

To elucidate how both TFs might integrate signals from different compartments and organelles, we aimed to decipher their regulation through interactome analysis. To this end, we generated transgenic plants expressing NAC53 or NAC78 tagged with eGFP at the N-terminus (N-ter), under control of the UBQ10 promoter (**Figure S1A**). Intriguingly, none of the generated lines displayed visible fluorescence under basal conditions (**Figure 2A**). Only upon proteasome inhibition with bortezomib (BTZ), GFP fluorescence was detected in nucleus (**Figure 2A**). These observations were confirmed by immunoblotting using an anti-GFP antibody (**Figure 2B**). Taken together, our results suggest that NAC53/78 are constitutively turned over by the proteasome implying the presence of an autoregulatory feedback loop.

To circumvent the short-lived feature of both NAC transcription factors in *A. thaliana*, and to proceed with our interactome study, we used *Agrobacterium*-mediated transient expression in *N. benthamiana* epidermal cells. Firstly, pUBQ10::GFP/RFP-NAC53/78 (hereafter referred as sTag-NACs, **Figure S1A**) were transiently expressed in *N. benthamiana* to obtain details on their subcellular localization in basal conditions. We could observe a fluorescence signal in reticulated structures reminiscent of the endoplasmic reticulum (ER) as confirmed by co-localization with an ER marker (mCherry-HDEL, **Figure 2C**). Such localization is consistent with the presence of a predicted transmembrane domain (TM) at the C-terminus of both proteins (**Figure S1A**). Due to this specific localization, we developed a second type of chimeric constructs. We tagged the proteins at both ends including a mCerulean3 (CFP) at the N-ter and a mCherry (RFP) at the C-terminus (C-ter), after the TM. These constructs were expressed under regulation of a tandem *Lotus japonicus UBQ1* promoter to obtain stronger expression (hereafter refers as dTag-NACs; **Figure S1A**; (Binder et al., 2014; Maekawa et al., 2008). Interestingly, we could observe the CFP signal was mainly located in the nucleus while the RFP remained strictly at the ER (**Figure 1D**). Both constructs appeared responsive to BTZ treatment that led to stabilization of both NAC transcription factors in *N. benthamiana* strengthening our findings that NAC53/78 are targets of the proteasome. (**Figure S1B and S1C**).

To decipher how both TFs might integrate signals from different compartments/organelles and if an autoregulatory feedback loop governs their function, we performed immuno-Precipitation (IP) followed by tandem Mass Spectrometry (MS/MS) with both constructs. We processed a total of 4 IP-MS/MS conditions for both NACs among 2 experiments. We performed IP of sTag-NACs in mock conditions and at 8 hours after bacterial infection, to induce proteoxic stress (**Figure S1D**). In parallel, we performed IP of dTag-NACs enriching for the N-ter or C-ter end of the proteins, which allowed us to characterize the interactome at a subcellular resolution (**Figure S1E**). For our downstream analysis, we focused on the common interactors for both NACs. Out of the 4 conditions we identified 245 unique *A. thaliana* orthologous proteins as interactor candidates (**Figure 2E and Table S1**).

We first analysed the localization profile of NAC53/78 common interactome using the Gene Ontology (GO) annotations for cellular components and the SUBA5 data base (https://suba.live/). The GO analysis displayed enrichment for terms mainly associated with the proteasome complex and plastid components (**Figure S1F**). This supports the importance of the proteasome complex as a central hub in the NAC53/78 interactome. Investigating the

SUBA5 annotation of NAC53/78 interacting candidates, we observed a specific subcellular

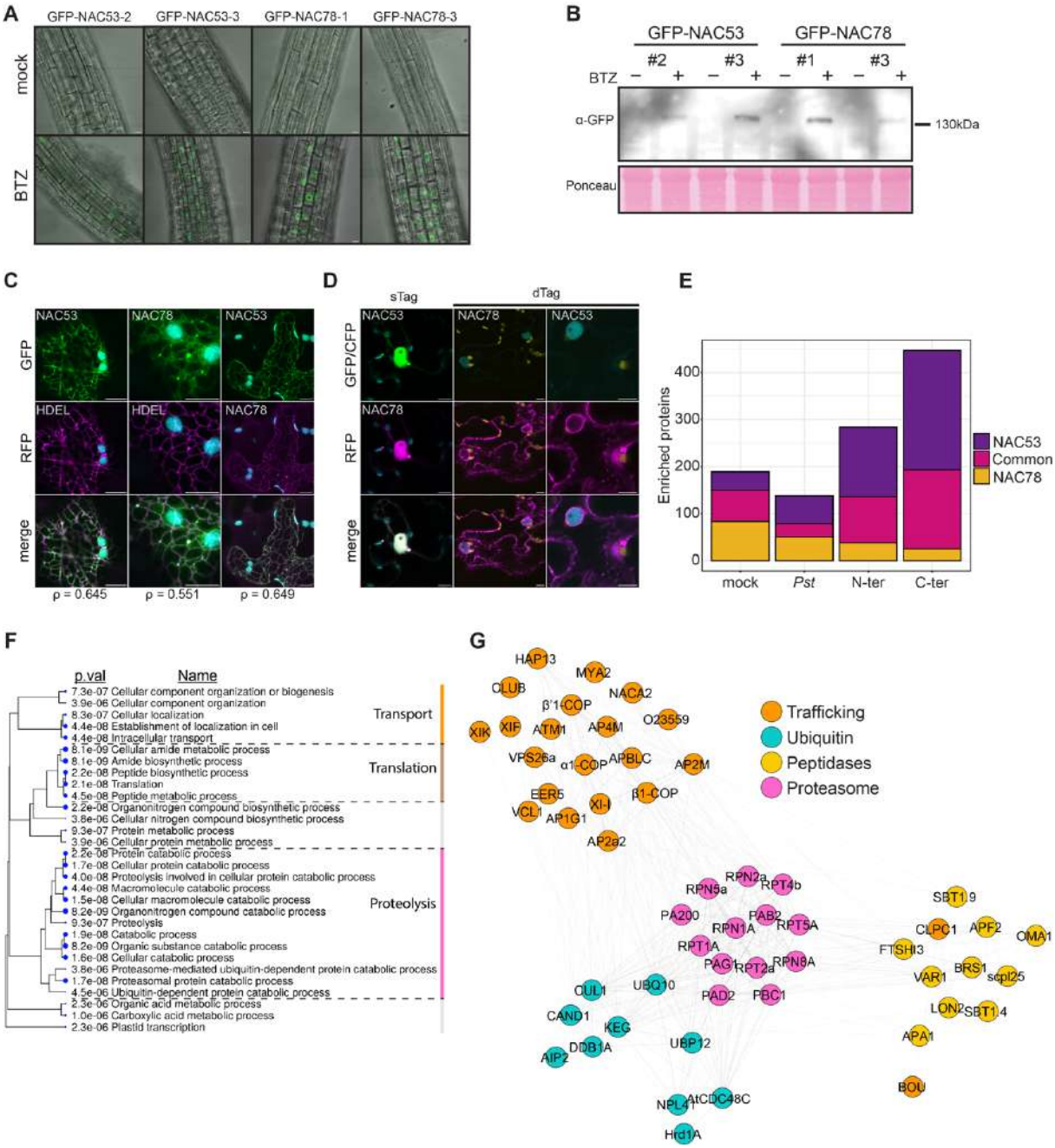

Figure 2. NAC53/78 are part of an autoregulatory proteasome feedback loop.
(A) Confocal microscopy pictures of roots of GFP-NAC53/78 *Arabidopsis thaliana* transgenics at 7dag exposed to mock or BTZ 10µM treatment for 3h. Treatments were repeated at least three times with similar observations.
(B) Immunoblot analysis against GFP on crude extract of seedlings related to panel A. Ponceau staining is used as loading control.
(C) Confocal microscopy pictures of transiently co-expressed sTag-NAC53/78 with prom35S::RFP-HDEL or together in *N. benthamiana* epidermis cells. Pearson index (ρ) represents co-localization index. Scale bars = 10µm
(D) Confocal microscopy pictures of transiently co-expressed sTag-NAC53/78 together or dTag-NAC53/78 alone in *N. benthamiana* epidermis cells. Scale bars = 10µm
(E) Bar plots representing the number of significantly enriched proteins in the 4 IP-MS/MS conditions for NAC53 only, NAC78 only and NAC53+NAC78 (Common).
(F) Cladogram of top 30 gene ontology (GO) terms for biological process (BP) enriched in the list of *A. thaliana* ortholog proteins found from NAC53/78 common interactome.
(G) Protein network of the interacting candidates related to the GO BP terms annotated as "Transport" and "Proteolysis" in panel F.

profile; we found enrichment for only 4 compartments: plastid, peroxisome, golgi, and endoplasmic reticulum (**Figure S1G**). The latter is in accordance with the observed localization (**Figure 2C**) and supports the importance of the ER-localization for the regulation of NAC53/78. To understand how this regulation takes place, we further extended our analysis. We performed GO analysis for biological processes and revealed that possible candidates were enriched in proteins related to three main biological process: proteolysis, trafficking and translation (**Figure 2F**). Based on our previous results we focused on the first two groups. We extracted the corresponding proteins and performed a protein network analysis (**Figure 2G**). This analysis highlighted the presence of numerous components of the ubiquitin-proteasome system (UPS) (**Figure 2G; Figure S1H and S1I**); confirming the strong interplay of NAC53/78 with ubiquitin-dependent proteasomal degradation. Comparison of the protein enrichment level in the several conditions revealed that association with the proteasome complex components was strongly reduced by bacterial infection and mainly enriched when targeting the ER-anchored end of the TFs (C-ter IP) (**Figure S1H**). It suggests that both proteasome regulators escape proteasomal degradation in the context of proteotoxic stress and that ER is the major site for their proteasomal removal. The latter was further supported by the presence of several ERAD components in the interactome (**Figure 2G and S1I**). Additionally, both TFs were associated with various trafficking components or peptidases (**Figure 2G**). Interestingly, the affinity with most of these proteins was substantially differing based on the analysed condition (**Figure S1J and S1K**). This indicates that the NAC53/78 interactome might involve further regulatory layers dynamically shaped in response to proteotoxic stress.

Taken together our analysis confirmed that both proteasome activators are short-lived proteins degraded by the proteasome. These findings reveal the presence of an autoregulatory feedback in plants, similar to what has been found in yeast and animal (Marshall & Vierstra, 2019). In addition, our interactome of NAC53/78 corroborates their role as integrators of subcellular proteostasis perturbations.

ER-Anchored Protein sorting (ERAPS) regulates the subcellular fate of NAC53 & NAC78

Our analysis of the NAC53/78 interactome revealed that NAC53 and NAC78 associate with proteins involved in the ubiquitin-proteasome system at the ER. Interestingly, among these candidates, three belonged to the ER-Associated Degradation (ERAD) machinery, including the membrane-bound E3 ligase HRD1 and the central component CDC48 (**Figure 2G and S1I**). Given the ER localization of the TFs (**Figure 2C**) and the strong enrichment of proteasome

subunits in the C-ter IP-MS/MS condition (**Figure S1I**) we hypothesized that the turnover of both NAC TFs are regulated by ERAD.

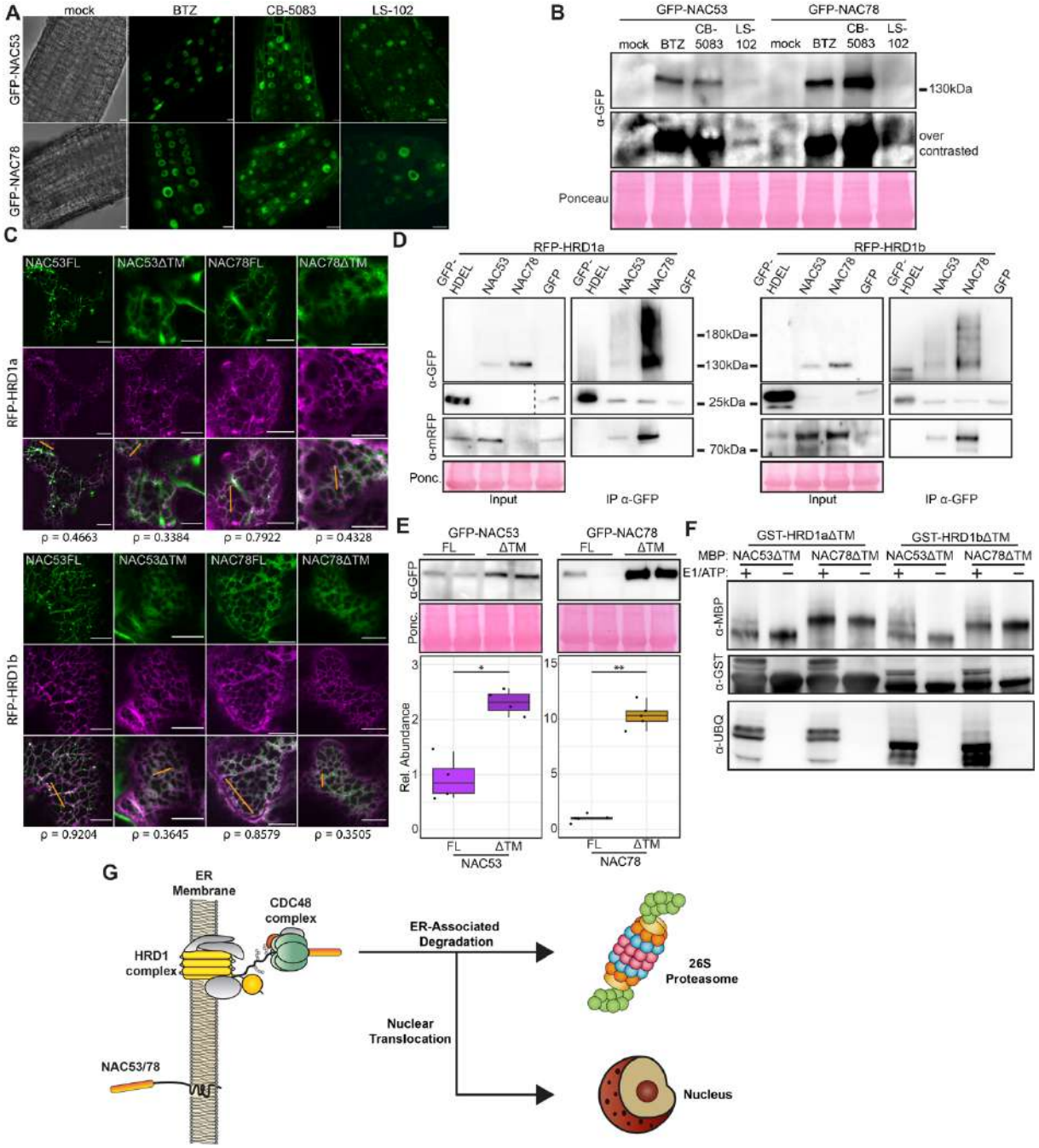

Figure 3. ER-Anchored Protein Sorting (ERAPS) coordinates the subcellular fate of NAC53 & NAC78.
(A) Confocal microscopy pictures of GFP-NAC53/78 expressing *A. thaliana* roots. 7 dag seedlings were exposed to mock treatment, BTZ 10µM, CB-5083 10µM or LS-102 100µM for 3h. The treatments were repeated at least three times with similar observations. Scale bars = 10µm
(B) Immunoblot against GFP on crude extracts of GFP-NAC53/78 *A. thaliana* adult plants infiltrated with mock treatment, BTZ 10µM, CB-5083 10µM or LS-102 100µM for 6h. Ponceau staining is used as loading control.
(C) Confocal microscopy pictures of *N. benthamiana* transiently co-expressing GFP-NAC53/78 full-length (FL) or deleted for the transmembrane domain (ΔTM) with RFP-HRD1a or RFP-HRD1b. Pearson index (ρ) indicates correlation index at the orange lines. Scale bars = 10µm
(D) Co-IP of RFP-HRD1a/b with GFP-NAC53/78. IP was performed with anti-GFP beads. GFP-HDEL and free-GFP were used as negative control. The experiment was repeated twice with similar results.
(E) Immunoblot against GFP on crude extract of *N. benthamiana* leaves transiently expressing GFP-NAC53/78FL or ΔTM. Ponceau was used as loading control. Boxplots represent the relative ΔTM abundance compared FL.

(F) *In vitro* trans-ubiquitination assays of GST-HRD1a/b against MBP-NAC53/78. Removal of E1 and ATP from the reaction was used as negative control. The experiment was repeated twice with similar results.
(G) Representation of the ER-Anchored Protein Sorting (ERAPS) mechanism. NAC53/78 are ER-anchored proteins recognized and ubiquitinated by the HRD1 complex. The CDC48 complex subsequently extracts NAC53/78 from the ER to mediate ER-Associated Degradation or allowing nuclear translocation in the context of proteasomal stress to mitigate proteotoxicity.

To investigate this possibility, we took advantage of previously characterized drugs: we treated the GFP-NAC53 and GFP-NAC78 transgenic lines with CB-5083 and LS-102, inhibitors of CDC48 and HRD1 proteins, respectively (Yagishita et al., 2012; Zhou et al., 2015). The effect of CB-5083 has already been characterized in plants (Li et al., 2022; Marshall et al., 2019), while LS-102 has not been characterized in plants to date. Our analysis revealed that LS-102 can efficiently inhibit both *A. thaliana* orthologs AtHRD1a and AtHRD1b *in vitro* (**Figure S2A and S2B**). Similar to BTZ treatment, CDC48 and HRD1 inhibition led to a stabilization of both proteins; visualized by confocal microscopy and through GFP immunoblotting (**Figure 3A and 3B**). Collectively, these results indicate that NAC53/78 are targets of ERAD. We next investigated whether NAC53 and NAC78 physically interact with both HRD1 isoforms. Transient co-expression of GFP-NACs with RFP-HRD1a/b revealed a strong association of NAC TFs with HRD1s at the ER, that was further confirmed by co-IP experiments (**Figure 3C and 3D**). The subcellular association was largely reduced upon deletion of the TM of both NAC TFs (ΔTM, **Figure 3C**). Interestingly, loss of ER association led to a strong stabilization of the proteins, supporting ERAD-dependent turn-over for both TFs (**Figure 3E**). These results support that NAC53/78 are targets of HRD1-mediated ubiquitination for proteasomal degradation.

To investigate whether HRD1s are indeed responsible for NAC ubiquitination, we performed *in vitro* ubiquitination assays using purified GST-HRD1a/b isoforms and MBP-NAC53/78 proteins. The assay revealed trans-ubiquitination of both NAC proteins in the presence of HRD1a and b that appeared in form of higher molecular weight bands of MBP-NAC proteins (**Figure 3E**). We could confirm the presence of ubiquitination marks at different sites via MS/MS analysis of the *in vitro* ubiquitination reactions (**Figure S2C and S2E**). In addition, ubiquitin marks were consistently inhibited by the addition of the inhibitor LS-102 to the *in vitro* ubiquitination assay (**Figure S2F**). The *in vitro* data was corroborated by identification of several ubiquitination sites on NAC53 and 78 in our *in vivo* IP-MS/MS analysis (**Figure S2D and S2E**). We confirmed *in planta* ubiquitination by performing ubiquitin IP on *N. benthamiana* leaves transiently expressing the dTag-NACs constructs (**Figure S2G**). Mutation of identified lysine residues substantially reduced the association with anti-ubiquitin beads *in planta* (**Figure S2H and S2I**). Altogether, our *in vivo* and *in vitro* analysis demonstrate that

NAC53 and NAC78 are directed to proteasomal degradation via ERAD through HRD1 ubiquitination.

During our analysis we could observe that NAC53/78 did not respond similarly to the tested inhibitors. Indeed, upon BTZ or CB-5083 treatment, GFP signal in the transgenic lines displayed different subcellular localization (**Figure 2A**). While BTZ led to a strong nuclear localization; CDC48 inhibition by CB-5083 led to a nuclear localization and cytoplasmic dot-like structures. To rule out the possibility of difference in drug potency, we treated plants with higher concentration of both drugs. While double amount of BTZ resulted in a stronger nuclear localization, an increase in CB-5083 concentration resulted in the accumulation of dot-like structures (**Figure S3A**), which could be potential sites of CDC48/NAC association. Co expression of *A. thaliana* CDC48 isoform (AtCDC48c) with both NACs revealed that CDC48 and NAC53/78 were able to associate in dot-like structures (**Figure S3B**). This indicates that upon CDC48 inhibition in *A. thaliana*, NAC53/78 accumulate at sites of CDC48 action. Given the role of CDC48 in retro-translocation of ER proteins to the cytosol, it could prevent degradation of NAC53/78 but also perturb their subcellular sorting. To test this, we compared the GFP signal intensity in the nucleus and cytoplasm upon BTZ and CB-5083 treatments (**Figure S3C**). Upon CB-5083 treatment the mean GFP intensity per cell was generally higher than upon BTZ (**Figure S3C**). This is consistent with a more diffuse localization of GFP signal. However, we observed that upon BTZ treatment more than 50% of the signal was found in the nucleus compared to 30% upon CB-5083 (**Figure S3D**). In addition, analysing the nucleus/cytoplasm mean intensity ratio revealed that NAC53/78 concentrate 6 times more in the nucleus upon BTZ compared to CB-5083 (**Figure S3E**). This analysis strongly suggests that CDC48 is partially involved in the nuclear translocation of NAC53 and NAC78 in addition to its role in proteasomal degradation.

In summary, we showed that the subcellular fate of NAC53 and 78 and hence the autoregulatory feedback loop is coordinated by the ERAD machinery. The turnover of ER-anchored NACs and their subsequent physiological impact is also the first example of the plant ERAD machinery having a role beyond quality control of aberrant proteins. In parallel this mechanism is responsible for their nuclear translocation (**Figure 3G**). Thus, we propose to refer to this mechanism as ERAPS (ER-Anchored Protein Sorting).

The transcriptional landscape of proteotoxic stress

Having established that ERAPS is controlling the proteasome autoregulatory feedback loop in plants, we wanted to understand why the *nac53-1 78-1* mutant is more tolerant to organelle-directed proteotoxic stress while it is hypersensitive to general proteotoxic stress (**Figure 1B**). To decipher the underlying mechanism, we utilized the fact that *Pseudomonas synringae* infection is causing proteotoxic stress through the suppression of proteasome activity and broad modification of chloroplast proteome (Littlejohn et al., 2021; Üstün et al., 2018; Üstün et al., 2016). We first characterized the involvement of the proteasome autoregulatory feedback loop during bacterial infection. Monitoring mRNA levels for both TFs genes, revealed an induction of *NAC53* and *78* upon infection (**Figure 4A**). In addition, transcriptional activation of proteasome genes was dependent on the presence of *NAC53* and *NAC78* WT alleles (**Figure 4B**). This was also consistent with an impaired protein accumulation of proteasome subunits in *nac53-1 78-1* upon infection (**Figure 4C**). Finally, we observed that bacterial infection was associated with the stabilization of NAC53 and NAC78 in *N. benthamiana* and *A. thaliana* (**Figure 4E and 4F**). Altogether these results demonstrate that bacterial infection displays all the features associated with proteotoxic stress that is dependent on the presence of both proteasome activators. As such, this system is ideal to unveil the function of the proteasome autoregulatory feedback loop in response to environmental perturbation.

To obtain a global idea on what else beyond the proteasome genes might be affected in *nac53-1 78-1* plants we undertook a transcriptomic analysis. We first analysed the transcriptomic profile of *nac53-1 78-1* infected with *Pst*. Interestingly, *nac53-1 78-1* displayed only 7 differentially expressed genes (DEGs) compared to Col-0 in mock (**Figure 4G)**, confirming that NAC53/78 are mainly involved in stress responses (Seo et al., 2008). Comparing the *nac53-1 78-1* to Col-0 in the context of bacterial infection revealed 945 DEGs. Strikingly, most of the genes display a positive Log2FC (**Figure 4H**). This suggests that NAC53/78 are major transcriptional repressors upon bacterial infection induced proteotoxic stress. We could confirm that bacterial infection triggers a general NAC53/78-dependent transcriptional up-regulation of proteasome related genes (**Figure S4A**). These results are in accordance with the involvement of the proteasome regulatory feedback loop during infection. Further investigation of which biological processes are enriched within the DEGs in our *nac53-1 78-1* transcriptome revealed photosynthesis, glucosinolates, cell wall and auxin signalling as major terms (**Figure 4I**). To refine our investigation and to include a broader view of the transcriptome landscape during proteotoxic stress, we included two other datasets into our analysis. Firstly, we generated

another transcriptome in response to pathogenic bacteria, subjecting the *rpt2a-2* proteasome

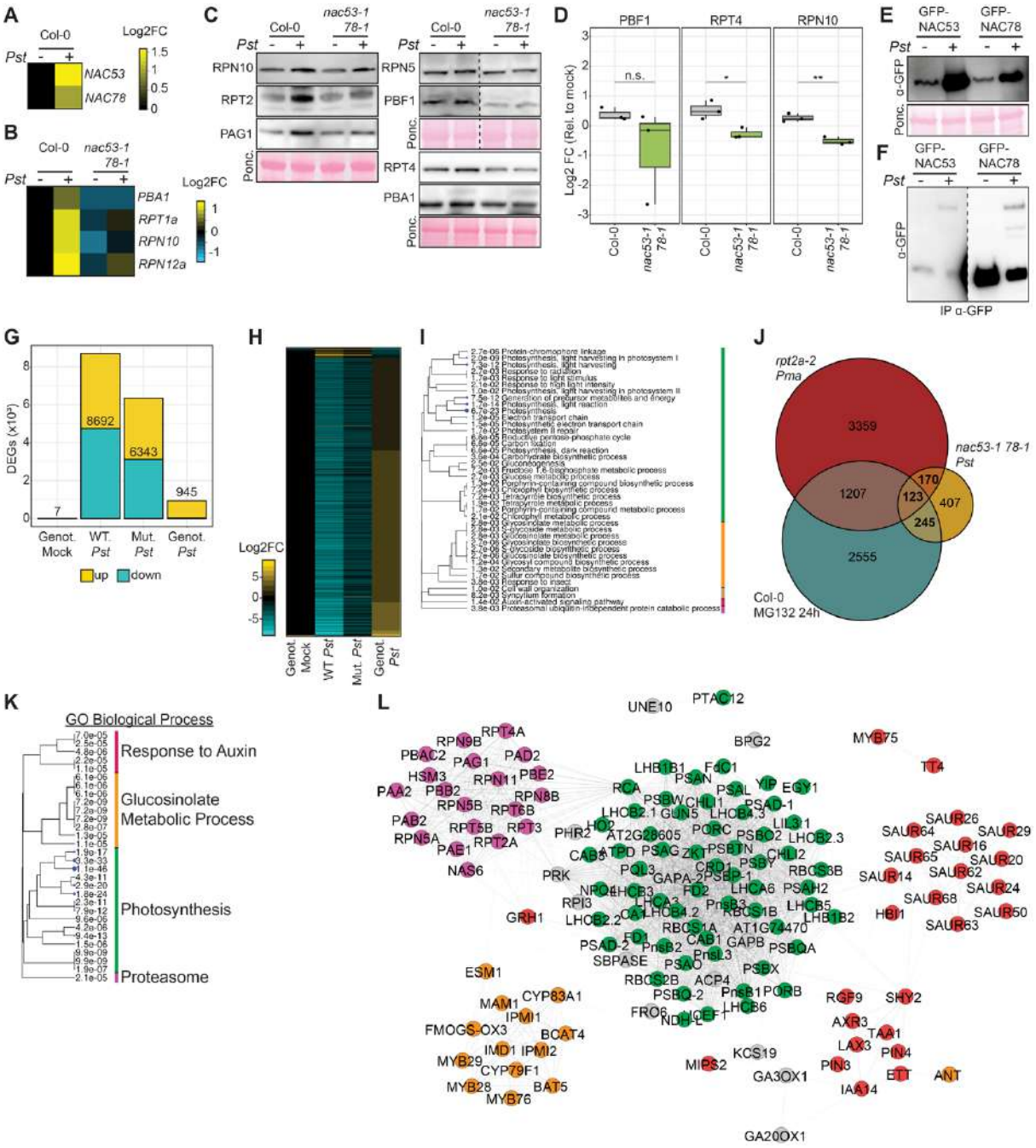

Figure 4. The transcriptional landscape of proteotoxic stress

(A) Log2FC mRNA levels of *NAC53* and *NAC78* transcripts after *Pst* infection of adult Col-0 plant leaves. The heatmap represent the mean of 4 biological replicates.

(B) Log2FC mRNA levels of 26S proteasome transcripts after *Pst* infection of Col-0 or *nac53-1 78-1* adult plant leaves. The heatmap represent the mean of 4 biological replicates. The experiment has been repeated 3 times with consistent results.

(C) Immunoblot against multiple 26S proteasome subunits on crude extracts of Col-0 or *nac53-1 78-1* adult plant leaves inoculated with *Pst* or mock solutions for 24h. Ponceau staining is used as loading control.

(D) Relative Log2FC abundance of representative 26S proteasome subunits in Col-0 or *nac53-1 78-1* adult plant leaves. The abundance is calculated relative to the mock conditions. Statistical differences are assessed via a Welch t.test (p values: n.s > 0.05, * < 0.05, ** < 0.01).

(E) Immunoblot against GFP on crude extract of *N. benthamiana* leaves transiently expressing GFP-NAC53/78 after mock treatment or *PstΔHopQ* infection for 8h. Ponceau staining is used as loading control.

(F) Immunoblot against GFP on extract of adult *A. thaliana* transgenics GFP-NAC53/78 subjected to mock treatment or *Pst* infection 8h by vacuum infiltration followed by IP with anti-GFP beads.

(G) Number of differentially expressed genes (DEGs) in the different conditions of the *nac53-1 78-1 Pst* RNAseq analysis. Total number of DEGs per condition is indicated. Colors indicate the proportion of DEGs up-regulated and down-regulated. DEGs are considered when |Log2FC| > 1.5. Genot. mock: *nac53-1 78-1* mock vs. Col-0 mock; WT *Pst*: Col-0 *Pst* vs. Col-0 mock; Mut. *Pst*: *nac53-1 78-1 Pst* vs. *nac53-1 78-1* mock; Genot. *Pst*: *nac53-1 78-1 Pst* vs. Col-0 *Pst*.
(H) Level of differential expression (Log2FC) of the 945 DEGs found in Genot. *Pst* (see panel G) for the several conditions analyzed.
(I) Cladogram of top 40 GO terms for BP enriched in the list of 945 DEGs. Colors represent broad GO clusters.
(J) Venn diagram representing the overlap between the 945 DEGs and DEGs from *rpt2a-2 Pma* (|Log2FC| > 0.5) or Col-0 MG132 24h (|Log2FC| > 0.5).
(K) Cladogram of top 30 GO terms for BP enriched in the list of 538 DEGs extracted from the combined analysis (panel J). For conciseness terms are hidden and grouped in 4 processes.
(L) Protein network of the genes from the 945 DEGs list related to the GO BP terms from panel K. Node colors refers to the 4 GO clusters from panel K.

mutant to *Pseudomonas syringae pv. maculicola* (*Pma*) infection. Contrary to *nac53-1 78-1,* this genotype displayed 251 DEGs in mock conditions (**Figure S4B**); indicating a basal stress response, including upregulation of proteasome genes, consistent with previous report (Lee et al., 2011). Upon infection we observed a large transcriptome variation compared to WT plant; with 981 DEGs identified specific to *rpt2a-2 Pma* condition (**Figure S4B and S4C**). Analysing the transcriptomic response of the proteasome complex, we found that most of the genes were further activated in response to infection in *rpt2a-2* background (**Figure S4D**). Interestingly, beyond terms associated with the proteasome, GO analysis on the 981 DEGs revealed others enriched process overlapping in both, *nac53-1 78-1* and *rpt2a-2*, transcriptomes (**Figure 4I and S4G**). Secondly, we included a previously characterized transcriptome analysis on Col-0 plants upon MG132 treatments (Gladman et al., 2016). This led to three distinct proteotoxic stress transcriptomes induced by drugs, infection and/or genetic mutations.

The comparison of all three datasets allowed us to extract a core set of 538 DEGs present in the *nac53-1 78-1* dataset and one or both others (**Figure 4J, Table S2**). Strikingly, GO enrichment on this subset of genes revealed 4 distinct biological processes involved (**Figure 4K**). Extracting the genes associated with these processes from the *nac53-1 78-1* 945 DEGs, we could define the core transcriptional network associated with proteotoxic stress (**Figure 4L**). This network is comprised of 4 modules: the proteasome genes, a major cluster of Photosynthesis associated nuclear genes (PhANGs), glucosinolate and auxin signalling pathways (**Figure 4K and 4L**). Analysing the transcriptional profile of the several clusters we identified interesting patterns (**Figure S4F**). While the proteasome cluster was present in all three datasets (**Figure S4C and S4F,** (Gladman et al., 2016), the glucosinolate related cluster was infection specific and the auxin cluster was found only in *nac53-1 78-1 Pst* and MG132 24h (**Figure S4H**). This further emphasized the specificity and complexity of the proteotoxic stress response. The photosynthesis cluster was found in significant proportions in all three datasets with 68 DEGs for *nac53-1 78-1 Pst*, 23DEGs for *rpt2a-2 Pma* and 57DEGs for MG132

24h (**Figure S4H, Table S2**). This suggests that PhANGs transcriptional repression is a recurrent response to proteotoxic stress. Strikingly, similar to the transcriptional response of proteasome genes, the differential expression of the other clusters is also happening in opposite manner in *nac53-1 78-1 Pst* compared to *rpt2a-2 Pma* or MG132 24h (**Figure S4H**). It shows that the observed transcriptional response is not due to an indirect effect of dysfunctional proteasome in *nac53-1 78-1* background as our previous results could have suggested.
Altogether our analysis revealed a so far unidentified link between NAC53/78 and the transcriptional regulation of PhANGs in response to proteotoxic stress.

NAC53 and NAC78 coordinate the regulation of proteasome and photosynthesis gene expression through the same cis-element

To identify whether NAC53/78 mediate a link between proteasome activation and repression of photosynthesis, we hypothesized NAC53/78 can act as novel repressors of PhANGs. Previous reports have shown that NAC TFs are involved in transcriptional repression (Hao et al., 2010; Shih et al., 2014). We therefore speculated PhANGs being direct targets of NAC53 and NAC78. This was also corroborated by the detailed analysis of distinct photosynthetic processes: While many processes were downregulated in the proteotoxic stress core transcriptome in the *rpt2a-2 Pma* and MG132 data sets, the absence of NAC53/78 had the opposite effect, indicating a possible repression via the NAC53/78 module (**Figure S5A**). To investigate a possible direct repression of PhANGs, we extracted the promoter regions of the 4 gene clusters from our transcriptional network (**Figure 4K and 4L**). Running enrichment analysis for specific cis-element, we found that Proteasome and PhANGs promoters share a similar cis-element characterized by the PRCE-like [TGGGC] motif, while the other clusters did not (**Figure 5A**). This further supported the link between PhANGs regulation and the proteasome regulatory feedback loop. In line with this, PRCE-like elements appeared homogeneously distributed among PhANGs (**Figure S5B**). Additionally, analysis of the cis-element position revealed a high frequency of occurrence and enrichment close to the transcription starting site, similar to proteasome promoters (**Figure S5B and S5C**). We then extracted two candidates' regions from LHCa3 and PSAD1 promoters (**Figure 5B**), respectively members of the light harvesting complex I and photosystem I (**Figure S5A,** (Leister, 2003). Performing electromobility shift assay (EMSA), we could confirm NAC53 and NAC78 were able to associates with these elements (**Figure 5C**). Consistently, this association was dependent on the presence of their respective DNA recognition motif (**Figure 5C**).

Furthermore, we confirmed the TGGGC motif as being the driver of this association, as mutated

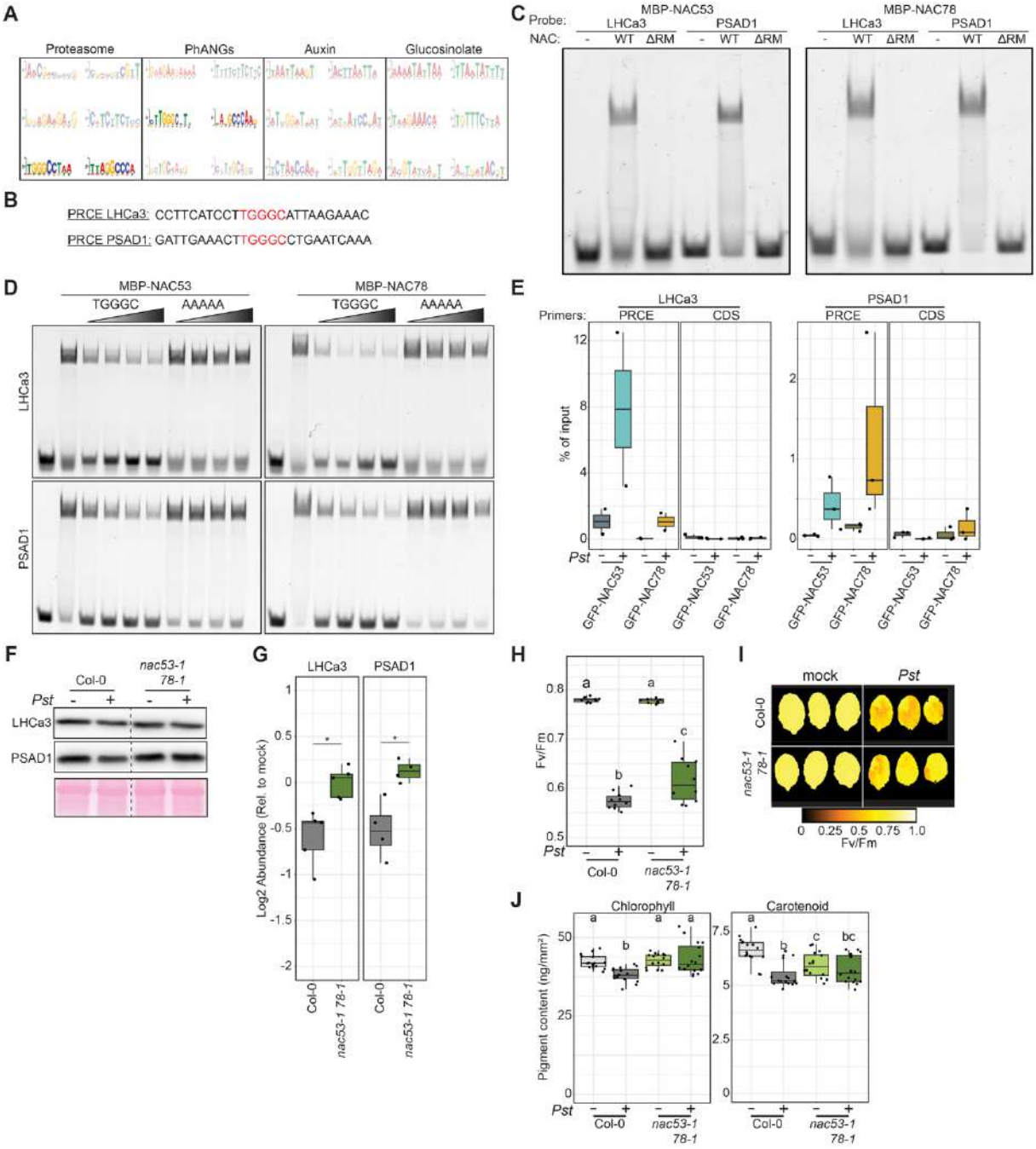

Figure 5. NAC53 and NAC78 coordinate the regulation of proteasome and photosynthesis gene expression through the same cis-element.

(A) Top 3 motifs found by STREME software in the promoter regions from the 4 network clusters (Figure 4L). PRCE-like elements from proteasome and PhANGs clusters are highlighted.

(B) 25bp region comprising the PRCE-like elements from LHCa3 and PSAD1 promoters used in this figure. The region corresponds to the probe sequence used in panel C and D. The PRCE is highlighted in red.

(C) Electro-Mobility Shift Assay (EMSA) of MBP-NAC53/78 with LHCa3/PSAD1 probes (see panel B). As a negative control, probes were incubated without MBP-NAC53/78 (-) or with MBP-NAC53/78 deleted for their DNA recognition motif (ΔRM). Experiment was repeated twice with similar results.

(D) EMSA competition assay of MBP-NAC53/78 association with LHCa3/PSAD1 probes. Competitor is applied at a concentration gradient (25X, 50X, 75X and 100X) indicated by the shade of grey. WT and mutated competitors are labelled TGGGC and AAAAA, respectively. Experiment was repeated twice with similar results.

(E) Boxplot representing association of GFP-NAC53/78 with LHCa3/PSAD1 PRCE in adult *A. thaliana* transgenics lines infected with *Pst* or mock for 8h after Chromatin Immunoprecipitation. The association is quantified as % of input and amplification of a region in the CDS is used as negative control.

(F) Immunoblot against mature PhANGs proteins in Col-0 or *nac53-1 78-1* adult plant leaves inoculated with *Pst* or mock solutions for 24h. Ponceau staining is used as loading control.
(G) Relative Log2FC abundance of PhANGs mature proteins immunoblotted in panel F. The abundance is calculated relative to the mock conditions. Statistical differences are assessed via a Welch t.test (p values: n.s > 0.05, * < 0.05, ** < 0.01).
(H) Photosystem II (PSII) activity measurement on Col-0 or *nac53-1 78-1* adult plants inoculated with *Pst* or mock solutions for 24h. Letters indicate the statistical group assessed by pairwise Welch t.test (p value < 0.05). The experiment was repeated 3 times with consistent results.
(I) Representative pictures of measurements from panel I. Fv/Fm values are represented by false color as indicated by the color gradient legend.
(J) Total chlorophylls and carotenoids from Col-0 or *nac53-1 78-1* adult plant leaves inoculated with *Pst* or mock solutions for 24h. Letters indicate the statistical group assessed by pairwise Wilcoxon-Mann-Whitney test (p value < 0.05). The experiment was repeated 3 times with consistent results.

oligos were unable to outcompete the association of NAC53/78 with the probes (**Figure 5D**). To corroborate our findings *in vivo*, we performed chromatin IP followed by qPCR in the context of bacterial-induced proteotoxic stress (**Figure 5E**). As expected, we could see that bacterial infection triggers the association of both TFs to both promoter regions, confirming the direct targeting of NAC53/78 to PhANGs promoters. To assess the regulatory role of NAC53/78 on PhANGs promoter activity, we used the luciferase reporter system in protoplasts (Yoo et al., 2007). Our analysis revealed that the PSAD1 promoter activity was consistently repressed by NAC53 and 78, which did not occur in *nac53-1 78-1* mutant protoplasts (**Figure S5D**). Deletion of the PRCE motif in PSAD1 abolished NAC78-mediated repression, while led NAC53 to mediate an increase in promoter activity (**Figure S5E**). In contrast, LHCa3 promoter activity appeared to be rather induced by NAC53 and unchanged by NAC78 (**Figure S5D**), with NAC53-mediated activation dependent on the PRCE motif (**Figure S5E**). This difference might be due to the fact that both TFs are expressed without a TM domain, bypassing ERAPS, in a rather artificial system. To circumvent this problem, we analysed the gene expression of *LHCa3* and *PSAD1* in the transgenic NAC53 and 78 lines upon BTZ treatment. Proteasome inhibition in the transgenic NAC53 and 78 lines partially enhanced the repression of PhANGs, supporting the notion that NAC53/78 act as repressors of photosynthesis during proteotoxic stress (**Figure S5F**). In addition, both lines showed an increase in *PBA1* and *RPT2a* mRNA (**Figure S5G**), confirming that NAC53/78 can act concomitantly as transcriptional repressor and activator. These results confirmed the importance of the PRCE-like element in PhANGs promoters, suggesting that NAC53 and NAC78 possess the ability to modulate each other's activity and highlights the complexity of the NAC53/78-PRCE regulatory module mediating transcriptional repression and activation on distinct gene cluster.

As NAC53 and NAC78 can associate with the PRCE-like element in PhANGs promoters to dampen their transcriptional activity, it is likely that they act as novel repressors of photosynthesis. To confirm this hypothesis, we analysed the protein abundance of LHCa3 and

PSAD1 proteins in the context of bacterial infection (**Figure 5F and 5G**). Immunoblot revealed that contrary to Col-0, infection induced reduction of photosynthesis-associated proteins appeared less pronounced in the *nac53-1 78-1* background (**Figure 5F**). Semi-quantitative analysis on several replicates confirmed this observation (**Figure 5G**). This confirms that the observed transcriptional repression mediated by the NACs has a major impact on PhANGs protein levels. To test if this protein pool perturbation would impact photosynthesis, we monitored PSII activity during infection. We found that *nac53-1 78-1* displayed significantly less PSII activity reduction compared to Col-0 (**Figure 5H and 5I**). In addition, when monitoring photosynthetic pigment content in the same context, we observed that total chlorophyll and carotenoid content reduction during infection occurred to a lesser extent in the *nac53-1 78-1* background (**Figure 5J**). Consistently with these findings, subjecting the NAC53/78 transgenics to constant proteasome inhibition resulted in strong developmental defect compared to WT (**Figure S5H and S5I**), suggesting that the role of NAC53/78 on photosynthesis repression is not restricted to bacterial infection.

Altogether, we demonstrate the unique ability of NAC53 and NAC78 to mediate activation and repression of target genes through the PRCE transcriptional module. This makes them novel repressors of photosynthesis during bacterial infection-induced proteotoxic stress. It also might explain our previous findings that the NAC mutant was more tolerant to organelle-directed proteotoxic stress, suggesting that photosynthesis repression is a general feature of the proteasome autoregulatory feedback loop to cope with proteotoxicity.

The proteasome autoregulatory feedback loop monitors photosynthesis homeostasis during stress responses

Our results show that NAC53/78 co-regulate proteasome and PhANGs by recognizing the same cis-element during bacterial infection induced proteotoxic stress. However, this feature does not only occur during bacterial infection as the PhANGs repression was also observed when proteasome was chemically inhibited (**Figure 4L, S5A, S5F and S5G**). Consistent with this, we have observed that the *nac53-1 78-1* mutant also performed better when we perturbed organellar proteostasis (**Figure 1B**). In addition, recent evidence suggests that loss of proteasome function in a chloroplast import deficient mutant increased photosynthetic capacity due to a lack of chloroplast precursor proteins degradation (Grimmer et al., 2020). Altogether, this hints towards a general role of the proteasome activators NAC53/78 to co-ordinate photosynthesis and proteasome homeostasis during proteotoxic stress.

To investigate to which extend NAC53/78 were involved in response to chloroplast perturbation, we analysed the photosynthetic response of *nac53-1 78-1* plants upon Bortezomib and Lincomycin treatments. Our analysis revealed that the decrease in pigment content was impaired in *nac53-1 78-1* in comparison to Col-0 plants upon BTZ and Lincomycin treatment (**Figure 6A**). Consistent with this, repression of PhANGs was less pronounced in the double mutant (**Figure 6B**) which resulted in a higher photosynthetic activity in *nac53-1 78-1* upon Lin treatment (**Figure S6A**).

To directly study the involvement of the proteasome autoregulatory feedback coordination of cellular proteostasis and photosynthesis, we decided to analyse the central ERAPS regulators HRD1a/b utilizing the inhibitors that were used in the NAC double mutant phenotyping (**Figure 1**). Proteasome inhibition rendered the *hrd1a 1b* more tolerant in comparison to Col-0 (**Figure 6C**), which is consistent with its role in negatively regulating NAC53/78 stability (**Figure 3G**). In contrast, all other tested drugs or bacterial infection rendered the *hrd1a 1b* mutant more susceptible (**Figure 6C and 6D**). The reduced growth of *hrd1a 1b* upon chloroplastic perturbations (Cml and Lin) are consistent with our previous results (**Figure 1B**), as stabilisation of NACs would lead to increased repression of PhANGs and growth reduction (**Figure S5A, S5H and S5I**). The impaired performance of *hrd1a 1b* upon CDC48 inhibition, pathogen infection or ER stress induction might be due to the general function of HRDs in ERAD (Chen et al., 2016) and thus appear to be pleiotropic. Consistent with this idea, analysis of the photosystem II activity revealed a stronger reduction in the *hrd1a 1b* double mutant (**Figure S6B**) upon infection corroborating our findings that ERAPS coordinate proteasome and photosynthesis through NAC53/78 stability. In addition, these data suggest that organellar perturbation would lead the NAC53/78 activation. Indeed, subjecting GFP-NACs transgenics to several organellar perturbators led to stabilization and nuclear localization of both TFs (**Figure S6C**). Taken together our analysis illustrates the importance of the proteasome autoregulatory feedback loop in maintaining the fine equilibrium of proteostasis to ensure normal response to proteotoxic stress.

We found that regardless the genetic mutations impacting the feedback loop, the plants displayed an increased susceptibility to bacterial infection (*rpt2a-2*, Üstün et al. (2016)). This finding demonstrates the importance of this mechanism in agronomically important context and raises the question if the autoregulatory feedback loop is involved in other conditions. To

answer this, we performed a large-scale transcriptomic analysis using the recently developed

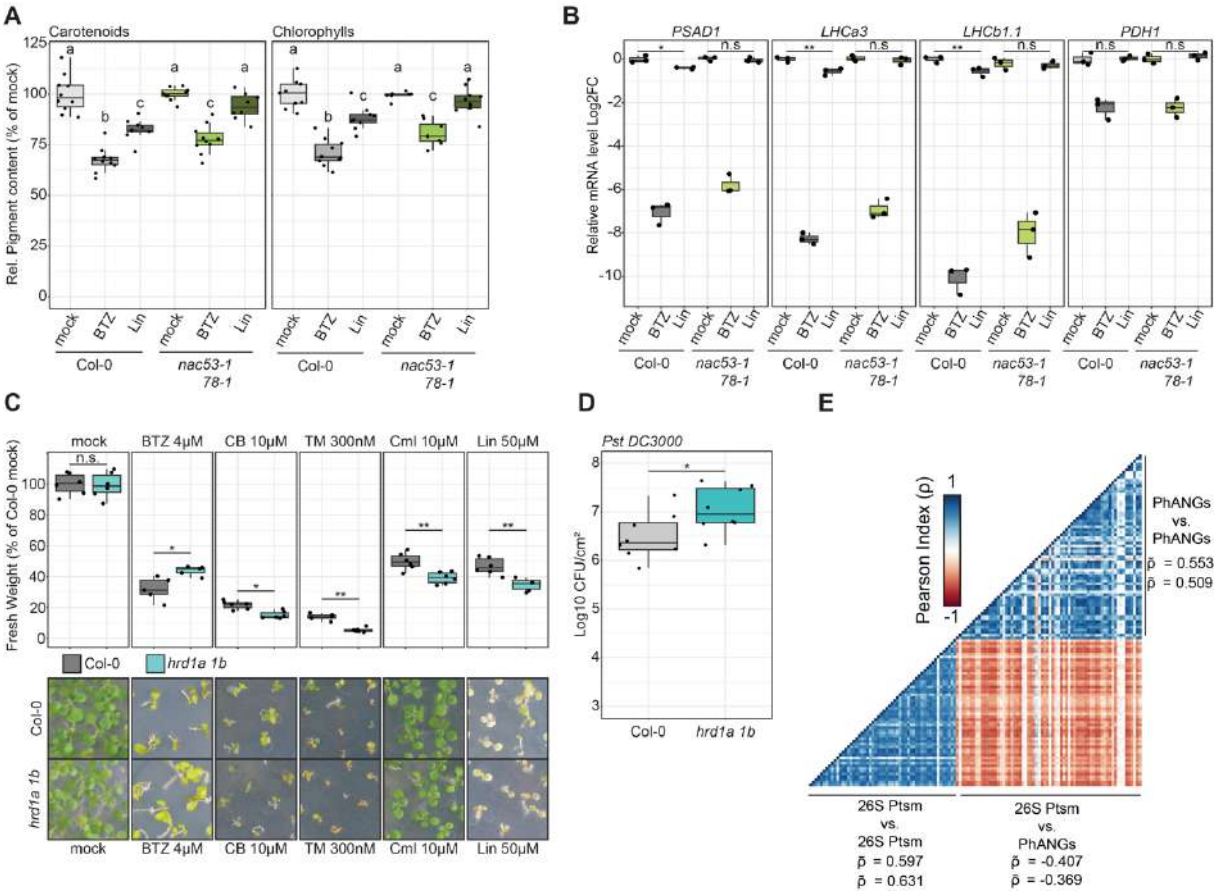

Figure 6. The proteasome autoregulatory feedback loop monitors photosynthesis homeostasis during stress responses

(A) Photosynthetic pigment content from Col-0 or *nac53-1 78-1* adult plant leaves infiltrated with Lin 200µM, BTZ 2µM or mock solutions for 24h. Content is expressed in percentage relative to Col-0 mock. Letters indicate the statistical group assessed by pairwise Wilcoxon-Mann-Whitney test (p value < 0.05). The experiment was repeated 3 times with consistent results.

(B) Log2FC mRNA level of the indicated transcripts in Col-0, *nac53-1 78-1* adult plants leaves Lin 200µM, BTZ 2µM or mock solutions for 24h. Log2FC is calculated from Col-0 mock and *PDH1* is used as negative control. Statistical differences are assessed with a Welch t-test (p values: n.s. > 0.05, * < 0.05, ** < 0.01). The experiment was repeated twice with consistent results.

(C) Fresh weight of seedlings grown under the indicated treatments at 10-14 day after germination. The fresh weight is represented as a percentage of Col-0 mock conditions. Letters indicate the statistical groups assessed by pairwise Wilcoxon-Mann-Whitney test (p value < 0.05). Every treatment has been repeated at least twice with consistent results. Representative phenotypic pictures are included.

(D) Bacterial density shown as Log10 Colony-Forming-Unit (CFU) per leaf cm² in Col-0 and *hrd1a hrd1b* plants. Statistical significance is assessed by a Welch t-test (p values: * < 0.05). The experiment has been repeated three times with consistent results.

(E) Correlation heatmap of the 54 26S proteasome subunit genes and the expression of 68 PhANGs from publicly available 1223 RNAseq libraries identified in this study.

Arabidopsis RNAseq data base (Zhang et al., 2020). We first investigated the relationship of transcript abundance between the 54 genes encoding 26S proteasome subunits and the 68 PhANGs associated with proteotoxic stress (**Figure 4**). We first extracted 165 unique projects of interest (see Methods, **Table S3**) to perform a correlation analysis between mRNA abundance of individual genes from both clusters (**Figure 6E**). We could observe that genes within each

cluster displayed a strong positive correlation ($\rho \approx 0.6$ and $\rho \approx 0.5$ for 26S Proteasome and PhANGs, respectively). Strikingly, analysing relationship between the two clusters showed a significant negative correlation ($\rho \approx -0.4$). It demonstrates that both clusters are regulated in opposite manner (**Figure S4H**) and that this is a general feature of stress responses. We therefore refined our analysis to define the spectrum of conditions displaying this transcriptional signature (see Methods). Thus, we extracted 43 projects in which 26S Proteasome and PhANGs appear transcriptionally co-regulated (**Table S3**). From these 43 projects, 35 displayed an opposite regulation for 26S Proteasome and PhANGs mRNA level (**Figure S6G**), confirming that both clusters undergo recurrent contrasting co-regulation. Looking at the conditions related to these datasets revealed that bacterial, oomycete infection or elicitation, led to a negative correlation of proteasome gene expression and PhANGs expression. This is in line with our previous observation using *Pst* infection. Beyond biotic stress, our analysis unveiled several other contexts, such as cold, dark and drought treatments as factors triggering this negative correlation (**Figure S6G**). Furthermore, we found that treatment with trans-chalcone a phytotoxin notably causing shoot bleaching (Diaz-Tielas et al., 2019) also resulted in a similar response. In addition to abiotic stress, nutrient stress and circadian rhythm triggered the same transcriptional signature. It suggests that coordination of PhANGs/Proteasome is not only a feature of plant stress response but also a characteristic of developmental processes which is additionally mirrored in hormone treatments such as SA and Auxin (**Figure S6G**).

Taken together, we found that the role of NAC53/78 in repression of photosynthesis is a general feature of proteotoxic stress at any subcellular level. We discovered that the coordination of proteasome activation and PhANGs repression is a key feature of the *Arabidopsis thaliana* transcriptome in response to multiple biotic, abiotic, and developmental cues. Given the conserved nature of the autoregulatory feedback loop in yeast, plants and animals, our findings bear the potential that proteasome activators are general gatekeepers of the interplay between the proteasome and energy metabolism across the tree of life.

Discussion

Understanding how eukaryotic organisms orchestrate proteostasis in a complex compartmentalized cellular environment is a long-standing question. Although the proteasome can degrade proteins from different compartments and organelles, how these different subcellular signals are integrated upon external cues and coordinated to maintain overall proteostasis was unknown.

Here, we have characterized that the proteasome autoregulatory feedback loop, involving the transcriptional NAC53/78-PRCE module, acts as a gatekeeper to facilitate the communication between the triangle chloroplast-proteasome-nucleus during proteotoxic stress (**Figure 7**).

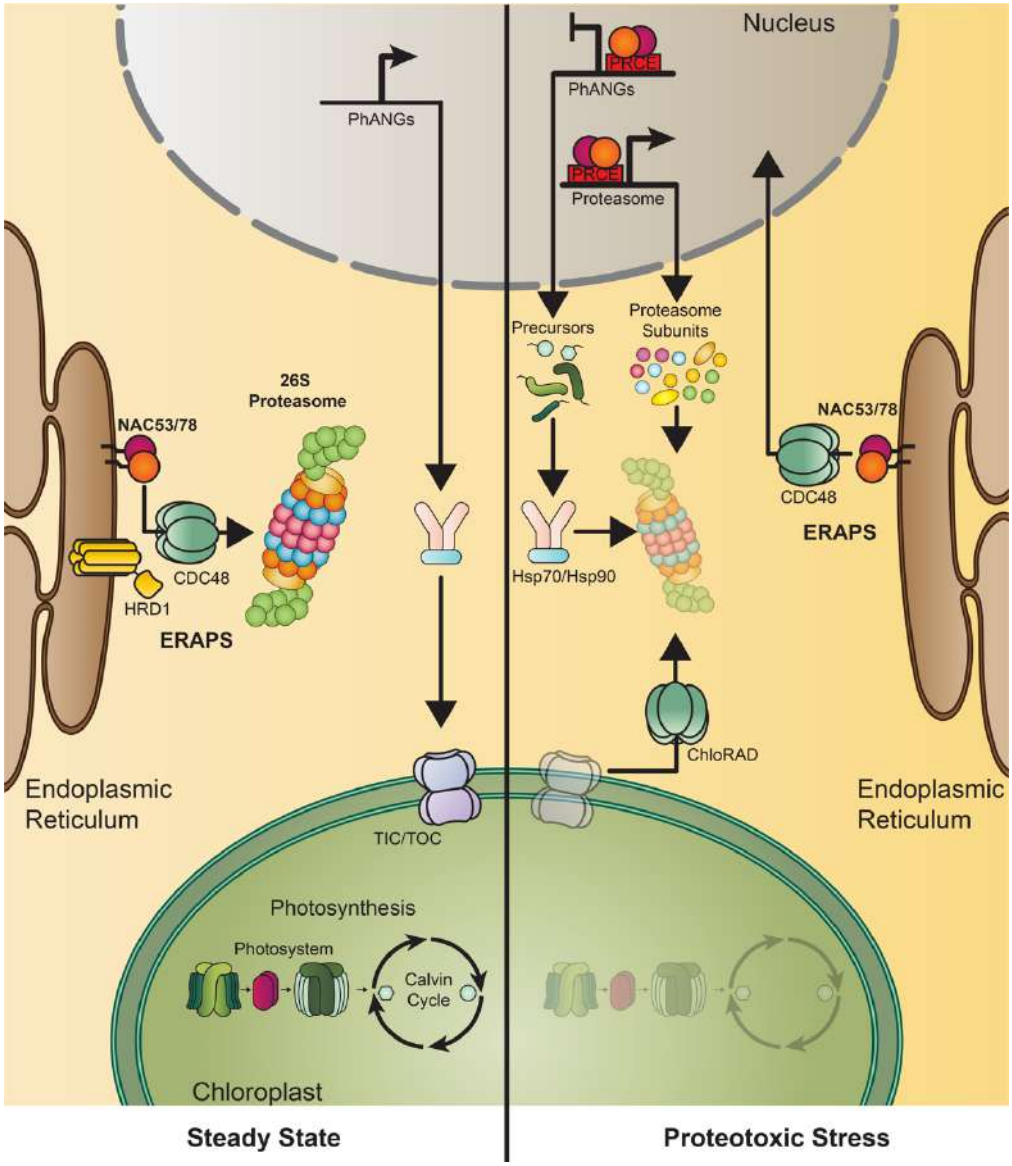

Figure 7. ER-anchored protein sorting (ERAPS) controls the fate of two proteasome activators for intracellular organelle communication during proteotoxic stress.
In steady state conditions, the ER-anchored protein sorting system (ERAPS) promotes the constitutive degradation of NAC53/78 via the 26S proteasome. Meanwhile, PhANGs expression is activated and subsequent chloroplastic import permits the maintenance of active photosynthesis. Upon proteotoxic stress, the chloroplast import machinery is targeted for proteasomal degradation. This leads to an accumulation of PhANGs precursors which are therefore subjected to proteasomal degradation, inducing proteotoxicity. Thus, to avoid proteotoxicity, the ERAPS system facilitates the nuclear translocation of NAC53/78, to activate the production of a new proteasome complex and to repress PhANGs expression to mitigate substrate accumulation.

We have shown that the trade-off between proteasome activation and photosynthesis downregulation is activated in response to various environmental and developmental cues

including disease. Using bacterial infection induced proteotoxic stress, we have identified ERAPS as the key regulatory node of this feedback loop and how the latter shapes and maintains subcellular proteostasis in plants. Considering that the autoregulatory feedback loop is mechanistically conserved across kingdoms, similar control mechanisms of subcellular proteostasis are possible in yeast and in animals (Marshall and Vierstra, 2019). While in yeast the main proteasome regulator is the cytosolic TF Rpn4; in animal systems, SKN-1A/Nrf1 is an ER-anchored protein which has also been shown to be subjected to ERAD (Radhakrishnan et al., 2014; Ruvkun and Lehrbach, 2023; Steffen et al., 2010). It suggests further mechanistic similarities between plant and animal systems, despite proteasome activators distinct evolutionary origins, as our study demonstrates the importance of ERAPS for the subcellular fate of NAC53/78, to a similar extend to what was reported for Nrf1 (Ruvkun and Lehrbach, 2023), emphasizing the conserved role ERAPS in regulating the proteasome activators. However, our data might suggest that nuclear translocation of NAC53 and 78 is only partially dependent on CDC48, as both NACs are still present in the nucleus upon CDC48 inhibition. In addition, the phenotypes observed using the *hrd1a hrd1b* mutant and the localization of both TFs upon LS-102 treatment suggest that HRD1-mediating ubiquitination is not strictly required for NAC53/78 nuclear translocation. Thus, it is likely that the ERAPS system involves alternative actors or other regulatory layers to mediate the transport of both TFs into the nucleus. For instance, SKN-1A/Nrf1 TFs were reported to be targeted by the ubiquitin-dependent DDI1/2 aspartyl-proteases for cleavage, downstream of their retro-translocation (Ruvkun and Lehrbach, 2023). Although NAC53/78 are evolutionary distinct from SKN-1A/Nrf1 and do not share the known DDIs cleavage site, we cannot exclude similar activation process due to the presence of an ortholog, DDI1, in *A. thaliana* (Farmer et al., 2010). In addition, a recent report has proposed a second ubiquitination step for Nrf1 in the cytosol which would facilitates DDI2-mediated cleavage (Hu et al., 2023). The presence of cytosolic E3 in NAC53/78 interactome could support similar mechanisms.

The ERAPS-dependent autoregulatory pathway proposed here would permit a rapid integration of proteotoxic signals from various compartments. As such, it would allow the communication between different organelles such as chloroplast or mitochondria with the nucleus, a process referred as retrograde signaling, known as the modulation of nuclear encoded gene expression in response of organellar proteostasis modification (Woodson and Chory, 2012). This communication is essential to respond to sudden changes in the environment. As such, retrograde signaling from mitochondria or chloroplast to the nucleus involves massive transcriptional changes that in turn influence organelle function (Richter et al., 2023). Thus, it

requires tight transcriptional regulation to respond to signals from different organelles. Some nuclear communicators have been identified to mediate retrograde signaling (Richter et al., 2023). However, to date, transcription factors GLK1 and 2, are the only known PhANGs activators (Waters et al., 2009), while putative repressors ABI4 and PTM could not be verified as retrograde signaling components (Kacprzak et al., 2019; Koussevitzky et al., 2007; Page et al., 2017; Sun et al., 2011). Here we have identified that plants have evolved a dual-regulatory system through the proteasome autoregulatory feedback loop: the NAC53/78-PRCE module acts as a novel retrograde signaling component, repressing PhANGs expression during prolonged proteotoxic stress. By binding to the same cis-element the NAC53/78 module is able to activate proteasome genes and repress PhANGs. In this scenario, (i) repression of PhANGs by NAC53/78 may be a strategy to cope with the excess of precursor accumulation due to proteasomal stress (**Figure 7**) which is corroborated by our findings that the *nac53-1 78-1* mutant is more tolerant to photosynthesis stress and HSP90 inhibition which activate NAC53/78 nuclear localization but also (ii) to counteract the overactivation of PhANGs by GLK1 that is degraded by the proteasome (Tokumaru et al., 2017). Although, NAC TFs have been reported to possess a repressor domain (NARD) (Hao et al., 2010), an intriguing question remains: how are NAC53/78 acting as activators and repressors using the same cis-element? Future investigations on this are necessary to improve our understanding how NACs activate and repress gene expression simultaneously or in a concurrent manner to mediate retrograde signaling.

In line with our findings, similar strategies to cope with the trade-off between proteasome activation and energy producing organelles have been established in yeast for mitochondrial associated proteins (Boos et al., 2019; Weidberg and Amon, 2018). In this case proteasome activator Rpn4 is activated upon accumulation mitochondrial precursor protein accumulation to turn on a second regulator Pdr3 which triggers the so called mitochondrial compromised protein import response (mitoCPR) (Kramer et al., 2021). This rather constitutes an indirect mechanism to transcriptionally repress the mitochondrial oxidative phosphorylation machinery (OXPHOS). This implies a divergence between yeast and plants on subcellular proteostasis coordination. It is tempting to propose these differences have emerged due to multicellularity allowing an improved flexibility depending on the tissue or cell types. This hypothesis is supported by the lack of the PRCE cis-element in the proteasome gene promoters of the monocellular algae *Chlamydomonas reinhardtii* (Nguyen et al., 2013). In addition, we could observe NAC53/78 activation in root cells, which lacks chloroplasts.. This observation further supports the general function of the proteasome regulatory feedback loop in maintenance of

subcellular proteostasis upon stress, not limited to chloroplastic impairment. To our knowledge, a similar system has not been found in other multicellular organisms such as animals. However, the characterization of OXPHOS gene repression by ATFS-1 during mitochondrial unfolded protein response (Shpilka et al., 2021), the importance SKN-1A/Nrf1 upon oxidative stress and the role of Nrf2/Nrf1 in mitochondrial biogenesis and proteasome activation (Ruvkun and Lehrbach, 2023) strongly suggests a tight link between proteasome and mitochondrial proteostasis in animals. Interestingly, another NAC TF, ANAC017 was characterized to mediate mitrochondria-nucleus retrograde signaling (Ng et al., 2013). As NAC TFs are known to function as homo or hetero-dimers (Welner et al., 2016), it is tempting to speculate that the proteasome autoregulatory feedback loop involves additional NAC in concert with NAC53/78, or other TFs, orchestrating the specificity of the transcriptional response.

Various environmental perturbations impede the balance between protein translation, sorting and degradation resulting in proteotoxicity. This has a global effect on proteostasis, and as mounting evidence highlights a role for the proteasome in clearing organelle-associated proteins it is essential to decipher how signals from different compartments and organelles are integrated to maintain proteostasis and avoid proteotoxicity. As such, our findings here lay the foundation to study whether the role as communicators between organelles during proteotoxic stress is a common feature of proteasome activators in different kingdoms.

Acknowledgments

We thank Yasin Dagdas and Marja Timmermans for critical discussions during the thesis advisory committee meeting. We are thankful to Ophélie Léger and Paul Gouguet for stimulating discussions. We thank Nan Wang for technical advice on the Ch-IP procedure, Robert Morbitzer for technical support on the golden gate molecular cloning. We are grateful to Ana Gabriela Andrade-Galan and Lars Pospisil for technical support on the Photosystem II activity measurement. Stefan Bieker for the help with the computational analysis. We are thankful to Jos Schippers, Yasin Dagdas and Richard Vierstra for sharing published material. This work was supported by an Emmy Noether Fellowship GZ: UE188/2-1 from the Deutsche Forschungsgemeinschaft (DFG; to S.Ü.) and through the collaborative research council 1101 (SFB1101; to G.L.). We thank the confocal microscopy facility of ZMBP that is supported by funds from DFG (INST 37/819-1 FUGG and INST 37/965-1 FUGG) and the confocal microscopy facility of RUB (DFG Project number 523980288, GZ:INST 213/1180-1 FUGG). Macek Lab is supported by DFG funds (INST 37/1050-1 FUGG and INST 37/1255-1 FUGG).

Author Contribution

S.Ü. conceived the project. G.L. performed most experiments, analyzed the data, and performed all computational analysis. M.R. performed the *in vitro* ubiquitination assays. D.B performed the EMSA, assisted with the Luciferase reporter assay and the molecular cloning. D.S. generated the *rpt2a-2 Pma* transcriptome under the supervision of F.B..M.F.W and B.M. performed LC-MS/MS analysis. S.Ü. wrote the manuscript together with G.L..

Experimental model and Subject Details

Arabidopsis thaliana lines and growth conditions

A. thaliana Columbia-0 (Col-0) ecotype was considered as WT. T-DNA insertion mutants for *NAC53* (*nac53-1*, SALK_009578C) and *NAC78* (*nac78-1*, SALK_025098) were obtained from Richard Vierstra and previously described (Gladman et al., 2016). T-DNA insertion mutants for *RPT2a* was previously described (Lee et al., 2011; Üstün et al., 2016). T-DNA insertion mutants for *HRD1a (hrd1a*, SALK_032914) and *HRD1b* (*hrd1b,* SALK_061776) were obtained from Yasin Dagdas and previously described (Su et al., 2011).

promUBQ10::GFP-NAC53 and *promUBQ10*::GFP-NAC78 transgenics lines were obtained by *Agrobacetrium tumefaciens* floral dipping (Clough and Bent, 1998) of Col-0 plants. Positive transformants were selected by BASTA spraying and seeds were harvested individually. The following generations were sawed on ½ Murashige and Skoog (MS) media supplemented with 10µM phosphinotricin for segregation analysis. Two independent lines showing a 75% survival rate for each construct were kept for subsequent experiments.

For experiments on seedlings, seeds were surface sterilized 10min with 1.3% sodium hypochlorite. Seeds were then sown on ½ MS medium supplemented with 1% sucrose and stratified for 2 days in cold room to synchronize germination. Plants were next grown under long day conditions (light/dark cycles: 16h 22°C/8h 20°C, 130µmol.mm².s^{-1} light intensity, 70% relative humidity).

For experiments on adult plants, seeds were sown on soil soaked with water in individual pots. Trays were put directly in the growth chamber under short day conditions (light/dark cycles: 12h 22°C/ 12h 20°C, 90µmol.mm².s^{-1} light intensity, 70% relative humidity). Seven days after germination, excessive number of seedlings were removed from individual pots to obtain one plant per pot. Plants were grown under same conditions until use (typically 21 to 28 more days).

Nicotiana benthamiana growth

N. benthamiana plants were grown under long day conditions (light/dark cycles: 16h/8h, at 21°C and 70% humidity) and typically used 4 weeks after germination for confocal microscopy experiments and 5 weeks after germination for co-immunoprecipitation experiments.

Bacterial strains

For Pseudomonas syringae pv. *tomato* DC3000 wild-type and *Pseudomonas syringae* pv. *maculicola* strains ES4326 were grown on King's B medium containing rifampicin 100µg.mL^{-1} at 28°C. For floral dipping and transient expression in *Nicotiana benthamiana* leaves, *Agrobacterium tumefaciens* C58C1 strain was grown in LB broth high salt (Duchefa L1704) containing the required antibiotics at 28°C. For molecular cloning, *Escherichia coli* Top10 strain was grown in LB broth high salt (Duchefa L1704) containing the required antibiotics at 37°C. For protein purification, *Escherichia coli* BL21 (DE3) was grown in LB broth high salt (Duchefa L1704) containing the required antibiotics at 37°C or 16°C.

Method Details

Molecular cloning

For chimeric protein constructs generated in this study, protein coding sequence (CDS) of the desired genes were amplified from *A. thaliana* cDNA with addition of flanking region for subsequent cloning process.

For Golden Gate based cloning (Binder et al., 2014), CDS were amplified with addition of flanking regions including BpiI/BsaI sites (Fw: 5'-GAGAAGACGATACGGGTCTCACACC-3'; Rv: 5'-GAGAAGACGACAGAGGTCTCACCTT-3'). PCR products were gel purified and inserted into LI module (Binder et al., 2014) backbone using BpiI/T4 ligase (both Thermo Scientic) cut-ligation procedure (40 cycles, 37°C 2min/16°C 5min). The resulting product was transformed into *E. coli* Top10 followed by gentamycin selection. Positive clones were used for plasmid miniprep (NEB) and verified by sanger sequencing. For generation of expression constructs, the LI CDS module and desired other modules (e.g., promoter, tag, terminator etc.) were assembled in the LIIa F 1-2 vector (Binder et al., 2014) using BpiI/T4 ligase (both Thermo Scientic) cut-ligation procedure (40 cycles, 37°C 2min/16°C 5min). Resulting product was transformed into *E. coli* Top10 followed by spectinomycin selection. Positive clones were verified for correct assembly by colony PCR following by enzyme restriction analysis. The obtained construct was then transformed into *A. tumefaciens* C58C1 for subsequent use.

For GATEWAY™ based cloning, CDS were amplified with addition of attb1/attb2 flanking regions (attb1-fw 5'-GGGGACAAGTTTGTACAAAAAAGCAGGCTTC-3'; attb2-rv 5'-

GGGGACCACTTTGTACAAGAAAGCTGGGT-3'). PCR products were gel purified and inserted into pDONR221 via BP clonase™ II enzymatic reaction. Alternatively, GATEWAY™ compatible entry clone was generated by performing a BsaI/T4 ligase cut-ligation from LI module to pENTR-BsaI (Binder et al., 2014). Resulting product was transformed into *E. coli* Top10 followed by kanamycin selection. Positive clones were used for plasmid miniprep (NEB) and verified by sanger sequencing. For generation of expression constructs, pDONR/pENTR clone was used for LR Clonase™ II enzymatic reaction into the desired destination vectors. Resulting product was transformed into *E. coli* Top10 followed by spectinomycin or carbenicillin selection. Positive clones were verified by colony PCR. The obtained construct was then transformed into *A. tumefaciens* C58C1 or *E. coli* BL21 (DE) for subsequent use.

Seedlings phenotyping

For phenotyping assay, seeds were sown on ½ MS 1% sucrose round petri dish supplemented with the indicated concentration of drug or a mock treatment.

After 10 to 14 days of growth fresh weight was measured. Seedlings were carefully extracted from the media with a curved tweezer (Dumont Nr. 7) ensuring that the entire root was taken. For one replicate, 5 representative seedlings were scaled together on an analytical scale (resolution 0.0001g). Typically, 5 replicates were measured for subsequent statistical analyses.

Transient expression in *N. benthamiana* leaves

Bacterial suspension was centrifuged for 4min at 4000g after overnight incubation of *A. tumefaciens* strain carrying the desired expression construct. Supernatant was removed and pellet was resuspended in 500µl of agroinfiltration buffer (10mM $MgCl_2$, 10mM MES pH 5.7). OD600 was measured and infiltration solutions were diluted to reach final 0.5 OD600 in agroinfiltration buffer supplemented with 200µM acetoseryringone. Solutions were incubated in dark at least 1h prior to infiltration. Infiltrated tissues were used 30h post infiltration for subsequent experimental procedures.

Protein purification

Recombinant proteins were expressed in E. coli BL21(DE3) by IPTG induction. Bacterial solution was centrifuged 20min at max speed and pellet was subjected to sonication after resuspension in 1mL MBP-buffer (20 mM TRIS-HCl pH 7.5, 200mM NaC, 1mM EDTA) or 1mL IPP50 (10 mM Tris-HCl, pH 8.0. 150mM NaCl, 0.1% NP40). Sonicated samples were used for purification by affinity chromatography using amylose resin (New England Biolabs)

for MBP-NAC53/78 or glutathione sepharose 4B (cytiva) for GST-HRD1a/b. For recombinant His-UBA1 and His-UBC8 protein were purified using Ni-Ted resin (Macherey-Nagel).

***In vitro* ubiquitination assay**

In vitro ubiquitination assay was performed as previously described (Leong et al., 2022). Purified proteins were used for in vitro ubiquitination assays. Each reaction of 30 ml final volume contained 25 mM Tris–HCl, pH 7.5, 5 mM MgCl2, 50 mM KCl, 2 mM ATP, 0.6 mM DTT, 2 µg ubiquitin, 200 ng E1 His- AtUBA1, 1.2 µg E2 His-AtUBC8, 2 µg of GST-HRD1a/b, and 0.3 µg of MBP-NAC53/78. Samples were incubated for 1 h at 30°C, and the reaction was stopped by adding SDS loading buffer and incubated for 10 min at 68°C. Samples were separated by SDS–PAGE electrophoresis using 4–15% Mini-PROTEAN® TGX™ Precast Protein Gels (BioRad) followed by detection of the ubiquitinated substrate by immunoblotting using anti-MBP (New England Biolabs), anti-GST and anti-ubiquitin (Santa Cruz Biotechnology) antibodies.

Co-immunoprecipitation

Plant tissue was homogenized in a mortar with liquid nitrogen to keep the sample frozen during the process. The powder was then transferred into a 50mL centrifuge tube and 1ml of extraction buffer (10% glycerol, 25 mM Tris pH 7.5, 1 mM EDTA, 150 mM NaCl, 1 mM DTT, 0.5% Triton X, 1X protease cocktail inhibitor (Sigma)) was added per gram of tissue. Obtained sample were vortexed for 3min and incubated in cold room on rotator in cold room for 10min following a 30min centrifugation at 4000g, 4°C. Supernatant was filtered through 3 layers of miracloth (Merck 475855-1R) in a 15mL centrifuge tube. 50µl of filtrate was sampled as input at this step, supplemented with 12.5µL laemmli buffer 4X (Biorad) and boiled for 10min at 90°C. Next, 10µl of ChromoTek GFP-Trap® or RFP-Trap Agarose beads per gram of tissue were added and tubes were incubated 2-3h in cold room. Tubes were then centrifuge at 800g for 1min; supernatant was carefully removed and pelleted beads were transferred to 1.5mL microcentrifuge tube in 1mL of washing buffer (10% glycerol, 25 mM Tris pH 7.5, 1 mM EDTA, 150 mM NaCl, 0.5% Triton X-100, 1X protease cocktail inhibitor (Sigma)). Washing was perfomed by centrifugation at 800g for 1min using 1mL washing buffer. After last washing, 10µL of Laemmli buffer 2X (Biorad) was added to equal amounts of beads and sample was boiled 10min at 90°C.

RNA isolation & RT-qPCR

Total RNA isolation was performed using RNeasy Plant Mini Kit (Qiagen 74904). All steps were performed according to manufacturer instructions. To exclude potential contaminant DNA, RNA samples were subjected to DNase I treatment (Thermo scientific™) following provider instructions. For RNA sequencing, integrity and RNA concentration was determined (2100 Bioanalyzer, Agilent). For RT-qPCR sample analysis was adapted from Langin and Üstün (2023); cDNA synthesis was performed using LunaScript® RT SuperMix Kit (NEB) following provider recommendation. qPCR was performed using MESA BLUE qPCR 2X MasterMix Plus for SYBR® Assay (Eurogentec) using a 2-step reaction protocol for 40cycles with systematic evaluation of primer melting curve. mRNA level was quantified based on the ΔΔCt method followed by Log2 transformation.

NanoLC-MS/MS analysis and data processing

For purification, proteins were subjected to a NuPAGE 12% gel (Invitrogen) and in-gel trypsin digestion was done on Coomassie-stained gel pieces, as described previously (Borchert et al, 2010) with a modification: iodoacetamide was used instead of chloroacetamide for carbamidomethylation of cysteine residues to avoid formation of lysine modifications isobaric to two glycine residues left on ubiquitinylated lysine after tryptic digestion. Next, peptides mixture were desalted using C18 Stage tips and run on an Easy-nLC 1200 system coupled to a Q Exactive HF-X mass spectrometer (both Thermo Fisher Scientific) as described elsewhere (Kliza et al., 2017) with some modifications: separation of the peptide mixtures was done using a 87-min segmented gradient from 10-33-50-90% of HPLC solvent B (80% acetonitrile in 0.1% formic acid) in HPLC solvent A (0.1% formic acid) at a flow rate of 200 nl/min. The seven most intense precursor ions were sequentially fragmented in each scan cycle using higher energy collisional dissociation (HCD) fragmentation. In all measurements, sequenced precursor masses were excluded from further selection for 30 s. The target values were 105 charges for MS/MS fragmentation and 3 × 106 charges for the MS scan.

Acquired MS spectra were processed with MaxQuant software package version 1.5.2.8 with an integrated Andromeda search engine. For *in vivo* IP samples, database search was performed against a *N. benthamiana* database containing 74,802 protein entries (Kourelis et al., 2019), the sequences of eGFP-NAC53/78, mCerrulean3-NAC53/78-mCherry and 285 commonly observed contaminants.

For *in vitro* ubiquitination samples, database search was performed against the Uniprot *E. coli* database, the sequences of MBP-NAC53/78, GST-HRD1a/b and 285 commonly observed contaminants.

Endoprotease trypsin was defined as a protease with a maximum of two missed cleavages. Oxidation of methionine, phosphorylation of serine, threonine, and tyrosine, GlyGly dipeptide on lysine residues, and N-terminal acetylation were specified as variable modifications. Carbamidomethylation on cysteine was set as a fixed modification. Initial maximum allowed mass tolerance was set to 4.5 parts per million (ppm) for precursor ions and 20 ppm for fragment ions. Peptide, protein, and modification site identifications were reported at a false discovery rate (FDR) of 0.01, estimated by the target-decoy approach (Elias and Gygi). The iBAQ (Intensity Based Absolute Quantification) and LFQ (Label-Free Quantification) algorithms were enabled, as was the "match between runs" option (Schwanhäusser et al., 2011).

Photosynthesis monitoring

For photosynthetic pigment concentration, 2 leaf discs (6mm) were sampled in a 2mL microcentrifuge tube after the indicated treatments and incubated over-night in 1mL acetone 100% on a rotating wheel in cold room. Tubes were next centrifuged for 3min at 400g. 200µl of was then pipetted in a transparent 96-well plate and absorbance was measured at 470nm, 646nm and 663nm using a plate reader (Tecan Infinite 200 PRO®). Acetone 100% was used as blank. Concentration was calculated as following:

Total Chlorophylls ($\mu g.ml^{-1}$): $((12.25*A_{662}) - (2.79*A_{646}) + (21.5*A_{646}) - (5.1*A_{663}))/0.2$

Total Carotenoids ($\mu g.ml^{-1}$): $((1000*A470-1.63*((12.25*A_{662}) - (2.79*A_{646})) - 85.02*((21.5*A_{646}) -(5.1*A_{663})))/221)/0.2$

The equations for concentration calculation and procedure were obtained from Karlsruher Institut für Technologie (KIT, https://www.jkip.kit.edu/molbio/998.php, "Chlorophyll and Carotenoid determination in leaves") as an updated version of the original procedure (Lichtenthaler, 1987).

Values were then then expressed as $ng.mm^2$ by dividing them by the total leaf area used for extraction (typically $56.55mm^2$).

For photosynthetic efficiency, photosystem II (PSII) activity was measured by quantifying the maximum photosystem II yield, Fv/Fm via the saturation pulse methods on dark acclimated plants (Schreiber, 2004). After treatments, plants were acclimated in dark for 15min. Next, leaves were detached and PSII activity was assessed by Fv/Fm values using the Imaging-PAM chlorophyll fluorometers: Maxi version v2-46i, for measurements related to Figure 5 and Dual-PAM100, for measurements related to Figure 6 (Walz GmbH, Effeltrich, Germany).

Bacterial Infection

For bacterial infections, *Pst* overnight liquid culture was centrifuged for 15min at 4000g. Bacterial pellet was resuspended in 5mL of $MgCl_2$ 10mM prior to OD600 measurement.

For qPCR, RNAseq and western blot analysis; a *Pst* solution at OD600=0.2 was used. Adult plant leaves were infiltrated with a 1mL syringe (Braun) with the *Pst* infiltration solution or a control solution (10mM $MgCl_2$) and put back in growth chamber for 24h until sampling or further analysis.

For IP and Chromatin-IP on *A. thaliana*, *Pst* infiltration was prepared as explained above and detached whole rosettes of adult plants were vacuum infiltrated 2 times 2 min at < 15mbar. For mock, control solution (10mM $MgCl_2$) was used similarly. Rosettes were put back in the growth chamber for 8h on multiple layers of wet tissue.

For assessment of bacterial density (related to Figure 1C and 6D); *Pst* infiltration solution was prepared in 10mM $MgCl_2$ at an OD600 of 0.0001. Adult plant leaves were infiltrated with a 1mL syringe (Braun) with the *Pst* infiltration solution and put back in growth chamber for 72h in high humidity conditions. After 3 days, 2 leaf disks per replicates were sampled with a biopsy punch 6.0mm (Harris Uni-Core) in a 1.5mL microcentrifuge tube. Tissue was homogenized in 200µl 10mM and a serial dilution of factor 10 was done for each replicate in 200µL nano pure water until 10^{-6} dilution was reached. For bacterial counting, 20µL of several resulting dilutions (typically 10^{-5} and 10^{-6}) were plated on KB media with rifampicin for each replicate. Growing colony-forming units were counted and Log10CFU/cm² was calculated for graphical representation and statistical testing.

Chromatin Immuno-Precipitation

For Chromatin-IP, after Arabidopsis rosettes were vacuum infiltrated for 30min with a fixation buffer solution (1% formaldehyde, 10mM KH2PO4 pH 7, 50mM NaCl, 0.1M sucrose, 0.01% Triton X-100) to cross-link protein-DNA. Plant material (typically 1g) was dried and frozen in liquid nitrogen for each replicate. Tissue was next ground in 5mL nuclei isolation buffer (20mM Hepes pH8, 250mM sucrose, 1 mM $MgCl_2$, 5mM KCl, 40% Glycerol, 0.25% Triton X-100, 0.1mM PMSF, 0.1% 2-mercaptoethanol, 1µM BTZ). The resulting solution was filtered through three layers of miracloth paper in a 50mL centrifuge tube following 10min centrifugation at 4°C, 3000g. Pellet was resuspended in 1mL nuclei isolation buffer and transferred into a 1.5mL microcentrifuge tube. Tube was centrifuged 5min, at 4°C, 3000g and the previous step was repeated once. Pellet was resuspended in 200µl M3 buffer (10mM KH2PO4 pH7, 0.1mM NaCl, 10mM 2-mercaptoethanol) and recentrifuged 5min, 4°C, 3000g. Nuclei pellet was resuspended in 1mL sonication buffer (10mM KH2PO4 pH7, 0.1mM NaCl,

0.5% Sarkosyl, 10mM EDTA). Sonication was performed with an Active Motif Sonicator (Amp 25%; Pulse: 30sec ON – 30sec OFF; Timer: 300sec). Sonicated sample was centrifuged for 5min, 4°C at max speed. Supernatant was tranferred to a new 1.5mL microcentrifuge tube and 10% (v/v) Triton X-100 was added to neutralize the sarkosyl. 5% (v/v) of this solution was saved in another 1.5mL microcentrifuge as input sample. For IP, 15µL ChromoTek GFP-Trap® were activates in 15µL IP buffer (50mM Hepes pH 7.5, 150mM NaCl, 5mM $MgCl_2$, 10uM ZnSO4, 1% Triton X -100, 0.05% SDS) and added to the tube and incubated for 3h on a rotating wheel at 4°C. Beads were washed for 4 rounds by centrifuging for 30sec, at 1000g and subsequent incubation on rotating wheel in 500µL buffer for 3 min; twice in IP buffer, once in LNDET buffer (0.25 LiCl, 1% NP-40, 1% deoxycholate, 1mM EDTA pH 8, 10mM Tris pH 8) and once in TE buffer (10mM Tris pH 8, 1mM EDTA pH 8). After the last washing step, beads were centrifuged for 30sec at 1000g, resuspended in 200µL EB buffer (50mM Tris pH 8, 10mM EDTA pH 8, 1% SDS) supplemented with 8µL 5M NaCl to reverse cross-linking and incubated at 65°C for at least 6h. At this step input sample was added and treated similarly. For protein digestion, 1µL of Proteinase K (Thermo Scientific) was added and incubated for 1h at 45°C. Next, DNA was purified using a PCR purification kit (NEB) following manufacturer instructions.

For DNA quantification, qPCR was performed using MESA BLUE qPCR 2X MasterMix Plus for SYBR® Assay (Eurogentec) using a 2-step reaction protocol for 40 cycles and each sample was processed in technical triplicates. For quantification, % of input was calculated and used for graphical representation and statistical analysis.

Immunoblot analysis

For immunoblot analysis, sample processing was adapted from (Langin and Üstün, 2023); 2 leaf discs from *N. benthamiana* or *A. thaliana* were sampled using a biopsy punch 6mm (Harris Uni-Core) in 2mL microcentrifuge tube containing 2 glass beads (2mm) for one replicate in the given condition and frozen in liquid nitrogen. Tissue was homogenized using a Tissue Lyzer II (Qiagen), 2 times 30sec, frequency: 25; followed by the addition of 150µL protein extraction buffer (100mM Tris-HCl pH 7.5, 3% SDS, 10mM EDTA) per tube. Tubes were next mixed with the Tissue Lyzer II, 2 times 15sec, frequency: 15. Finally, 50µL laemmli buffer 4X (biorad) was added and samples were boiled for 10min at 95°C. Tubes were centrifuged for 1min at 13000g and 150µL of the supernatant was transferred in a new 1.5mL microcentrifuge tube and kept at -20°C until use.

Western blotting was done by SDS-PAGE using TGX FastCast 10% Acrylamide gels (Biorad) with 1.0 mm spacer plates according to manufacturer recommendations. SDS-PAGE was performed in TGS running buffer (25 mM Tris pH 8.3, 192mM glycine, 0.1% SDS) and proteins were transferred on PVDF membrane 0.2mm (Biorad) using Trans-Blot Turbo system (Biorad) according to manufacturer recommendations. PVDF membranes were incubated for 1h in TBST (50mM Tris-HCl pH 7.5, 150mM NaCl, 0.1% Tween20) solution containing 5% Skimmed-Milk followerd by antibody incubation in TBST 5% Milk for 1h at RT or over-night at 4°C. Membranes were washed 3 times in TBST for 5min and 1 time in TBS for 5min. HRP chemiluminescence was detected using Amersham™ ECL Select™ detection reagent and images were taken using a CCD camera.

Electromobility Shift Assay

For EMSA assays, complementary DNA oligos were synthesized by EuroFins Genomics with ATTO565 dye linked to the 5' end of minus strand for probes. To generate double stranded probes, complementary oligos were incubated at 2µM in annealing buffer (25mM HEPES-KOH pH 7.8, 40mM KCl) at 70°C for 5min and cool down to room temperature.

EMSA reactions were performed in 20µL reaction buffer (25 mM HEPES-KOH pH 7.8, 40 mM KCl, 1 mM DTT, 10% Glycerol) using 1µg purified MBP-NAC53/78 and 50ng DNA probe for 30min at 25°C. Reactions were subjected to native polyacrylamide migration with TGX FastCast 7.5% Acrylamide gels (Biorad) in TAE (Tris-base 40 mM pH 8.3, 20mM acetic acid, 1mM EDTA). After migration, probes were imaged using a Typhoon FLA 9000 Gel Scanner.

Luciferase reporter assay in Protoplasts

For promoter activity analysis, *Arabidopsis* mesophyll protoplasts were generated adapted from Yoo et al., 2007. Leaves from adult plants were cut into strips (0.5mm) and incubated in the Maceroenzyme R-10 (Duchefa M8002) and Cellulase Onozuka R-10 (Duchefa C8001) solution for 3h. Solution was subsequently filtered through 3 layers of miracloth paper (Merck 475855-1R) in a 50mL centrifuge tube. Protoplast suspension was centrifuged for 1min at 200g at 4°C and supernatant was carefully removed from the protoplast pellet. Pellet was washed twice with W5 buffer (Yoo et al., 2007) in ice. Protoplasts were resuspended in MMG buffer (Yoo et al., 2007), 200µL dispatched in 2mL microcentrifuge tube and 5µg of each plasmid were transfected by addition of 220µL 30% PEG4000 (Sigma-Aldrich 81240) solution for 15min. 880µL of W5 was added to stop the reaction followed by 1min centrifugation at 200g. Supernatant was removed and transfected protoplast pellet were resuspended in 250µL WI

buffer (Yoo et al., 2007). Tubes were left over night in dark for construct expression prior to measurements.

Luciferase quantification was performed according to Dual-Luciferase® Reporter Assay System from Promega recommendation (see link). Protoplast expressing the desired contructs were centrifuged for 15sec at max speed. Supernatant was removed and protoplast pellet was resuspended in 100µl of 1X passive lysis buffer (see link). The lysed protoplast suspension was transferred into a white 96-well plate (Thermo Scientific™ Nunc™ MicroWell™). Measurement of Firefly Luciferase (FfLuc, reporter constructs) was performed by adding 40µl LARII reagent (see link) and luminescence was measured using a plate reader (Berthold Tristar LB 940). Measurement of Renilla Luciferase (RnLuc, internal control) was performed adding 40µl of Stop & Glo® (see link) and luminescence was measured. Due to an apparent cross-talk between NAC53/78ΔTM expression and the *prom35S*::*RnLuc* constructs (see AtNAM DBD and 35S promoter interaction, (Duval et al., 2002); the results showed Figure S5 are based on the FfLuc luminescence only.

QUANTIFICATION AND STATISTICAL ANALYSIS

For all statistical analysis, R programming language was used in the Rstudio environment.

For non-omics data, the statistical test and associated p value threshold for each analysis are indicated in the figure legends. Data dispersion, medians and quantiles are represented with boxplots and replicates displayed in every figures. For bar plots in Figure S2, number of replicates are indicated in the figure legend, error bars represent the standard deviation from the mean.

RNA sequencing

For *rpt2a-2 Pma* transcriptome, sequencing was performed by ATLAS Biolabs, Berlin. For *nac53-1 78-1 Pst* transcriptome, sequencing was performed by the NGS Competence Center, Tübingen. After quality control, reads were mapped to the *A. thaliana* TAIR10 reference genome. The mapped reads were counted with *htseq-count* for subsequent analysis. Log2FC and false discovery rate (FDR) were determined using R package DEseq2 (Love et al., 2014) with default settings. A gene is considered significantly differentially expressed when its FDR < 0.05. Log2FC threshold is indicated in the figure legends according to the analysis.

IP-MS/MS analysis

For IP-MS/MS analysis in Figure 2 and Figure S2, Log2FC and false discovery rate (FDR) for each protein group were determined using R package IPinquiry4 (Kuhn et al., 2023). For GFP-NAC53/78 mock conditions, free-GFP mock was used as control; for GFP-NAC53/78 *Pst* conditions, free-GFP *Pst* was used as control; for CFP-NAC53/78-RFP N-ter conditions, free-GFP was used as control; for CFP-NAC53/78-RFP C-ter conditions, mCherry-HDEL was used as control. For downstream analysis, to each protein group a unique Agi-code was assigned by blasting every *N. benthamiana* protein present in the protein group and taking the most frequent Agi-code with the best E-value. An e-value threshold of e-10 was used, in case of absence of *A. thaliana* the protein group was not considered for downstream analysis. For heatmap representation in Figure S1H-K, in case multiple protein groups correspond to the same *A. thaliana* orthologs the mean Log2FC is represented.

Meta-Transcriptomic analysis

For meta-transcriptomic analysis in Figure 6 and FigureS6, fragments per kilobase per million counts were retrieved from the data base (http://ipf.sustech.edu.cn/pub/athrna/). Log2FC for individual genes in every project was calculated based on the control RNAseq libraries as annotated in the original publication (Zhang et al., 2020). Filtering of relevant projects for subsequent correlation analysis was done based on the median |Log2FC|. Median|Log2FC| > 0.5 was used for identification of projects with at least one gene cluster transcriptionally impacted (see Table S3, related to Figure 6H) and median |Log2FC| > 0.3219 was used for identification of projects in which 26S proteasome and PhANGs clusters were co-transcriptionally impacted (see Table S3, related to Figure S6G). Pearson correlations were calculated using base R function. Only correlations with p-value < 0.05 were considered significant and used for calculation of mean/median.

Omics downstream analysis: Gene ontology, Protein Network, subcellular enrichment & cis-element analysis

For Gene Ontology enrichment, the list of Agi-code was uploaded into ShinyGO software (http://bioinformatics.sdstate.edu/go/, (Ge et al., 2020). Cladogram of the indicated number of top terms for the indicated type of terms was used for graphical representation. Table of annotations was extracted for further analysis.

For network creation, list of Agi-code was provided to the string database (https://string-db.org/). Table of interactions was extracted and uploaded to cytoscape software (https://cytoscape.org/) for network generation, design, and annotation. For purposes of clarity,

network nodes were manually arranged. Edge transparency relate to the strength of interaction with opaque edges corresponding to strong interactions and transparent edges to weak interactions. Node color corresponds to manual annotation inferred based on GO annotations and further curated from the literature.

For subcellular compartment enrichment, the list of Agi-code was uploaded into SUBA5db (https://suba.live/). Compartment annotation was extracted, and occurrence of every compartment was counted to estimate the list distribution. For theorical distribution 20 Agi-code lists of the same length were randomly generated and processed similarly. The mean distribution of the 20 lists was used as theorical distribution. Enrichment for every compartment was calculated as a Log2FC of the ratio between the observed proportion and the theorical one.

Cis-Regulatory Element analysis

For cis-regulatory element analysis, promoter sequences of 1000bp upstream of the transcription starting site were retrieved from plant ensembl database using biomart browser (https://plants.ensembl.org/biomart/). For identification of novel cis-regulatory elements in Figure 5A, promoter sequences of the several gene clusters were analyzed using the STREME software (https://meme-suite.org/meme/tools/streme) with default settings. For mapping and counting in Figure S5B and S5C, promoter sequences were analyzed in R using regular expression matching for “tgggc” or “gccca” pattern.

Immunoblot semi-quantitative analysis

Quantification of protein abundance based on immunoblot signals (related to Figure 4D and 5G) was adapted from (Gallo-Oller et al., 2018). Raw image of the immublot signals against the protein of interest and the corresponding loading control were processed using Fiji software (https://imagej.net/software/fiji/downloads). Image was converted to 8-bit format. A duplicated image was used to generate a background image using the function “Substract Background” with a ball radius value of 50 pixels and the option “create background (don’t substract) activated. The resulting background was then subtracted from the original 8-bit image with the function “Image Calculator”. Individual lanes were quantified by measurement of the peak area after circumscription with the rectangular ROI selection and “Gels” function. The obtained values for individual bands were normalized by the corresponding loading control values. For calculation of Log2FC in abundance, quantification of bands in infected sample were divided by the corresponding mock sample quantification of the same genotype; the obtained ratio was next transformed using Log2 function.

Confocal microscopy imaging

Confocal microscopy was done using an inverted Zeiss LSM 880 microscope, an upright Leica SP8 microscope or an inverted Leica Stellaris 8 microscope. For mCerrulean3 imaging, excitation was done using a 458nm laser and emission signal was measured from 465nm to 500nm; for eGFP or sGFP imaging, excitation was done using a 488nm laser and emission signal was measured from 510nm to 540nm; for mRFP or mCherry imaging, excitation was done using a 561nm laser and emission signal was measured from 590nm to 630nm; in addition chlorophyll auto fluorescence was measured in the far red wavelength (> 700nm). Images were acquired with a 40X water immersion objective, pinhole was set to 1 airy unit, resolution of acquisition was set to at least to 1024x1024 with a line average of 4.

After acquisition images were processed in Fiji Software. For images obtained from Leica microsystem devices, a gaussian blur (radius 0.75) was applied for a smoother rendering. For clarity purposes, contrast on the individual channels was manually adjusted.

For subcellular quantification of GFP signal (related to Figure S3), all images used were acquired on the Zeiss LSM 880 with a 16bits depth. Prior to imaging seedlings were incubated for 10min in a 10µM propidium iodide (PI) ½ MS solution followed by a brief washing in clear ½ MS. PI fluorescence was excited with the 488nm laser and measured from 590nm to 660nm. For all acquisitions within an experimental repetition the laser power and gain for the GFP channel was kept constant. For segmentation, images were processed in Fiji Software. Each cell was segmented using the polygon ROI selection tool. Each nucleus was segmented in the same order using the oval ROI selection tool. Next, mean intensity and integrated density of the whole cell, the nucleus, and the whole cell after removal of nucleus ROI (considered as cytosolic ROI) was measured. Signal proportion in the nucleus was quantified by the ratio between integrated density of nucleus ROI by whole cell ROI and ratio of signal between nucleus and cytosol was calculated by the ratio between nucleus ROI mean intensity and cytosolic ROI mean intensity.

For calculation of co-localization index in Figure 2C, the image J plugin “co-localization finder” was used and calculated pearson index is provided in the Figure. For calculation in Figure 3C, plot profile of GFP and RFP signals was extracted at the indicated line using Fiji software and the pearson index indicated on the Figure was calculated between the two profile values on R.

RESOURCE AVALAIBILITY

Source code of R and Python3 scripts used for the several computational analysis done in this study will be put available on https://github.com/Gogz31 or can be directly requested.

DATA AVAILABILITY

The mass spectrometry data from this publication will be made available on the PRIDE archive (https://www.ebi.ac.uk/pride/archive/) and with the identifier (PXDXXXXX; and (PXDXXXX). All relevant proteomics data are made available in the supplemental information.

SUPPORTING INFORMATION

Figure S1. Deciphering the details of NAC53/78 interactome. Related to Figure 2.
Figure S2. NAC53/78 are subjected to high level of poly-ubiquitination. Related to Figure 3.
Figure S3. NAC53/78 association with CDC48 is required for their nuclear translocation. Related to Figure 3.
Figure S4. Transcriptional analysis of proteotoxic stress reveals a trade-off between 26S proteasome and other biological process. Related to Figure 4.
Figure S5. Characterization of the NAC53/78-PRCE module in PhANGs promoters. Related to Figure 5.
Figure S6. The proteasome autoregulatory feedback loop transcriptional signature is a systemic response to environmental cues. Related to Figure 6.
Table S1. Spectral count enrichment of the protein groups identified in NAC53/78 common interactome. Related to Figure 2.
Table S2. Enrichment of mRNA of 538 DEGs in *nac53-1 78-1* Pst, overlapping with *rpt2a-2* Pma and/or MG132 24h data sets. Related to Figure 4.
Table S3. List of the several RNAseq projects identified in study in which 26S proteasome and/or PhANGs are differentially regulated. Related to Figure 6.

FIGURE LEGENDS

Figure 1. NAC53/78 are central integrators of various proteotoxic stress conditions.
(A) The role of the 26S Proteasome in degradation of proteins from distinct subcellular compartments. Prime site of action of the several treatments used in this study: Blunt head arrows indicate enzymatic activity suppression; pointed head arrows indicate trigger of substrate accumulation.
(B) Fresh weight of seedlings grown under the indicated treatments at 10-14 day after germination (dag). Fresh weight is expressed as a percentage of Col-0 mock conditions. Boxplots colors refer to the genotype. Statistical significance is assessed by a Wilcoxon-Mann-Whitney test (p values: n.s. > 0.05; * < 0.05; ** < 0.01). Every treatment has been repeated at least twice with similar results.
(C) Bacterial density in Log10 Colony-Forming-Unit (CFU) per leaf cm^2. Statistical significance is assessed by a Wilcoxon-Mann-Whitney test (p values: n.s. > 0.05; ** < 0.01). Boxplots colors refer to the genotype as in panel B. The treatment has been repeated three times with consistent results.
(B-C) Representative phenotypic pictures of Col-0 and *nac53-1 78-1* plants under several treatments are included.
Figure 2. NAC53/78 are part of an autoregulatory proteasome feedback loop.

(A) Confocal microscopy pictures of roots of GFP-NAC53/78 *Arabidopsis thaliana* transgenics at 7dag exposed to mock or BTZ 10µM treatment for 3h. Treatments were repeated at least three times with similar observations.
(B) Immunoblot analysis against GFP on crude extract of seedlings related to panel A. Ponceau staining is used as loading control.
(C) Confocal microscopy pictures of transiently co-expressed sTag-NAC53/78 with prom35S::RFP-HDEL or together in *N. benthamiana* epidermis cells. Pearson index (ρ) represents co-localization index. Scale bars = 10µm
(D) Confocal microscopy pictures of transiently co-expressed sTag-NAC53/78 together or dTag-NAC53/78 alone in *N. benthamiana* epidermis cells. Scale bars = 10µm
(E) Bar plots representing the number of significantly enriched proteins in the 4 IP-MS/MS conditions for NAC53 only, NAC78 only and NAC53+NAC78 (Common).
(F) Cladogram of top 30 gene ontology (GO) terms for biological process (BP) enriched in the list of *A. thaliana* ortholog proteins found from NAC53/78 common interactome.
(G) Protein network of the interacting candidates related to the GO BP terms annotated as "Transport" and "Proteolysis" in panel F.

Figure S1. Deciphering the details of NAC53/78 interactome. Related to Figure 2

(A) Chimeric NAC53/78 constructs generated in this study. Upstream promoter, fluorescent tag and protein domain of interests are represented.
(B) Immunoblot against GFP on crude extracts of *N. benthamiana* leaves transiently expressing sTag-NACs in addition to mock or 6h BTZ (10µM) treatment. Ponceau staining is used as loading control.
(C) Immunoblot against GFP or RFP on crude extracts of *N. benthamiana* leaves transiently expressing dTag-NACs in addition to mock or BTZ 10µM for 6h. Ponceau staining is used as loading control.
(D) Immunoblot against GFP after immunoprecipitation (IP) with anti-GFP agarose beads on *N. benthamiana* leaf extracts transiently expressing sTag-NACs after mock or *PstΔHopQ* infection for 8h. The same samples were used for subsequent MS/MS analysis.
(E) Immunoblot against GFP or RFP after IP with anti-GFP or anti-RFP agarose beads on *N. benthamiana* leaf extracts transiently expressing dTag-NACs. The same samples were used for subsequent MS/MS analysis.
(F) Cladogram of top 30 GO terms for cellular components enriched in the list of *A. thaliana* ortholog proteins found in NAC53/78 common interactome.
(G) Subcellular compartments enrichment in the list of *A. thaliana* proteins from NAC53/78 common interactome based on their SUBA5db annotation. Statistical significance is provided through a chi-square testing.
(H-K) Heatmap representing the peptide enrichment (Log2FC) of the protein clusters from the network Figure 2G.

Figure 3. ER-Anchored Protein Sorting (ERAPS) coordinates the subcellular fate of NAC53 & NAC78.

(A) Confocal microscopy pictures of GFP-NAC53/78 expressing *A. thaliana* roots. 7 dag seedlings were exposed to mock treatment, BTZ 10µM, CB-5083 10µM or LS-102 100µM for 3h. The treatments were repeated at least three times with similar observations. Scale bars = 10µm
(B) Immunoblot against GFP on crude extracts of GFP-NAC53/78 *A. thaliana* adult plants infiltrated with mock treatment, BTZ 10µM, CB-5083 10µM or LS-102 100µM for 6h. Ponceau staining is used as loading control.
(C) Confocal microscopy pictures of *N. benthamiana* transiently co-expressing GFP-NAC53/78 full-length (FL) or deleted for the transmembrane domain (ΔTM) with RFP-HRD1a or RFP-HRD1b. Pearson index (ρ) indicates correlation index at the orange lines.

(D) Co-IP of RFP-HRD1a/b with GFP-NAC53/78. IP was performed with anti-GFP beads. GFP-HDEL and free-GFP were used as negative control. The experiment was repeated twice with similar results.
(E) Immunoblot against GFP on crude extract of *N. benthamiana* leaves transiently expressing GFP-NAC53/78FL or ΔTM. Ponceau was used as loading control. Boxplots represent the relative ΔTM abundance compared FL.
(F) *In vitro* trans-ubiquitination assays of GST-HRD1a/b against MBP-NAC53/78. Removal of E1 and ATP from the reaction was used as negative control. The experiment was repeated twice with similar results.
(G) Representation of the ER-Anchored Protein Sorting (ERAPS) mechanism. NAC53/78 are ER-anchored proteins recognized and ubiquitinated by the HRD1 complex. The CDC48 complex subsequently extracts NAC53/78 from the ER to mediate ER-Associated Degradation or allowing nuclear translocation in the context of proteasomal stress to mitigate proteotoxicity.

Figure S2. NAC53/78 are subjected to high level of poly-ubiquitination. Related to Figure 3.

(A) *In vitro* analysis of LS-102 effect on HRD1a/b ubiquitination activity. Removal of E1 and ATP from the reaction was used as negative control.
(B) Quantification of the inhibitory effect of LS-102 (100µM) on HRD1 activity. Bar plots represent the mean of three independent replicates with error bars representing the standard deviation.
(C) Heatmaps representing the mean Log10 intensity of peptides bearing a di-glycine mark on the indicated lysin residue identified by MS/MS analysis of *in vitro* trans-ubiquitination reactions (see Figure 3F).
(D) Heatmaps representing the mean Log10 intensity of peptides bearing a di-glycine mark on the indicated lysin residue identified by MS/MS analysis of IP samples generated for Figure 2.
(E) Alignments of NAC53 and NAC78 peptide sequence regions around the identified lysin residues in panel C and D. Colors represent the residue conservation (green: conserved, shade of red: not conserved). All the identified lysins in one protein are conserved in the other. Underlined residues correspond to the mutated residues generated for the panel H and I.
(F) *In vitro* trans-ubiquitination assays of GST-HRD1a/b against MBP-NAC53/78 in the presence of LS-102 inhibitor. Removal of E1 and ATP from the reaction was used as negative control.
(G) Immunoblot analysis of *N. benthamiana* transiently expressing free-GFP, RFP-HDEL or dTag-NAC53/78 subjected to IP with anti-ubiquitin beads. The experiment was repeated twice with similar results.
(H) Immunoblot analysis of *N. benthamiana* transiently expressing GFP-NAC53/78 mutated for 5 lysins (Mut., see panel E) or not (WT) subjected to IP with anti- ubiquitin beads.
(I) Quantification of the relative ubiquitination levels assessed by the ratio between GFP signal and ubiquitin signal after IP as in panel H. Barplots represent the mean ratio of two replicates, normalized to the ratio of WT constructs with error bars representing the standard deviation.

Figure S3. NAC53/78 association with CDC48 is required for their nuclear translocation. Related to Figure 3.

(A) Confocal microscopy pictures of transgenic GFP-NAC53/78 root seedlings exposed to BTZ 10µM, BTZ 20µM, CB-5083 10µM or CB-5083 20µM for 3h. Scale bars = 10µm
(B) Confocal microscopy pictures of *N. benthamiana* leaves transiently co-expressing AtCDC48c-GFP with RFP-NAC53/78. Co-localization is visible in aggregate-like structures. Scale bars = 1µm
(C) Confocal microscopy representative pictures (used for panel D-E) of transgenic GFP-NAC53/78 roots treated with BTZ 10µM and CB-5083 10µM followed by Propidium Iodide staining. Scale bars = 10µm

(D-F) Boxplot representing the GFP signal quantification after confocal microscopy imaging of transgenic GFP-NAC53/78 roots exposed to BTZ 10µM or CB-5083 10µM. Black dots represent one cell. Statistical difference is assessed by a Wilcoxon-Mann-Whitney test.

Figure 4. The transcriptional landscape of proteotoxic stress

(A) Log2FC mRNA levels of *NAC53* and *NAC78* transcripts after *Pst* infection of adult Col-0 plant leaves. The heatmap represent the mean of 4 biological replicates.

(B) Log2FC mRNA levels of 26S proteasome transcripts after *Pst* infection of Col-0 or *nac53-1 78-1* adult plant leaves. The heatmap represent the mean of 4 biological replicates. The experiment has been repeated 3 times with consistent results.

(C) Immunoblot against multiple 26S proteasome subunits on crude extracts of Col-0 or *nac53-1 78-1* adult plant leaves inoculated with *Pst* or mock solutions for 24h. Ponceau staining is used as loading control.

(D) Relative Log2FC abundance of representative 26S proteasome subunits in Col-0 or *nac53-1 78-1* adult plant leaves. The abundance is calculated relative to the mock conditions. Statistical differences are assessed via a Welch t.test (p values: n.s > 0.05, * < 0.05, ** < 0.01).

(E) Immunoblot against GFP on crude extract of *N. benthamiana* leaves transiently expressing GFP-NAC53/78 after mock treatment or *PstΔHopQ* infection for 8h. Ponceau staining is used as loading control.

(F) Immunoblot against GFP on extract of adult *A. thaliana* transgenics GFP-NAC53/78 subjected to mock treatment or *Pst* infection 8h by vacuum infiltration followed by IP with anti-GFP beads.

(G) Number of differentially expressed genes (DEGs) in the different conditions of the *nac53-1 78-1 Pst* RNAseq analysis. Total number of DEGs per condition is indicated. Colors indicate the proportion of DEGs up-regulated and down-regulated. DEGs are considered when |Log2FC| > 1.5. Genot. mock: *nac53-1 78-1* mock vs. Col-0 mock; WT *Pst*: Col-0 *Pst* vs. Col-0 mock; Mut. *Pst*: *nac53-1 78-1 Pst* vs. *nac53-1 78-1* mock; Genot. *Pst*: *nac53-1 78-1 Pst* vs. Col-0 *Pst*.

(H) Level of differential expression (Log2FC) of the 945 DEGs found in Genot. *Pst* (see panel G) for the several conditions analyzed.

(I) Cladogram of top 40 GO terms for BP enriched in the list of 945 DEGs. Colors represent broad GO clusters.

(J) Venn diagram representing the overlap between the 945 DEGs and DEGs from *rpt2a-2 Pma* (|Log2FC| > 0.5) or Col-0 MG132 24h (|Log2FC| > 0.5).

(K) Cladogram of top 30 GO terms for BP enriched in the list of 538 DEGs extracted from the combined analysis (panel J). For conciseness terms are hidden and grouped in 4 processes.

(L) Protein network of the genes from the 945 DEGs list related to the GO BP terms from panel K. Node colors refers to the 4 GO clusters from panel K.

Figure S4. Transcriptional analysis of proteotoxic stress reveals a trade-off between 26S proteasome and other biological process. Related to Figure 4

(A) mRNA level Log2FC of all 26S proteasome genes and associated interactors/chaperones in several conditions of the *nac53-1 78-1 Pst* RNAseq.

(B) Number of differentially expressed genes (DEGs) in the different conditions of the *nac53-1 78-1 Pst* RNAseq analysis. Total number of DEGs per condition is indicated. Colors indicate the proportion of DEGs up-regulated and down-regulated. DEGs are considered when |Log2FC| > 1.5. Genot. mock: *rpt2a-2* mock vs. Col-0 mock; WT *Pma*: Col-0 *Pma* vs. Col-0 mock; Mut. *Pma*: *rpt2a-2 Pma* vs. *nac53-1 78-1* mock; Genot. *Pma*: *rpt2a-2 Pma* vs. Col-0 *Pma*.

(C) mRNA levels Log2FC of the 981 DEGs found in Genot. *Pma* (see panel D) for the several conditions analyzed.

(D) mRNA level Log2FC of all 26S proteasome genes and associated interactors/chaperones in the several conditions of the *rpt2a-2 Pma* RNAseq.

(E) Cladogram of top 40 GO terms for BP enriched in the list of 945 DEGs. Colors represent the broad GO clusters.

(F) mRNA level Log2FC of the genes present in the 4 network modules from Figure 4L in the 3 Transcriptome used.

Figure 5. NAC53 and NAC78 coordinate the regulation of proteasome and photosynthesis gene expression through the same cis-element.

(A) Top 3 motifs found by STREME software in the promoter regions from the 4 network clusters (Figure 4L). PRCE-like elements from proteasome and PhANGs clusters are highlighted.

(B) 25bp region comprising the PRCE-like elements from LHCa3 and PSAD1 promoters used in this figure. The region corresponds to the probe sequence used in panel C and D. The PRCE is highlighted in red.

(C) Electro-Mobility Shift Assay (EMSA) of MBP-NAC53/78 with LHCa3/PSAD1 probes (see panel B). As a negative control, probes were incubated without MBP-NAC53/78 (-) or with MBP-NAC53/78 deleted for their DNA recognition motif (ΔRM). Experiment was repeated twice with similar results.

(D) EMSA competition assay of MBP-NAC53/78 association with LHCa3/PSAD1 probes. Competitor is applied at a concentration gradient (25X, 50X, 75X and 100X) indicated by the shade of grey. WT and mutated competitors are labelled TGGGC and AAAAA, respectively. Experiment was repeated twice with similar results.

(E) Boxplot representing association of GFP-NAC53/78 with LHCa3/PSAD1 PRCE in adult *A. thaliana* transgenics lines infected with *Pst* or mock for 8h after Chromatin Immunoprecipitation. The association is quantified as % of input and amplification of a region in the CDS is used as negative control.

(F) Immunoblot against mature PhANGs proteins in Col-0 or *nac53-1 78-1* adult plant leaves inoculated with *Pst* or mock solutions for 24h. Ponceau staining is used as loading control.

(G) Relative Log2FC abundance of PhANGs mature proteins immunoblotted in panel F. The abundance is calculated relative to the mock conditions. Statistical differences are assessed via a Welch t.test (p values: n.s > 0.05, * < 0.05, ** < 0.01).

(H) Photosystem II (PSII) activity measurement on Col-0 or *nac53-1 78-1* adult plants inoculated with *Pst* or mock solutions for 24h. Letters indicate the statistical group assessed by pairwise Welch t.test (p value < 0.05). The experiment was repeated 3 times with consistent results.

(I) Representative pictures of measurements from panel I. Fv/Fm values are represented by false color as indicated by the color gradient legend.

(J) Total chlorophylls and carotenoids from Col-0 or *nac53-1 78-1* adult plant leaves inoculated with *Pst* or mock solutions for 24h. Letters indicate the statistical group assessed by pairwise Wilcoxon-Mann-Whitney test (p value < 0.05). The experiment was repeated 3 times with consistent results.

Figure S5. Characterization of the NAC53/78-PRCE module in PhANGs promoters. Related to Figure 5.

(A) mRNA level Log2FC of the PhANGs clusters from Figure 4L in the 3 transcriptomes used. Genes are separated based on their associated process in the photosynthetic pathway.

(B) Mapping of the PRCE-like motifs in PhANGs promoter regions from panel A. Promoter regions are organized according to the order of the genes from panel A. Purple marks represent the position of the motifs based on their distance from the transcription starting site (TSS). The two red arrows highlight LHCa3 and PSAD1 promoter regions.

(C) Histograms representing the number of occurrences of the PRCE-like motifs across the 4 genes cluster from the network Figure 4L. Each bar represents a 20bp region, frequency *f* of promoters bearing at least one motif is indicated as a percentage.

(D) LHCa3/PSAD1 promoter activity measured by luminescence in Col-0 or *nac53-1 78-1* protoplasts extract transiently co-expressing LHCa3/PSAD1 reporter constructs and NAC53/78ΔTM. Log2FC is calculated from the luminescence level of protoplasts expressing

the reporter construct alone. Replicates are a pool of at least two independent experiments. Letters indicate the statistical group assessed by pairwise Wilcoxon-Mann-Whitney test (p value < 0.05).
(E) Promoter activity as calculated in panel D for LHCa3/PSAD1 promoters deleted for their respective DNA regions from Figure 5B. Replicates are a pool of at least two independent experiments. Letters indicate the statistical group assessed by pairwise Wilcoxon-Mann-Whitney test (p value < 0.05).
(F-G) Boxplot representing the Log2FC mRNA level the indicated transcripts in Col-0, GFP-NAC53 or GFP-NAC78 seedlings treated with BTZ 10µM or mock solutions for 6h. Log2FC is calculated from Col-0 mock. Letters indicate the statistical group assessed by pairwise Wilcoxon-Mann-Whitney test (p value < 0.05).
(H) Fresh weight of seedlings from indicated genotypes grown under the indicated treatments at 10 days after germination. Letters indicate the statistical group assessed by pairwise Wilcoxon-Mann-Whitney test (p value < 0.05). Experiment was repeated 3 times with consistent results.
(I) Representative phenotypic pictures related to panel D.

Figure 6. The proteasome autoregulatory feedback loop monitors photosynthesis homeostasis during stress responses

(A) Photosynthetic pigment content from Col-0 or *nac53-1 78-1* adult plant leaves infiltrated with Lin 200µM, BTZ 2µM or mock solutions for 24h. Content is expressed in percentage relative to Col-0 mock. Letters indicate the statistical group assessed by pairwise Wilcoxon-Mann-Whitney test (p value < 0.05). The experiment was repeated 3 times with consistent results.
(B) Log2FC mRNA level of the indicated transcripts in Col-0, *nac53-1 78-1* adult plants leaves Lin 200µM, BTZ 2µM or mock solutions for 24h. Log2FC is calculated from Col-0 mock and *PDH1* is used as negative control. Statistical differences are assessed with a Welch t-test (p values: n.s. > 0.05, * < 0.05, ** < 0.01). The experiment was repeated twice with consistent results.
(C) Fresh weight of seedlings grown under the indicated treatments at 10-14 day after germination. The fresh weight is represented as a percentage of Col-0 mock conditions. Letters indicate the statistical groups assessed by pairwise Wilcoxon-Mann-Whitney test (p value < 0.05). Every treatment has been repeated at least twice with consistent results. Representative phenotypic pictures are included.
(D) Bacterial density shown as Log10 Colony-Forming-Unit (CFU) per leaf cm² in Col-0 and *hrd1a hrd1b* plants. Statistical significance is assessed by a Welch t-test (p values: * < 0.05). The experiment has been repeated three times with consistent results.
(E) Correlation heatmap of the 54 26S proteasome subunit genes and the expression of 68 PhANGs from publicly available 1223 RNAseq libraries identified in this study.

Figure S6. The proteasome autoregulatory feedback loop transcriptional signature is a systemic response to environmental cues. Related to Figure 6.

(A) PSII activity measurement on Col-0 and *nac53-1 78-1* treated as indicated in Figure 6A. Replicates are a pool of 3 independent experiments. Letters indicate the statistical group assessed by pairwise Wilcoxon-Mann-Whitney test (p value < 0.05).
(B) PSII activity measurement on Col-0 and *hrd1a hrd1b* adult plant leaves inoculated with *Pst* or mock solutions for 24h. Letters indicate the statistical group assessed by pairwise Welch t.test (p value < 0.05). The experiment was repeated 2 times with consistent results.
(C) Confocal microscopy pictures of transgenic GFP-NAC53/78 *A. thaliana* roots exposed to mock treatment, MV 100µM, GDA 100µM and Lin 100µM for 2h. The treatments were repeated at least three times with similar observations. Scale bars = 10µm
(D) Density functions of the 54 26S proteasome genes and 68 PhANGs transcripts (Log2FC) in the different transcriptome projects. Log2FC limits are -10 to +10. Treatment types and

relevant condition information are provided in the figure. Plots are separated by treatment groups and subdivided by experiments.

Figure 7. ER-anchored protein sorting (ERAPS) controls the fate of two proteasome activators for intracellular organelle communication during proteotoxic stress.

In steady state conditions, the ER-anchored protein sorting system (ERAPS) promotes the constitutive degradation of NAC53/78 via the 26S proteasome. Meanwhile, PhANGs expression is activated and subsequent chloroplastic import permits the maintenance of active photosynthesis. Upon proteotoxic stress, the chloroplast import machinery is targeted for proteasomal degradation. This leads to an accumulation of PhANGs precursors which are therefore subjected to proteasomal degradation, inducing proteotoxicity. Thus, to avoid proteotoxicity, the ERAPS system facilitates the nuclear translocation of NAC53/78, to activate the production of a new proteasome complex and to repress PhANGs expression to mitigate substrate accumulation.

REFERENCES

Albert, S., Wietrzynski, W., Lee, C.W., Schaffer, M., Beck, F., Schuller, J.M., Salome, P.A., Plitzko, J.M., Baumeister, W., and Engel, B.D. (2020). Direct visualization of degradation microcompartments at the ER membrane. Proc Natl Acad Sci U S A *117*, 1069-1080.

Baird, L., Tsujita, T., Kobayashi, E.H., Funayama, R., Nagashima, T., Nakayama, K., and Yamamoto, M. (2017). A Homeostatic Shift Facilitates Endoplasmic Reticulum Proteostasis through Transcriptional Integration of Proteostatic Stress Response Pathways. Mol Cell Biol *37*.

Binder, A., Lambert, J., Morbitzer, R., Popp, C., Ott, T., Lahaye, T., and Parniske, M. (2014). A modular plasmid assembly kit for multigene expression, gene silencing and silencing rescue in plants. PLoS One *9*, e88218.

Boos, F., Kramer, L., Groh, C., Jung, F., Haberkant, P., Stein, F., Wollweber, F., Gackstatter, A., Zoller, E., van der Laan, M.*, et al.* (2019). Mitochondrial protein-induced stress triggers a global adaptive transcriptional programme. Nat Cell Biol *21*, 442-451.

Bragoszewski, P., Turek, M., and Chacinska, A. (2017). Control of mitochondrial biogenesis and function by the ubiquitin-proteasome system. Open Biol *7*.

Chen, Q., Zhong, Y., Wu, Y., Liu, L., Wang, P., Liu, R., Cui, F., Li, Q., Yang, X., Fang, S.*, et al.* (2016). HRD1-mediated ERAD tuning of ER-bound E2 is conserved between plants and mammals. Nat Plants *2*, 16094.

Christianson, J.C., and Ye, Y. (2014). Cleaning up in the endoplasmic reticulum: ubiquitin in charge. Nat Struct Mol Biol *21*, 325-335.

Clough, S.J., and Bent, A.F. (1998). Floral dip: a simplified method for Agrobacterium-mediated transformation of Arabidopsis thaliana. Plant J *16*, 735-743.

Colberg, L., Cammann, C., Greinacher, A., and Seifert, U. (2020). Structure and function of the ubiquitin-proteasome system in platelets. J Thromb Haemost *18*, 771-780.

Diaz-Tielas, C., Grana, E., Sanchez-Moreiras, A.M., Reigosa, M.J., Vaughn, J.N., Pan, Z., Bajsa-Hirschel, J., Duke, M.V., and Duke, S.O. (2019). Transcriptome responses to the natural phytotoxin t-chalcone in Arabidopsis thaliana L. Pest Manag Sci *75*, 2490-2504.

Duval, M., Hsieh, T.-F., Kim, S.Y., and Thomas, T.L. (2002). Molecular characterization of AtNAM: a member of theArabidopsis NAC domain superfamily. Plant Molecular Biology *50*, 237-248.

Farmer, L.M., Book, A.J., Lee, K.H., Lin, Y.L., Fu, H., and Vierstra, R.D. (2010). The RAD23 family provides an essential connection between the 26S proteasome and ubiquitylated proteins in Arabidopsis. Plant Cell *22*, 124-142.

Fonseca, D., and Carvalho, P. (2019). EGAD! There is an ERAD doppelganger in the Golgi. EMBO J *38*, e102679.

Gallo-Oller, G., Ordoñez, R., and Dotor, J. (2018). A new background subtraction method for Western blot densitometry band quantification through image analysis software. Journal of Immunological Methods *457*, 1-5.
Ge, S.X., Jung, D., and Yao, R. (2020). ShinyGO: a graphical gene-set enrichment tool for animals and plants. Bioinformatics *36*, 2628-2629.
Gladman, N.P., Marshall, R.S., Lee, K.H., and Vierstra, R.D. (2016). The Proteasome Stress Regulon Is Controlled by a Pair of NAC Transcription Factors in Arabidopsis. Plant Cell *28*, 1279-1296.
Grimmer, J., Helm, S., Dobritzsch, D., Hause, G., Shema, G., Zahedi, R.P., and Baginsky, S. (2020). Mild proteasomal stress improves photosynthetic performance in Arabidopsis chloroplasts. Nat Commun *11*, 1662.
Gureev, A.P., Shaforostova, E.A., and Popov, V.N. (2019). Regulation of Mitochondrial Biogenesis as a Way for Active Longevity: Interaction Between the Nrf2 and PGC-1alpha Signaling Pathways. Front Genet *10*, 435.
Hao, Y.J., Song, Q.X., Chen, H.W., Zou, H.F., Wei, W., Kang, X.S., Ma, B., Zhang, W.K., Zhang, J.S., and Chen, S.Y. (2010). Plant NAC-type transcription factor proteins contain a NARD domain for repression of transcriptional activation. Planta *232*, 1033-1043.
Hristou, A., Grimmer, J., and Baginsky, S. (2020). The Secret Life of Chloroplast Precursor Proteins in the Cytosol. Mol Plant *13*, 1111-1113.
Hu, X., Zou, R., Zhang, Z., Ji, J., Li, J., Huo, X.-Y., Liu, D., Ge, M.-X., Cui, M.-K., Wu, M.-Z., *et al.* (2023). UBE4A catalyzes NRF1 ubiquitination and facilitates DDI2-mediated NRF1 cleavage. Biochimica et Biophysica Acta (BBA) - Gene Regulatory Mechanisms *1866*, 194937.
Jayaraj, G.G., Hipp, M.S., and Hartl, F.U. (2020). Functional Modules of the Proteostasis Network. Cold Spring Harb Perspect Biol *12*.
Kacprzak, S.M., Mochizuki, N., Naranjo, B., Xu, D., Leister, D., Kleine, T., Okamoto, H., and Terry, M.J. (2019). Plastid-to-Nucleus Retrograde Signalling during Chloroplast Biogenesis Does Not Require ABI4. Plant Physiol *179*, 18-23.
Kliza, K., Taumer, C., Pinzuti, I., Franz-Wachtel, M., Kunzelmann, S., Stieglitz, B., Macek, B., and Husnjak, K. (2017). Internally tagged ubiquitin: a tool to identify linear polyubiquitin-modified proteins by mass spectrometry. Nature Methods *14*, 504-512.
Kourelis, J., Kaschani, F., Grosse-Holz, F.M., Homma, F., Kaiser, M., and van der Hoorn, R.A.L. (2019). A homology-guided, genome-based proteome for improved proteomics in the alloploid Nicotiana benthamiana. BMC Genomics *20*, 722.
Koussevitzky, S., Nott, A., Mockler, T.C., Hong, F., Sachetto-Martins, G., Surpin, M., Lim, J., Mittler, R., and Chory, J. (2007). Signals from Chloroplasts Converge to Regulate Nuclear Gene Expression. Science *316*, 715-719.
Kramer, L., Groh, C., and Herrmann, J.M. (2021). The proteasome: friend and foe of mitochondrial biogenesis. FEBS Lett *595*, 1223-1238.
Kuhn, L., Vincent, T., Hammann, P., and Zuber, H. (2023). Exploring Protein Interactome Data with IPinquiry: Statistical Analysis and Data Visualization by Spectral Counts. In Statistical Analysis of Proteomic Data: Methods and Tools, T. Burger, ed. (New York, NY: Springer US), pp. 243-265.
Langin, G., Gonzalez-Fuente, M., and Üstün, S. (2023). The Plant Ubiquitin-Proteasome System as a Target for Microbial Manipulation. Annu Rev Phytopathol *61*, 351-375.
Langin, G., Gouguet, P., and Üstün, S. (2020). Microbial Effector Proteins - A Journey through the Proteolytic Landscape. Trends Microbiol *28*, 523-535.
Langin, G., and Üstün, S. (2023). A Pipeline to Monitor Proteasome Homeostasis in Plants. In Plant Proteostasis: Methods and Protocols, L.M. Lois, and M. Trujillo, eds. (New York, NY: Springer US), pp. 351-363.
Lee, K.H., Minami, A., Marshall, R.S., Book, A.J., Farmer, L.M., Walker, J.M., and Vierstra, R.D. (2011). The RPT2 subunit of the 26S proteasome directs complex assembly, histone

dynamics, and gametophyte and sporophyte development in Arabidopsis. Plant Cell *23*, 4298-4317.

Leister, D.S., A. (2003). From Genes to Photosynthesis in Arabidopsis thaliana. Int Rev Cytol *228*.

Leong, J.X., Raffeiner, M., Spinti, D., Langin, G., Franz-Wachtel, M., Guzman, A.R., Kim, J.G., Pandey, P., Minina, A.E., Macek, B.*, et al.* (2022). A bacterial effector counteracts host autophagy by promoting degradation of an autophagy component. Embo J *41*, e110352.

Li, J., Yuan, J., Li, Y., Sun, H., Ma, T., Huai, J., Yang, W., Zhang, W., and Lin, R. (2022). The CDC48 complex mediates ubiquitin-dependent degradation of intra-chloroplast proteins in plants. Cell Rep *39*, 110664.

Liao, P.C., Wolken, D.M.A., Serrano, E., Srivastava, P., and Pon, L.A. (2020). Mitochondria-Associated Degradation Pathway (MAD) Function beyond the Outer Membrane. Cell Rep *32*, 107902.

Lichtenthaler, H.K. (1987). [34] Chlorophylls and carotenoids: Pigments of photosynthetic biomembranes. In Methods in Enzymology (Academic Press), pp. 350-382.

Ling, Q., Broad, W., Trosch, R., Topel, M., Demiral Sert, T., Lymperopoulos, P., Baldwin, A., and Jarvis, R.P. (2019). Ubiquitin-dependent chloroplast-associated protein degradation in plants. Science *363*.

Littlejohn, G.R., Breen, S., Smirnoff, N., and Grant, M. (2021). Chloroplast immunity illuminated. New Phytol *229*, 3088-3107.

Love, M.I., Huber, W., and Anders, S. (2014). Moderated estimation of fold change and dispersion for RNA-seq data with DESeq2. Genome Biology *15*, 550.

Ma, M., and Liu, Z.L. (2010). Comparative transcriptome profiling analyses during the lag phase uncover YAP1, PDR1, PDR3, RPN4, and HSF1 as key regulatory genes in genomic adaptation to the lignocellulose derived inhibitor HMF for Saccharomyces cerevisiae. BMC Genomics *11*, 660.

Maekawa, T., Kusakabe, M., Shimoda, Y., Sato, S., Tabata, S., Murooka, Y., and Hayashi, M. (2008). Polyubiquitin Promoter-Based Binary Vectors for Overexpression and Gene Silencing in Lotus japonicus. Molecular Plant-Microbe Interactions *21*, 375-382.

Mannhaupt, G., Schnall, R., Karpov, V., Vetter, I., and Feldmann, H. (1999). Rpn4p acts as a transcription factor by binding to PACE, a nonamer box found upstream of 26S proteasomal and other genes in yeast. FEBS Letters *450*, 27-34.

Marshall, R.S., Hua, Z., Mali, S., McLoughlin, F., and Vierstra, R.D. (2019). ATG8-Binding UIM Proteins Define a New Class of Autophagy Adaptors and Receptors. Cell *177*, 766-781 e724.

Marshall, R.S., and Vierstra, R.D. (2019). Dynamic Regulation of the 26S Proteasome: From Synthesis to Degradation. Front Mol Biosci *6*, 40.

Ng, S., Ivanova, A., Duncan, O., Law, S.R., Van Aken, O., De Clercq, I., Wang, Y., Carrie, C., Xu, L., Kmiec, B.*, et al.* (2013). A membrane-bound NAC transcription factor, ANAC017, mediates mitochondrial retrograde signaling in Arabidopsis. Plant Cell *25*, 3450-3471.

Nguyen, H.M., Schippers, J.H., Goni-Ramos, O., Christoph, M.P., Dortay, H., van der Hoorn, R.A., and Mueller-Roeber, B. (2013). An upstream regulator of the 26S proteasome modulates organ size in Arabidopsis thaliana. Plant J *74*, 25-36.

Orosa, B., Üstün, S., Calderon Villalobos, L.I.A., Genschik, P., Gibbs, D., Holdsworth, M.J., Isono, E., Lois, M., Trujillo, M., and Sadanandom, A. (2020). Plant proteostasis - shaping the proteome: a research community aiming to understand molecular mechanisms that control protein abundance. New Phytol *227*, 1028-1033.

Page, M.T., Kacprzak, S.M., Mochizuki, N., Okamoto, H., Smith, A.G., and Terry, M.J. (2017). Seedlings Lacking the PTM Protein Do Not Show a genomes uncoupled (gun) Mutant Phenotype. Plant Physiol *174*, 21-26.

Pastor-Cantizano, N., Ko, D.K., Angelos, E., Pu, Y., and Brandizzi, F. (2020). Functional Diversification of ER Stress Responses in Arabidopsis. Trends Biochem Sci *45*, 123-136.

Peters, L.Z., Hazan, R., Breker, M., Schuldiner, M., and Ben-Aroya, S. (2013). Formation and dissociation of proteasome storage granules are regulated by cytosolic pH. J Cell Biol *201*, 663-671.

Radhakrishnan, S.K., den Besten, W., and Deshaies, R.J. (2014). p97-dependent retrotranslocation and proteolytic processing govern formation of active Nrf1 upon proteasome inhibition. Elife *3*, e01856.

Raffeiner, M., Zhu, S., Gonzalez-Fuente, M., and Üstün, S. (2023). Interplay between autophagy and proteasome during protein turnover. Trends Plant Sci *28*, 698-714.

Richter, A.S., Nagele, T., Grimm, B., Kaufmann, K., Schroda, M., Leister, D., and Kleine, T. (2023). Retrograde signaling in plants: A critical review focusing on the GUN pathway and beyond. Plant Commun *4*, 100511.

Ruvkun, G., and Lehrbach, N. (2023). Regulation and Functions of the ER-Associated Nrf1 Transcription Factor. Cold Spring Harb Perspect Biol *15*.

Sampaio-Marques, B., and Ludovico, P. (2018). Linking cellular proteostasis to yeast longevity. FEMS Yeast Res *18*.

Schreiber, U. (2004). Pulse-Amplitude-Modulation (PAM) Fluorometry and Saturation Pulse Method: An Overview. In Chlorophyll a Fluorescence: A Signature of Photosynthesis, G.C. Papageorgiou, and Govindjee, eds. (Dordrecht: Springer Netherlands), pp. 279-319.

Schwanhäusser, B., Busse, D., Li, N., Dittmar, G., Schuchhardt, J., Wolf, J., Chen, W., and Selbach, M. (2011). Global quantification of mammalian gene expression control. Nature *473*, 337-342.

Seo, P.J., Kim, S.G., and Park, C.M. (2008). Membrane-bound transcription factors in plants. Trends Plant Sci *13*, 550-556.

Sha, Z., and Goldberg, A.L. (2014). Proteasome-mediated processing of Nrf1 is essential for coordinate induction of all proteasome subunits and p97. Curr Biol *24*, 1573-1583.

Shih, C.F., Hsu, W.H., Peng, Y.J., and Yang, C.H. (2014). The NAC-like gene ANTHER INDEHISCENCE FACTOR acts as a repressor that controls anther dehiscence by regulating genes in the jasmonate biosynthesis pathway in Arabidopsis. J Exp Bot *65*, 621-639.

Shirozu, R., Yashiroda, H., and Murata, S. (2015). Identification of minimum Rpn4-responsive elements in genes related to proteasome functions. FEBS Lett *589*, 933-940.

Shpilka, T., Du, Y., Yang, Q., Melber, A., Uma Naresh, N., Lavelle, J., Kim, S., Liu, P., Weidberg, H., Li, R*., et al.* (2021). UPR(mt) scales mitochondrial network expansion with protein synthesis via mitochondrial import in Caenorhabditis elegans. Nat Commun *12*, 479.

Steffen, J., Seeger, M., Koch, A., and Kruger, E. (2010). Proteasomal degradation is transcriptionally controlled by TCF11 via an ERAD-dependent feedback loop. Mol Cell *40*, 147-158.

Su, W., Liu, Y., Xia, Y., Hong, Z., and Li, J. (2011). Conserved endoplasmic reticulum-associated degradation system to eliminate mutated receptor-like kinases in Arabidopsis. Proceedings of the National Academy of Sciences *108*, 870-875.

Sun, X., Feng, P., Xu, X., Guo, H., Ma, J., Chi, W., Lin, R., Lu, C., and Zhang, L. (2011). A chloroplast envelope-bound PHD transcription factor mediates chloroplast signals to the nucleus. Nat Commun *2*, 477.

Tanaka, K., Mizushima, T., and Saeki, Y. (2012). The proteasome: molecular machinery and pathophysiological roles. Biol Chem *393*, 217-234.

Tokumaru, M., Adachi, F., Toda, M., Ito-Inaba, Y., Yazu, F., Hirosawa, Y., Sakakibara, Y., Suiko, M., Kakizaki, T., and Inaba, T. (2017). Ubiquitin-Proteasome Dependent Regulation of the GOLDEN2-LIKE 1 Transcription Factor in Response to Plastid Signals. Plant Physiol *173*, 524-535.

Ulasov, A.V., Rosenkranz, A.A., Georgiev, G.P., and Sobolev, A.S. (2022). Nrf2/Keap1/ARE signaling: Towards specific regulation. Life Sci *291*, 120111.

Üstün, S., Hafrén, A., Liu, Q., Marshall, R.S., Minina, E.A., Bozhkov, P.V., Vierstra, R.D., and Hofius, D. (2018). Bacteria Exploit Autophagy for Proteasome Degradation and Enhanced Virulence in Plants. Plant Cell *30*, 668-685.

Üstün, S., Sheikh, A., Gimenez-Ibanez, S., Jones, A., Ntoukakis, V., and Börnke, F. (2016). The Proteasome Acts as a Hub for Plant Immunity and Is Targeted by Pseudomonas Type III Effectors. Plant Physiol *172*, 1941-1958.

Wang, X., Xu, H., Ju, D., and Xie, Y. (2008). Disruption of Rpn4-induced proteasome expression in Saccharomyces cerevisiae reduces cell viability under stressed conditions. Genetics *180*, 1945-1953.

Wang, X., Yen, J., Kaiser, P., and Huang, L. (2010). Regulation of the 26S proteasome complex during oxidative stress. Sci Signal *3*, ra88.

Waters, M.T., Wang, P., Korkaric, M., Capper, R.G., Saunders, N.J., and Langdale, J.A. (2009). GLK transcription factors coordinate expression of the photosynthetic apparatus in Arabidopsis. Plant Cell *21*, 1109-1128.

Weidberg, H., and Amon, A. (2018). MitoCPR-A surveillance pathway that protects mitochondria in response to protein import stress. Science *360*.

Welner, D.H., Deeba, F., Lo Leggio, L., and Skriver, K. (2016). NAC Transcription Factors: From Structure to Function in Stress-Associated Networks. In Plant Transcription Factors, pp. 199-212.

Woodson, J.D., and Chory, J. (2012). Organelle signaling: how stressed chloroplasts communicate with the nucleus. Curr Biol *22*, R690-692.

Wu, G.Z., Meyer, E.H., Richter, A.S., Schuster, M., Ling, Q., Schottler, M.A., Walther, D., Zoschke, R., Grimm, B., Jarvis, R.P.*, et al.* (2019). Control of retrograde signalling by protein import and cytosolic folding stress. Nat Plants *5*, 525-538.

Xie, Y., and Varshavsky, A. (2001). RPN4 is a ligand, substrate, and transcriptional regulator of the 26S proteasome: A negative feedback circuit. Proceedings of the National Academy of Sciences *98*, 3056-3061.

Xie, Y.V., A. (2001). RPN4 is a ligand, substrate, and transcriptional regulator of the 26S proteasome: A negative feedback circuit. Proc Natl Acad Sci U S A *98*, 3056-3061.

Yagishita, N., Aratani, S., Leach, C., Amano, T., Yamano, Y., Nakatani, K., Nishioka, K., and Nakajima, T. (2012). RING-finger type E3 ubiquitin ligase inhibitors as novel candidates for the treatment of rheumatoid arthritis. Int J Mol Med *30*, 1281-1286.

Yoo, S.D., Cho, Y.H., and Sheen, J. (2007). Arabidopsis mesophyll protoplasts: a versatile cell system for transient gene expression analysis. Nat Protoc *2*, 1565-1572.

Zhang, H., Zhang, F., Yu, Y., Feng, L., Jia, J., Liu, B., Li, B., Guo, H., and Zhai, J. (2020). A Comprehensive Online Database for Exploring approximately 20,000 Public Arabidopsis RNA-Seq Libraries. Mol Plant *13*, 1231-1233.

Zhou, H.J., Wang, J., Yao, B., Wong, S., Djakovic, S., Kumar, B., Rice, J., Valle, E., Soriano, F., Menon, M.K.*, et al.* (2015). Discovery of a First-in-Class, Potent, Selective, and Orally Bioavailable Inhibitor of the p97 AAA ATPase (CB-5083). J Med Chem *58*, 9480-9497.

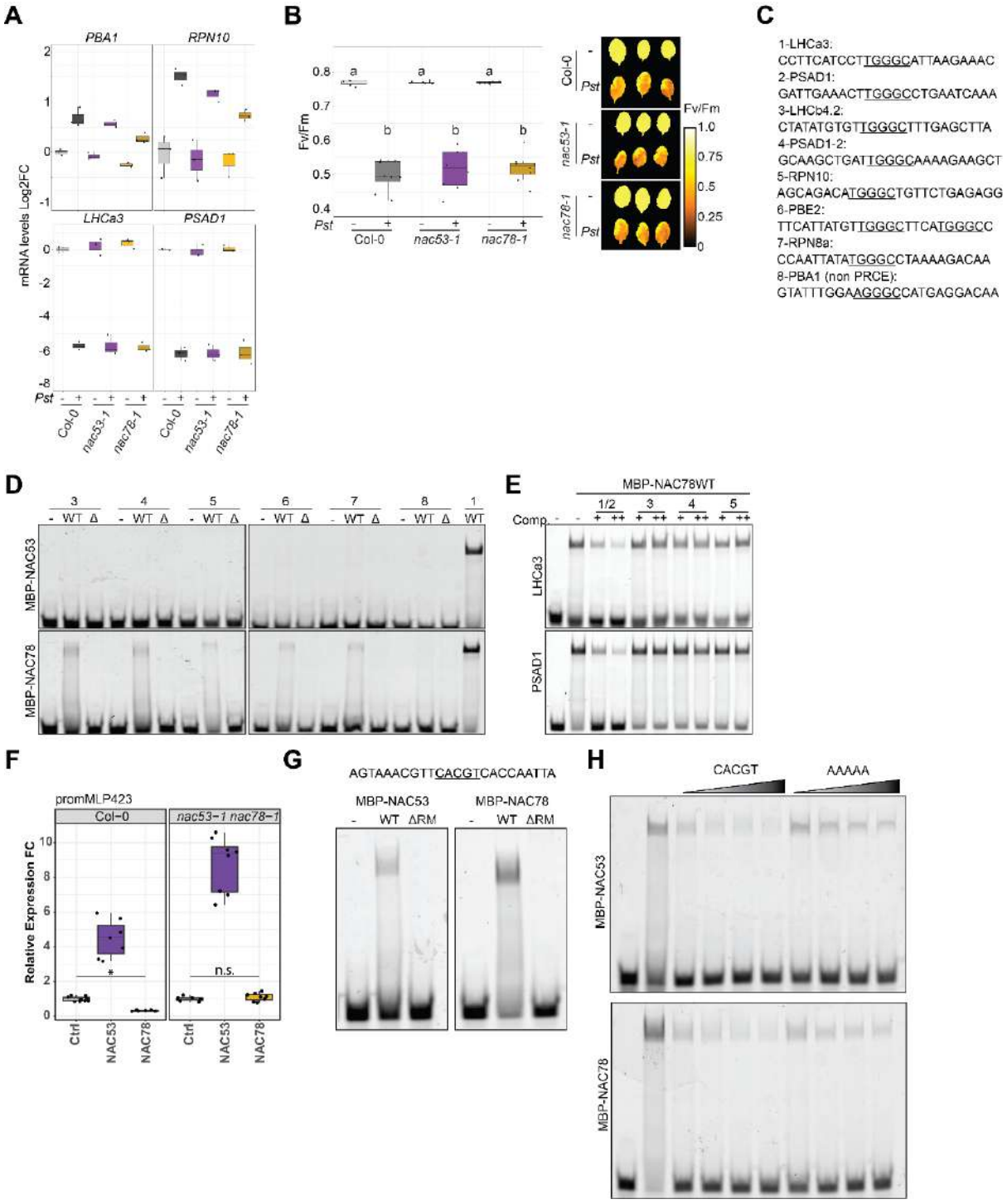

Figure 3. Specificity of NAC53/78 mediated promoter regulation.

A. Boxplot representing the Log2FC mRNA level the indicated transcripts in *Col-0*, *nac53-1* and *nac78-1* upon *Pst* infection in adult plant leaves. **B.** Boxplots representing the photosystem II (PSII) activity measurement on Col-0, *nac53-1* and *nac78-1* adult plant inoculated with *Pst* or mock solutions for 24h. PSII activity is represented by Fv/Fm value. Letters indicate the statistical group assessed by pairwise Welch t.test (p value < 0.05). **C.** 25bp region comprising the PRCE-like elements from several promoters. **D.** Electro-Mobility Shift Assay (EMSA) of MBP-NAC53/78 with probes described in panel C. For negative controls probes were incubated without MBP-NAC53/78 (-) or with MBP-NAC53/78 deleted for their DNA recognition motif (Δ). Experiment was repeated twice with similar results. **E.** EMSA competition of MBP-NAC78 association with LHCa3 or PSAD1 probes competed by each other or other PhANGs probes. Competitor probe is applied at 25X (+) or 100X (++) and indicated by the number from panel C. **F.** Boxplot representing the Fold Change (FC) in LHCa3/PSAD1 promoters activity measured from luminescence of Col-0 or *nac53-1 78-1* protoplasts extract transiently expressing firefly Luciferase under regulation of MLP423 promoters and NAC53/78ΔTM under regulation of 35S promoter. Statistical differences were tested with Wilcoxon-Mann-Whitney test (n.s. : p value >0.05; *: p value < 0.05) **G.** EMSA of MBP-NAC53/78 with indicated probe from MLP423 promoter. For negative controls probes were incubated without MBP-NAC53/78 (-) or with MBP-NAC53/78 deleted for their DNA recognition motif (ΔRM). **H.** EMSA competition of MBP-NAC78 association with MLP423 probe competed by MLP423 probe mutated or not for its G-box. Competitor probe is applied as a gradient of concentration 25X (+) or 100X (++).

b. Additional Results and Discussion

1. The dual regulatory function of the PRCE-NAC53/78 module and associated signaling

In Chapter Va, we demonstrated that proteotoxic stress displays a typical transcriptional signature notably characterized by concomitant activation of proteasome genes and the repression of photosynthesis associated nuclear genes (PhANGs). Interestingly, our analysis showed that the proteasome activators NAC53/78 mediate PhANGs transcriptional repression via association with a similar cis-element than the one found in proteasome promoters (e.g. PRCE) and responsible for transcriptional activation (Nguyen et al., 2013). This dual function of the same NAC53/78-PRCE regulatory module is an intriguing feature and raises several hypotheses on the nature of the underlying mechanism.

The first possibility would be that contrary to proteasome activation, PhANGs repression is not a redundant function of NAC53/78. Indeed, our analysis (**Chapter Va**) tends to suggest that NAC53 acts rather as an activator on PhANGs promoter, and the repression would be solely due to NAC78. However, analyzing the mRNA levels of the identified target PhANGs as well as photosynthetic activity in the single mutants *nac53-1* and *nac78-1* during bacterial infection did not result in significant differences compared to WT plants (**Figure 3A & 3B**). Confirming that like proteasome activation; PhANGs repression is a function depending on both TFs.

A second hypothesis would come from the nature of the cis-elements. While in both promoter groups the association is driven by the TGGGC core sequence, it cannot be excluded that the PhANGs and Proteasome cis-element have some divergences. To test this, we performed EMSA experiments with a broader number of probes coming from proteasome genes or PhANGs promoters. Strikingly, for the 5 other probes bearing a TGGGC core sequence, none of them were bound by NAC53 (**Figure 3C & 3D**). Additionally, the association observed with NAC78 was rather weak that could be further confirmed by competition assays with the two identified probes from Chapter Va (**Figure 3E**). This would strongly suggest that the nature of the PRCE-like motif can differ, playing a significant role in the affinity of the interaction with NAC53/78. From our analysis, it is tempting to conclude that the strong interaction is dependent on the **CT**TGGGC motif possibly resulting in promoter repression, perhaps due to a low reversibility of the NAC53/78-PRCE module, blocking transcriptional factors at its docking site (Rojo, 2001). This is supported by the observation that deletion of the PSAD1 motif results in

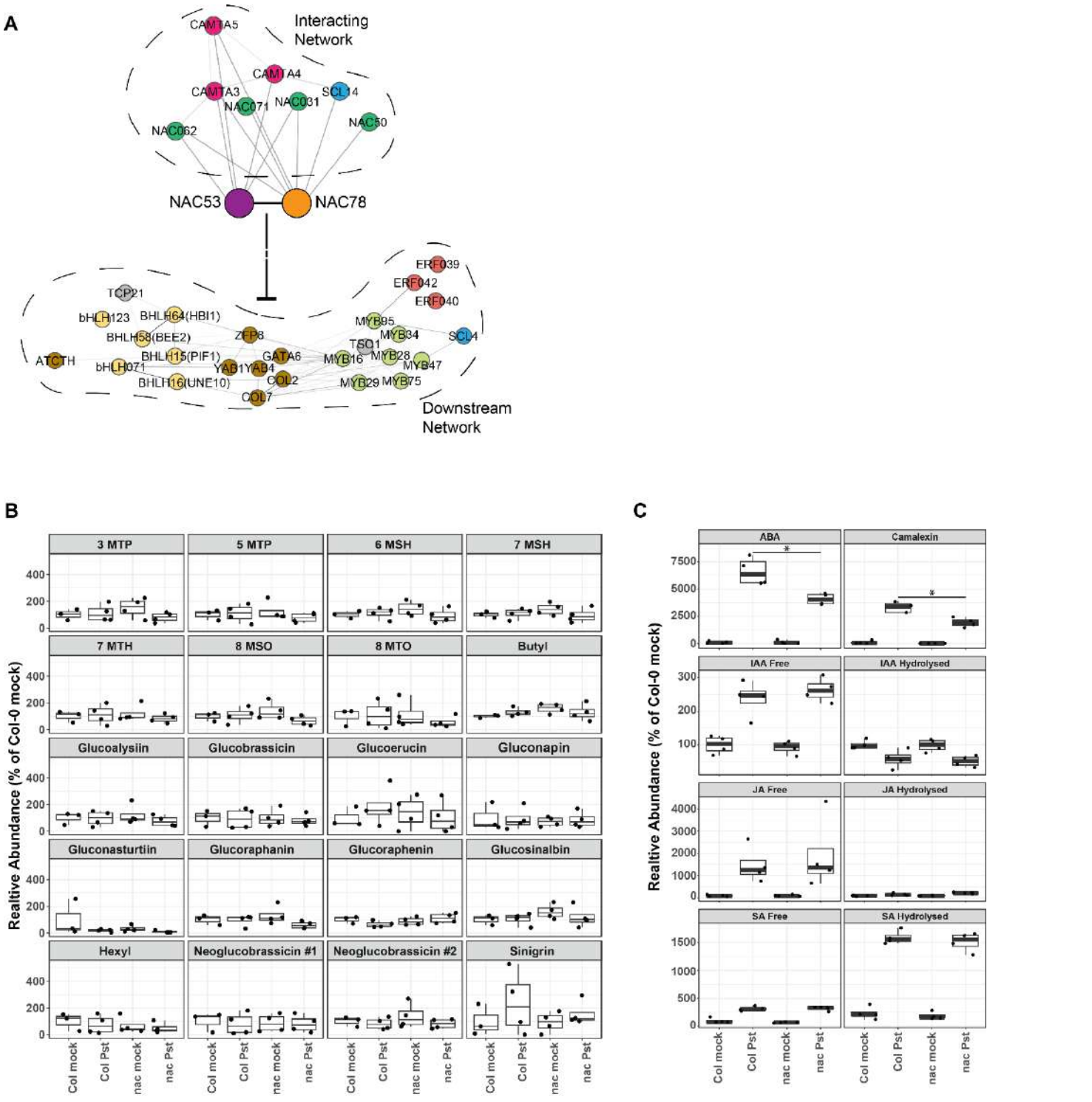

Figure 4. NAC53/78-associated transcription factors network signaling.

A. Protein network of the transcription factors identified in the IP-MS/MS and transcriptomic analysis from Chapter V. Interacting network represent TFs found in the IP-MS/MS for either NAC53 or NAC78. Downstream network represents TFs for which mRNA level was significantly higher in *nac53-1 78-1* leaves upon *Pst* infection compared to Col-0 infected leaves. **B.** Boxplots representing the level of the several glucosinolates in Col-0 plants and *nac53-1 78-1* (nac) plants infected with *Pst*. Metabolites abundance is represented relative to Col-0 mock sample. **C.** Boxplots representing the level of the several plant metabolites in Col-0 plants and *nac53-1 78-1* (nac) plants infected with *Pst*. Metabolites abundance is represented relative to Col-0 mock sample. Statistical differences are tested with Welch T-test (*: p value < 0.05).

hyper activation by NAC53 as PSAD1 promoter possesses a second motif downstream tested as low affinity (**Chapter Va**, **Figure3D** & **3E**). However, this is not in adequation with the observation that NAC53 activates LHCA3 promoter which possess only one motif neither with the absence of such “strong” cis-element in LHCB4.2, found among many others PhANGs as negatively regulated by NAC53/78 presence.

Another aspect that could be considered is the presence of other cis-elements that are recognized by NAC53/78. Indeed, the NAC family has been found to recognize different sequences from one member to another (Lindemose et al., 2014). It cannot be excluded that the same TF can associate with multiple cis-element. This is supported by the observation made during our analysis that NAC78 can induce the repression of the MLP423 promoter (**Figure 3F**), from the MLP423 gene, a candidate initially found as one of the most differentially expressed genes in *nac53-1 78-1 Pst* transcriptome. This promoter does not display a PRCE-like element in proximity to its transcription starting site but bears a G-box related element in this region. This type of element is known to be recognized by some NAC TFs (Welner et al., 2016). We then assessed the association of NAC53 and NAC78 with it by EMSA (**Figure 3G**). Here, we found that both TF were able to interact with the element, partially dependent on the presence of the CACGT core motif (**Figure 3H**). It suggests that both TFs can associate with several elements in their target promoter regions, adding another layer of complexity in the mechanism leading to their transcriptional output.

Additionally, NACs TF are known to homo-/hetero-dimerize (Welner et al., 2016). First, this aspect raises the possibility that the homo-/hetero-dimers NAC53-NAC53; NAC78-NAC78 and NAC53-NAC78 do not share the same regulatory features. This can be supported by the fact that single mutants seem to show mild defects in term of proteasome gene activation (**Figure 3A**), suggesting that the heterodimer NAC53-NAC78 has a higher activity than the homodimers. However, as discussed above, regarding the regulation of PhANGs, homodimers seem to be sufficient for the observed transcriptional repression. Arabidopsis encodes more than 100 NAC TFs, therefore we cannot rule out the possibility that NAC53 and/or NAC78 interact with other members of the NAC family and with other TF family members. By further analyzing the interactome of both proteins (deciphered in **Chapter Va**) we could support this hypothesis as several other NACs were present in association with NAC53 and/or NAC78. In addition, multiple Calmodulin-associated transcriptional activators (CAMTA) were present in the NAC53/78 interactome (**Figure 4A**). This suggests that NAC53/78 could associate with other TFs to mediate the downstream transcriptional regulation of target genes. Those other TFs might share a similar transcriptional impact than NAC53/78, which could explain why in the transcriptomic analysis from Chapter V, we could observe slight activation of some proteasome genes in *nac53-1 78-1* plants upon *Pst* infection.

This is also in line with the observation that the repression of PhANGs is still partially occurring in the NAC mutant. Therefore, investigating this putative TF network would be helpful to fully understand the NAC53/78-dependent transcriptional reprogramming.

While we focused our attention on the NAC-dependent direct regulation of PhANGs transcription, deciphering the transcriptional landscape associated with proteotoxic stress highlighted the presence of other gene clusters that seem specific to proteotoxicity at a certain degree. Indeed, we observed the enrichment of SAURs gene present in the dataset "*nac53-1 78-1 Pst*" and "Col-0 MG132" while we found glucosinolate metabolic process in the dataset "*nac53-1 78-1 Pst*" and "*rpt2a-2 Pma*" (**Chapter Va**). These findings strongly suggest that the proteasome regulatory feedback loop can regulate multiple gene clusters, and that this regulation happens in a context specific manner. While the discussion above could be extended to the case mentioned here, where other cis elements could be targeted in these genes' promoters or association of NAC53/78 with other TFs could lead to regulation of these downstream targets, another possibility needs to be mentioned. Looking at the gene's mis-regulated upon stress in *nac53-1 78-1* reveals the presence of numerous transcription factors. Strikingly, several TF families seem enriched as putative NAC53/78 downstream target (**Figure 4A**). This opens the possibility that NAC53/78 will modulate the expression of other TFs to mediate the required transcriptional reprogramming. This aspect of TF cascades, mentioned in **Chapter I.b.1**, could allow NAC53/78 to impact transcriptional level of multiple gene clusters without directly targeting them. This is further supported by the presence of the MYB28/29 TF pair known to be key regulators of glucosinolate metabolism genes (**Figure 4A**), which might explain the presence of glucosinolate metabolic process gene cluster (**Chapter Va**).

We have revealed that the NAC53/78-dependent transcriptional reprogramming could involve a complex transcriptional network. These types of networks have often been related to hormone signaling, hormones being master signaling compounds in all plant life context (Bittner et al., 2022). It is therefore likely that hormones play also a role in regulating the transcriptional landscape of proteotoxic stress. This is further supported by the known role of Salicylic acid in activating proteasome genes as well as proteasome activity in plants (Üstün et al., 2013). To investigate the possible involvement of hormones or other metabolites in our context, we performed a metabolome profiling of *nac53-1 78-1* plants upon *Pst* infection. Surprisingly, glucosinolates quantification did not reveal any striking differences when comparing Col-0 and *nac53-1 78-1* upon infection; despite the enrichment of genes involved in this metabolic process in the transcriptomic analysis (**Figure 4B**, **Chapter Va: Figure 4**). Similarly, Jasmonic acid, Auxin or Salicylic acid (SA) levels are not impacted by *nac53-1 78-1* mutations (**Figure 4C**). This would suggest the role of SA in proteasome genes activation

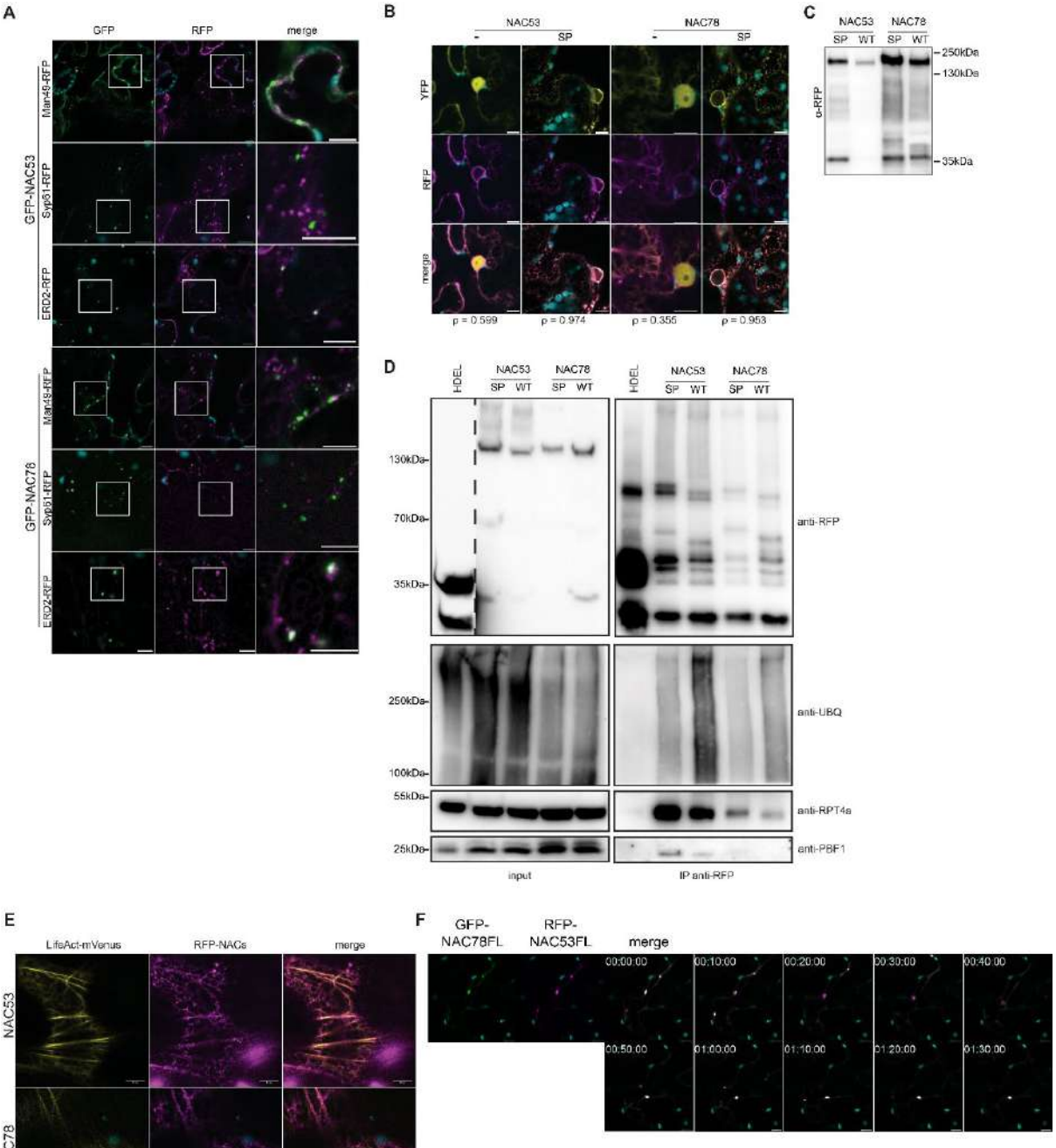

Figure 5. NAC53/78 subcellular dynamic.

A. Confocal microscopy pictures of transiently co-expressed GFP-NAC53/78 and subcellular marker tagged with RFP. Merges represent a close-up view on the indicated region. Scale bars represent 10µm. **B.** Confocal microscopy pictures of transiently expressed (SP-)YFP-NAC53/78-RFP. Colocalization index between YFP and RFP signal are indicated. **C.** Immunoblot against RFP on crude extract of *N. benthamiana* leaves transiently expressing (SP-)YFP-NAC53/78-RFP constructs as in B. **D.** Immuno pull-down against RFP on *N. benthamiana* leaves transiently expressing (SP-)YFP-NAC53/78-RFP. Immunoblot analysis was performed with anti-RFP, anti-ubiquitin (UBQ), anti-RPT4a and anti-PBF1. **E.** Confocal microscopy pictures of transiently co-expressed RFP-NAC53/78 with LifeAct-mVenus. Scale bars represent 10µm. **F.** Confocal microscopy kinetic pictures of transiently co-expressed GFP-NAC78 and RFP-NAC53. Kinetic was imaged for 1min30 every 10 seconds. **G.** Confocal microscopy pictures of transiently co-expressed GFP-NAC78ΔTM and RFP-NAC53ΔTM. Scale bars 10µm.

would occur upstream of NAC53/78 regulation. Interestingly, while glucosinolate levels seem to be unimpacted, we observed a tendency for reduced camalexin accumulation induced by *Pst* in *nac53-1 78-1* (**Figure 4C**). While a direct link with the transcriptome analysis is not obvious; the molecular cross-talk between glucosinolates and camalexin biosynthesis could serve as a starting point for further investigation (Stotz et al., 2011). Finally, we also observed a reduction in ABA accumulation in the mutant background (**Figure 4C**). This interestingly echoes the growth to defense trade-off observed in the NAC53/78-mediated transcriptional reprogramming and photosynthesis repression as reports have pointed out the function of ABA in regulating such trade-offs (Ortiz-García et al., 2023). Together, these data indicate an unknown link between the proteasome regulatory feedback and plant metabolome with a highlight on the ABA metabolism.

2. Subcellular sorting of NAC53/78

We have identified that the ER-anchored NAC TFs act as coordinators of subcellular proteostasis through a molecular system, we termed as ERAPS, allowing the integration of the proteasome status at the ER interface. Interestingly, while we found a direct connection between NAC-mediated proteasome activation and PhANGs repression, we also showed that the lack of NAC53/78 perturbs the plant response to stress occurring at several subcellular compartments (**Chapter Va: Figure 1**). These findings suggest that ERAPS could act locally in the cell, for instance concomitantly directing NAC53/78 for proteasomal degradation or nuclear translocation based on their subcellular localization. This hypothesis is particularly relevant given the known function of the ER network to connect cellular organelles (Wu et al., 2018). However, it would suggest the presence of several actors/mechanisms to locally regulate NAC53/78 ERAPS.

During our investigation we observed the formation of aggregates in response to CDC48 inhibition or NAC53/78 transient over-expression. Based on our analysis, we propose these structures as sites where CDC48 is active and facilitates the retro-translocation of NAC53/78 during ERAPS. Colocalization studies with several endomembrane system markers revealed that these structures appear distinct from the golgi network but could colocalize with the ER retention signal receptor ERD2 strengthening our hypothesis that these aggregates correspond to protein accumulation at local ER sites (**Figure 5A**). Additionally, developing a chimeric construct bearing a signal peptide at the N-ter of the NACs TFs, we could abolish their nuclear translocation as the protein remained strictly at the ER (**Figure 5B**). This indicates 1) their trafficking does not involve the secretory pathway; 2) the topology of their

anchoring is essential for subsequent processing. These additional data support the importance of the ER in the subcellular sorting of NAC53/78. Surprisingly, further investigation on the processing of these constructs through western blotting revealed a similar proteolytic processing between SP and WT constructs (**Figure 5C**). This data is surprising given the known importance of proteases in the release of membrane bound TFs for subsequent nuclear translocation, which has been shown for the animal counterpart Nrf1/SKN1 (Hu et al., 2023b; Lehrbach and Ruvkun, 2016). Further investigation of this aspect by IP highlighted differences in processing of the several constructs (**Figure 5D**). Additionally, analyzing co-pulldown with proteasome subunits and total ubiquitin levels revealed an interesting trade-off. While the SP constructs seem to associate more with proteasome subunits, they were less enriched in ubiquitin marks (**Figure 5D**). It suggests that the SP constructs are still subjected to ERAD, and distinct NAC53/78 ubiquitination marks are necessary for degradation and intracellular trafficking.

Our NAC53/78 interactome found an additional strong association between both NACs and myosin XI proteins, as they were the most enriched proteins. Myosin XI are actin-based molecular motor predominantly involved in vesicular and organelle trafficking (Duan and Tominaga, 2018). This suggests a link between the actin cytoskeleton and NAC53/78. Preliminary experiments showed that the observed aggregate-like structures exhibit colocalization with the actin cytoskeleton (**Figure 5E**). Kinetic analysis of these structures highlighted their subcellular mobility (**Figure 5F**). These data suggest these structures can be vesicles and/or structures belonging to the endomembrane system (Šamaj et al., 2004; Yuen et al., 2023). Involvement of vesicular trafficking in NAC53/78 regulation is intriguing as neither their proteasomal degradation nor their nuclear translocation should require such a process. Additionally, subcellular analysis of NAC53/78 lacking the TM domain resulted in the formation of similar structures (**Figure 5G**), indicating these structures do not depend on the NAC membrane-anchoring. While these data remain elusive, it highlights NAC53/78 subcellular dynamics and supports a link with actin cytoskeleton. Interestingly, the myosin XI-K from Arabidopsis has been reported to be essential for ER motility, actin organization and organellar trafficking (Duan and Tominaga, 2018; Ueda et al., 2010). Given our evidence that NAC53/78 can integrate signal from diverse subcellular sites, actin network could be an important player in connecting NAC53/78 dynamic with the different subcellular compartment. Interestingly, actin cytoskeleton has been recently shown to be essential for maintenance of proteasome homeostasis in yeast (Williams et al., 2022), hence a similar link could be possible in plants.

Our MS/MS analysis not only permitted analysis NAC53/78 interactome but also allowed the identification of PTMs for both TFs. Notably, we could identify several sites of ubiquitination on both proteins, for a total of 9 lysin residues (**Figure 6**). While investigation of these residues permitted to confirm their importance of NAC53/78 ubiquitination (see **Chapter V**), a role in the regulation of the protein's stability could not be clearly established. Given the number of identified sites, it is likely that mutations of 5 residues are not sufficient to display a clear effect on their proteasomal degradation; however, it also raises other possibilities. Indeed, while ubiquitination has been primarily studied on its role regarding protein degradation; it can also play a significant role in other types of regulations. This is due to the possibility of a ubiquitin chain attached to the substrate to possess different topologies based on how the chain has been formed. This is referred to as the ubiquitin code, which associate the different topologies to define regulatory process (Dikic and Schulman, 2023). Given the above-mentioned aspect of NAC53/78 dynamics (**Figure 5**), it is plausible that some of the identified marks would be sites of ubiquitin chains regulating protein trafficking rather than degradation. In this scenario, defining the precise role of the HRD1 E3 ligases in the ubiquitination process would be crucial for a precise understanding of the ERAPS machinery defined in **Chapter Va**. Indeed, ERAD pathways have been associated with several types of ubiquitin chain topologies (Albert et al., 2020; Tang et al., 2011; Xu et al., 2009). While most of the findings have been done on topologies related to proteasomal degradation, we cannot exclude that ERAPS also relies on non-proteolytic related ubiquitin chain types. This is supported by the fact that ubiquitination is required for ER to cytosol retro-translocation and subsequent recognition by the CDC48 complex (Radhakrishnan et al., 2014). Hence, NAC53/78 ubiquitination would serve as retro translocation signal, degradation signal and putatively trafficking signal. It would suggest that this process involves more than one E3 ligase, this assumption is supported by the presence of several cytosolic E3 ligases in NAC53/78 interactome (**Chapter Va: Figure 1**).

In animal, the ER anchored TF (Nrf1) acting as proteasome transcriptional activator has been found to be processed through a similar mechanism (Marshall and Vierstra, 2019). First, glycosylation permits recognition by the Hrd1 ERAD complex; second, ubiquitination and retro translocation is initiated by Hrd1 E3 ligase; third, CDC48 complex extracts the protein from the ER membrane for proteasomal degradation. In case of proteasomal stress, the degradation would not occur and an E4 ligase will lead to ubiquitin chain elongation (Hu et al., 2023b). These long chains have been proposed to be recognized by the ubiquitin-dependent DDI1/2 proteases for proteolytic cleavage of the TF allowing release from the CDC48 complex and nuclear translocation. Our investigation strongly suggests that NAC53/78 are subjected to a similar mechanism and the presence of DDI1 in *A. thaliana* (Farmer et al., 2010) supports

the involvement of this protease in NAC53/78 dissociation from CDC48 prior to nuclear translocation.

We just highlighted the possible importance of ubiquitination in regulation of the proteasome transcriptional activator for their intracellular processing from degradation to translocation. In addition to ubiquitin marks, our analysis showed the presence of several phosphorylation sites. Interestingly, the phosphorylation sites are found, for most of them, near ubiquitination sites (**Figure 6**). This suggests another layer of signaling in the sorting of NAC53/78. It is known that phosphorylation and ubiquitination can be concomitantly involved in protein regulation and signaling (Mithoe and Menke, 2018). Interestingly, previous reports have been shown the role of PI4Kγ5 in phosphorylation and activation of NAC78 (Tang et al., 2016). This supports the importance of phosphorylation in NAC53/78 regulation and encourages further investigation in this direction.

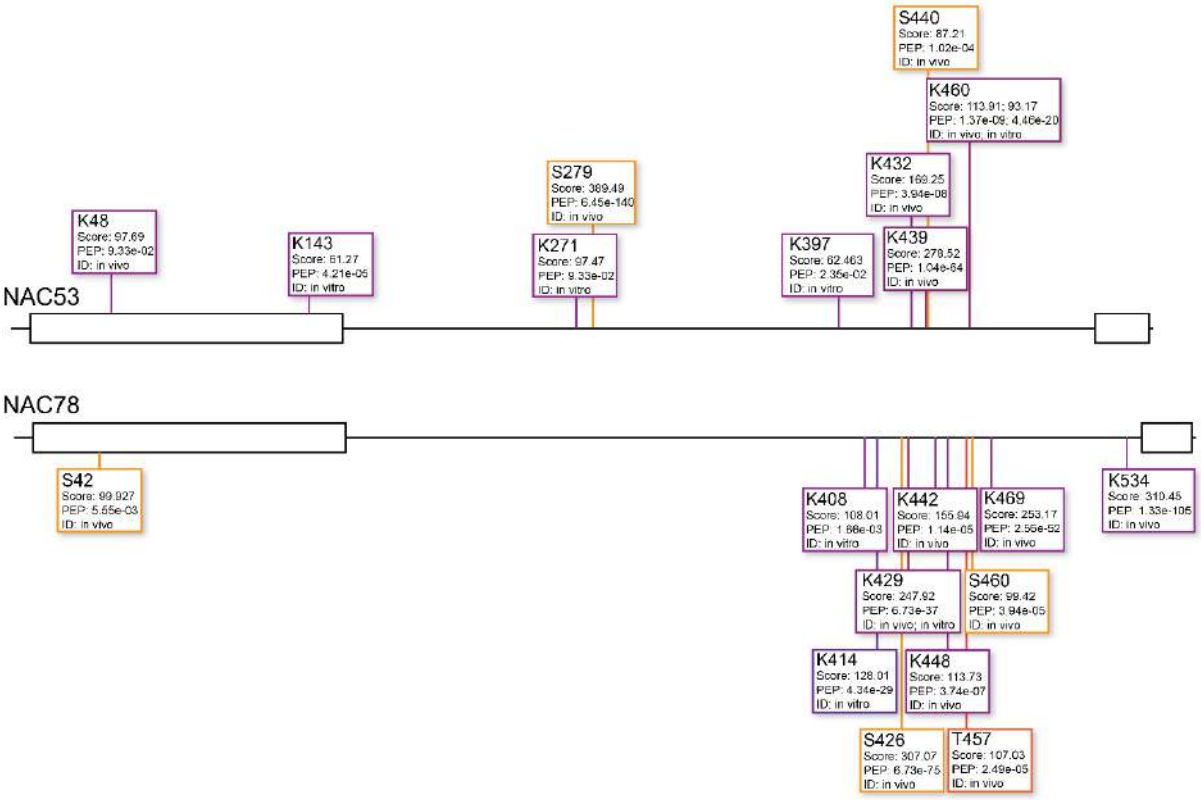

Figure 6. NAC53/78 post-translational modifications.

Schematic representation of the position of identified PTMs in the analysis from Chapter V. Analysis score (Score), confidence index (PEP) and context of identification (ID) are indicated for every residue. Lysins displaying ubiquitination marks are indicated in purple. Threonins or Serins displaying phosphorylation marks are indicated in orange.

3. The specificity of 26S Proteasome regulation

The 26S proteasome complex is often presented as a unique entity within a cell but is present in numbers. Given the size and complexity of these structures, it is probable that complex can differ from one another in the same cell or between cells, but little emphasis has been brought to this aspect. However, it is known that the complex can be regulated at several steps as reported in **Chapter II** and more strikingly can differ in its subunit's composition. The most striking example of such specificity comes from medical studies where it is known that specific subunits possess multiple copies in the mammalian genome. These homologs have been found to be specifically expressed in context or cell type dependent manner, leading to the formation of what is called immunoproteasome complex or thymoproteasome complex (Murata et al., 2018). Interestingly, *A. thaliana* possesses an extensive number of duplicated proteasome subunits genes (**Figure 7A**). It has been reported that upon proteasome inhibition, NAC53/78-mediated proteasome gene expression activation seems to be biased toward certain gene copies over others (Gladman et al., 2016). Interestingly, during our analysis we refined the transcriptional landscape of proteotoxicity, showing that bacteria-induced proteotoxicity and proteasome inhibition share similar transcriptional footprints. Performing hierarchical clustering of the proteasome subunits could confirm specific activation of certain subunit copies upon stress (**Figure 7B**). Interestingly, this classification highlights a preference for certain duplicated genes to be transcriptionally modulated over their paralog. It suggests a functional purpose for the large proteasome genes duplication observed in *Arabidopsis* and would support the presence of a stress-specific 26S proteasome complex, assembled with preferential subunits. While characterizing the nature of this specific complex would require further investigation, the difference could arise from multiple aspects such as certain paralogs to be subjected to unique PTMs (Hirano et al., 2016), the position of these genes in the plant genome (which could impact transcriptional regulation based on chromatin status, (Klemm et al., 2019)) or the necessity to express similar protein through distinct mRNA molecules to allow precise post-transcriptional regulation (Iñiguez and Hernández, 2017).

During our analysis we monitored total ubiquitin level as well as proteasomal proteolytic activity upon bacterial infection (**Figure 7C & 7D**). Surprisingly, despite a striking effect of the *nac53-1 78-1* mutations on the activation of proteasome genes and accumulation of proteasome subunits (**Chapter Va**), we observed only mild differences for both measurements. As discussed in **Chapter IV**, proteasome homeostasis mis-regulation is expected to impact the activity of the proteases and thus, the turnover of ubiquitinated proteins. However, the absence of a strong effect suggests a certain level of specificity behind the NAC-mediated activation of the proteasome genes.

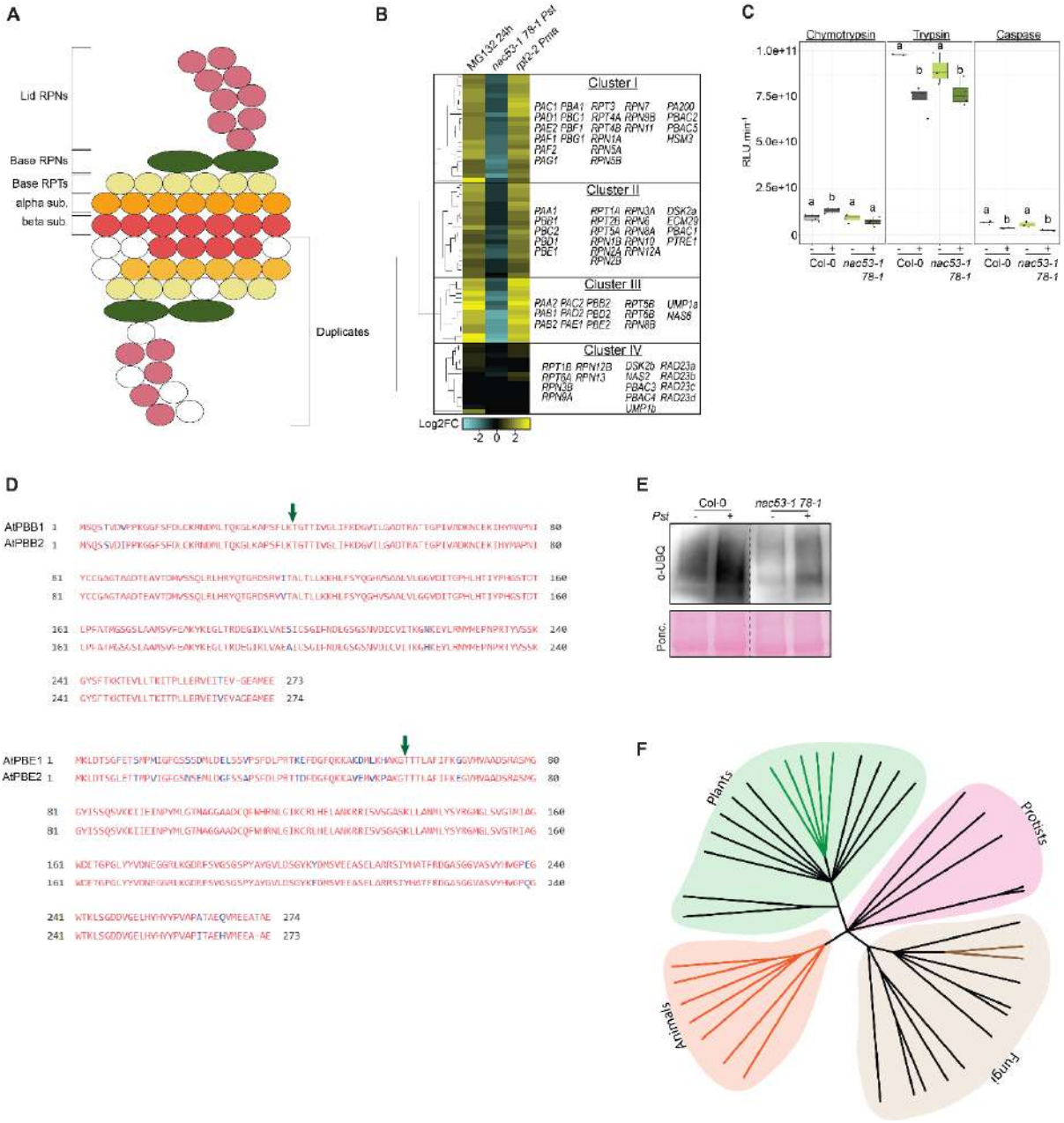

Figure 7. Specificity of the proteasome complex.

A. Schematic representation of the gene number encoding proteasome subunits in *A. thaliana* **B.** Hierarchical clustering of proteasome complex genes and associated proteins based on the transcriptomic analysis from Chapter V. **C.** Boxplot representing proteasome protease activity measurement in Col-0 and *nac53-1 78-1* adult plant leaves inoculated with Pst or mock solutions for 24h. Activity is represented as a percentage of Col-0 mock. Letters indicate the statistical group assessed by pairwise Wilcoxon-Mann-Whitney test (p value < 0.05). **D.** Sequence alignment of PBBs and PBEs paralogs. Identical residues are represented in red, diverging ones in blue. Green arrow indicated the cleavage site of the subunits propeptides. **E.** Immunoblot against ubiquitin in Col-0 and *nac53-1 78-1* adult plants leaves inoculated with *Pst* or mock solutions for 24h. Ponceau staining is used as loading control. **F.** Phylogenic tree of representative species from the 4 eukaryotic kingdoms. Colored lines represent the species with conserved known proteasome transcriptional activators within each kingdom.

Indeed, measuring the proteasome activity we could observe that Chymotrypsin-like activity tends to increase in Col-0 background while it is decreased in *nac53-1 78-1*. Out of the three subunits possessing proteolytic activity, two are duplicated in *Arabidopsis*: beta-2 (PBB1 and PBB2) and beta-5 (PBE1 and PBE2); respectively responsible for Trypsin-like and Chymotrypsin-like activity. In both cases, the duplicated genes show strong differences in stress-dependent transcriptional activation (**Chapter Va**, **Figure 5B**). Hence, it is tempting to speculate that the chymotrypsin-like activity differences observed in *nac53-1 78-1* compared to Col-0 would be due to differences between the two paralogs PBE1 and PBE2. This could be contradicted by the absence of impact on Trypsin-like activity despite similar transcriptional disparities between PBB1 and PBB2. However, looking at amino acids' sequences alignment between the 2 paralogs pair showed that the PBEs show more divergence than the PBBs (**Figure 7C**). Interestingly, most of the polymorphism happened in the N-terminal region, corresponding to a propeptide cleaved upon assembly of the subunits (**Figure 7C**). This region has been reported to be the main driver of the differential assembly between stan dard and immuno-proteasome, notably due to large differences in the amino acids composition between the mammalian paralogs defining either type of complex (Jayarapu and Griffin, 2007). While the differences observed between PBE1 and PBE2 are not as drastic as the ones observed for their animal counterpart (Li et al., 2016); based on our observations it is tempting to propose a similar mechanism in which plants have evolved a system favoring assembly of certain paralogs hence adapting overall proteasome activity upon stress. Analyzing total ubiquitin level in *nac53-1 78-1* upon infection did not show strong difference compared to WT (**Figure 7D**), supporting a specific function of proteasome gene activation upon infection. On another level, it must be noted that the activity monitoring performed here does not distinguish between 26S proteasome activity and 20S proteasome activity. Indeed, the proteasome complex is not exclusively present in form of 26S complex as a significant proportion of it can be found in its 20S form, lacking the base and the lid subunits (Sahu et al., 2021). This 20S complex can alternatively be capped with other ATPase rings (Pick and Berman, 2013). In plants the proportion and context in which the 20S complex plays a role are still poorly characterized but given its function in other eukaryote in coping with proteotoxicity (Demasi and da Cunha, 2018), it would not be surprising that these type(s) of proteasomes play a significant role in similar plant-related context. Therefore, being unable to distinguish between these forms could explain the inability to see strong differences in *nac53-1 78-1* at the proteolytic level.

The data discussed here suggests a certain level of specificity in the proteasome activation characterized *in planta*. The discussion above mostly focused on the characteristics of *Arabidopsis* to possess multiple copies of multiple proteasome subunits genes. Interestingly, while duplications have occurred largely in plants it is not restricted to, as mammals also

possess certain proteasome gene paralogs, as mentioned previously (**Figure 7A**). This similar feature raises questions about the conservation of the proteasome regulation. Strikingly, despite a mechanistic conservation, the known proteasome regulators are from distinct evolutionary origin (Marshall and Vierstra, 2019). This divergence contrasts with the conserved aspect of the proteasome complex. More strikingly, the regulators identified in yeast and plants are specific to a relatively restricted clade in their respective kingdoms (**Figure 7E**). It suggests that the evolutionary path has systematically adapted the proteasome regulators to specific requirements across species. Understanding the diversity of the regulators and the nature of such requirements would be a key step in the understanding of proteostasis regulation in eukaryotes.

4. Conclusion

In this chapter, we have deciphered the mechanism that we refer to as the proteasome regulatory feedback loop in the model plant *Arabidopsis thaliana*. Interestingly, we could identify a direct relationship between proteasome gene activation and PhANGs repression. Given the large proportion of PhANGs encoded in term of gene number (up to 15% of total gene number, (Nellaepalli et al., 2023) and total protein amount (van Wijk et al., 2021), it is not surprising that plants evolved a direct molecular link between the major degradation machinery and the most abundant subcellular proteome. Interestingly, a similar link exists between the yeast proteasome transcriptional activator Rpn4p and mitochondrial nuclear encoded genes (Boos et al., 2019). However, in yeast this trade-off relies on multiple actors acting through a TFs cascade rather than a direct co-regulation through action of the same proteins. Nevertheless, it suggests a recurrent connection between the 26S proteasome complex and its substrates via the proteasome regulatory feedback loop. Interestingly, while our analysis focused on the PhANGs, we observed the enrichment for other gene clusters sharing a similar transcriptional pattern. With the difference that this other gene cluster appeared specific to certain conditions, (e.g. glucosinolate enriched in infectious context, SAURs enriched in chemical proteasome inhibition and proteasome activation defective mutant *nac53-1 78-1,* see **Chapter Va**). Hence it is tempting to speculate that the observed trade-off between proteasome transcriptional activation and proteasome substrate repression is a context-specific response that could be impacted by the type of stress and/or the tissue affected by the stress.

In such a scenario, the 26S proteasome complex would act as a central signaling hub able to sense local perturbations of the cellular proteome due to an increase or a decrease of substrate abundance, constituting a proteasome-integrated signaling pathway. The modulation of substrate abundance would directly impact the ability of the proteasome

complex to degrade the transcriptional activators resulting in modulation of the TF abundance in the nucleus and associated transcriptome response. We have mentioned above multiple aspects of NAC53/78 potential regulation additionally to their proteolytic turn-over. These additional components would permit to shape the specificity of the proteasome-integrated signaling response based on the stress context, site of perturbation and overall proteome status.

This is reminiscent of the characterized animal mechanism called ISR (integrated stress response), which allows stress adaptation of the cellular translatome via specific phosphorylation of the translation initiation factor, eIF2α (Ryoo, 2024). This mechanism relies on several kinases activated by specific stresses initiating a shared signaling output. Interestingly, a connection between the proteasome activator Nrf2 and the ISR has recently emerged in the context of mitochondrial dysfunction (Bilen et al., 2022). It suggests an elaborated signaling network comprising ISR and the proposed proteasome-integrated signaling pathway to coordinate cellular stress response. However, from the four kinases identified as ISR initiators in animals, only one (GCN2) seems to be conserved across kingdoms and in yeast the ISR output involves a non-conserved TF (Postnikoff et al., 2017). This example highlights again the presence of similar stress integration mechanisms with molecular divergences being driven by evolution. Altogether, this knowledge points toward a universal stress integration signaling network including ISR, proteasome-integrated signaling pathway and likely other known or unknown mechanisms. This network would share mechanistic principles via divergent actors at several nodes. These specificities would have been developed through evolutionary adaptations reflecting the needs of every species to specifically shape their proteome in response to environmental cues.

In conclusion, the proteasome-integrated signaling pathway would constitute a molecular system allowing to unify eukaryotic proteostasis. This signaling network centered around the 26S proteasome would allow, in connection with other mechanism, precise adaptation of the cellular proteome.

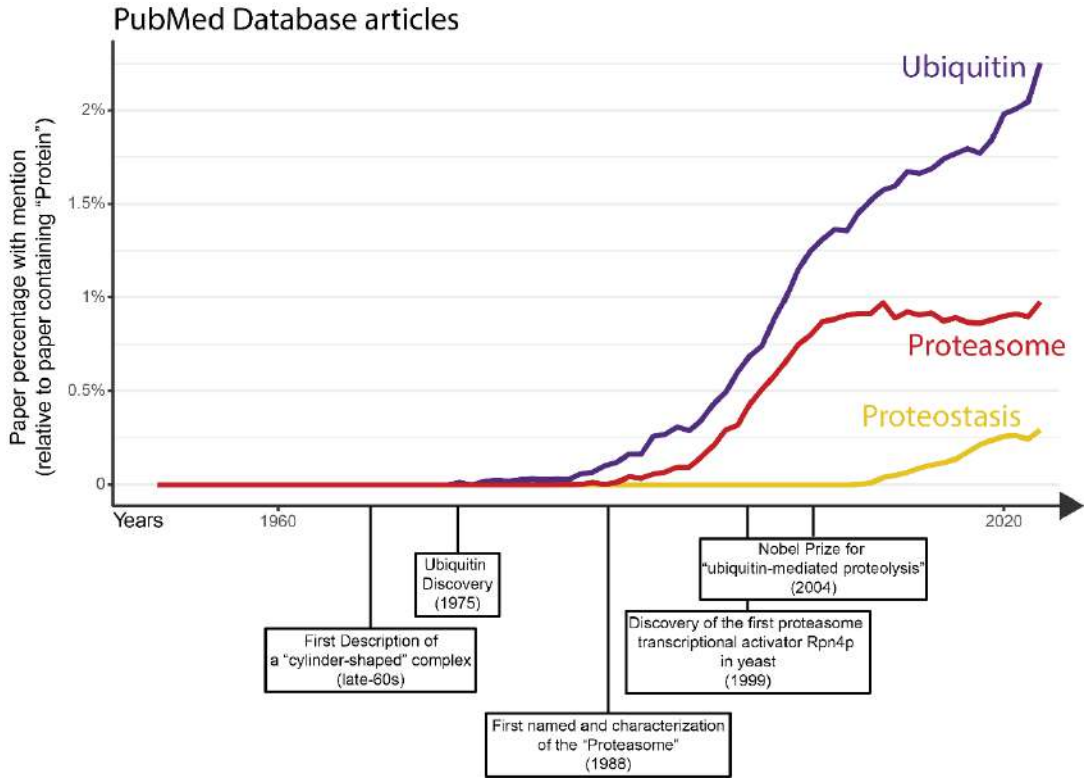

Figure 8. The recent increased interests for the concept of Proteostasis.

VI. Future perspectives

It has been now nearly 60 years since the first description of a “cylinder-shaped” protein complex ((Baumeister et al., 1998), **Figure 8**). This first description has been followed by the purification and discovery of the ubiquitin peptide in 1975. After this a succession of studies during the late 70s and early 80s permitted to characterize the presence of an ATP dependent, ubiquitin-mediated protein degradation (Nobel prize 2004). While the original focus was to identify the protease, the results directed the research into the characterization of the ubiquitination machinery. It is in 1988, that the first characterization and naming of the “proteasome” was provided to the community (Arrigo et al., 1988). Eleven years later, the first proteasome transcriptional activator was identified in yeast and in 2004 the nobel prize of advanced chemistry was attributed for the discovery and characterization of the “ubiquitin-mediated proteolysis”. It shows that the study of UPS has been an important field of research since the breakthrough of biochemistry and molecular biology. However, as reflected by the proportion of published studies related to UPS during this time, the interest in this field has never stopped growing (**Figure 8**). Interestingly, the interest in the concept of proteostasis seemed to have appeared relatively late, as the mention in scientific paper increased since 2010.

This observation can be correlated with the rise of the omics era in the early 2000 (Pavlopoulos et al., 2013). Indeed, the ability to picture global changes in transcriptome or proteome likely promoted the interest of identifying processes explaining general regulation of the cellular molecular network. Indeed, we know now that the cellular functions and response to environment are regulated by intricated molecular networks. Hence, it became clear that despite major pathways being involved in every biological context, these pathways always rely on a more complex system, often linking them together. This complexity makes it essential to understand how this molecular network is orchestrated.

The work presented here fits in with this aspect. While we connect proteasome-mediated degradation, transcriptional reprogramming and energetic metabolism, it is plausible that such link exists between many, if not all, fundamental processes. Being able to identify these connections would be helpful to provide the knowledge to develop biological tools necessary to face today’s societal challenges.

For instance, we can discuss two major worldwide problematics of the human modern era that can be connected to the present work. On a biomedical angle, cancer has emerged as one of the major global health issue (Bray et al., 2024). Hence, for decades, efforts have been focused on the development of novel and more efficient therapeutic approaches. Interestingly,

since more than 20 years, proteasome targeting for cancer therapy holds promise. Indeed, in the late 90s preclinical studies on Bortezomib have shown efficient antitumor activity and render malignant cells and tumors more sensitive to other conventional treatment (Teicher et al., 1999). Further studies in the 21st century, could confirm the efficacy of bortezomib promoting investigation on novel proteasome inhibitors (Manasanch and Orlowski, 2017). The identification of such molecules and clinical trials could confirm the interest in proteasome inhibition. However, these treatments pose several significant challenges. As often with targeting of pleiotropic mechanisms, drug administration can lead to secondary effect associated with development of other diseases or can trigger development of resistant tumors (Manasanch and Orlowski, 2017). Hence, interest has focused on identifying more specific means to target UPS in cancerous cells. This has mostly been investigated through protein-targeting chimeric molecules (PROTACs) that induce proteasome-mediated degradation of specific protein targets (Gao et al., 2020; Manasanch and Orlowski, 2017). While this technology provided encouraging results, it relies on identification of precise targets and subsequent specific chimeric molecules which can be challenging. Therefore, other strategies to manipulate the 26S proteasome complex would be interesting. This is further supported by the implication of the main animal proteasome transcriptional activator, Nrf1, in several tumoral context (Liu et al., 2023). In this work we show that plants have evolved a system to coordinate subcellular proteostasis. This system allows the 26S proteasome complex to act as a signaling hub able to integrate proteotoxic signals. While substantial evidence exists to support the existence of a similar system in yeast (Krämer et al., 2021) and evidence that Nrf1, and its paralog Nrf2, control further proteostasis associated processes (Ruvkun and Lehrbach, 2023), a similar system unifying subcellular proteostasis is probable but yet to be defined in biomedical research. Understanding the conserved features of this system would certainly help develop new therapeutic approaches with a broad tumoral impact on while mitigating side effects of pleiotropic treatment.

On an agronomical aspect, to face hunger crisis molecular biology research to improve crop yield have historically focused on developing crops with increased productivity and decreased susceptibility to pathogens (Palmgren et al., 2015). These goals have been investigated, for instance, through improvement of photosynthetic efficiency and identification of pathogen virulence factors and associated host targeted pathways. While the involvement of the UPS has been identified in plant immunity (see **Chapter III**); its role in coordinating chloroplast proteostasis has been characterized relatively recently (Nellaepalli et al., 2023). A challenging aspect of plant breeding is the trade-off between growth and defense (He et al., 2022). In short, plant rapid growth is associated with increased susceptibility and, conversely, plants with defense mechanisms onset often show reduced agronomical traits. Hence, it is critical to

understand the molecular mechanism underlying this tradeoff. The work presented here fits in, as plant defective for proteasome transcriptional activators concomitantly display increased susceptibility to pathogenic bacteria but improved photosynthetic efficiency upon infection (see **Chapter V**). Additionally, a determinant limitation of the improvement of plant immunity is the capacity of microorganisms to evolve faster than their host, due to higher generation rate, thus leading to a high capacity to overcome newly acquired resistance in crops, especially if the latter is provided by a single gene (Gou et al., 2023). Therefore, identifying immunity mechanisms that rely on general proteostasis regulators such as the 26S proteasome would be a promising direction to develop sustainable resistant traits. This has been recently illustrated by the discovery of a natural allele providing broad scale resistance in rice plants without impact on yield (Hu et al., 2023a). Finally, our investigation suggests that the coordination of proteostasis by the proteasome-integrated signaling pathway is not limited to bacterial infection but occurs also in other agronomically relevant contexts (see **Chapter Va**). Taking these aspects together, further investigations of the specificity of proteostasis coordination via the proteasome regulatory feedback loop, could permit to identify novel principles behind the trade-off between growth and stress responses, providing interesting frameworks for the development of improved plant resistance traits against pathogens or other agronomical problematics.

These two examples highlight the importance of understanding general processes linking fundamental molecular processes to efficiently develop the required biological tools. They reflect the limitations of detailed studies on single pathways, often neglecting their connection with global proteome and the necessity of being able to encompass the entire molecular complexity of life for future challenges.

VII. Additional Methods

Quantification of plant metabolites

For quantification of plant metabolites upon infection, 4 weeks old leaves of Col-0 and *nac53-1 78-1* infiltrated with mock solution ($MgCl_2$ 10mM) or *Pst* solution (OD_{600}: 0.2) for 24h were harvested and flash freezed. After grinding tissue was extracted in 2 x 750 µl Ethyl acetate (EtAc) with 0.1% Formic acid containing the internal standard (3HOBA 60ng, DHJA 80ng and 5IFA 50ng per ml) followed by 10min sonication in Ultra sonic bath. Tubes were mixed by shaking for 1h at 28°C, 1400rpm and centrifuged 10min at 13000rpm (Hettich tabletop Micros 220C centrifuge). 1200µL Supernatant was transferred in a new tube and pellet kept.

For supernatants, EtAc solvent was dried from supernatant with an Eppendorf Vacuum concentrator at 30mbar for 1h. Next, 70µL of Methanol/ Trimethylsilyldiazomethan (1:1) was added and tubes were incubated 35min at 24°C, 1200rpm following by a short centrifugation phase prior to submission for Gas Chromatography-Mass Spectrometry (GC-MS) in split less MRM Mode.

For pellets, the remaining EtAc was removed as much as possible, and the pellet was let to evaporate. Next, 300µl 3M HCl was added followed by 1h incubation at 70°C, 1400rpm. Then, 300µL 3M NH3 was added followed by vortexing and 1mL of Extraction solution was added. Tubes were incubated 1h at 28°C, 1400rpm and centrifuged 10min at 13000rpm (Hettich tabletop Micros 220C centrifuge). 700µL supernatant was transferred to a new tube. EtAc solvent was dried from supernatant with an Eppendorf Vacuum concentrator at 30mbar for 1h. Next, 70µL of Methanol/ Trimethylsilyldiazomethan (1:1) was added and tubes were incubated 35min at 24°C, 1200rpm following by a short centrifugation phase prior to submission for Gas Chromatography-Mass Spectrometry (GC-MS) in split less MRM Mode.

Protein Alignment and representative phylogeny

For protein alignment, alignment was performed using Clustal Omega software (https://www.ebi.ac.uk/jdispatcher/msa/clustalo). Amino acids conservation was represented in red, polymorphism in blue.

For representative species phylogenic tree, the tree information was extracted from NCBI Taxonomy browser (https://www.ncbi.nlm.nih.gov/Taxonomy/Browser/wwwtax.cgi) for the following species:

(Fungi) *Aspergillus nidulans, Saccharomyces cerevisiae, Neurospora crassa, Schizosaccharomyces pombe, Candida Albicans, Botrytis cinerea, Sclerotinia sclerotiorum, Coprinopsis cinerea, Cryptococcus neoformans, Rhizophagus irregularis, Schizophyllum commune, Ustilago maydis.*

(Plants) *Chlamydomonas reinhardtii, Arabidopsis thaliana, Glycine max, Marchantia polymorpha, Oryza sativa, Physcomitrium patens, Populus trichocarpa, Selaginella moellendorfii, Solanum lycopersicum, Gingko biloba, Ceratopteris richardii, Cryptomeria japonica, Zygnema cylindricum, Chlorokybus atmophyticus, Ostreococcus tauri, Anthoceros agrestis.*

(Animals) *Caenorhabditis elegans, Danio rerio, Drosophila melanogaster, Homo sapiens, Mus musculus, Xenopus tropicalis, Gallus gallus.*

(Protists) *Hyaloperonospora arabidopsidis, Phytophthora infestans, Phytophthora sojae, Leishmania major, Paramecium tetraurelia, Plasmodium falciparum*

VIII. Bibliography

Agarwal, P.K. (2006). Enzymes: An integrated view of structure, dynamics and function. Microbial Cell Factories *5*, 2.

Albert, S., Wietrzynski, W., Lee, C.W., Schaffer, M., Beck, F., Schuller, J.M., Salome, P.A., Plitzko, J.M., Baumeister, W., and Engel, B.D. (2020). Direct visualization of degradation microcompartments at the ER membrane. Proc Natl Acad Sci U S A *117*, 1069-1080.

Arndt, N.T., and Nisbet, E.G. (2012). Processes on the Young Earth and the Habitats of Early Life. Annual Review of Earth and Planetary Sciences *40*, 521-549.

Arrigo, A.-P., Tanaka, K., Goldberg, A.L., and Welch, W.J. (1988). Identity of the 19S 'prosome' particle with the large multifunctional protease complex of mammalian cells (the proteasome). Nature *331*, 192-194.

Balchin, D., Hayer-Hartl, M., and Hartl, F.U. (2016). In vivo aspects of protein folding and quality control. Science *353*, aac4354.

Baumeister, W., Walz, J., Zühl, F., and Seemüller, E. (1998). The proteasome: paradigm of a self-compartmentalizing protease. Cell *92*, 367-380.

Bilen, M., Benhammouda, S., Slack, R.S., and Germain, M. (2022). The integrated stress response as a key pathway downstream of mitochondrial dysfunction. Current Opinion in Physiology *27*, 100555.

Bittner, A., Cieśla, A., Gruden, K., Lukan, T., Mahmud, S., Teige, M., Vothknecht, U.C., and Wurzinger, B. (2022). Organelles and phytohormones: a network of interactions in plant stress responses. Journal of Experimental Botany *73*, 7165-7181.

Boos, F., Kramer, L., Groh, C., Jung, F., Haberkant, P., Stein, F., Wollweber, F., Gackstatter, A., Zoller, E., van der Laan, M.*, et al.* (2019). Mitochondrial protein-induced stress triggers a global adaptive transcriptional programme. Nat Cell Biol *21*, 442-451.

Bray, F., Laversanne, M., Sung, H., Ferlay, J., Siegel, R.L., Soerjomataram, I., and Jemal, A. (2024). Global cancer statistics 2022: GLOBOCAN estimates of incidence and mortality worldwide for 36 cancers in 185 countries. CA: A Cancer Journal for Clinicians *74*, 229-263.
Brix, K.S., Walter (2013). Proteases: Structure and Function.
Cohen, S., Valm, A.M., and Lippincott-Schwartz, J. (2018). Interacting organelles. Current Opinion in Cell Biology *53*, 84-91.
Consortium, T.U. (2022). UniProt: the Universal Protein Knowledgebase in 2023. Nucleic Acids Research *51*, D523-D531.
de Mendoza, A., and Sebé-Pedrós, A. (2019). Origin and evolution of eukaryotic transcription factors. Current Opinion in Genetics & Development *58-59*, 25-32.
Demasi, M., and da Cunha, F.M. (2018). The physiological role of the free 20S proteasome in protein degradation: A critical review. Biochimica et Biophysica Acta (BBA)- General Subjects *1862*, 2948-2954.
Dever, T.E., Dinman, J.D., and Green, R. (2018). Translation Elongation and Recoding in Eukaryotes. Cold Spring Harb Perspect Biol *10*.
Dikic, I., and Schulman, B.A. (2023). An expanded lexicon for the ubiquitin code. Nature Reviews Molecular Cell Biology *24*, 273-287.
Duan, Z., and Tominaga, M. (2018). Actin–myosin XI: an intracellular control network in plants. Biochemical and Biophysical Research Communications *506*, 403-408.
Eberhard, S., Finazzi, G., and Wollman, F.-A. (2008). The Dynamics of Photosynthesis. Annual Review of Genetics *42*, 463-515.
Fagan, W.F., Lewis, M.A., Auger-Méthé, M., Avgar, T., Benhamou, S., Breed, G., LaDage, L., Schlägel, U.E., Tang, W.-w., Papastamatiou, Y.P*., et al.* (2013). Spatial memory and animal movement. Ecology Letters *16*, 1316-1329.
Farmer, L.M., Book, A.J., Lee, K.H., Lin, Y.L., Fu, H., and Vierstra, R.D. (2010). The RAD23 family provides an essential connection between the 26S proteasome and ubiquitylated proteins in Arabidopsis. Plant Cell *22*, 124-142.

Gao, H., Sun, X., and Rao, Y. (2020). PROTAC Technology: Opportunities and Challenges. ACS Medicinal Chemistry Letters *11*, 237-240.
Gilbert, W.V., and Nachtergaele, S. (2023). mRNA Regulation by RNA Modifications. Annual Review of Biochemistry *92*, 175-198.
Gladman, N.P., Marshall, R.S., Lee, K.H., and Vierstra, R.D. (2016). The Proteasome Stress Regulon Is Controlled by a Pair of NAC Transcription Factors in Arabidopsis. Plant Cell *28*, 1279-1296.
Gou, M., Balint-Kurti, P., Xu, M., and Yang, Q. (2023). Quantitative disease resistance: Multifaceted players in plant defense. Journal of Integrative Plant Biology *65*, 594-610.
Gray, M.W. (1999). Evolution of organellar genomes. Current Opinion in Genetics & Development *9*, 678-687.
Grudnik, P., Bange, G., and Sinning, I. (2009). Protein targeting by the signal recognition particle. Biological Chemistry *390*, 775-782.
Hao, Y.J., Song, Q.X., Chen, H.W., Zou, H.F., Wei, W., Kang, X.S., Ma, B., Zhang, W.K., Zhang, J.S., and Chen, S.Y. (2010). Plant NAC-type transcription factor proteins contain a NARD domain for repression of transcriptional activation. Planta *232*, 1033-1043.
Harms, M.J., and Thornton, J.W. (2013). Evolutionary biochemistry: revealing the historical and physical causes of protein properties. Nature Reviews Genetics *14*, 559-571.
He, Z., Webster, S., and He, S.Y. (2022). Growth–defense trade-offs in plants. Current Biology *32*, R634-R639.
Hightower, L.E. (1991). Heat shock, stress proteins, chaperones, and proteotoxicity. Cell *66*, 191-197.
Hirano, H., Kimura, Y., and Kimura, A. (2016). Biological significance of co- and post-translational modifications of the yeast 26S proteasome. Journal of Proteomics *134*, 37-46.
Hu, X.-H., Shen, S., Wu, J.-L., Liu, J., Wang, H., He, J.-X., Yao, Z.-L., Bai, Y.-F., Zhang, X., Zhu, Y.*, et al.* (2023a). A natural allele of proteasome maturation factor improves rice resistance to multiple pathogens. Nature Plants *9*, 228-237.
Hu, X., Zou, R., Zhang, Z., Ji, J., Li, J., Huo, X.-Y., Liu, D., Ge, M.-X., Cui, M.-K., Wu, M.-Z.*, et al.* (2023b). UBE4A catalyzes NRF1 ubiquitination

and facilitates DDI2-mediated NRF1 cleavage. Biochimica et Biophysica Acta (BBA)- Gene Regulatory Mechanisms *1866*, 194937.
Iñiguez, L.P., and Hernández, G. (2017). The Evolutionary Relationship between Alternative Splicing and Gene Duplication. Frontiers in Genetics *8*.
Jackson, R.J., Hellen, C.U.T., and Pestova, T.V. (2010). The mechanism of eukaryotic translation initiation and principles of its regulation. Nature Reviews Molecular Cell Biology *11*, 113-127.
Jayarapu, K., and Griffin, T.A. (2007). Differential intra-proteasome interactions involving standard and immunosubunits. Biochem Biophys Res Commun *358*, 867-872.
Kim, M., Xi, H., and Park, J. (2021). Genome-wide comparative analyses of GATA transcription factors among 19 Arabidopsis ecotype genomes: Intraspecific characteristics of GATA transcription factors. PLOS ONE *16*, e0252181.
Kim, S.-Y., Kim, S.-G., Kim, Y.-S., Seo, P.J., Bae, M., Yoon, H.-K., and Park, C.-M. (2007). Exploring membrane-associated NAC transcription factors in Arabidopsis : implications for membrane biology in genome regulation. Nucleic Acids Research *35*, 203-213.
Klemm, S.L., Shipony, Z., and Greenleaf, W.J. (2019). Chromatin accessibility and the regulatory epigenome. Nature Reviews Genetics *20*, 207-220.
Knop, M., Schiffer, H.H., Rupp, S., and Wolf, D.H. (1993). Vacuolar/lysosomal proteolysis: proteases, substrates mechanisms. Current Opinion in Cell Biology *5*, 990-996.
Koonin, E.V., Fedorova, N.D., Jackson, J.D., Jacobs, A.R., Krylov, D.M., Makarova, K.S., Mazumder, R., Mekhedov, S.L., Nikolskaya, A.N., Rao, B.S.*, et al.* (2004). A comprehensive evolutionary classification of proteins encoded in complete eukaryotic genomes. Genome Biology *5*, R7.
Koonin, E.V., and Novozhilov, A.S. (2017). Origin and Evolution of the Universal Genetic Code. Annual Review of Genetics *51*, 45-62.
Krämer, L., Groh, C., and Herrmann, J.M. (2021). The proteasome: friend and foe of mitochondrial biogenesis. FEBS Letters *595*, 1223-1238.

Lee, Y., and Rio, D.C. (2015). Mechanisms and Regulation of Alternative Pre-mRNA Splicing. Annual Review of Biochemistry *84*, 291-323.
Lehrbach, N.J., and Ruvkun, G. (2016). Proteasome dysfunction triggers activation of SKN-1A/Nrf1 by the aspartic protease DDI-1. Elife *5*.
Lentjes, M.H., Niessen, H.E., Akiyama, Y., de Bruïne, A.P., Melotte, V., and van Engeland, M. (2016). The emerging role of GATA transcription factors in development and disease. Expert Rev Mol Med *18*, e3.
Li, X., Li, Y., Arendt, C.S., and Hochstrasser, M. (2016). Distinct Elements in the Proteasomal beta5 Subunit Propeptide Required for Autocatalytic Processing and Proteasome Assembly. J Biol Chem *291*, 1991-2003.
Liu, X., Xu, C., Xiao, W., and Yan, N. (2023). Unravelling the role of NFE2L1 in stress responses and related diseases. Redox Biology *65*, 102819.
Manasanch, E.E., and Orlowski, R.Z. (2017). Proteasome inhibitors in cancer therapy. Nature Reviews Clinical Oncology *14*, 417-433.
Mann, S. (2012). Systems of Creation: The Emergence of Life from Nonliving Matter. Accounts of Chemical Research *45*, 2131-2141.
Marshall, R.S., and Vierstra, R.D. (2019). Dynamic Regulation of the 26S Proteasome: From Synthesis to Degradation. Front Mol Biosci *6*, 40.
Maugarny-Calès, A., Gonçalves, B., Jouannic, S., Melkonian, M., Ka-Shu Wong, G., and Laufs, P. (2016). Apparition of the NAC Transcription Factors Predates the Emergence of Land Plants. Molecular Plant *9*, 1345-1348.
Mayans, O., van der Ven, P.F., Wilm, M., Mues, A., Young, P., Fürst, D.O., Wilmanns, M., and Gautel, M. (1998). Structural basis for activation of the titin kinase domain during myofibrillogenesis. Nature *395*, 863-869.
Miller, M.B., and Bassler, B.L. (2001). Quorum Sensing in Bacteria. Annual Review of Microbiology *55*, 165-199.

Mithoe, S.C., and Menke, F.L.H. (2018). Regulation of pattern recognition receptor signalling by phosphorylation and ubiquitination. Current Opinion in Plant Biology *45*, 162-170.
Murata, S., Takahama, Y., Kasahara, M., and Tanaka, K. (2018). The immunoproteasome and thymoproteasome: functions, evolution and human disease. Nature Immunology *19*, 923-931.
Nellaepalli, S., Lau, A.S., and Jarvis, R.P. (2023). Chloroplast protein translocation pathways and ubiquitin-dependent regulation at a glance. Journal of Cell Science *136*.
Neph, S., Stergachis, Andrew B., Reynolds, A., Sandstrom, R., Borenstein, E., and Stamatoyannopoulos, John A. (2012). Circuitry and Dynamics of Human Transcription Factor Regulatory Networks. Cell *150*, 1274-1286.
Nguyen, H.M., Schippers, J.H., Goni-Ramos, O., Christoph, M.P., Dortay, H., van der Hoorn, R.A., and Mueller-Roeber, B. (2013). An upstream regulator of the 26S proteasome modulates organ size in Arabidopsis thaliana. Plant J *74*, 25-36.
Orosa, B., Üstün, S., Villalobos, L.I.A.C., Genschik, P., Gibbs, D., John Holdsworth, M., Isono, E., Lois, M., Trujillo, M., and Sadanandom, A. (2020). Plant proteostasis – shaping the proteome

a research community aiming to understand molecular mechanisms that control protein abundance. The New Phytologist *227*, 1028-1033.
Ortiz-García, P., González Ortega-Villaizán, A., Onejeme, F.C., Müller, M., and Pollmann, S. (2023). Do Opposites Attract? Auxin-Abscisic Acid Crosstalk: New Perspectives. International Journal of Molecular Sciences *24*, 3090.
Pakos-Zebrucka, K., Koryga, I., Mnich, K., Ljujic, M., Samali, A., and Gorman, A.M. (2016). The integrated stress response. EMBO reports *17*, 1374-1395.
Palmgren, M.G., Edenbrandt, A.K., Vedel, S.E., Andersen, M.M., Landes, X., Østerberg, J.T., Falhof, J., Olsen, L.I., Christensen, S.B., Sandøe, P*., et al.* (2015). Are we ready for back-to-nature crop breeding? Trends in Plant Science *20*, 155-164.
Pavlopoulos, G.A., Iacucci, E., Iliopoulos, I., and Bagos, P. (2013). Interpreting the Omics 'era' Data. In Multimedia Services in Intelligent

Environments: Recommendation Services, G.A. Tsihrintzis, M. Virvou, and L.C. Jain, eds. (Heidelberg: Springer International Publishing), pp. 79-100.
Paysan-Lafosse, T., Blum, M., Chuguransky, S., Grego, T., Pinto, B.L., Salazar, Gustavo A., Bileschi, Maxwell L., Bork, P., Bridge, A., Colwell, L., *et al.* (2022). InterPro in 2022. Nucleic Acids Research *51*, D418-D427.
Pick, E., and Berman, T.S. (2013). Formation of alternative proteasomes: Same lady, different cap? FEBS Letters *587*, 389-393.
Postnikoff, S.D.L., Johnson, J.E., and Tyler, J.K. (2017). The integrated stress response in budding yeast lifespan extension. Microb Cell *4*, 368-375.
Radhakrishnan, S.K., den Besten, W., and Deshaies, R.J. (2014). p97-dependent retrotranslocation and proteolytic processing govern formation of active Nrf1 upon proteasome inhibition. Elife *3*, e01856.
Rojo, F. (2001). Mechanisms of transcriptional repression. Current Opinion in Microbiology *4*, 145-151.
Ruvkun, G., and Lehrbach, N. (2023). Regulation and Functions of the ER-Associated Nrf1 Transcription Factor. Cold Spring Harb Perspect Biol *15*.
Ryoo, H.D. (2024). The integrated stress response in metabolic adaptation. Journal of Biological Chemistry *300*.
Sahu, I., Mali, S.M., Sulkshane, P., Xu, C., Rozenberg, A., Morag, R., Sahoo, M.P., Singh, S.K., Ding, Z., Wang, Y., *et al.* (2021). The 20S as a stand-alone proteasome in cells can degrade the ubiquitin tag. Nature Communications *12*, 6173.
Šamaj, J., Baluška, F.e., Voigt, B., Schlicht, M., Volkmann, D., and Menzel, D. (2004). Endocytosis, Actin Cytoskeleton, and Signaling. Plant Physiology *135*, 1150-1161.
Seo, P.J., Kim, S.G., and Park, C.M. (2008). Membrane-bound transcription factors in plants. Trends Plant Sci *13*, 550-556.
Shibata, Y., Hu, J., Kozlov, M.M., and Rapoport, T.A. (2009). Mechanisms Shaping the Membranes of Cellular Organelles. Annual Review of Cell and Developmental Biology *25*, 329-354.
Song, L., Huang, S.-s.C., Wise, A., Castanon, R., Nery, J.R., Chen, H., Watanabe, M., Thomas, J., Bar-Joseph, Z., and Ecker, J.R. (2016). A

transcription factor hierarchy defines an environmental stress response network. Science *354*, aag1550.
Stotz, H.U., Sawada, Y., Shimada, Y., Hirai, M.Y., Sasaki, E., Krischke, M., Brown, P.D., Saito, K., and Kamiya, Y. (2011). Role of camalexin, indole glucosinolates, and side chain modification of glucosinolate-derived isothiocyanates in defense of Arabidopsis against Sclerotinia sclerotiorum. The Plant Journal *67*, 81-93.
Tang, F., Wang, B., Li, N., Wu, Y., Jia, J., Suo, T., Chen, Q., Liu, Y.-J., and Tang, J. (2011). RNF185, a Novel Mitochondrial Ubiquitin E3 Ligase, Regulates Autophagy through Interaction with BNIP1. PLOS ONE *6*, e24367.
Tang, Y., Zhao, C.-Y., Tan, S.-T., and Xue, H.-W. (2016). Arabidopsis Type II Phosphatidylinositol 4-Kinase PI4Kγ5 Regulates Auxin Biosynthesis and Leaf Margin Development through Interacting with Membrane-Bound Transcription Factor ANAC078. PLOS Genetics *12*, e1006252.
Teicher, B.A., Ara, G., Herbst, R., Palombella, V.J., and Adams, J. (1999). The Proteasome Inhibitor PS-341 in Cancer Therapy. Clinical Cancer Research *5*, 2638-2645.
Ueda, H., Yokota, E., Kutsuna, N., Shimada, T., Tamura, K., Shimmen, T., Hasezawa, S., Dolja, V.V., and Hara-Nishimura, I. (2010). Myosin-dependent endoplasmic reticulum motility and F-actin organization in plant cells. Proceedings of the National Academy of Sciences *107*, 6894-6899.
Üstün, S., Bartetzko, V., and Börnke, F. (2013). The Xanthomonas campestris Type III Effector XopJ Targets the Host Cell Proteasome to Suppress Salicylic-Acid Mediated Plant Defence. PLOS Pathogens *9*, e1003427.
van der Lee, R., Buljan, M., Lang, B., Weatheritt, R.J., Daughdrill, G.W., Dunker, A.K., Fuxreiter, M., Gough, J., Gsponer, J., Jones, D.T*., et al.* (2014). Classification of Intrinsically Disordered Regions and Proteins. Chemical Reviews *114*, 6589-6631.
van Wijk, K.J., Leppert, T., Sun, Q., Boguraev, S.S., Sun, Z., Mendoza, L., and Deutsch, E.W. (2021). The Arabidopsis PeptideAtlas: Harnessing worldwide proteomics data to create a comprehensive community proteomics resource. The Plant Cell *33*, 3421-3453.

Vogel, C., and Marcotte, E.M. (2012). Insights into the regulation of protein abundance from proteomic and transcriptomic analyses. Nature Reviews Genetics *13*, 227-232.
Welner, D.H., Deeba, F., Lo Leggio, L., and Skriver, K. (2016). Chapter 13- NAC Transcription Factors: From Structure to Function in Stress-Associated Networks. In Plant Transcription Factors, D.H. Gonzalez, ed. (Boston: Academic Press), pp. 199-212.
Williams, T.D., Cacioppo, R., Agrotis, A., Black, A., Zhou, H., and Rousseau, A. (2022). Actin remodelling controls proteasome homeostasis upon stress. Nature Cell Biology *24*, 1077-1087.
Wu, H., Carvalho, P., and Voeltz, G.K. (2018). Here, there, and everywhere: The importance of ER membrane contact sites. Science *361*, eaan5835.
Xu, P., Duong, D.M., Seyfried, N.T., Cheng, D., Xie, Y., Robert, J., Rush, J., Hochstrasser, M., Finley, D., and Peng, J. (2009). Quantitative proteomics reveals the function of unconventional ubiquitin chains in proteasomal degradation. Cell *137*, 133-145.
Yuen, E.L.H., Shepherd, S., and Bozkurt, T.O. (2023). Traffic Control: Subversion of Plant Membrane Trafficking by Pathogens. Annual Review of Phytopathology *61*, 325-350.

Acknowledgments

I would like to sincerely thank Suayb for giving me the chance to work on this fantastic project and for always encouraging my scientific creativity. This guidance has played a significant role in shaping the scientist I am today.

Thank to Paul, my enduring colleague in Germany, for engaging and inspiring discussions on both scientific topics and beyond, as well as for the laughs and good times outside of work.

I am grateful to Marja Timmermans and Yasin Dagdas, my TAC committee members, for their critical advice during my PhD, which helped steer this project in meaningful directions.

A special thanks to the Üstün Lab for the enjoyable time we spent together.

To my family—my mother, Mary, and my father, Dominique—thank you for fostering my love for nature and always believing in me, even during difficult times. To my brother, Guillaume, thank you for being a role model and for sharing my curiosity about life and the universe.

Finally, to my partner in life and in crime, Ophélie: thank you for being my love through all these years, for supporting me unconditionally, and for being by my side throughout this journey. Your presence has made so many beautiful moments possible and made this cycle of my life unique and unforgettable.